OLLSCOIL NA GAILLIMHE
UNIVERSITY OF GALWAY

MODELLING THE RESPONSE OF INFLUENT VOLUMES OF WASTEWATER TREATMENT PLANTS UNDER CURRENT AND FUTURE CONDITIONS FOR EFFECTIVE WASTEWATER MANAGEMENT IN COMBINED SEWERAGE SYSTEMS

By

Sukanya D Saikia

A thesis submitted to the College of Science and Engineering, University of Galway, in partial fulfilment of the requirements for the Degree of Doctor of Philosophy

2023

Academic supervisors: Dr. Eoghan Clifford, Dr. Paraic Ryan

Declaration

I, the undersigned, hereby declare that this thesis, entitled, ‘Modelling the response of influent volumes of wastewater treatment plants under current and future conditions for effective wastewater management in combined sewerage systems”, is entirely my own work. The thesis has not been submitted in whole or in part to any other university or institution. All sources used have been acknowledged and referenced in the text.

Sukanya Diganta Saikia

Acknowledgements

Firstly, I would like to thank Dr. Eoghan Clifford for supervising me with utmost dedication and patience. His guidance and support helped me overcome my inhibitions. He was present whenever I sought his advice, and I am very grateful for his time. I would also like to thank Dr. Paraic Ryan for agreeing to co-supervise me. His attention to detail pushed me to try and achieve the highest standard and nothing less only ever. Both their supervision enhanced my critical thinking skills and I believe, made me a better researcher.

I am grateful to the Energy System Integration Partnership Programme (ESIPP) for funding the research. I would also like to thank the College of Science and Engineering in University of Galway for supporting this research. I am grateful to my graduate research committee Prof. Padraic O'Donoghue, Dr. Mark Healy and Dr. Stephen Nash for believing in me. Thanks to Irish Water for providing me with the data for this thesis. Special thanks to Dr. Paul Nolan from Irish Centre for High-End Computing, who despite his busy schedule, always responded promptly to my doubts and gave me a word of encouragement when I needed. Thanks to Sudeep and Ronan for being there whenever I needed to chat. Sharing the struggles and the successes made the journey more enjoyable.

My beloved friends, Jenny, Soorya, Nikita, Anand, Cerine, Jiahui, Cleressa, Rajib and Hugh helped me cope with homesickness. They made me feel at home, even though I was thousands of miles away, in a different country. I will always be grateful for them, for lending me an ear when I needed one, their shoulders to lean on, when I felt like everything was going wrong! I am very grateful to Tara, without whom, I wouldn't have had a home in Ireland while finishing my thesis. She gave me a safe space to work with a stable mind when I had no place to stay.

My mother and my sister were the greatest strengths from the very beginning of my PhD and throughout life. Despite being miles away, they made sure they talk to me each and every single day on the phone. Be it the highs or the lows, they have been there for me and helped me to remain motivated and be persistent. They always looked out for me, mentally, emotionally and financially despite all the troubles. Their unconditional love and support made my PhD journey a tad bit easier. My brother-in-law was also there in every step of the way, inspiring me and making me believe that I can do this. My heart is

full of gratitude and love for each one of them. I am also very grateful to my late father who dreamt of a brighter future for me and believed in my quality education that has helped to build a strong foundation. I am sure he is smiling seeing his name (my middle name) on the thesis! His presence is missed every single day.

Last, but certainly not the least, my heartfelt gratitude to Abhishek, who was my biggest support through my entire PhD. He was there on the phone, listening and talking to me through all my problems. He was there each and every time I was close to giving up, pushing me, encouraging me to always face the challenges and believing in me, more than I believed in myself. The distance, the pandemic and everything else, although extremely difficult to tackle, never really mattered because he was always there, on the other end of the phone, smiling at me, telling me that if there is anyone who could do this, it is me. I cannot thank my stars enough to have received so much support from him. I will be forever grateful. I could not have done this without him.

Abstract

Wastewater treatment plants (WWTPs) are critical infrastructure globally and are essential to protect public health and the environment. With factors such as population growth, urbanisation, increase in water consumption etc., the amount of wastewater generated has increased significantly, which impact the operations of WWTPs. Of particular concern are WWTPs with combined sewerage systems (CSSs) which treat foul and storm wastewater collectively. Such WWTPs are also influenced by changes in the intensity and frequency of precipitation events. During instances of increased precipitation intensity and frequency of storm events, WWTPs with CSSs might encounter hydraulic overloading and release of untreated wastewater called combined sewer overflows (CSOs). On the other hand, lack of precipitation can lead to reduced flow and increased contaminant loading. In both the cases, with climate change and the associated changes in precipitation patterns, WWTPs with CSSs may become more susceptible to system failures that pose a threat to the receiving waters and the surrounding natural environment.

As stricter environmental regulations are enforced to limit the occurrences of CSOs, it has become increasingly important to identify the variables that impact the functioning of WWTPs with CSSs. However, unavailability of real data is a key challenge in the research area of monitoring the performance of WWTPs and sewerage systems. Studies have conventionally used modelled data simulated from hydraulic models that do not cater to local characteristics of individual WWTPs and hence are often associated with large uncertainties. While considerable attention has been given to the impacts of climate variables (current and future) and urbanisation on effluent quantity and quality and the performance of the sewerage systems focusing on CSOs, the same cannot be said for wastewater influent volumes. Influent volume characteristics function differently as compared to CSOs and effluent volumes. Once CSOs leave the sewerage system, there are still variations in the flow that proceed towards the WWTPs during or after the spill. Hence influent volumes have a significant impact on subsequent WWTP processes and predicting how they might change can help prevent occurrences of overflows and aid in achieving resilience of WWTPs. Studies investigating the degree to which precipitation change (current and future), tidal level, river level, and urbanisation impacts influent volumes of WWTPs with CSSs remain unexplored.

This research addresses these gaps by studying influent volume response characteristics of 14 WWTPs of varying sizes, connected with CSSs, that are spatially distributed over Ireland. The thesis uses real spatio-temporal datasets of precipitation, influent volumes and location-specific data of tidal and river level. The objective of this study was to develop methodologies under practical data constraints to build models that could define meaningful relationships among the different variables. Daily precipitation and daily mean river level were found to be statistically significant predictor variables of influent volumes at a daily scale. On a monthly basis, monthly average daily precipitation, number of wet days in a month (and thus zero rainfall days) were observed to be statistically significant. The daily and monthly variations in influent volumes for each of the WWTPs were assessed with the help of simple and multiple linear regression modelling analysis. These individual WWTP models helped to capture local characteristics specific to each WWTP. In addition, a novel pooled model was developed through spatio-temporal analysis across all the 14 WWTPs to derive generic trends in influent volumes across any WWTP. Probability of exceedance curves linking daily precipitation and influent volumes were also developed that could aid in identifying storm overflow events under various precipitation categories. These graphs could be potentially used for future climate scenarios using precipitation projections to estimate the projected frequency of storm overflow events.

This research also analysed, for the first time, the evolution of influent volumes during mid-century period (2041 – 2060) as compared to current period. It predicted future influent volumes by leveraging high resolution multi-model regional climate model projections of precipitation intensity and extreme events for each WWTP and linking them to the developed data-driven models and probability of exceedance curves. This analysis offers valuable insights into how WWTPs might get impacted in future (e.g., exceedance of peak design capacity under extreme weather conditions) due to climate change.

Finally, this research aims to investigate the degree to which urbanisation might potentially impact influent volumes of WWTPs with CSSs. Landsat 5 and Landsat 8 satellite images were used to perform landuse landcover classification of all the 14 agglomerations corresponding to each WWTP to estimate the change in built-up area. Percentage change in built-up area relative to agglomeration area was found to be statistically significant with moderate degree of correlation with influent volumes across

all agglomerations. The findings of this research will help wastewater utilities (particularly the ones connected with CSSs) as end-users, take informed decision in their planning and adaptation strategies in order to establish resilient wastewater infrastructure at regional and local WWTP scales.

Table of Contents

List of Figures

List of Tables

Nomenclature

ADIV	Average daily influent volume over a month
ADP	Average daily precipitation over a month
AOI	Area of Interest
AR	Assessment Report
BMPs	Best Management Practices
CERFACS	Centre Européen de Recherche et de Formation Avancée
CMIP	Coupled Model Intercomparison Project
CNRM-GAME	Centre National de Recherches Météorologiques—Groupe d'études de l'Atmosphere Météorologique
CRU	Commission for Regulation of Utilities
COSMO-CLM	Consortium for Small-scale Modeling – Climate Limited-area Modelling
CSO	Combined sewer overflow
CSS	Combined sewerage system
DCIA	Directly Connected impervious area
DJF	December January February
DWF	Dry weather flow
EM	Electromagnetic
EPA	Environmental Protection Agency
ESRI	Environmental Systems Research Institute
EU	European Union

FCC	False Colour Composite
GCM	General circulation model
GEE	Google Earth Engine
GHG	Greenhouse gas
GIS	Geographical Information System
HadGEM2-ES	Hadley Centre Global Environment Model version 2 Earth System
IDE	Integrated Development Environment
IPCC	Intergovernmental Panel on Climate Change
JJA	June July August
LID	Low Impact Development
LULC	Landuse land cover
m^3/day	Cubic Meter per day
MAM	March April May
MIROC	Model for Interdisciplinary Research on Climate
MLR	Multiple Linear Regression
mm/day	Millimetre per day
MPI-ESM-LR	Max Planck Institute-Earth System Model-Low Resolution
MSS	Multispectral Scanner
NASA	National Aeronautics Space Administration
NDC	Nationally Determined Contribution

NIR	Near-infrared
OPW	Office of the Public Works
P	Daily precipitation
p-value	Statistical level of significance
PD	Peak design capacity
PE	Population Equivalent
POTW	Publicly owned treatment work
Q	Daily influent volume
RCM	Regional Climate Model
RCP	Representative Concentration Pathway
RGB	Red-green-blue
RL	Daily mean river level
RSE	Residual Standard Error
RMSE	Root mean square error
ROI	Region of Interest
RS	Remote Sensing
SDSM	Statistical DownScaling Model
SLC	Scan Line Corrector
SLCF	Short-lived Climate Forcers
SLR	Simple linear regression
SNR	Signal to noise ratio

SON	September October November
SRES	Special Report on Emission Scenarios
SSO	Sanitary sewer overflow
SSP	Shared Socio-economic Pathway
SWMM	Storm Water Management Model
T	Daily maximum tidal level
TCC	True Colour Composite
TIA	Total Impervious area
TM	Thematic Mapper
ZRD	Number of zero rainfall days in a month
UNFCCC	United Nations Framework Convention on Climate Change
USGS	United States Geological Survey
UWWTD	Urban Waste Water Treatment Directive
VIF	Variance Inflation Factor
WD	Number of wet days in a month
WRF	Weather Research Forecasting
WWAP	World Water Assessment Program
WWTP	Wastewater treatment plant

List of Notation

y	Dependent variable
x	Predictor variable
β	Coefficient of the predictor variable in a linear regression equation
c	Intercept
$\in$	Model Error
n	Number of predictor variables
o	Number of observations
R^2	Regression coefficient or coefficient of determination
Q	Observed daily influent volume
Q_{min}	Minimum observed daily influent volume
Q_{max}	Maximum observed daily influent volume
Q'_D	Normalised daily influent volume
$ADIV$	Observed monthly average daily influent volume
$ADIV_{min}$	Minimum observed monthly average daily influent volume
$ADIV_{max}$	Maximum observed monthly average daily influent volume
Q'_M	Normalised monthly average daily influent volume
Q'_{Dwdy}	Predicted normalised daily influent volume of WWTP w, on day d and year y

P_{wdy}	Observed daily precipitation of WWTP w, on day $d$and year y
Q'_{Mwmy}	Predicted normalised monthly average daily influent volume of WWTP w, in month m and year y
ADP_{wmy}	Observed monthly average daily influent volume of WWTP w, in month m and year y
ZRD_{wmy}	Observed number of zero rainfall days of WWTP w, in month m and year y
Q_{PD}	Predicted daily influent volume
Q_{PM}	Predicted monthly average daily influent volume
Q_m	Observed average daily influent volume in month m
$Q_{m,p}$	Predicted future average daily influent volume in month m
$RC_{O,m}$	Observed reserved capacity in month m
PD	Peak design capacity
$BU_t\%$	Percentage change in built-up area over time interval t
BU_{ts}	Built-up area of the subsequent year ts
BU_{tp}	Built-up area of the antecedent year tp
$BU_{tA}\%$	Percentage change in built-up area to total agglomeration area
A	Total agglomeration area
$BU_{tR}\%$	Rate of urbanisation / average annual rate of change in built-up area

BU_{tf}	Built-up area in the final year tf
BU_{ti}	Built-up area in the initial/first year ti

1. INTRODUCTION

1. Introduction

1.1. Background

Global water use is increasing at the rate of 1% per year and has increased 6-fold over the past 100 years due to increases in population, economic development and changing consumption patterns (UNESCO, 2020). Wastewater is "used" water contaminated with pollutants by human activities (Jones et al., 2021). Therefore, increase in water use inherently leads to surge in the quantity of wastewater generated that puts additional pressure on the wastewater infrastructure services (Teklehaimanot et al., 2015). Ongoing increases in wastewater generation can lead to increased pollution loads within receiving waters and can pose a serious threat to our aquatic ecosystems, human health and livelihoods of communities and economy (Astaraie-Imani et al., 2012; García-Ávila et al., 2021; Sahu, 2019).

The risk of contaminated water being discharged without any treatment is further exacerbated by various factors such as change in sea level, urbanisation marked by a rise in impervious surfaces, population growth etc. (Astaraie-Imani et al., 2012; Hussain et al., 2022; Kleidorfer et al., 2009; Mohammed et al., 2021; Semadeni-Davies et al., 2008; Shakeri et al., 2021; Teklehaimanot et al., 2015). Furthermore, according to the International Panel on Climate Change (IPCC), human and natural systems have already encountered some irreversible impacts of climate change arising from exposure to irregular weather patterns and extreme weather events (IPCC, 2022). These variables are known to be key factors influencing hydraulic characteristics of WWTPs both in terms of wastewater quality and quantity; but in some cases, their effects on wastewater volumes are not well understood.

Wastewater treatment facilities are considered as critical infrastructure globally (Hawchar et al., 2020), and are affected by changes in the intensity and frequency of precipitation events (Gooré Bi et al., 2015; Langeveld et al., 2013; Li et al., 2018; Mines et al., 2007; Mohammed et al., 2021). For example, increased rainfall intensity and frequency of extreme rainfall events will result in increased wastewater influent volumes due to inflow and infiltration and flow from combined sewerage systems (CSSs) that collect both wastewater and stormwater (Hughes et al., 2021). Decreased rainfall will lead to the contrary outcome of reduced flow and inflow and infiltration, resulting in

increased contaminant concentrations (from reduced dilution capacity) due to reduced volumes of wastewater (Hughes et al., 2021, Zouboulis and Tolkou, 2015). Furthermore, extreme weather events such as floods or droughts will likely decrease the efficiency of treatment processes in WWTPs (Reznik et al., 2020). Storm events can trigger overflow of excess untreated wastewater, called the combined sewer overflows (CSOs) (Gooré Bi et al., 2015) whereas drought events can lead to settled debris in the pipelines (Draude et al., 2019). In case of a combination of extreme events such as an extended dry period followed by a storm event, the settled debris is carried to the receiving waters resulting in increased pollutant loading (Langeveld et al., 2013). The performance characteristics of influent volumes, CSOs and effluent volumes for WWTPs connected to CSSs are different (discussed in detail in Chapter 2, Section 2.3.1). While the response of CSO and effluent characteristics to rainfall have been studied extensively, the degree to which rainfall patterns may impact WWTP influent volumes has not been widely investigated, particularly in the context of expected changing rainfall patterns to mid-century and beyond.

In addition to climatic parameters, the degree to which stormwater might affect a CSS, in the event of extreme precipitation, may be linked to existing landuse land cover (LULC) around the catchment or agglomeration from where the CSS is connected. In the case of urban areas, LULC comprises significant amounts of impermeable surfaces increasing the amount of stormwater runoff, and can overburden sewer networks (Yao et al., 2016) though the degree to which this may impact WWTPs is also not well understood.

Along with changes in precipitation variables (current and future) and urbanisation, changes in tidal level and river level can also cause challenges for the design and operation of wastewater collection and treatment systems (Lian et al., 2013; Yin et al., 2011). Indeed, WWTPs in coastal areas are prone to tidal inflow that can enter the sewer systems of coastal WWTPs via CSO outfall pipes and can thus influence influent volumes to WWTPs. For example the effects (individually or combined) of tidal inflow and precipitation can lead to higher influent volumes, partly induced by elevated groundwater levels, and, consequently increase operational costs and reduce treatment capacities (Cahoon & Hanke, 2017; Cahoon and Hanke, 2019; Flood & Cahoon, 2011). However, the degree to which influent volumes of WWTPs with CSSs, which are constructed close

to rivers or in coastal regions, may be impacted by tidal and river water levels has not been investigated previously to the best knowledge of the author.

1.2. Knowledge Gaps

This research aims to address several key gaps in the field of urban wastewater management studies which are summarised below:

- It is clear that limiting the number of CSOs and instances of hydraulic overloading are becoming increasingly important due to the risks they pose to the environment and public health (Astaraie-Imani et al., 2012; Butler et al., 2016; Gooré Bi et al., 2015; Li et al., 2012; Olds et al., 2018). Management of influent volumes, which is a significant WWTP parameter, will help in minimizing such risks. To the best knowledge of the author, research investigating the impacts of precipitation on influent volumes of WWTPs are limited to three studies (Langeveld et al., 2013; Li et al., 2018; Mines et al., 2007). These studies investigated either only one WWTP over a long time period (temporal aspect), or several WWTPs over a very short time period (spatial aspect). Thus, there is a clear gap in modelling the variation of the impacts of precipitation variables (Peleg et al., 2016) on influent volume characteristics over space and time (spatial-temporal aspect). Other studies have assessed the impacts of precipitation on the performance of sewerage systems focusing on CSOs and not on influent volumes (Gooré Bi et al., 2015; Hlodversdottir et al., 2015; Schroeder et al., 2011). A majority of these studies have used hydrodynamic pipe flow models or other pre-defined hydraulic models to simulate wastewater flows rather than real data. Therefore, there is a lack of understanding of responses of influent volumes to different precipitation variables, particularly for WWTPs connected to CSSs. There is a need to develop models that use a range of spatial and temporal real data to derive relationships between precipitation and influent volumes which can be generally applied at a regional level.
- Previous studies that have focused on the impacts of tidal levels on wastewater quantity and flooding include Cahoon & Hanke, (2017; 2019), Flood & Cahoon, (2011); Lian et al., (2013) and Yin et al., (2011). To the best knowledge of this author there has not been a previous study focusing on the impact of river levels on wastewater influent volumes. This may be particularly significant in the case

of tidal rivers where river level may be impacted both by precipitation changes and tidal changes.

- Analysis of potential climate change impacts has generally investigated the performance of sewerage systems and not WWTP influent volumes (Gooré Bi et al., 2015; Hlodversdottir et al., 2015; Kleidorfer et al., 2009). In addition, these studies involved application of fixed percentage change to observed datasets to generate climate change induced simulations, instead of using high-resolution climate model simulations. These fixed percentages are assumptions and hence lack a degree of scientific basis provided by the latest climate models in terms of future climate change impacts. Therefore, analysis of how influent volumes may be impacted by changes in future precipitation projections (derived from high-resolution climate models) are required.
- Studies conducted to investigate the impacts of urbanisation on sewer systems (Hussain et al., 2022; Loperfido et al., 2014; Ravagnani et al., 2009; Yao et al., 2016; Zhou et al., 2019) are limited to studying the response behaviour of stormwater runoff. To the best knowledge of author, previous studies do not reflect the degree to which it might affect wastewater influent volumes.

1.3. Research Aims and Objectives

The overall aim of this research was to thoroughly investigation the nature of response of influent volumes to WWTPs – a critical parameter as a function of precipitation (current and future), tidal and river levels and urbanisation, and provide a number of tools to stakeholders (e.g., utilities, researchers, engineers, and other wastewater operating/managing personnel) in this sector which could be applied at regional and national levels to derive generic trends. This was achieved by targeting the knowledge gaps and shortcomings identified above (Section 1.2) and undertaking the following objectives:

- Analyse the response characteristics of influent volumes of WWTPs, connected to CSSs, to precipitation, using extensive observational datasets and develop a pooled model from detailed spatio-temporal data analysis, that could be used to derive general trends of influent volumes across WWTPs of various sizes, while accounting for local characteristics. This research uses data from 14 WWTPs spatially distributed across Ireland, to establish the relationship between the

precipitation variables, and the response characteristic of influent volumes to WWTPs. Additionally, a new, but simple means to examine expected influent volumes resulting from particular precipitation events is proposed by means of probability of exceedance curves.

- Develop an understanding of the impacts of tidal level and river levels on wastewater influent volumes, and the potential relationships amongst these variables using data from different WWTPs located near rivers or coasts.
- Use the above models (relationships between current precipitation and influent volumes) to analyse evolution of wastewater influent volume characteristics by mid-century (2041 – 2060) at WWTP scale based on future projected change in mean precipitation intensity and frequency of extreme events derived from high-resolution Regional Climate Models (RCMs) outputs. The use of probability of exceedance curves to investigate the projected impacts of high and very high rainfall days on the frequency of events exceeding the peak design capacity of WWTPs is examined.
- Enhance the understanding of the potential effects of urbanisation on the influent volumes of WWTPs connected to CSSs by using supervised classification techniques to calculate change in builtup areas and analyse this in the context of WWTP influent volumes over those periods of time (and in the context of the above objectives).

1.4. Structure of the dissertation:

This research thesis is structured into 7 different chapters and an appendix. Chapter 1 presents a brief introduction to the research area of wastewater infrastructure and an overview of the challenges faced by wastewater utilities, the knowledge gaps identified through literature review, the research aims and objectives, the dissertation structure, and the contribution of this thesis to existing literature.

Chapter 2 presents a literature review which provides background on wastewater treatment plants, the way they function, the types of sewerage systems, focusing on combined sewerage systems. It discusses the impacts of precipitation variability (current and future), tidal and river levels, and urbanisation on the operation and maintenance of wastewater infrastructure. Chapter 2 also discusses in detail the existing literature in this field, the knowledge gaps and how this research aims to cover some of these gaps.

Chapter 3 describes the data sources and the data used in this research. It identifies the significant variables impacting influent volumes of WWTPs with combined sewerage systems and presents the methodologies used to model these relationships in Chapters 4, 5 and 6.

Chapter 4 presents the results of analysis of observed historical precipitation records, river and tidal levels and their impacts on the influent volume characteristics of 14 WWTPs of varying sizes. The chapter develops and presents a number of models and explains how probability of exceedance curves can be used to capture the influent volume response characteristics specific to each WWTP and across all WWTPs. The results demonstrate the usability and predictive capacity of the models developed and the curves in predicting influent volume to WWTPs based on variables for current period. This chapter has been published as a peer reviewed paper.

Chapter 5 of this thesis presents an analysis of future precipitation projections on influent volume characteristics of combined sewerage systems. It takes into consideration the latest climate model projections available and depicts an analysis of evolution of influent volumes by mid-century (2041 – 2060) as compared to a historical reference period (1981 – 2000) and the current period (2005 – 2018). It focuses on the projected change in precipitation intensity and frequency to illustrate the results, showing the evolution of wastewater influent volumes under RCP 4.5 and RCP 8.5.

Chapter 6 explains in detail the methodology adopted to estimate the change in landuse land cover at an urban catchment scale and investigates its influence on wastewater influent volumes. It also investigates impacts of urbanisation (individually or combined with precipitation), on influent volume changes in the WWTPs examined. The chapter discusses the different outcomes and provides thorough justification of the results.

Chapter 7 outlines the conclusions of the thesis. It starts with an overview of the research questions and the aims and objectives addressed in the PhD thesis. The chapter then highlights the main conclusions discussing the novel approaches utilised to address the research gaps and the main results obtained. It also discusses the limitations of the research and finally, it provides recommendations on promising future research scope.

1.5. Contribution to existing literature:

1.5.1. Journal Papers

- Saikia, S.D., Ryan, P., Nuyts, S., Clifford, E. (2022). Precipitation, tidal and river level impacts on influent volumes of combined wastewater collection systems: A regional analysis. *Results in Engineering*, 15, 100588, https://doi.org/10.1016/j.rineng.2022.100588
- Saikia, S.D., Ryan, P., Nuyts, S., Nolan, P. Clifford, E., (2023). Impacts of projected future changes in precipitation on the WWTP influent volumes connected by combined sewer collection systems. *Climate Services (Under Review)*
- Saikia, S.D., Ryan, P., Clifford, E. (2023). Understanding the relative response of influent volumes to urbanisation and precipitation for WWTPs connected by combined sewerage systems. *Urban Water Journal (Under preparation)*

1.5.2. Conferences

- Saikia, S.D., Ryan, P., Clifford, E. (2020). Modelling wastewater treatment plant dry and all-weather influent volumes as a function of tidal water level and precipitation in Ireland, Civil Engineering Research in Ireland, Cork, Ireland, 27th – 28th August.
- Saikia, S.D., Clifford, E., Ryan, P. (2020). Modelling the precipitation impacts on wastewater influent volumes in Galway, Ireland, European Geosciences Union General Assembly, Vienna, Austria, 3rd – 8th May.
- Saikia, S.D., Ryan, P., Clifford, E. (2020). Analysing influent volumes as a function of tidal water level and precipitation in Ireland, ENVIRON 2020 conference, Dublin, Ireland, 20th October 2020.
- Saikia, S.D., Clifford, E., Nair, S., Ryan, P., (2019). Impacts of precipitation variability on wastewater systems, 9th International Young Water Professionals Conference, Toronto, Canada, 23rd – 27th June 2019.
- Saikia, S.D., Clifford, E., Nair, S., Ryan, P., (2019). Observing the impacts of extreme precipitation events on wastewater systems, ENVIRON 2019 conference, Carlow, Ireland, 15th – 17th April 2019.

2. LITERATURE REVIEW

2. Literature review

2.1. Overview

Proper functioning of wastewater treatment plants (WWTPs) is essential to protect public health and the environment. There are several external factors such as demographics, climate change, urbanisation etc., that influence the operations of WWTPs (Gooré Bi et al., 2015; Hawchar et al., 2020; Hughes et al., 2021; Kleidorfer et al., 2009; Reznik et al., 2020; Semadeni-Davies et al., 2008; Zhou et al., 2019). Various studies have analysed the impacts of climate change and urbanisation on wastewater effluent discharge quantity and quality (Astaraie-Imani et al., 2012; Butler et al., 2016; Gooré Bi et al., 2015; Li et al., 2012; Olds et al., 2018) or on the hydraulic performance of the sewer systems (Fortier & Mailhot, 2015; Gooré Bi et al., 2015; Hlodversdottir et al., 2015; Mohammed et al., 2021; Shakeri et al., 2021). However, while influent to WWTPs is critical in terms of the operation and design of WWTPs (Giokas et al., 2002), there have been limited studies on analyzing the wastewater influent volumes (Langeveld et al., 2013; Y. Li et al., 2018; Mines et al., 2007). This chapter outlines the present state-of-the-art literature and the methodologies involved in studying the impacts of hydrological parameters such as precipitation and tidal levels, climate change and urbanisation on WWTPs and their associated sewer/sewerage systems, with a focus on the importance of wastewater influent characteristics. To establish context for this research, the initial sections review relevant literature regarding wastewater treatment plants and the different types of sewerage systems. The chapter then reviews literature regarding climate change model projections and scenarios. The core principles of remote sensing are also discussed to set the foundation for using this technology in this research. The chapter concludes with an overview of the key knowledge gaps identified and how they are addressed in part in this study.

2.2. Wastewater and Wastewater Treatment Systems

Wastewater contains a number of pollutants and harmful micro-organisms. Because of its highly contaminated nature, it needs to be safely carried away and treated to avoid negative impacts to the environment and public health. There are two broad categories of wastewater: i) domestic sewage, ii) infiltration and industrial wastewater (Sperling 2007). Domestic sewage wastewater includes water from toilets, bathrooms, kitchens, hospitals

etc. This type of wastewater is generated on a daily basis and depends on the per capita use. Infiltration and industrial wastewater, on the other hand, mainly comprises of water from commercial activities such as manufacturing, chemical processes, industries and stormwater and surface runoff from rain and flooding and can be collectively termed as non-sewage wastewater since it does not contain human waste.

In most cases, wastewater from a given area is transferred and directed towards public sewer systems and then to wastewater treatment plants (WWTPs). The area served by a WWTP is known as an agglomeration and is defined by the European Union Urban Waste Water Directive (UWWTD) as "an area where the population and/or economic activities are sufficiently concentrated for urban waste water to be collected and conducted to an urban waste water treatment plant or to a final discharge point" (European Commission, 2007). On the contrary, in rural areas, where there might not be any wastewater network serving the area, individual households have sewer/ septic tanks which are private and are also called domestic wastewater treatment systems.

2.2.1. Types of wastewater sewerage collection systems

Wastewater sewerage systems are designed to collect and convey wastewater generated by their agglomerations, for treatment in WWTPs. Hence the term wastewater sewerage system comprises the collection, treatment, and disposal systems (Sperling 2007). In this thesis, sewerage system is interchangeably used with the terms sewer system/ network, or, in the context of some literature, drainage system. The part of the sewerage system that collects the wastewater from its sources is the sewerage collection system. For efficient conveyance, WWTPs are generally located in low lying areas where wastewater can naturally and progressively flow, with the help of gravity. For the WWTPs which are not located in lower elevations and for agglomerations with varied topography and relatively long pipe networks, pumping stations are required to transfer the wastewater upwards from the sources. The design of the wastewater infrastructure is determined by a specific hydraulic treatment capacity which is generally called the population equivalent (PE) of the urban area served (Irish Water, 2015). There are three main categories of sewerage collection systems aimed to collect wastewater or stormwater: (i) sanitary sewers, (ii) storm sewers and (iii) combined sewerage system (CSS). The following sub-sections describe the different WWTP sewerage collection systems.

2.2.1.1. Sanitary sewers

Sanitary sewers are designed in such a way that the sewage, in this case, wastewater, is transported from its sources to the WWTPs without being mixed with stormwater. Under ideal conditions, sanitary sewers transfer wastewater from its sources to the WWTPs and thereby help prevent discharge of untreated wastewaters into the environment. However, when a system's capacity is exceeded or due to leakage or other faults in the network, these systems can be prone to sanitary sewer overflows (SSOs) (Cahoon & Hanke, 2017). During wet weather conditions, additional extraneous flows of stormwater or groundwater can infiltrate the sewer network, and might cause SSOs (Water Environment Federation, 2011). On the other hand, SSOs might also occur prior to reaching the WWTPs, resulting from blockages in the sewer network, during dry weather conditions (US EPA, 2004). Draude et al., (2019) defined blockages as "any obstruction in the sewer that has resulted in a reportable service failure that impacts customers or the environment". Dry weather can cause increase in settled debris in the sewer network due to the reduced hydraulic flow. When such a dry spell is followed by a rainy event, the debris gets accumulated within the network resulting in blockages. During wet weather, the increased flowrate carries the debris through the network or build up until it restricts the flow, resulting in flooding from SSOs (Draude et al., 2019).

2.2.1.2. Storm sewers

A storm sewer or storm drain collects surface water (they are not designed to carry wastewater) from rain, melted snow etc. and channel it to streams, rivers, coastal waters, estuaries, and other water bodies. By draining and diverting the excess stormwater and runoff collected from impervious surfaces such as paved roads, parking lots, footpaths, roofs etc., these storm sewer systems help prevent flooding. However, the surface runoff from impervious surfaces might carry pollutants which without treatment can impact the water quality of the natural water bodies. Nevertheless, these systems help minimize the problem of inflow and infiltration in sanitary sewers during wet weather events.

2.2.1.3. Combined sewerage systems

CSSs are sewer infrastructure designed to collect both wastewater (from its sources) and stormwater (from surface runoff), for transfer to a WWTP for treatment. CSSs functions differently in dry and wet weather conditions (Figure 2.1). On a day marked by heavy

intensity precipitation event, these systems may not have the capacity to cope with the total amount of incoming wastewater and stormwater. During such an event the systems can discharge excess flows to rivers and streams and other receiving water bodies without the wastewater undergoing any kind of treatment. Hence combined sewer overflows (CSOs) can happen during times of precipitation events.

This deviation of excess flows to the receiving waters acts like a relief valve that prevents wastewater backing up in the system that could cause flooding, health issues and system failure and blockages (Irish Water, 2015). This system becomes a problem when overflows happen too frequently, or if the receiving waters are negatively impacted by such overflows (Irish Water, 2015).

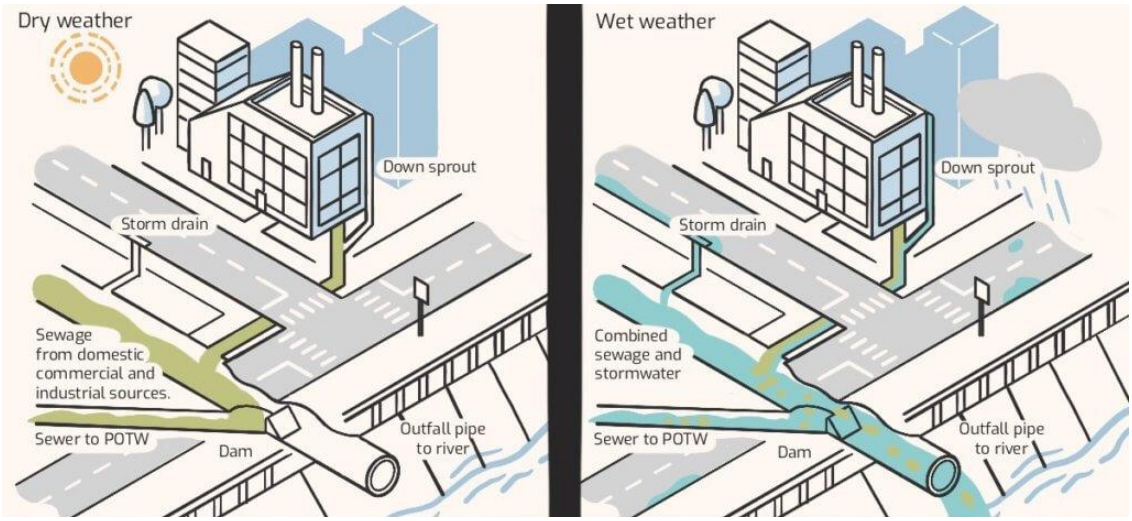

Figure 2.1: Operation of combined sewerage collection system under dry and wet weather conditions, starting from collection to transfer to publicly owned treatment works (POTW) (Source: Thompson, 2020)

On the contrary, prolonged dry periods also lead to blockages in the sewer network affecting the operation of the wastewater systems (Draude et al., 2019). Drought periods also reduce the base flow of the streams and the rivers where effluent is discharged (Zouboulis and Tolkou, 2015). As a result, when a consecutive number of dry days are followed by the first flush of wet weather events, the solid waste settled upstream from the CSO, gets carried away due to the rain and can be a significant source of pollution to the receiving water (McDonnell et al., 2014). Figure 2.2 gives examples of how very wet or prolonged dry periods can impact wastewater treatment infrastructure.

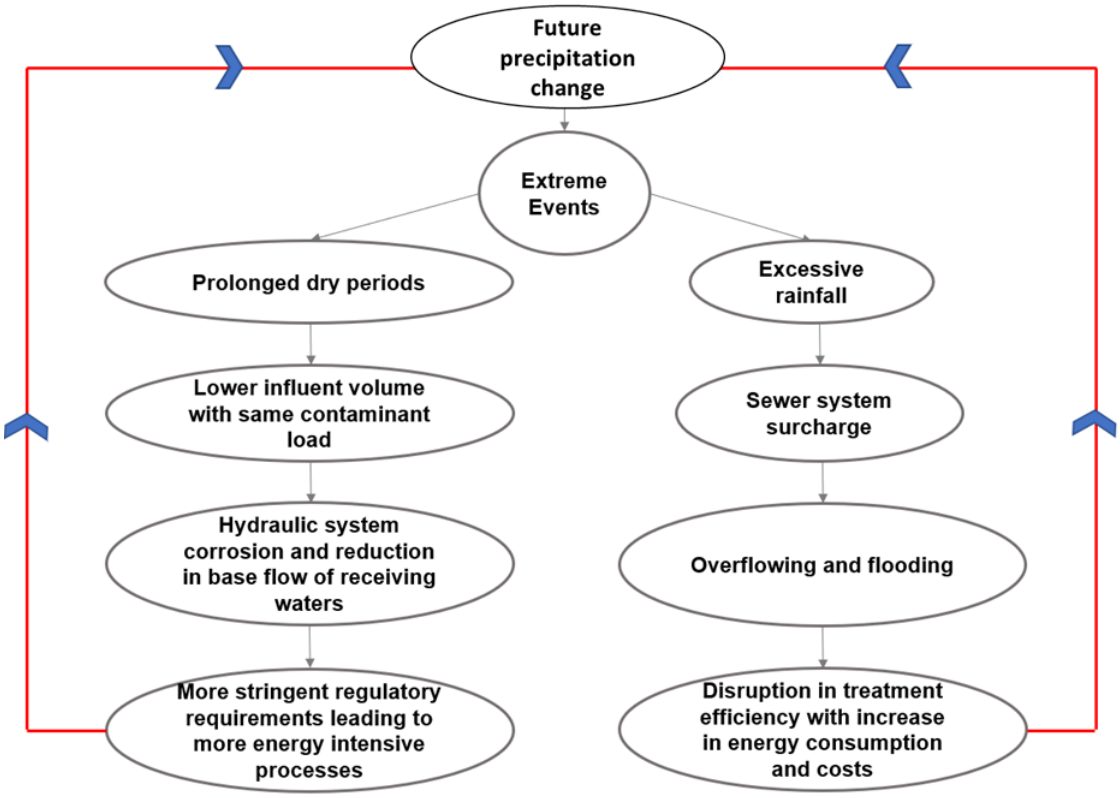

Figure 2.2: Loop showing the relationships between extreme events impacts on wastewater systems

2.2.2. Global wastewater treatment and sustainable wastewater management

Depending on the contaminant load, regulatory requirements, level of infrastructure and investment, the treatment of wastewater comprises some or all of the following stages: preliminary treatment, primary treatment, secondary treatment, floc formation, final settlement, tertiary treatment, nutrient removal and quality control[1], after which, it is finally being released into the environment. A recent study by Jones et al., (2021) estimated that only 52% of the amount of wastewater produced globally are treated (Figure 2.3). They also stated that the collection and treatment rates were highest in western Europe and lowest in South Asia and sub-Saharan Africa. High-income countries treat 70% of the wastewater generated on average (WWAP, 2017). In case of upper and lower middle-income countries, the figure drops to 38% and 28% respectively, whereas in low-income countries, only 8% receive treatment of any kind (WWAP, 2017). Thus,

[1] https://www.water.ie/help/wastewater/treatment/ (Accessed in Feb 2022)

significant volumes of wastewater continue to be discharged to the environment with little or no treatment.

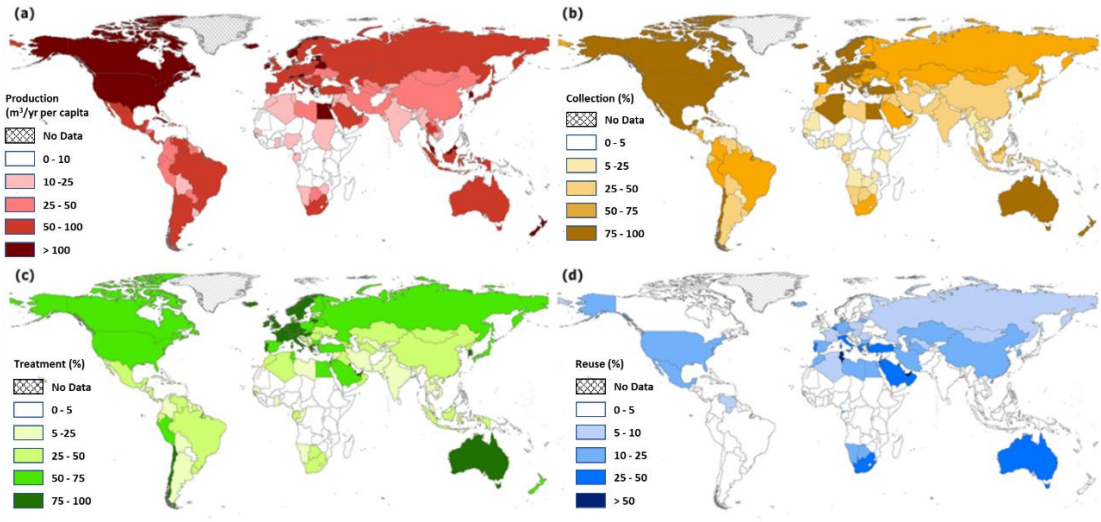

Figure 2.3: Country scale world map depicting a) wastewater production (m^3/year/capita); b) percentage of wastewater collected; c) percentage of wastewater treated and d) percentage of wastewater reused (Jones et al., 2021).

The United Nations (UN) General Assembly adopted an agenda called the Sustainable Development Goals (SDGs) in 2015 with an aim to end poverty, protect the environment and ensure prosperity to all by 2030 (UNESCO, 2017). It is crucial to identify the potential synergies between the UNSDGs and sustainable wastewater management to ensure the protection of the natural environment. Sustainable wastewater management contributes towards 7 out of 17 UNSDGS: Goal 3 – Good health and well-being, Goal 6 – Clean water and sanitation, Goal 8 – Decent work and economic growth, Goal 11 – Sustainable cities and communities, Goal 13 – Climate action, Goal 14 – Life below water and Goal 15 – Life on land (UNESCO, 2017). Therefore, sustainable wastewater management will help achieve water and sanitation services for all, promote good health and well-being, thereby preventing diseases, reducing WWTP operation failures and treatment costs. Building resilient wastewater infrastructure will contribute towards economic growth by preventing losses, help in safeguarding the agglomerations from climate change hazards (floods and droughts), mitigate greenhouse gas (GHG) emissions, and protect the aquatic and terrestrial ecosystem.

2.2.3. Wastewater treatment in Ireland

In Ireland, Irish Water is the national water utility that provides water and wastewater services in the country. There are approximately 1000 WWTPs and collection systems serving around 3.3 million people in Ireland (Irish Water, 2015). Irish Water ensures the maintenance and operation of wastewater treatment facilities and is responsible for the planning and adaptation of wastewater infrastructure in future. The Environmental Protection Agency (EPA) of Ireland is the environmental regulator of Irish Water which sets emission limits of wastewater discharges post treatment to be released back into the environment, to safeguard the aquatic ecosystem of the receiving waters and public health (EPA, 2021). The Commission for Regulation of Utilities (CRU) of Ireland, on the other hand, is the financial regulator of Irish Water as it regulates the revenue and charges of water and wastewater services such that these facilities are provided at a reasonable cost to the public[2]. It also cooperates with EPA in regulating the environmental discharges.

2.2.3.1. Legislation in Ireland

The Water Framework Directive (2000/60/EC) is the European Union (EU) directive adopted in 2000 that requires all the member states to protect and improve water quality in all waters to achieve good ecological status by 2015, or latest by 2027[3]. It was implemented in Ireland by the European Communities (Water Policy) Regulations 2003. Ireland follows the UWWTD (EU, 1991) which states that, for all discharges from agglomerations with greater than 10,000 population equivalents (PE), collection and secondary treatment processes are mandatory (Morgan et al., 2017). The same treatment processes are also required for discharges to fresh waters and estuaries from agglomerations with greater than 2000 PE (Morgan et al., 2017). Morgan et al., (2017) stated that for agglomerations with less than 2000 PE, appropriate treatment should be provided to wastewater entering collection systems for discharges to fresh waters and estuaries. The authors also reported that the Directive requires appropriate treatment for discharges to coastal waters for agglomerations with less than 10,000 PE. For all agglomerations with WWTPs of hydraulic treatment capacity greater than 10,000 PE., tertiary treatment must be provided for discharges to sensitive areas (Morgan et al., 2017).

[2] https://www.cru.ie/professional/water-2/ (Accessed in Feb 2022)
[3] https://www.gov.ie/en/publication/f7c76-water-framework-directive/#what-the-eu-water-framework-directive-wfd-is (Accessed in Oct 2022)

Pre-authorisation of all urban wastewater discharges, along with monitoring and reporting of the performance of the WWTPs and the water quality of the receiving water bodies are also required as per the Directive.

2.2.3.2. Wastewater collection network in Ireland

The majority of the urban areas in Ireland are connected to combined sewerage collection systems (Morgan et al., 2017). Irish Water policy is, where possible, manage pollution related to CSOs resulting from occurrence of a heavy precipitation event, by diverting the first flush from going into the environment (Irish Water, 2022)[4]. An impact assessment of CSOs in Ireland under the Water Framework Directive concluded that the cumulative annual spill volumes were in the order of 5-10% of the total annual combined flows (Camp Dresser & McKee, 2009). In order to address the problem of CSO spills, improving the sewerage collection systems need to be prioritised to prevent such spills to occur again in future. According to the recent 2021 report by EPA Ireland, there still exists seven collection systems in Ireland that requires an upgrade. It is therefore crucial to understand the influent volume response characteristics of WWTPs and the factors that potentially affect these systems, to prevent hydraulic overloading leading to operation and system failures.

2.3. Factors impacting sewerage systems and WWTP operations

There are several drivers influencing the maintenance and operations of WWTPs and their associated sewerage systems. Climate variables such as precipitation and temperature, population, human behaviour, urbanisation etc. are some of the variables that have been studied to understand their impacts on the hydraulic performance of WWTPs and sewerage systems (Astaraie-Imani et al., 2012; Butler et al., 2007; Gooré Bi et al., 2015; Hussain et al., 2022; Kleidorfer et al., 2009; Langeveld et al., 2013; Mohammed et al., 2021; Shakeri et al., 2021; Teklehaimanot et al., 2015; Zhou et al., 2019). Among all these factors, precipitation (current and future) and urbanisation are considered as the most influential factors that challenge the operation of WWTPs and their associate sewerage systems (Li et al., 2018; Zhou et al., 2019). Studies carried out to analyse the impacts of precipitation and urbanisation on the hydraulic performance of

[4] https://www.water.ie/conservation/business/business-conservation-tips/construction/ (Accessed in Sep 2022)

WWTPs and sewerage systems have mainly focused on 1) wastewater quantity, as measured by peak flows, CSO frequency, volume discharge, storage capacity, events of flooding and sewer system blockage etc. and 2) wastewater quality, i.e., the wastewater contaminant concentrations which eventually impact the receiving waters. However, there are still key gaps in understanding how wastewater influent volumes are impacted by precipitation and may be in the future by climate change and urbanisation. As influent volumes approach the design capacity of the WWTP, its response to these variables is crucial, particularly as many WWTP operational decisions are based on the influent wastewater entering the WWTP. In addition to this, location-specific variables such as WWTPs located near coasts or rivers may also be impacted by saltwater intrusion, or infiltration during peak flows of high rainfall combined with high tidal level (Irish Water, 2015).

This sub-section presents a detailed discussion on the impact of precipitation and related hydrological parameters on wastewater treatment infrastructure (and storm water infrastructure where relevant). Discussions related to climate change and urbanisation are presented in Sections 2.4 and 2.5 respectively.

2.3.1. Quantitative assessment of precipitation impacts on wastewater treatment systems

Unlike variables such as peak flow, CSO volume or frequency, effluent volume etc., that define the performance of the wastewater sewerage systems, influent volume, i.e., the total amount of wastewater that finally arrives at the WWTP inlet, defines the WWTP functions. Peak flows might not take into account any leakage in or out of the WWTP, if the measuring meter is placed after the leaking point in the sewer system. Hence peak flows do not represent the impact on WWTP operations. Any change in the peak flow after it is recorded, is thereby taken into account by the influent volume parameter. Since influent volume is the amount of untreated wastewater ready for the treatment process, it will impact all the other processes in the WWTP. Moreover, the pattern of influent and effluent volume on a daily basis on a normal weather day can be disturbed during storm events, when the amount of influent volume can differ from the amount of wastewater effluent volume. In such cases, the amount of wastewater influent going into a WWTP is regulated by reserving the excess amount in storage tanks, which changes the amount of wastewater coming out of the WWTP as shown in Figure 2.4.

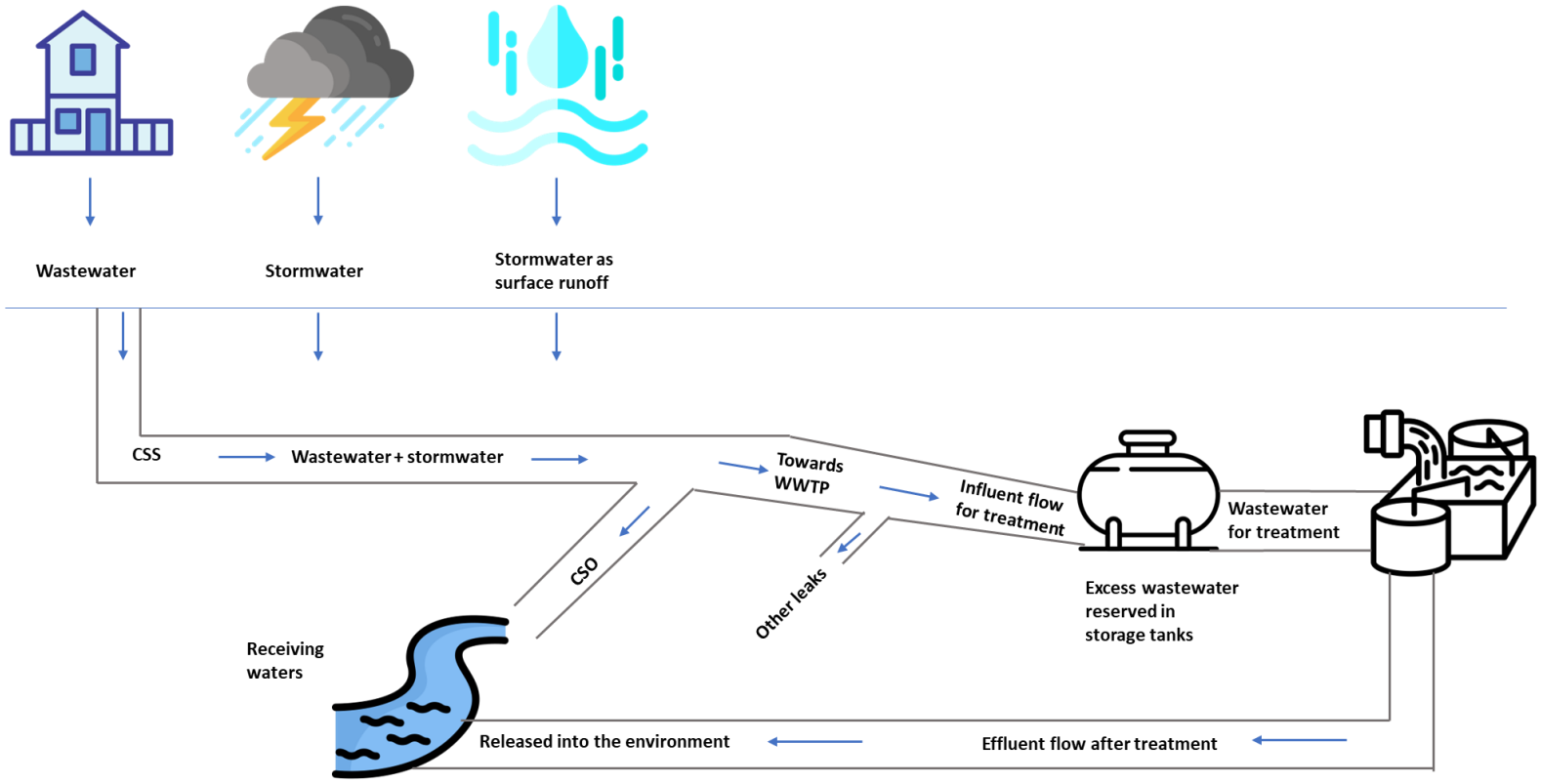

Figure 2.4: A schematic of the different characteristics of CSO, influent and effluent flows

On a subsequent day, when the wastewater influent volume is manageable, the amount stored in the storage tanks are treated and released into the environment, making the amount of effluent volume higher than the influent volume. Due to this difference in the influent wastewater volume and the effluent wastewater quantity (which is frequently studied), studies investigating influent volume will provide a different perspective when trying to achieve a better understanding of WWTP functions and operations under different weather conditions. However, such studies are few in number, which might be due to the limitations of the approaches used. For example, key limiting factors can include the issue of availability of real data from WWTPs (Langeveld et al., 2013; Li et al., 2018) and unavailability of long-term observed data of CSO events required to design efficient CSO control measures (Fortier & Mailhot, 2015; Schroeder et al., 2011).

2.3.1.1. Assessment of precipitation impacts on hydraulic characteristics of the sewer system

Generally, when monitored observational datasets of wastewater systems are unavailable, studies have adopted software-based hydraulic models to generate simulated data of sewer systems. The most commonly used model is the Storm Water Management Model (SWMM) developed by the United States Environmental Protection Agency. This is an open-source free software used in the design, planning and analysis of data related to stormwater runoff, combined and sanitary sewers and other drainage systems (US, EPA, 2022)[5]. SWMM allows for hydraulic and water quality simulation while accounting for hydrologic processes. There are other such models like the MIKE MOUSE (MOdel of Urban SEwers) water modelling software by Danish Hydraulic Institute that models the sewer hydraulics.

Gooré Bi et al., (2015) carried out an impact assessment of a number of precipitation variables such as rainfall intensity and duration on volume discharge and peak CSO flowrate between May and October 2013, in a CSS in Longueuil, Canada. They observed that 8 rainfall events during this period led to CSOs which they used to calibrate a PCSWMM, which is a personal computer version of SWMM. It was found that high intensity events could be more accurately modelled than longer duration or low intensity

[5] https://www.epa.gov/water-research/storm-water-management-model-swmm (Accessed in Sep 2022)

events. The drawback associated with this model as pointed out by the authors was it performed relatively poorly in modelling events marked with low intensity rainfall that could potentially lead to concentrated discharges in the receiving waters. Another study of a CSS by Hlodversdottir et al., (2015) assessed the flood hazard in the CSS network. They used the MIKE MOUSE software package to model the runoff and sewer flows in the combined or stormwater pipes by using historical 10-minute intervals precipitation data (1998 – 2008) as inputs. Domestic wastewater was negligible during high rainfall days and hence was not considered by the authors. Flood hazard was assessed in terms of the sum of the number of flooded manholes and the number of manholes with water level 1 m below ground. The model output suggested that 3% of the public network manholes were vulnerable to flooding during short-term high rainfall events.

Model-based approaches are usually carried out when physical characteristics of the sewer networks are available but day-to-day operational data or data at sub-daily levels are unavailable. Hence, a majority of the research using hydraulic modelling techniques use limited observational data for calibrating the model or validating model outputs (Gooré Bi et al., 2015; Hussain et al., 2022; Kleidorfer et al., 2009; Schroeder et al., 2011; Semadeni-Davies et al., 2008; Zhou et al., 2019). These studies focus on the hydraulic characteristics of the sewer network rather than WWTPs itself. Moreover, model-based analyses have a major drawback as they can only take into account the processes that are incorporated into the models and hence the outputs may not be useful in making more general observations (Langeveld et al., 2013).

Research that uses real data are restricted to studying CSO characteristics such as volume and frequency of CSOs. With a limited set (2 years) of CSO discharge data of the Berlin CSS and rainfall data, Schroeder et al., (2011) demonstrated the efficiency of CSO control measures in four catchments. The authors developed a methodology that enables the prediction of CSO occurrences from rainfall data based on 2 years of CSO volume discharge data. From the CSO data, a subset was used to determine the rainfall depth threshold value which led to CSOs of a given probability. This was followed by validating the identified rainfall depth with the remaining subset of the CSO data which in turn enabled long term modelling of the responses of CSSs to changing precipitation. As stated by the authors, this method is applicable when long-term rainfall records are available but the CSO discharge data is limited. Mailhot et al., (2015) leveraged the

previous study to develop a rainfall threshold-based model to forecast the occurrence of CSOs using observed rainfall and CSO datasets. They carried out an accuracy assessment of the threshold model to assess whether the forecast was statistically significant using the Odds Ratio Skill Score and found that this threshold model could significantly forecast the CSO frequency.

The common thread between these studies is the focus on the sewer system performance rather than the WWTPs. Such studies can help in assessing sewer system performance, but do not give us outputs associated with the changing influent volume characteristics, that can be used to assess the impacts on WWTPs itself. The subsequent section reviews the research that has been carried out to assess the precipitation impacts on influent volume at the inlet of the WWTPs.

2.3.1.2. Assessment of precipitation impacts on WWTP influent volume characteristics

As previously discussed, it is important to understand the characteristics of influent wastewater to ensure the smooth functioning of WWTPs under various weather conditions (wet and dry). If influent wastewater can be correctly managed and designed, it will be a significant part of ensuring efficient WWTP operation and in avoiding all the subsequent problems associated with non-compliance of effluent standards (Giokas et al., 2002) or occurrence CSOs or spills. Furthermore, it is necessary to understand both current influent characteristics and also those that might occur throughout the WWTP design life cycle. Across all types of collection networks, but particularly CSSs, influent volumes (the key characteristic of focus in this study) are significantly impacted by precipitation.

Langeveld et al., (2013) investigated the impacts of a specific precipitation event in 2007, characterised by a 38-day long dry event followed by an intense storm event in Eindhoven, Netherlands. The prolonged dry period showed typical dry weather flow values which decreased over the 6 weeks due to decrease in the extraneous flows into the sewer system. The storm event following the dry period had a precipitation amount of 33 mm. They found that the dry spell resulted in deposition of debris in the culverts through which the discharge arrives at the WWTP. Due to this reason, during the hours of the storm event, no large wet weather flows were arriving at the WWTP. However, the

authors observed a sudden increase of flows in the influent chamber after the storm event. They explained this phenomenon by stating that, as the culverts were blocked during the storm event, by switching to a spare culvert, the WWTP pumping station could have emptied the sewer system after the storm ended. This resulted in the delayed response of increase in influent flows. The authors also suggested that the blockage caused a CSO further upstream of the sewer system to discharge for a longer duration of time, thereby increasing the spill volume. Li et al., (2018) assessed the relationship between monthly precipitation and monthly influent volume in one WWTP over a 3-year period and found a strong linear relationship between the two parameters. However, this linear relationship ceased to exist beyond the total monthly precipitation value of 193.2 mm, where monthly inflow rate became stagnant. This indicates that the sewer system surpassed its full capacity beyond 193.2 mm and occurrence of CSOs were implied as demonstrated by the unchanged monthly influent volume. Another study by Mines et al., (2007) carried out linear regression for 24 WWTPs over a single year to asses the impact of rainfall on WWTP influent flows. When all the WWTPs were analysed together, weak correlations were found between average monthly influent volume and average monthly precipitation. Hence, in order to derive more generic and meaningful trends, the authors pooled subsets of WWTPs of similar size and characteristics to investigate the relationship between average monthly influent volume and average monthly precipitation. This resulted in moderate to strong correlations between these variables for each subset of similar WWTPs. However, the authors did not consider more independent precipitation variables to explain influent volume nor propose a model that could be used across all the 24 WWTPs of varying sizes. Moreover, daily relationships between precipitation and influent volumes were not explored that could provide more insights into the probability of exceedance of influent volumes that could potentially lead to CSOs under various precipitation intensities.

Thus, Li et al., (2018) focused on a single case-study, (Langeveld et al., 2013) focused on a single storm event and (Mines et al., 2007) studied several WWTPs over one year. Consequently, there is a gap in relation to studying several WWTPs, of varying size across a number of years, to try and identify broader trends in relation to precipitation and influent wastewater.

2.3.2. Quantitative assessment of tidal and river level impacts on wastewater treatment systems

In the context of tidal level impacts on urban wastewater, drainage and storm water infrastructure, the focus, to date, has been urban flooding (Lian et al., 2013; Tang et al., 2017; Williams et al., 2016; Yin et al., 2011). Other research analyses the impacts of inflow and infiltration on the operations of coastal wastewater infrastructure or impacts of flooding from storm events and high tides on coastal sewer networks (Cahoon & Hanke, 2017, 2019; Flood & Cahoon, 2011).

Flood & Cahoon, (2011) studied the impacts of tidal level individually and with precipitation on daily flows to four central wastewater treatment systems. They found that infiltration of elevated groundwater, influenced by heavy precipitation or variation in tidal levels, significantly contributed towards increased influent volumes. Cahoon & Hanke, (2019) studied the impacts of rainfall, sea level and temperature on 19 wastewater collection systems in the coastal regions of North Carolina. These parameters were found to be significant drivers of inflow and infiltration into the collection systems. When analysed separately, it was found that the flows (consisting of inflow and infiltration) of 95% of the 19 WWTPs in coastal North Carolina, studied over a period of two years, were significantly impacted by tidal levels.

Although tidal level is found to be a significant contributor to flows into wastewater collection systems, studies investigating impacts on influent volumes, particularly for CSSs are limited to the best knowledge of the author. Moreover, catchments with tidal rivers might also influence wastewater collection systems. While there have been studies to understand the effect of wastewater effluent on river water quality (Bo, 2014; Colson et al., 2019; Mascher et al., 2017; River et al., 2016; Ryu et al., 2014) or impacts of precipitation extreme events leading to variability in streamflow (Coffey et al., 2016; Kiely, 1999; Murphy and Charlton, 2006). There has been no study to date, to the best knowledge of the author, which analyses the impacts of river levels on WWTP influent volumes. With climate change expected to impact sea and river levels (Coffey et al., 2016; Vousdoukas et al., 2017), analysing the effects of these hydrological parameters on the wastewater influent volumes and consequently, on the operations of WWTPs is necessary and is an important gap in ensuring wastewater infrastructure can respond to

these challenges. Other studies carried out to evaluate the impacts of precipitation and tidal levels on WWTPs and their associate sewerage systems are presented in Table 2.1.

Table 2.1: Research studying the impacts of precipitation variables and tidal level on WWTPs and their associate sewerage systems

References	Objective	Key features and outcomes of study
Studies based on precipitation and tidal levels (using observed datasets)		
(Draude et al., 2019)	Analysis of sewer blockages as an effect of dry weather days	Statistical techniques used to demonstrate the relationships between rainfall, number of dry days and consecutive number of dry days on sewer blockage. The study found that consecutive preceding dry days is more likely to influence sewer blockages as compared to rainfall or number of dry days.
(Mohammed et al., 2021)	Modelling the performance of a sanitary sewer system under precipitation events of different return periods	Performance of the sanitary sewer before and after stormwater leakage event was assessed using an SWMM. Model calibration was performed using observed leaked surface runoff data and dry weather flow. Model validation was carried out using another single event based observed data. Model was found to have good fit with a correlation coefficient of 0.86 between observed and modelled data. When return period increased, the precipitation intensity increase resulting in stormwater leakage during wet weather

		days. The study found that the system operated well during dry weather days.
(Peleg et al., 2016)	Understanding the influence of climate variability and spatial rainfall variability, jointly and individually on the response of a calibrated hydrodynamic urban drainage model	This study used a stochastic high resolution rainfall generator to simulate many realizations of rainfall accounting for both climate (temporal variability over 30 years) and spatial rainfall variability. The generated rainfall data was incorporated into a calibrated SWMM to simulate surface runoff and channel flow for a small urban catchment. Peak flows at three different locations in the sewer network for different return periods of 5 to 15 years was also assessed. It was found that the variation in flow was significantly impacted by variation in climate. The effect of the spatial rainfall variability on flow extremes depended on the return period, with a greater contribution observed for events of high return periods. The results indicated the importance of studying both spatial and temporal variation in flows.
(Cahoon & Hanke, 2017)	Impact assessment of rainfall induced inflow and infiltration in coastal wastewater treatment systems	Investigated the influence of inflow and infiltration arising due to rainfall events or sea level rise that might lead to sanitary system overflows was studied with a focus on coastal WWTPs. Regression analysis of system flow responses to

		rainfall was carried out. Rainfall effects were found to be statistically significant.
(Lian et al., 2013)	Analysis of combined impacts of rainfall and tidal level on flooding in a coastal city with a complex river network	Flood severity and flood probability was studied under a range of precipitation intensities of different return periods and tidal level were assessed using a hydrodynamic model. It was found that the greatest threat to flooding was from heavy rainfall. However, tidal level was found to increase the risk of flood severity and flood frequency, if ignore, could lead to underestimation of the flood risk.

2.4. Climate change

Climate is defined as the observed patterns of average weather of a particular location over a time period in terms of mean and variability of climate variables such as precipitation, temperature, wind etc. (Intergovernmental Panel on Climate Change (IPCC), 2014 a). The time period referred to in terms of climate is generally decades or longer. Climate change, on the other hand, is the alterations in the state of climate, i.e., the change in the statistical mean or variability of a particular variable, analysed and detected by statistical tests (IPCC, 2014 a). The United Nations Framework Convention on Climate Change (UNFCCC) distinguishes the causes of climate change into two categories: i) due to natural internal processes and ii) due to external forcing such as volcanic eruptions or persistent anthropogenic activities contributing towards changing atmospheric composition. Anthropogenic activity is a broader term that includes deforestation, forest fragmentation, agriculture, land use change, burning of fossil fuels, urbanisation, vehicular emission, industrial uses, to name a few, that contribute to greenhouse gas (GHG) emissions (Mahmoud et al., 2018). Natural events like volcanic eruptions, solar activity, variations in the oceanic and atmospheric circulation also lead to climate change. However, the effects of natural causes are much smaller in comparison to the effects of increase in greenhouse gases due to human activities (IPCC, 2022).

A major consequence of human-induced climate change is the increasing frequency of extreme events such as heat waves, drought, large storms, floods etc. (US EPA, 2022)[6]. It is now accepted that a changing climate will lead to changes in the frequency, intensity, spatial extent, duration, and timing of extreme weather and climate events (IPCC, 2022). Such events will have severe implications on both natural resources and man-made assets and infrastructure (IPCC, 2014 b; 2022).

Infrastructure that is designed in the present with the purpose of serving many years down the line are likely to experience the effects of climate change 30 to 50 years from now (Meyer et al., 2012). Dawson et al., (2018) reported that $2.5 trillion a year is invested on infrastructure which are typically designed to last long (at least decades). During this time, changing climate may alter the performance and operation of such services. In the

[6] https://www.epa.gov/climate-indicators/weather-climate#:~:text=Scientific%20studies%20indicate%20that%20extreme,storms%2C%20floods%2C%20and%20droughts. (Accessed in Sep 2022)

context of wastewater infrastructure, with climate change, extreme weather events such as floods and droughts will decrease the efficiency and increase the costs of treatment processes in WWTPs (Reznik et al., 2020). Kirchhoff & Watson (2019), revealed that a majority of wastewater managers are implementing changes in the wastewater networks to build in climate-resilience based on the historical storm events rather than future climate change analyses. Therefore, there is a high probability that these infrastructures will continue to experience impacts of climate variability in the future. Research studying the climate extremes and its impacts on the wastewater systems in various parts of the world is discussed in Section 2.4.3.

2.4.1. Future climate scenarios and projections

Weather and climate vary spatially and temporally. As changes in climate at a regional scale might impact climate change at the global scale and vice-versa, an understanding of this interaction between regional and global climate change is important in order to set effective global climate policy targets and designing scenarios (Tebaldi et al., 2015). Such climate scenarios are designed on the basis of GHG emissions which determine the atmospheric composition. The IPCC has found a parameter to measure the amount of GHG emission in terms of Radiative Forcing. Radiative forcing is the net change in the energy (irradiance) balance of the earth system caused by external influence across a temporal range, usually represented as the value due to changes between pre-industrial times and present-day (Huang et al., 2013). It is a quantitative measure widely implemented by scientists and researchers that provides the basis of comparison of potential climate response characteristics to various external drivers.

Quantifying radiative forcing from GHG emissions needs to take into account a number of factors such as population growth, technological and economic development etc. which renders the prediction of changes in future climate patterns difficult to achieve (Santoso et al., 2008). That is why, different scenarios are developed which aid in the process of identifying possible impact of climate change. These future climate conditions are developed by the IPCC in the form of trajectories or pathways of radiative forcing levels or CO_2-equivalent concentrations. These pathways are called the Representative Concentration Pathways or RCPs. These RCPs are also termed as climate scenarios that depict the various emission possibilities in future.

According to the IPCC's 5th Assessment Report (AR5), 2014, there are four RCPs that depict the range of possible impacts based on GHG emissions (Figure 2.5). These scenarios do not take into account the possible changes in natural forcings. These four scenarios are: i) RCP 2.6 or the stringent/ low emission pathway that limits CO_2 emissions and requires it to start declining by 2020 to zero at the end of the century, ii) RCP 4.5 is the intermediate pathway with no climate policies adopted, and represents the peak in CO_2 emissions around 2040 followed by a decline, iii) RCP 6.0 which shows CO_2 emissions peak around 2080 followed by a decline and iv) RCP 8.5 which is the high emission or the worst-case scenario depicts an increase in CO_2 emissions through the century until 2100[7]. The annual GHG emission pathways are included in AR5 (Figure 2.6).

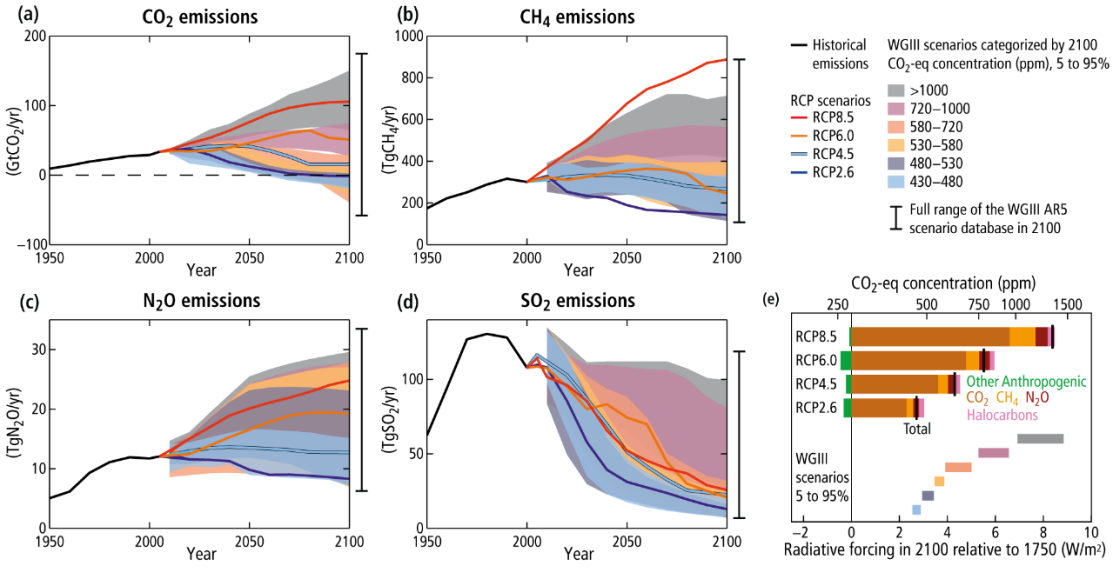

Figure 2.5: The four RCPs based on different greenhouse gas emissions (IPCC AR5 Synthesis Report, 2014 c)

[7] https://en.wikipedia.org/wiki/Representative_Concentration_Pathway (Accessed in Jan 2019)

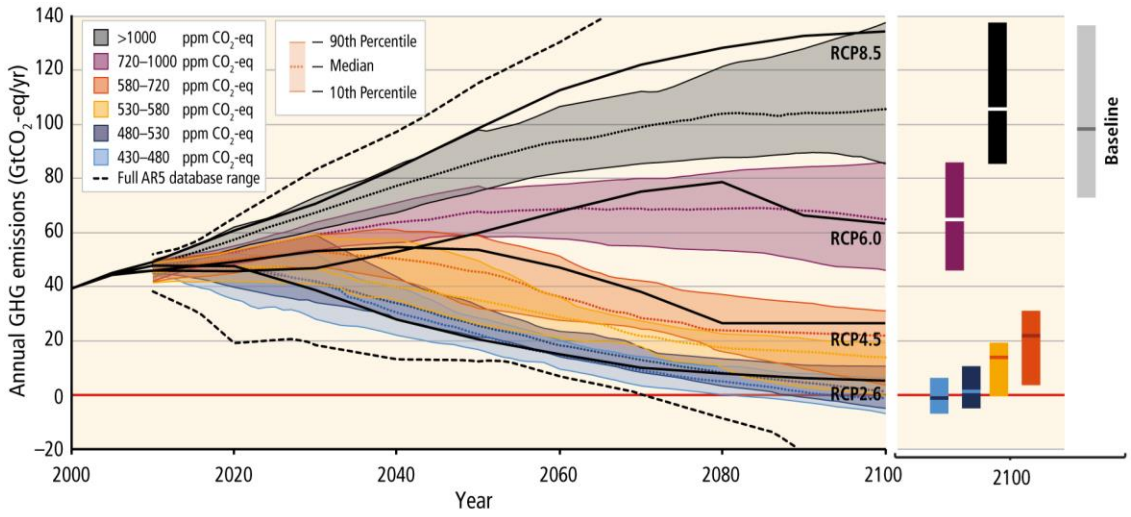

Figure 2.6: Annual GHG emission pathways 2000 - 2100 (IPCC AR5 Synthesis Report, 2014 c).

The IPCC in their 6th Assessment Report, has introduced the latest climate scenarios, as a set of 9 emission and concentration scenarios. These scenarios are built on a range of radiative forcings and five shared socio-economic pathways (SSPs) (IPCC, 2021 a; 2021 b). The SSPs are different socio-economic storylines developed on the basis of population, urbanisation, human and technological development etc. that describe a range of potential future worlds (IPCC, 2021 a). This new set of scenarios, referred to as SSPX-Y, where X represents the socio-economic pathways 1 – 5 and Y refers to the radiative forcings 1.9, 2.6, 3.4, 4.5, 6.0, 7.0 and 8.5 provides a wider range of future worlds as compared to RCPs (Table 2.2) and thus, fill some gaps.

Table 2.2: Description of the SSPX-Y Scenarios and comparison to RCPs (Source: IPCC, 2021 a)

SSPX-Y Scenario	Description From an Emissions/Concentrations Perspective	Closest RCP Scenarios
SSP1-1.9	Implies net-zero CO_2 emissions around the middle of the century.	Not available. No equivalently low RCP scenario exists.
SSP1-2.6	Implies net-zero CO_2 emissions in the second half of the century.	RCP 2.6, although RCP 2.6 might be cooler for the same model settings.
SSP4-3.4	A scenario between SSP1-2.6 and SSP2-4.5 in terms of end-of-century radiative forcing.	3.4 level of end-of-century radiative forcing was not available in the RCPs. Nominally SSP4-3.4 sits between RCP 2.6 and RCP 4.5, although SSP4-3.4 might be more similar to RCP 4.5. Also, in the early decades of the 21st century, SSP4-3.4 is close to RCP 6.0, which featured lower radiative forcing than RCP 4.5 in those decades.
SSP2-4.5	Scenario approximately in line with the upper end of aggregate nationally determined contribution (NDCs) emissions levels by 2030 [NDCs are each country's target to reduce emissions to adapt to climate change]. CO_2 emissions remaining around current levels until the middle of the century. New or updated NDCs by the end	RCP 4.5 and, until 2050, also RCP 6.0. Forcing in the latter was even lower than RCP 4.5 in the early decades of the 21st century.

	of 2020 did not significantly change the emissions projections up to 2030, although more countries adopted 2050 net-zero targets in line with SSP1-1.9 or SSP1-2.6. The SSP2-4.5 scenario deviates mildly from a 'no-additional-climate-policy' reference scenario.	
SSP4-6.0	The end-of-century nominal radiative forcing level of 6.0 W m^{-2} can be considered a 'no-additional-climate-policy' reference scenario, under SSP1 and SSP4 socio-economic development narratives.	RCP 6.0 is nominally closest in the second half of the century.
SSP3-7.0	An intermediate-to-high reference scenario resulting from no additional climate policy under the SSP3 socio-economic development narrative. CO_2 emissions roughly double from current levels by 2100. SSP3-7.0 has particularly high non-CO_2 emissions, including high aerosols emissions.	Between RCP 6.0 and RCP 8.5, although SSP3-7.0 non-CO_2 emissions and aerosols are higher than in any of the RCPs.
SSP3-7.0-lowNTCF	A variation of the intermediate-to-high reference scenario SSP3-7.0 but with mitigation of CH_4 and/or short-lived species such as black carbon and other short-lived climate forcers (SLCF). Variants of SSP3-7.0-	SSP3-7.0-lowNTCF is between RCP 6.0 and RCP 8.5, as RCP scenarios generally incorporated a narrow and comparatively low level of SLCF emissions across the range of RCPs.

	lowNTCF differ in terms of whether CH_4 emissions are reduced.	
SSP5-3.4-OS (Overshoot)	A mitigation-focused variant of SSP5-8.5 that initially follows unconstrained emissions growth in a fossil fuel-intensive setting until 2040 and then implements the largest net negative CO_2 emissions of all SSP scenarios in the second half of 21st century to reach SSP1-2.6 forcing levels in the 22nd century.	Not available. Initially, until 2040, similar to RCP 8.5.
SSP5-8.5	A high-reference scenario with no additional climate policy. CO2 emissions roughly double from current levels by 2050. Emissions levels as high as SSP5-8.5 are not obtained under any of the SSPs other than the fossil-fuelled SSP5 socio-economic development pathway.	RCP 8.5, although CO_2 emissions under SSP5-8.5 are higher towards the end of the century. CH4 emissions under SSP5-8.5 are lower than under RCP 8.5. When used with the same model settings, SSP5-8.5 may result in slightly higher temperatures than RCP 8.5

2.4.2. Climate models

Climate models are developed using mathematical equations that helps in simulating weather patterns in future or in the past. They are used to identify and estimate future climate projections (simulations) of various parameters like precipitation, temperature etc based on climate scenarios. Generally, various models and scenarios are used to generate a range of projections that provide alternatives to the policymakers in order to map their activities. All models represent real-world phenomena but always have an associated error between the observed and the predicted values. Different climate models provide a range of representations of the Earth's response to the different forcings as mentioned above. It also takes into account the natural variability of climate (IPCC, 2013). The IPCC uses the results of a representative climate model project called the Coupled Model Intercomparison Project (CMIP) in the assessment reports (Ohba, 2021). This project was initiated by the World Organization Research Program in 1995. The latest CMIP is the CMIP Phase 6 which aims to fill the scientific gaps remaining in the previous CMIP, i.e., the CMIP Phase 5 which were incorporated into the IPCC AR5. CMIP6 considers the socio-economic conditions by linking the SSPs to RCPs (Table 2.2), thereby enhancing the robustness of the projections (Zhang & Ayyub, 2021).

Each CMIP project involves different scientific modelling groups across the world to provide General Circulation Models (GCMs). GCMs are models that yield large-scale simulations representing the physical, atmospheric, and oceanic processes of Earth. However, they are restricted to coarser resolutions due to computational constraints. Although CMIP 6 is the most up-to-date climate model project, GCM projections from CMIP 6 are still in the process of becoming available. Hence, Shakeri et al., (2021) stated that the GCMs from CMIP 5 are considered the most reliable and current climate model which included simulations at a coarse resolution for assessment in the IPCC's AR5. However, precipitation effects vary spatially, depending on local topography, and cannot be captured in such coarse resolution simulations. Hence, such large-scale projections are not suitable for analysis and planning at local levels (Peng et al., 2023). Estimating climate change projections at finer regional or local scales, requires that global large scale simulations are downscaled using high-resolution Regional Climate Models (RCMs), which take into account the finer level local conditions (Nolan and Flanagan, 2020). As all models, RCMs also have model errors that flow from the GCMs in the process of

downscaling the observations. However, one advantage of RCMs in addition to better representation of local climate effects is that they produce improved simulations with relatively small spatial and temporal character (Nolan and Flanagan, 2020). Downscaled RCM simulations from CMIP 6 GCMs are still not widely available yet (Peng et al., 2023).

In relation to WWTPs , these climate model projections of high spatial and temporal resolution under various scenarios can be used to model key parameters such as influent volume, effluent characteristics etc., analysing future performance of wastewater infrastructure under future climate scenarios (Arnbjerg-Nielsen, 2012). The following section details the work done in investigating the future change in precipitation induced by climate change and its impacts on WWTPs and their associated sewerage systems.

2.4.3. Impacts of precipitation change on wastewater systems in future – state-of-the- art

There have been several studies (Abdellatif et al., 2014; Arnbjerg-Nielsen, 2012; Butler et al., 2007; Gooré Bi et al., 2015; Hlodversdottir et al., 2015; Jung et al., 2015; Kleidorfer et al., 2009; Semadeni-Davies et al., 2008; Shakeri et al., 2021; Willems, 2013; Zhou et al., 2019) that have used model projections of GCMs and RCMs to establish that increased intensity of precipitation is a primary driver that will influence the design and operation of WWTPs and their associated sewer systems. These studies have used different approaches depending on the use of climate projections (GCMs or RCMs), and the parameter that is modelled such as peak flow, hydrologic runoff, storage capacity of the sewer network, CSO frequency etc. These are characteristics that can be used to measure the performance of sewer network. Each approach is described below using example case studies.

Zhou et al., (2019) investigated the effects induced by climate change on hydrological runoff and urban flood volumes in northern China to emphasize the importance of drainage adaptation and planning. They used projections from five GCMs from the CMIP5 archive under RCP 2.6 and RCP 8.5 climate scenarios. A change factor methodology was applied to these raw projections with large uncertainties to obtain more confidence in the projected changes. Change factor methodology is commonly used in climate change impact studies where the difference between future and baseline GCM or

RCM simulations, termed as the climate change factor, is estimated, which is then applied to the raw projections (Zhou et al., 2019). The climate change factors are the projected changes which (Zhou et al., 2019) stated to have more confidence on, as compared to the absolute values of the projections. The authors then used the resulting projections from the change factor methodology in the SWMM to understand the hydraulic response characteristics of sewer systems to climate change. They observed that under future climate scenarios, the ratio of total flood volume (overflows from overloading manholes) to surface runoff volume, increases with increase in rainfall intensities. Moreover, they also concluded that total flood volume increases in the future for all return periods from 1 to 100 years, with higher increases for heavier precipitation events. On the other hand, Butler et al., (2007) studied the impacts of climate change on storage tanks of sewer networks in North London, UK, which are generally used to limit overflows into the environment. Using the climate predictions for UK derived from the Hadley Centre's Europe RCM, under IPCC medium-high emission scenario, the authors generated a long-term synthetic rainfall time series and predicted that under future rainfall conditions, a 35% increase in storm events was observed that could lead to 57% increase in the requirement of storage tank capacity.

CSO characteristics (volume discharge and peak flow) under current and future climate was studied by Gooré Bi et al., (2015) using observed overflow events in 2013 in a combined sewer system in Canada, leading from a 20% increase in rainfall intensity of 8 observed rainfall events. They based their research on the projections of the Canadian Regional Climate Model that suggests an increase in extreme precipitation events by 2050. Using the SWMM model, they found a 15% – 500% increase in volume discharge and a 13% – 148% increase in peak flow in 2050 as compared to the 2013 period. Fortier & Mailhot (2015) conducted a study considering 30 CSO outfalls in southern Quebec for 3 years for the period of May to October. They estimated the rainfall threshold at which CSOs might occur based on the methodology adopted by Schroeder et al., (2011) (described in Section 2.3.1.1) and used the Canadian RCM to estimate the change in CSO frequency in future. The authors found that on a monthly basis, CSOs are expected to be more frequent in future for the months of May and October but decrease in the summer months of July and August. These methodologies featured the use of limited event-based rainfall data and focused on CSO characteristics. The model applied to simulate some of

the quantitative variables does not incorporate the process descriptions representing the dynamics observed in monitoring data.

With respect to wastewater volumes, a recent study by (Shakeri et al., 2021) assessed the potential impact of the change in climate variables on the change in wastewater production in Tehran. The authors used climate projections from CMIP5 models downscaled using a Statistical DownScaling Model (SDSM), and finally forecasted wastewater production volume under RCPs 2.6, 4.5 and 8.5 using Multi-Layer Perceptron Network and Fuzzy model. However, as wastewater networks in Tehran feature separate storm and wastewater sewerage systems, the research found temperature, relative humidity, sunshine hours, and population as significant variables of wastewater volumes rather than precipitation.

While the importance of studying wastewater influent volumes in WWTP design and operation has been recognised (discussed in Section 2.3.1), as has the influence of climate change on (future change in precipitation variables and extreme events) on wastewater systems (Reznik et al., 2020), to date, no study has investigated how changes in climate (and in particular precipitation) will impact influent wastewater volumes in the coming decades. Thus there are gaps in knowledge as to the robustness of WWTPs in meeting future climate-related challenges. Table 2.3 presents a literature review of various studies based on the impacts of future precipitation change on WWTPs and their associate sewerage systems.

Table 2.3: Research studying the impacts of climate change on WWTPs and their associate sewerage systems

References	Objective	Key features and outcomes of study
Studies based on impacts of future precipitation change		
(Berggren et al., 2012)	Analysis of the hydraulic performance of urban drainage systems based on precipitation changes induced by climate change	Two hydraulic parameters were studied: water levels in nodes (represented by the number of floods and frequency and duration of floods) and pipe flow ratio. It was found that the number of flooded nodes, geographical distribution of floods, flooding frequency and flood duration will increase in the future. The pipe flow ratio was found to improve the understanding of system capacity while delineating critical areas when presented graphically.
(Kirchhoff & Watson 2019)	Assessment of how wastewater managers are adapting the wastewater infrastructure to climate change	Surveys and interviews were carried out to understand the methods and techniques of wastewater managers to adapt to climate change. 78% of WW managers were found to making changes to the design of wastewater infrastructure as per the storms that they experienced in the past instead of considering future climate change impacts.

(Arnbjerg-Nielsen, 2012)	Quantitative analysis of the climate change impacts on precipitation which is used for hydrologic design	These studies are all centered around climate change impacts on the design parameters of urban drainage systems based on the rainfall characteristics. Use of historical rainfall data RCM projections. Results suggest change in the design intensities and storage facilities in future reflecting increase in both the design parameters, implying the change in the response of the urban drainage systems in future as compared to current period.
(Willems, 2013)	Revision of urban drainage system design based on climate change impacts on precipitation	
(Arnbjerg-Nielsen et al., 2013)	Review of climate change impacts on rainfall extremes and urban drainage systems	Both these studies are reviews of the methods involving the climate change impacts on precipitation intensity and precipitation extremes that can eventually impact the urban drainage systems.
(Willems et al., 2012)	Impact assessment of climate change on urban rainfall extremes and urban drainage	
(Jung et al., 2015)	Analysis of the effects of climate change on runoff in an urban drainage system	Linear regression analysis was carried out for observed rainfall data of different duration (1 hour, 24 hours and 10 minutes) to analyse the trend and extrapolate future climate change scenarios. Design rainfall intensity and peak discharge of the urban drainage basin were calculated using a calibrated SWMM to evaluate the effect of the variation in rainfall events on increased runoff.

		Statistically significant upward trends were observed for 1 hour and 24 hours rainfall duration. However, the steepest slope was observed for the shortest rainfall duration, although it was nearly significant at 90% level of confidence. Simulated peak discharge increased with increase in the short duration rainfall intensity.
(Gooré Bi et al., 2017)	Review of downscaled data for climate change impact studies in urban areas	Trends and approaches to study climate change impacts with a focus on urban drainage systems are reviewed.
(P. Nolan et al., 2017)	Climate change impacts on rainfall by mid-century in Ireland using RCM ensemble approach	Detailed the precipitation projection in Ireland by mid-century. Precipitation amounts showed significant projected decrease as opposed to extreme events such as heavy precipitation events and extended dry periods which showed significant projected increase.
(Hughes et al., 2021)	Analysis of impacts and implications of climate change on wastewater systems	Impacts such as spill and odour nuisance leading to flooding, water quality deterioration due to uncontrolled discharges and damage to infrastructure were shown as direct climate-related impacts. Long-term implications of these impacts were demonstrated.

In addition to precipitation variables, changes in land use land cover (LULC) due to urban development can increase the amount of impermeable surfaces in agglomerations. This combined with increasing populations can also overburden existing WWTPs (Kleidorfer et al., 2009; Semadeni-Davies et al., 2008), particularly WWTPs with CSSs, making such infrastructure vulnerable to the variable nature of influent wastewater volume (Marlow et al., 2013; Willuweit and O'Sullivan, 2013). Therefore, it is important to analyse how changing LULC may impact the design and operation of urban wastewater infrastructure.

2.5. Land use land cover

Land use is a description based solely on the human activity or function of an area of land (US EPA, 2021)[8] and refers to the purpose that the land serves. Examples of land use types include agricultural, residential industrial, transport, commercial etc. Land cover refers to the physical and biological characteristics that cover the earth's surface (US EPA, 2021). It describes the type of land being used and is captured in the distribution of forest, grassland, open water, marsh land, agriculture, developed/ built-up / urban land (impervious), barren land etc. Land cover changes can result from anthropogenic activities, though such changes do not necessarily imply degradation of land. The land use land cover (LULC) pattern of a region is an outcome of natural and socio-economic factors and their changes in time and space (Rimal, 2011).

Of particular concern are urban areas, where half of the world's population live (Ritchie and Roser, 2020) (Figure 2.7). Urbanisation is a complex and heterogeneous process involving various factors such as population growth of urban areas, economic development, migration of people from rural to urban areas, spatial rearrangement, and adaptation of settlements, landuse land cover (LULC) change etc.[9]

[8] https://www.epa.gov/report-environment/land-use (Accessed in Dec 2021
[9] https://www.conserve-energy-future.com/urbanization-and-urban-growth.php (Accessed in Sep 2022)

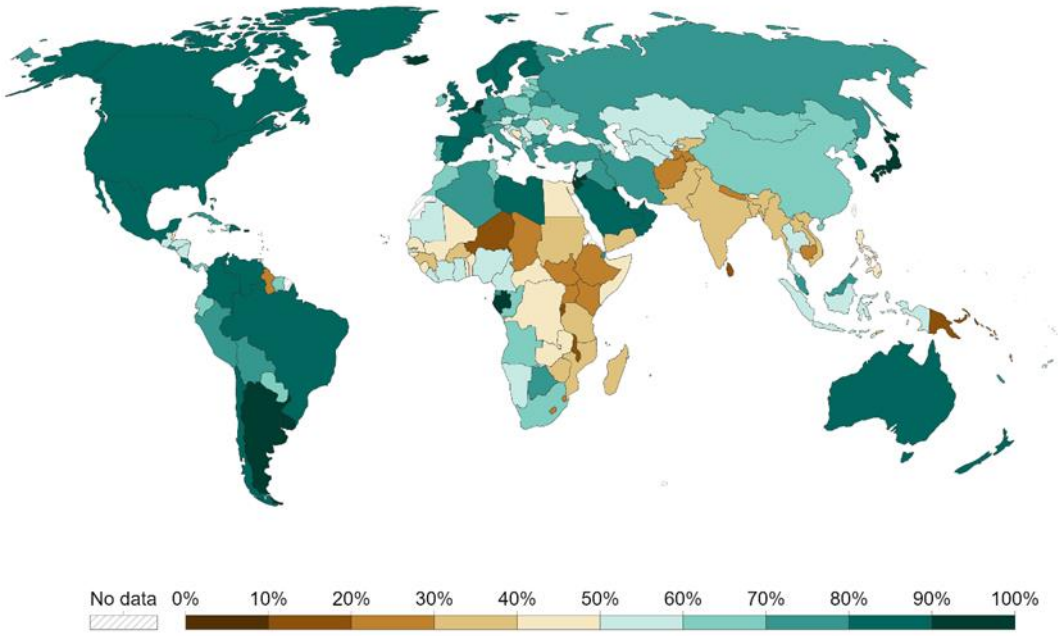

Figure 2.7: World map showing proportion people living in urban areas, Source: UN Population Division (via World Bank, 2022)

These factors are intricately linked with one another, and hence multifaceted, as economic growth leads to migration of people, leading to population growth. Population growth inherently brings about changes in the LULC (Shukla et al., 2018) as human activities and economic growth are also observed to follow an upward trend (Mushtaq & Lala, 2017). Urbanisation also refers to a change in landuse type and is defined as the "development of modern urban infrastructure and public service facilities that cater to the changing economic and social circumstances of the working population such as changes in their thinking patterns, lifestyle, behaviour etc." (Chaolin, 2020). As of 2021, approximately 57% of the world population live in urban areas. In case of Ireland, 64% of the population live in urban areas[10] (World Bank, 2022). In the past decade (2011 – 2021), the urbanisation has increased by 2.2%.

2.5.1. Monitoring LULC change using Remote Sensing and GIS

Remote Sensing (RS) is the process of acquiring information of an area of interest from a distance, by monitoring its physical characteristics measured by its reflected and

[10] https://data.worldbank.org/indicator/SP.URB.TOTL.IN.ZS?locations=IE (Accessed in June 2022)

emitted radiation, thereby detecting any kind of dynamic phenomenon happening on the surface of the Earth (Read & Torrado, 2009). RS is most commonly used to map landuse land cover changes because of its efficiency in collecting multi-temporal, multi-spectral, and multi-location data (Saraswat et al., 2016). Geographical Information System (GIS) is a "spatial system that creates, manages, analyses, and maps all types of data. It helps users understand patterns, relationships, and geographical context" (Environmental Systems Research Institute[11]). It enables users to identify problems, monitor them and manage and respond to such events. Integration of GIS and RS are fundamental for monitoring LULC change and are extremely useful for future planning. The core principles of RS are presented in the following section to underpin the methodology used in this thesis to estimate LULC change (Chapter 6).

2.5.1.1. Electromagnetic Radiation

Electromagnetic (EM) radiation spans over a broad spectrum from very long radio waves to very short gamma rays (Butcher, et al., 2016) as shown in Figure 2.8. The portion of the spectrum visible to our eye is a narrow range between 380 – 700 nanometres. These ranges of different wavelengths are also called spectral bands.

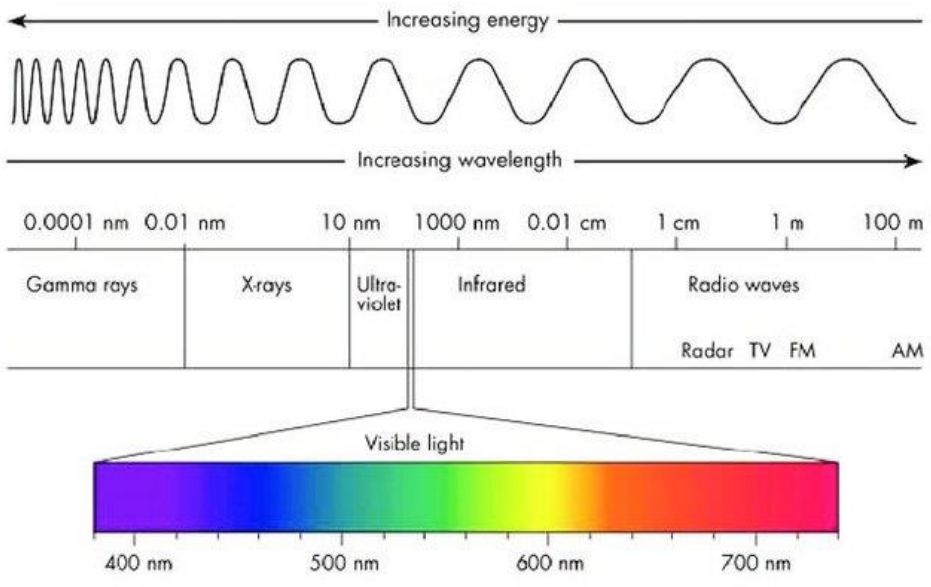

Figure 2.8: Electromagnetic spectrum – the spectral range of different wavelengths (Szantoi, 2013)

[11] https://www.esri.com/en-us/what-is-gis/overview (Accessed in Aug 2022)

Some of this energy is reflected back into the atmosphere where it is then scattered, due to interactions with particles in the air, before reaching a remote sensor (Figure 2.9). Clouds can also cause colours to appear faint and hazy because the EM radiation we see is mostly scattered light. It is therefore important in RS to use images with little to no cloud cover so that visual and digital image interpretation is easier as colours are brighter and surface features are clearer. Visible radiation can readily pass through the atmosphere and microwaves can even transmit through clouds making them the best wavelength to undergo remote sensing.

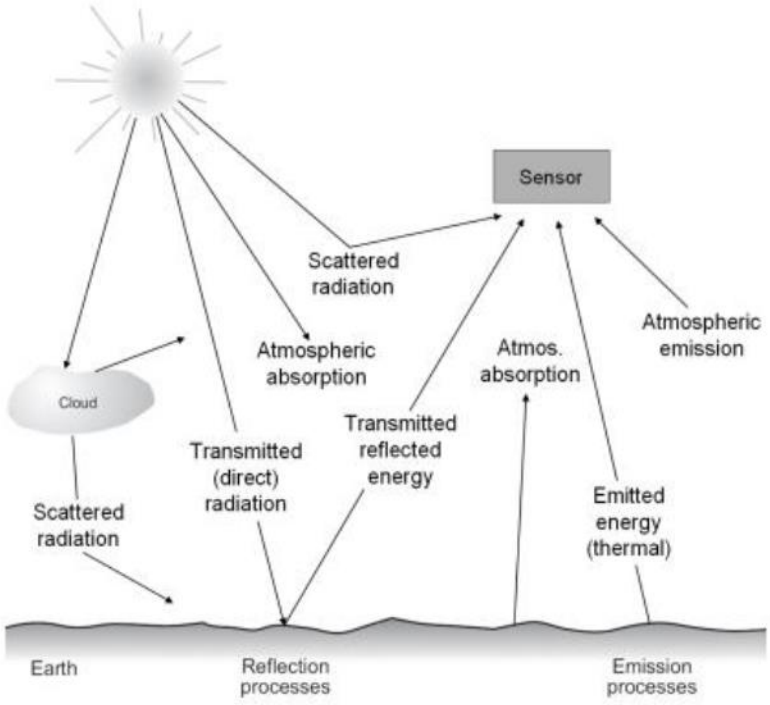

Figure 2.9: Energy interactions in the atmosphere (Bakker et al., 2000)

2.5.1.2. Spectral Reflectance

The radiation emitted by an object is normally perceived as the object colour by humans. For example, healthy vegetation is perceived as green in colour because plants absorb the red and blue incident light for photosynthesis and reflect the green light (DeRiggi, 2017). However, vegetation has the highest reflectance in near-infrared (NIR) wavelength (Figure 2.10). Thus, the reflectance of different land cover type depends on the wavelength of the electromagnetic spectrum. When this reflectance or spectral response of an object is represented graphically, over the range of electromagnetic spectrum, characterised by the different wavelengths, it is called spectral reflectance curve or

spectral signature. Spectral signatures can be a strong tool to interpret remotely sensed images.

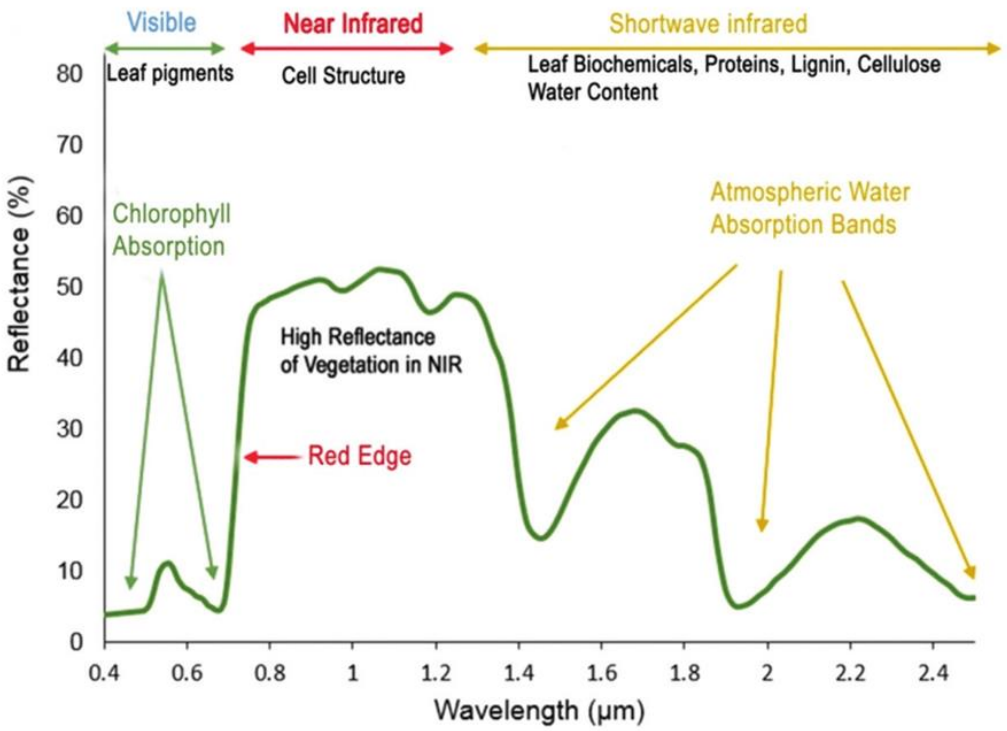

Figure 2.10: Spectral signature of vegetation (Roman and Ursu, 2016)

2.5.1.3. Band combinations and satellite images

In terms of mapping, there are two primary colour models used to visualise satellite images and these are i) the red-green-blue (RGB) colour model or the additive colour model, and ii) the subtractive colour model. The RGB colour model is based on the theory that a very broad range of visible colours can be seen by mixing the three primary colours red, green and blue. The RGB colour model is used for screen displays such as when remote sensing technology is accessed through computer graphics applications. In contrast, the subtractive colour model is when the primary colours are subtracted from white light to get yellow, magenta or cyan. This model is used for device outputs such as printed hardcopies of photos.

The RGB colour model can be used in different ways of spectral band combinations, called colour schemes, in order to achieve composite images based on the visual requirements of the user. True colour composite scheme is when the red, green and blue visible spectral bands of the image is aligned with the red, green and blue input channels

of a monitor. The resulting composite image is perceived in the same way as it occurs naturally on ground. For example, vegetation in true colour composite image would appear as green pixels as it would appear normally on ground. On the contrary, false colour composite (FCC) scheme is when the red, blue and green values of the image do not align with the true red, green, blue planes of the monitor (input channel). This method of using band combinations is very beneficial in visualizing wavelengths that are not detected by human eye. For example, as per the spectral signature of vegetation (Figure 2.11), since high reflectance value is observed in NIR band (wavelength), a user whose study focuses on detecting vegetation would ideally select the NIR band to highlight vegetation. Therefore, to ensure efficient interpretation of vegetation, the NIR, red and green bands are aligned with the red, green and blue planes of the monitor respectively. An example of a typical FCC is shown in Figure 2.11.

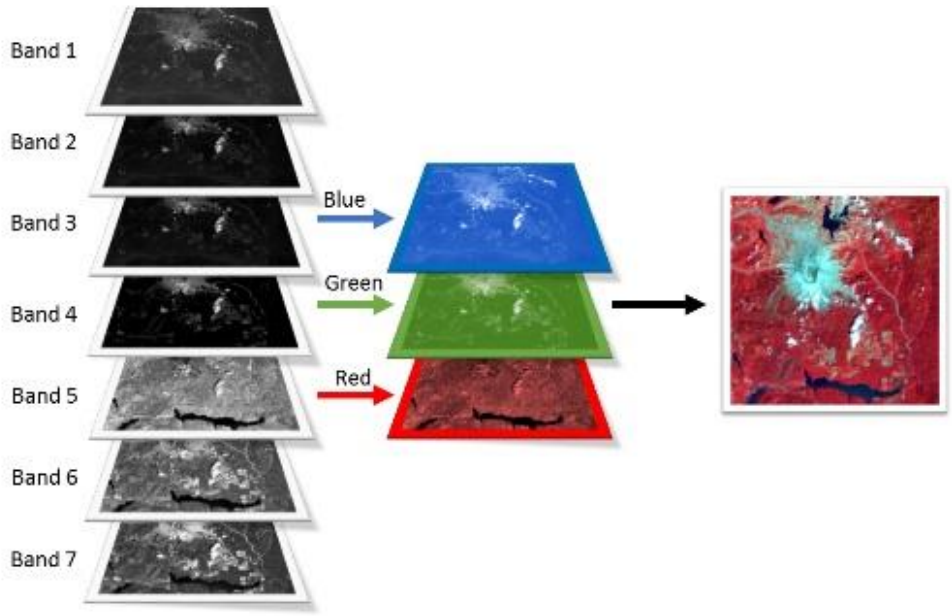

Figure 2.11: A typical FCC band combination for LANDSAT 8 for better visualization[12]

Different satellite images are characterised by a range of spectral bands. The researcher selects the satellite image and band combinations depending on factors such as their research interest, data availability, spatial resolution required etc. The Landsat satellite is one of the most robust satellites initiated by the joint program of National Aeronautics

[12] https://gsp.humboldt.edu/olm/Courses/GSP_216/lessons/composites.html (Accessed in Sep 2022)

Space Administration (NASA) and the United States Geological Survey (USGS). This satellite has been continuously orbiting the earth since 1972 (Google Earth Engine Data Catalog, 2020). Landsat captures satellite images of the entire earth at 30 m spatial resolution in the form of scenes or tiles, with each scene covering 180 X 185 km^2 (Roy et al., 2014), approximately once every two weeks. Landsat data is freely available, making it a unique resource for researchers working in agriculture, forestry, regional planning, mapping, education and global change research. Two such Landsat satellites are Landsat 5 and Landsat 8. Landsat 5 satellite of the Landsat program, launched in 1984 is the "Longest Operating Earth Observation Satellite" which was decommissioned in 2013[13] (USGS, 2022). Landsat 5 carried two sensors the Multispectral Scanner (MSS) and the Thematic Mapper (TM). While the MSS sensor consisted of four spectral bands: Visible green (0.5 – 0.6 µm), visible red (0.6 – 07 µm), NIR 1 (0.7 – 0.8 µm) and NIR 2 (0.8 – 1.1 µm), the TM sensor consisted of 7 bands (Table 2.4).

[13] https://www.usgs.gov/landsat-missions/landsat-5 (Accessed in Sep 2022)

Table 2.4: Landsat 5 bands

Bands	Description	Resolution	Wavelength
B1	Blue	30 m	0.45-0.52 µm
B2	Green	30 m	0.52-0.60 µm
B3	Red	30 m	0.63-0.69 µm
B4	Near infrared	30 m	0.77-0.90 µm
B5	Shortwave infrared 1	30 m	1.55-1.75 µm
B6	Thermal	30 m (While originally collected with a resolution of 120 m / pixel (60 m / pixel for Landsat 7), this band has been resampled using cubic convolution to 30 m)	10.40-12.50 µm
B7	Shortwave infrared 2		2.08-2.35 µm

Landsat 8 was launched in 2013 and is the first Landsat satellite of the 21st century. It consists of two sensor instruments, the Operational Land Imager (Band 1 to Band 9) and the Thermal Infrared sensor (Bands 10 and 11)[14] (Table 2.5).

[14] https://www.usgs.gov/landsat-missions/landsat-8 (Accessed in Sep 2022)

Table 2.5: LANDSAT 8 bands

Bands	Description	Resolution	Wavelength
B1	Coastal aerosol	30 m	0.43 - 0.45 μm
B2	Blue	30 m	0.45 - 0.51 μm
B3	Green	30 m	0.53 - 0.59 μm
B4	Red	30 m	0.64 - 0.67 μm
B5	Near infrared	30 m	0.85 - 0.88 μm
B6	Shortwave infrared 1	30 m	1.57 - 1.65 μm
B7	Shortwave infrared 2	30 m	2.11 - 2.29 μm
B8	Panchromatic	15 m	0.52 - 0.90 μm
B9	Cirrus	15 m	1.36 - 1.38 μm
B10	Thermal infrared 1, resampled from 100 m to 30 m	30 m	10.60 - 11.19 μm
B11	Thermal infrared 2, resampled from 100 m to 30 m	30 m	11.50 - 12.51 μm

2.5.2. Digital image classification of remotely sensed data

In order to convert band information of these satellite images into usable data that could be easily interpreted, digital image processing techniques are applied. These involve various procedures such as correcting data (e.g. correction for atmospheric conditions), digital enhancement for better visual interpretation (e.g. cloud masking), automated image classification etc. Following such corrections, digital image classification classifies and labels groups of pixels on a satellite image based on common features. These homogeneous collections of pixels or features are called feature classes. In the context of LULC classification, the different feature classes are characterised by different reflectance values of the pixels, perceived as different colours (whether in true or false colour composite) and represent the different LULC types. There are three different image classification techniques, and the background of each technique is provided in the sub-sections below.

2.5.2.1. Unsupervised classification

Unsupervised classification is used when the user does not possess specific (to the research interest) knowledge on the study area. For unsupervised classification, clustering algorithms are used to automatically identify and define a number of "clusters". The number of clusters generated depends on the user requirements. Fewer clusters lead to reduced variability implying more resemblance of pixels within groups as opposed to higher number of clusters.[15] Clustering algorithms are then used to group pixels into clusters based on their properties without the help of predefined class labels. The user then manually assigns feature classes (LULC class) to each cluster. Unsupervised classification may sometimes be preferred over supervised if the user requires a classified image quickly and with minimum effort. However, it is not well suited to applications where fine details are necessary in the resulting classified image.

2.5.2.2. Supervised classification

In the case of supervised classification approach, the user defines the feature classes in the satellite image based on the pixel reflectance. Hence, the selection of classes is 'supervised' by the operator. A representative training sample (or training set) is selected for each LULC class. The number of training sets needed for an accurate classification result depend on the classification algorithm being used, the number and distinctiveness of classes, the homogeneity of the image and the image signal to noise ratio (SNR). All the spectral information (bands, pixel reflectance values) of the training samples is stored in a file called "signature file". The final step is to use a classification algorithm to run classification based on the signature file. Although supervised classification is a longer process, it allows the user to be more specific about the definitions of the labels. Results produced by this method are therefore generally more accurate as the input data is well known.

2.5.2.3. Object-based classification

Unlike unsupervised and supervised classification which are pixel-based, object-based image classification segments an image by creating groups of pixels. These groups of pixels are called objects which are characterised by different geometries. These objects

[15] https://gisgeography.com/image-classification-techniques-remote-sensing/ (Accessed in Sep 2022)

can be classified based on their shapes, texture and spectral information. Therefore, object-based classification can be performed using very high-resolution images to distinguish between the different shapes and textures to create objects.

2.5.2.4. Validation of results

Classification of satellite images is always accompanied by a degree of error which might occur inherently during capturing the image or by the user while carrying out the process of LULC classification. Therefore, in order to validate the classification results, accuracy assessment is carried out, which is one of the most important stages of classification to ensure optimum quality of classified image (Hasmadi et al., 2009). In this validation process, the classified images are validated against true world reference data such as aerial maps, raw satellite images etc. This is key for precise representation of on-ground geographical features.

Accuracy assessment is carried out by a sampling approach where a number of sample points are selected from the classified images to be compared with reference data. There are different sampling schemes that can be used to select the sampling points. The quantity of samples required must be considered before deciding on a sampling scheme. One of the most common sampling schemes is random sampling (Bakker et al., 2000). Once the satellite images are classified, GIS can be integrated into the analysis for further post-processing of the images based on the requirements of the user. Validation and post-processing of classified images are further discussed in Chapter 6.

2.5.2.5. Various platforms for image classification and GIS processing

There are several remote sensing and GIS platforms available to conduct integrated RS and GIS applications. Platforms such as ERDAS, ENVI, ArcGIS, QGIS, and R allow users to conduct digital image processing techniques such as image classification. While ERDAS, ENVI and ArcGIS are expensive licensed software, QGIS and R are open source platforms, which provide the capability to run classification algorithms. The selection of platform depends on the needs of the user (research area) and the type of classification the user would like to run.

One platform that has been used in recent years with regard to RS applications is the Google Earth Engine (GEE) platform developed by Google. GEE uses JavaScript

programming language to analyse RS datasets, which are of massive volumes of data. These datasets are often difficult to handle in common software packages and desktop computing resources (Amani et al., 2020). In addition to this, processes such as appropriate data identification, data fusion, data visualization and interpretation is also challenging. GEE effectively addresses all these challenges by being a prominent cloud-based remote sensing and geospatial data processing platform (Amani et al., 2020). In a paper involving review of 450 journal articles from 150 journals, Amani et al., (2020) stated that GEE provides free access to numerous RS datasets and is the most popular big geodata processing platform. They found that it is most extensively used for analysing Landsat and Sentinel (10 m satellite by European Union's Copernicus Programme) satellite images. Another review by Wang et al., (2021) found that GEE has become one of the emerging platforms for studying specifically urban land change science.

For geospatial workflows, software packages such as ArcGIS Pro, QGIS, MapInfo etc are some of the most common GIS applications. ArcGIS platform by Environmental Systems Research Institute (ESRI) is extensively used for any kind of GIS-based analysis as it offers a wide range (1500+) of geoprocessing tools across 35 toolboxes, allows integration with ArcGIS online (Mariushko et al., 2018), enables customisation of workflows and toolboxes through Model Builder (Stefanidinis et al., 2021) and most importantly, because of its user-friendliness (Wi et al., 2017). However, one of its disadvantages is that it is an expensive licensed software as mentioned above as opposed to QGIS.

2.5.3. Urbanisation and its impacts on wastewater systems – state-of-the-art

As land changes from pervious (e.g. open fields) to impervious (e.g. paved roads) surfaces, water from rainfall that previously soaked through the grass, forests, soil and bedrock, is no longer intercepted (Farjad et al., 2017; Loperfido et al., 2014) . As a result, large volumes of water (stormwater runoff) gets prevented from infiltrating into the sub-surface layers of soil and flows without any interruption to local water bodies which can lead to flooding (Saraswat et al., 2016; Zope et al., 2016) as shown in Figure 2.12. With rapid urbanisation and decline in green cover, substantial amounts of stormwater runoff is generated (Yao et al., 2016) which will eventually flow to the inlets of the WWTPs (in case of CSSs) and can cause significant challenges for wastewater systems (Astaraie-Imani et al., 2012; Willuweit and O'Sullivan, 2013).

Recent literature has focused on the impacts of urbanisation on surface runoff, and, in turn, the hydraulic performance of sewerage systems or storm drainage systems (Hussain et al., 2022; Kleidorfer et al., 2009; Loperfido et al., 2014; Miller et al., 2014; Paule-Mercado et al., 2017; Ravagnani et al., 2009; Semadeni-Davies et al., 2008; Yao et al., 2016; Zhou et al., 2019). Other studies have analysed the response of sewerage systems and stormwater-runoff to rainfall events by implementing stormwater Best Management Practices (BMPs). To date, research that has studied the impacts of LULC changes in agglomerations on influent wastewater volumes have not been found. However, some the aforementioned work is reviewed below as some of the lessons and outputs are of relevance to this research.

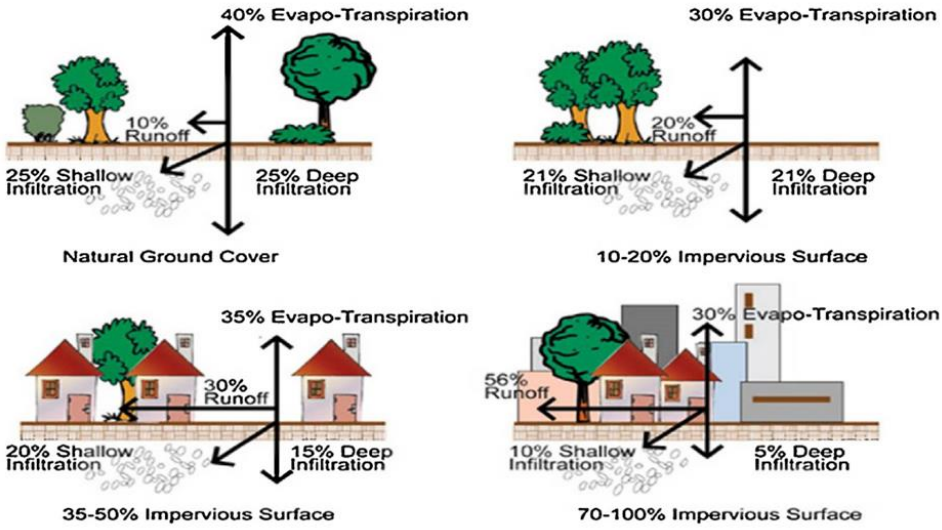

Figure 2.12: Change in runoff characteristics based on the degree of impervious surfaces present (Saraswat et al., 2016)

Yao et al., (2016) conducted a model-based analysis (SWMM) in a residential catchment in Beijing China. In this study they visually interpreted a satellite image of 0.6 m spatial resolution, in order to assess land cover. They also used GIS and field investigation to identify two parameters of imperviousness; (i) the whole fraction of the impervious area in a catchment, termed as total impervious area (TIA) and (ii) the part of TIA which is hydraulically connected to the drainage systems, known as directly connected impervious area (DCIA). They simulated three runoff metrics; total runoff depth, peak runoff depth and lag-time using the SWMM. Regression analyses were performed to understand the

relative impacts of the two impervious metrics on the runoff variables under various storm scenarios. Different storm conditions representing local characteristics were fed into the SWMM as input storms. The study found that lag-time was affected by DCIA to a greater extent than TIA which was found to be insignificant. With the increase in DCIA, lag-time reduced (R^2 value < 0.45), but this relationship weakened with increases in rainfall amount, rainfall peak ratio (ratio of the rainfall peak time to the total rainfall duration) and duration. On the other hand, it was found that TIA was a stronger contributor towards changing total runoff as compared to DCIA under various storm conditions. In terms of wastewater quantity, the added volume of stormwater runoff (contributed by impervious area and rainfall), in addition to the wastewater load that is generated, can result in hydraulic overloading in WWTPs with CSSs and lead to occurrence of CSOs.

In order to assess the impacts of urbanisation on the performance of CSSs for 250 virtual case studies, Kleidorfer et al., (2009) analysed two parameters as indicators of urbanisation: effective impervious fraction and dry weather flow. The virtual case-studies with varying system properties were generated using a case-study generator. A real-world case-study was also used for comparison. The authors simulated future scenarios of both parameters by implementing -60% to +60% changes from current conditions of the effective impervious fraction of the real-world case study. The authors reported that the area of impervious surfaces was a significant contributor to the percentage of runoff reaching the WWTP, when averaged over the simulation period of 10 years. While studying the comparative impacts of an increase in built-up areas and climate change, they found that a 20% increase in rainfall intensity had the same effect on the performance of the CSSs, as a 40% increase in impervious area. Semadeni-Davies et al., (2008) also investigated the relative effects of climate change and urbanisation on wastewater and stormwater flows in a WWTP connected by a CSS in Helsingborg, Sweden. The paper took into consideration inflows to the WWTP with respect to stormwater referred to as quick flows (impacted by the impervious areas) and sewer infiltration referred to as slow flows (contributed by permeable surfaces). The study considered the period 1994 – 2003 as the study period when 58% of the total annual inflow was wastewater, with the remaining being stormwater from inlets and sewer infiltration from groundwater. It was reported that during this period overflows occurred due to high intensity storm events. Using the Danish Hydrological Institute MOdel of

Urban Sewers (MOUSE) model, they simulated the CSS for the period 1994 – 2003 and for the period 2081 – 2090. For two climate change greenhouse gas (GHG) emission scenarios B2 (medium/low) and A2 (high) (IPCC Special Report on Emission Scenarios (SRES) Report, 2000), the change in present and future simulations at a monthly scale were applied to the existing rainfall series. Four urbanisation storylines were built based on the Swedish trends during the 1994 – 2003 period that represented city growth to urban renewal. These storylines were i) current situation with no change in the system but climate is changed, ii) increase in city size but no change in the sewerage system, iii) increase in city size but disconnection of 75% of the impervious areas to the CSS and iv) an ideal situation representing optimum management of the system. The highest impact on overflows was observed under the storyline characterised by city growth with no change in the drainage system and networks. Climate change exacerbated the effects on the CSS with or without city growth through increased wastewater inflows. The worst effect on the drainage system was demonstrated by city growth storyline in conjunction with A2 SRES scenario. From the findings of these studies, it can be concluded that strategies for adaptation of sewerage systems connected to WWTPs need to be taken to compensate for the dual effects of climate change and urbanization. Another case study by (Hussain et al., 2022) in Iraq carried out the comparison between the effects of climate change and urbanisation on stormwater sewer system using SWMM. They implemented a landuse change scenario where the surface area of the sub-catchment contributing to surface runoff (representing actual data in 2008) was doubled (resulting in a 58% increase in impervious area). It was found that the surface runoff volume and flooding volume also increased almost two-fold (Hussain et al., 2022). However, the authors found that the adverse impacts of climate change were higher than that of landuse change. The model was validated by comparing the maximum discharge in pipes predicted by SWMM with the observed data, which showed an R^2 value of 0.95.

Other aspects of sewer systems that might get affected due to amplified surface runoff are the response time properties of a catchment (e.g. peak time, i.e., the time between the start of the rainfall event and peak discharge and lag-time, defined in this paper as the time between the peak rainfall and peak discharge) (Tuohy et al., 2018) and discharge properties (e.g. peak flows) (Miller et al., 2014). Response time of a catchment is the time interval between a storm event and the response of a catchment in terms of achieving peak flows (peak time) or any other quantitative variable of interest. A study conducted

by Miller et al., (2014) aimed to investigate the response of stormwater runoff from two catchments of similar sizes in Swindon, UK, that transformed from rural to peri-urban areas. One of the catchments was highly urbanised and the other was a recently developed peri-urban area. The peri-urban catchment had two distinct areas of drainage where one consisted of both natural and built storm drainage pathways and the other comprised of only built storm drainage systems. Comparison of observed storm hydrographs demonstrated that the area served by storm drainage system was a stronger factor in determining stormwater runoff as compared to impervious area or development type. The authors used digitized historical topographic maps to map historical levels of urbanisation and impervious cover from the 1960s to 2010s. The results showed that the impervious area in the peri-urban catchment increased from 11% to 44% from 1960s to 2010s. Installation of a large-scale storm drainage network in the early 2000s resulted in the reduction of the characteristic flood duration by more than 50% and increase in peak flow by more than 400%. The runoff response to rainfall was contributed mainly by the type of drainage system (built storm drainage or natural) rather than the development type (urban or peri-urban). This was supported by the examples of the highly urbanised catchment and the part of the peri-urban catchment connected to the natural drainage system. Both these catchments that receive runoff from sub-surface pathways and storm drainage, had similar response to rainfall. However, the part of the peri-urban catchment connected to the built storm drainage that receive runoff solely from impervious area showed a rapid and flashy response to runoff.

From the above studies it can be concluded that, in the context of water and wastewater infrastructure services, ongoing urbanisation can potentially impact the response characteristics of the existing urban drainage systems (Zhou, 2014; Zhou et al., 2019) and urban water/ wastewater management systems (Astaraie-Imani et al., 2013; Farjad et al., 2017; Shukla et al., 2018). With increases in extreme precipitation events and in impermeable surfaces, wastewater flowrates (quantity), wastewater quality, entering the WWTPs, and response time, particularly for the WWTPs connected with CSSs, are affected, which eventually impacts the receiving waters. Remote sensing images can be very useful and precise in identifying changing patterns of urban land cover by estimating impervious surfaces to study peak discharge entering into storm sewer systems (Ravagnani et al., 2009). Although the urbanisation impacts on discharge wastewater quality has been studied before (Astaraie-Imani et al., 2012; Li et al., 2012) along with

sewer network studies, it is also vital to incorporate the change in LULC, to study wastewater influent volumes. This will enable wastewater utility managers to optimise WWTP performance, better manage stormwater and protect the environment by limiting the frequency of CSOs. However, to the best knowledge of the author, research carried out have not incorporated LULC to study the WWTP flows. Table 2.6 presents various studies investigating the impacts of LULC change on stormwater runoff and sewerage systems.

Table 2.6: Literature review of research studying the impact of LULC change on stormwater runoff and sewerage systems

References	Objective	Key features and outcomes of study
LULC change based studies		
(Saraswat et al., 2016)	Analysis of stormwater runoff management practices based on climate change and urbanisation	Studies are based on the assessment of management practices of stormwater runoff.
(Loperfido et al., 2014)	Assessment of distributed and centralized stormwater best management practices and land cover	Results display the importance of sustainable best management practices on mitigating stormwater runoff and the role of RS and GIS in identifying optimum measures to inform policy makers and researchers in the field of stormwater management.
(Paule-Mercado et al., 2017)	Analyse the influence of ongoing land development on stormwater runoff while integrating four different Low Impact Development and best management practice scenarios in a catchment of mixed LULC in South Korea connected to a sanitary sewer system.	The area upstream of the sanitary sewer had a natural drainage system receiving inflow from a forest, whereas the area downstream connected to the stormwater drainage system received inflow from both pervious and impervious areas. Data of 41 storm events (characterised by 3 antecedent dry days, 4 mm of rainfall and 6 hours of runoff duration) and monthly LULC were monitored. LULC map and network data was estimated by classifying an aerial image of 0.4 m spatial resolution accompanied by monthly field monitoring. A

		SWMM was used to simulate the monitored storm events by incorporating catchment characteristics, climate, LULC etc. Model validation showed that the model is fit and reliable to be used in this context. They also found that stormwater quality deteriorated with an increase in imperviousness. In addition to that, they emphasized the importance of implementing LID-BMPs as they can reduce runoff volume, peak flow and pollutant concentrations.
(Ravagnani et al., 2009)	Assessing the impact of urban impervious fraction on peak discharge entering a storm sewer system.	Use of RS technology to estimate the urban impervious fraction. Two issues regarding the margin of error in remotely sensed image and the unavailability of the information about the connection of impervious and pervious areas to the sewer system were addressed. It was found that the remote sensing image was sufficient and precise in mapping impervious and pervious areas without affecting the peak discharge. But if the information on how the different areas is connected is ignored, peak discharge is overestimated.

(**Sanyal et al., 2014)**	Investigating the impact of LULC changes at sub-catchment level on flood peak at a catchment outlet.	Classification of Landsat images to produce LULC maps and use of HEC-HMS hydrological model to simulate the rainfall-runoff process. They found a statistically significant linear relationship between the LULC changes and flood peak with an R^2 value of 0.53. However, a number of sub-catchments deviated from this relationship. The authors suggested that it is difficult to upscale the relationship between LULC changes and runoff due to localised change in landcover at sub-catchment scale.
(Zhou, 2014)	Review of sustainable urban drainage systems with respect to climate change and urbanisation impacts	Recent progress in sustainable drainage systems were reviewed considering climate change and urbanisation impacts
(Zhou et al., 2019)	Impact analysis of urban development on hydrological runoff and urban flood volumes.	They developed a geospatial database of landuse types, surface imperviousness and drainage systems and incorporated these into the SWMM urban drainage model. The study revealed that urban development, particularly accelerated urbanisation caused a large increase (208 – 413%) in surface runoff. However, the changes in the urban flood volumes depended on the performance of drainage systems.

(Yazdanfar & Sharma, 2015)	Investigation of different factors varying spatially and temporally, affecting the functioning of urban drainage system	Challenges in the urban drainage system designing due to climate change and urbanisation were reviewed.
(Amani et al., 2020)	Review of GEE Platform as compared to software or desktop programs	Review of 450 journal papers across 150 journals to demonstrate a deep understanding of GEE
(Wang et al., 2021)	Demonstrate the advances of GEE in studies related to urban land cover change	Reviewed GEE progress in four specific areas of urban studies: urban extent mapping, urbanisation estimation, urban ecosystem characterization, and city accessibility assessment.

2.6. Summary of literature review

It is evident from the published literature that there has been ongoing research investigating the impacts of climate variables (current and future) and urbanisation on the hydraulic efficiency of sewerage systems. Some research have also based their focus at the WWTP scale to study the quantitative and qualitative impacts on wastewater infrastructure. Table 2.1, Table 2.3 and Table 2.6 summarise the studies investigating the range of climate and urbanisation variables used to assess the degree to which WWTPs and its associated sewer network are impacted. It is evident that the number of studies investigating CSOs, and effluent are abundant as opposed to influent flows. As established in Figure 2.4, these parameters exhibit different characteristics. Influent volume characteristics is one of the most influential factors determining WWTP operations. Lack of understanding of influent volume variations can be addressed by a detailed study investigating influent volumes values representing a range of WWTPs and the factors affecting it. A key challenge in the research area of monitoring the performance of WWTPs and sewer systems is data unavailability. The majority of the literature published to date have used modelled data from hydraulic models with calibration and validation of models using limited observed data. Sewer process models are limited in terms of representing actual processes (Langeveld et al., 2013). For example, the limited data available for calibration and validation might not include rare extreme events. As such these models only represent the processes that are incorporated by the user and hence, cannot be applied in a generic way (Langeveld et al., 2013). With advancement in data monitoring, data-based analysis could be performed to tackle this problem. However, research using observed dataset are limited to demonstrating either spatial variability of wastewater characteristics based on rainfall characteristics (for a 1-year period) or the temporal variability of wastewater characteristics based on rainfall characteristics (for 1 case study). When models are fed with a single aspect, the impact of the spatio-temporal variability of rainfall on the response of the urban drainage system remains unexplored (Peleg et al., 2016). This drawback along with the drawback of lacking models that can be applied universally, can be addressed by developing a model that captures the spatio-temporal aspect and can be applied to any WWTP of any treatment capacity and size.

One aspect that is common across Table 2.1, Table 2.3 and Table 2.6 is the limited number of studies that focus on influent volumes, with the effluent discharge volume and performance of sewer systems being frequently studied. In addition to this, research addressing the tidal level impacts on wastewater flows are significantly limited. River level which may be influenced by tides, is another factor that will enhance the understanding of the response of wastewater flows but has not been investigated till date.

In terms of future climate change impacts, it can be noted from Table 2.3 that all the published literature are centered around the performance and design of the urban drainage system. As the impacts on wastewater influent flows as result of precipitation has been established, with the climate change induced change in precipitation patterns, analysis involving projected future influent wastewater flows as a function of projected change in future precipitation is highly valuable. However, such an analysis has not been studied till date. This will help wastewater utility managers in taking informed decision while strategizing adaptation techniques.

In relation to LULC based studies, Table 2.6 clearly demonstrates the impact of urbanisation on stormwater runoff. However, the author did not find any study that investigates the degree to which this runoff might impact the amount of wastewater influent to the WWTPs. This will provide deeper insight into the response of wastewater influent volume characteristic of WWTPs and help determine whether urbanisation induced surface runoff is a significant variable in terms of hydraulic overloading at the inlets of WWTPs with CSSs.

These findings underpin the objectives for this PhD and provide a focus for the remainder of the literature review. The objectives which address the gaps highlighted above are as follows:

1) Detailed understanding of influent volume characteristics that varies downstream after CSOs and define the WWTP operations.
2) Use of real spatio-temporal data to analyse wastewater influent volumes of WWTPs with CSSs as the variable of interest to enhance the understanding of WWTP responses to precipitation.
3) Consideration of tidal and river levels impacts incorporated in the analysis of wastewater influent volumes.

4) Consideration of climate change impacts to develop an understanding of the evolution of wastewater influent volume characteristics in future.
5) Study of urbanisation impacts on wastewater influent volumes.

Methodologies undertaking these objectives will help in the optimal management of wastewater quantity entering the WWTPs.

3. ANALYTICAL PROCEDURE

3. Analytical procedure

3.1. Overview

The aim of this chapter was to provide a summary of the study area of this research, the datasets obtained and used for the study. These datasets include precipitation, tidal and river levels, the future precipitation projections under various climate change scenarios, and data with respect to land use and land cover. This chapter describes the sources, resolution, and range of all the datasets. It describes the fourteen wastewater treatment plants of varied capacity and network size studied in this thesis. It also illustrates the methodologies which underpin the results in chapters 4, 5 and 6. Part of this chapter has already been published in Results in Engineering (Saikia, S.D., Ryan, P., Nuyts, S., Clifford, E. (2022). Precipitation, tidal and river level impacts on influent volumes of combined wastewater collection systems: A regional analysis. *Results in Engineering*, 15, 100588). The future datasets and methodology have been submitted to Climate Services.

3.2. Summary of Datasets

This section summarizes all the datasets used for the analysis in Chapter 4, 5 and 6.

3.2.1. Observed Datasets

3.2.1.1. Influent volume data

In order for a WWTP to be considered as part of this study, it needed 1) to have a CSS, 2) to have at least 3 years of daily data of influent volumes, and 3) have had limited recent network improvements/extensions, in order to exclude their impact from the analysis (albeit this criterion was not strictly applied given ongoing improvements in many locations in Ireland). Geographical spread and the size of the WWTPs were also considered. Data was obtained from Irish Water, and the data gathering process from the initiation of the talks with Irish Water to the final acquisition of the data involved approximately 16 months. This timeline also included a 6-month internship (4 months of work at their Mullingar office followed by 2-months remote work) and a 5-month post internship period for Irish Water to formally transfer the data. The Asset Management team of Irish Water assisted in the acquisition of the data. The data collection included

manual analysis of both online and "paper-based" records. The highest resolution of data available were daily datasets and were recorded in m^3/day unit of measurement. Sub-daily data although suitable for this research, were not available for a sufficient number of WWTPs. The data were in various formats including PDF, excel and word documents.

This eventually led to the selection of 14 different WWTPs with varying treatment capacities representing small to very large agglomerations (Table 3.1), geographically spread across Ireland. Out of the 14 WWTPs, 5 WWTPs are located in the west of the country, five in the east, one in the north and three are centrally located. Lastly, 6 of the WWTPs are in close proximity to rivers or to the coast. The location of the WWTPs were provided as shapefiles (.shp format) by Irish Water. The data available for each of the WWTPs is summarised in Table 3.2.

Table 3.1: Network categories

Range of Treatment Capacities (population equivalent - PE)	**Network Categories**
≥ 1,000 – 30,000	Small
> 30,000 – 100,000	Medium
> 100,000 – 450,000	Large
> 450,000 – 1,640,000	Very Large

Table 3.2: Summary of the 14 WWTPs

WWTPs	Treatment Capacity (PE)	Peak Design Capacity (m3/day)	Network Category	Average annual precipitation * (mm/year)	River/Tidal Analysis	Temporal Range of data availability (Current Period)		
						Influent Volume	Tidal Level	River Level
WWTP 1	1,86,000	88,500	Large	995	River	2014 - 2018	2014 - 2018	2014 - 2018
WWTP 2	4,13,200	3,59,592	Large	1044	Tidal	2005 - 2018	2010 - 2018	-
WWTP 3	28,000	23,814	Small	1632	-	2012 - 2018	-	-
WWTP 4	25,000	14,760	Small	1211	Tidal	2008 - 2018	2012 - 2018	-
WWTP 5	3,000	2,250	Small	1267	-	2014 - 2018	-	-
WWTP 6	40,000	32,400	Medium	1243	-	2015 – 2018	-	-
WWTP 7	55,000	37,125	Medium	1024	-	2014 - 2018	-	-

WWTP 8	1,70,000	1,35,000	Large	1352	Both	2011 - 2018	2011 - 2018	2011 - 2018
WWTP 9	39,000	23,400	Medium	837	-	2012 - 2018	-	-
WWTP 10	16,40,000	9,59,040	Very large	621	Both	2015 - 2018	2015 - 2018	2017 - 2018
WWTP 11	1,86,000	1,08,000	Large	716	-	2015 - 2018	-	-
WWTP 12	20,000	12,000	Small	965	Tidal	2008 - 2018	2012 - 2018	-
WWTP 13	24,834	5,063	Small	1171	-	2016 - 2018	-	-
WWTP 14	45,000	33,000	Medium	897	-	2014 - 2018	-	-

*Average annual precipitation calculated from years covering the available data of the influent volumes

3.2.1.2. Precipitation data

For 13 of the 14 wastewater treatment plants, daily precipitation data used in this study was obtained from weather stations nearest to the WWTPs, which are operated by Met Éireann (Irish national meteorological service). The one exception was WWTP 8. For this WWTP, precipitation data was obtained from a calibrated weather station at the University of Galway as this was the nearest calibrated weather station. All precipitation data were recorded in mm/day unit of measurement.

Wet days were defined as those with greater than 1 mm/day precipitation, and zero rainfall days defined as those with 0 mm/day rainfall (Met Éireann, 2019). Figure 3.1 summarizes monthly rainfall patterns in Ireland for the years 1981 – 2010 and shows that annual precipitation is significantly higher on the western seaboard compared to central and eastern areas of the country.

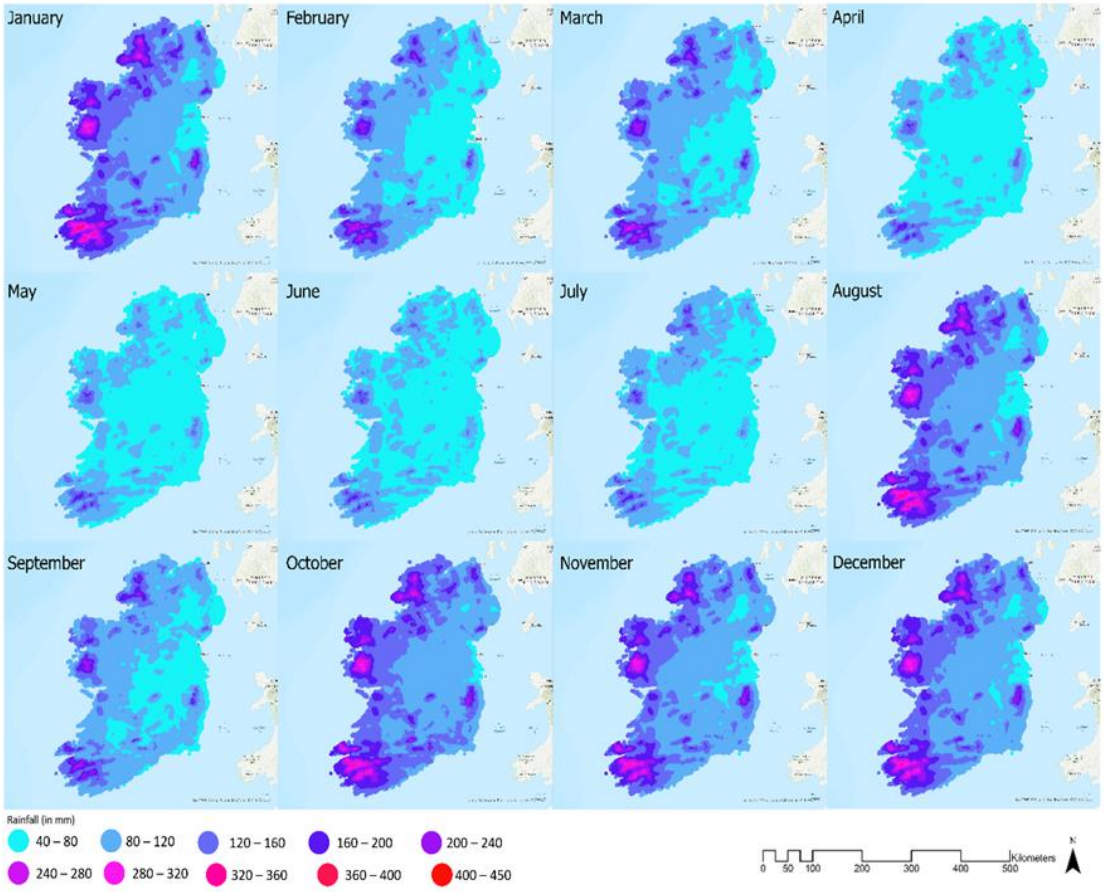

Figure 3.1: Monthly rainfall distribution map of Ireland depicting 1981 – 2010 monthly average rainfall data with 1 km spatial resolution (Data source: Met Éireann)

3.2.1.3. Tidal level and river level data

Tidal levels, recorded in metres (m), was available at a 5 – 6 minute resolution from the Marine Institute of Ireland. From this, the daily maximum tidal data was extracted for WWTPs 2, 4, 8 10 and 12, i.e., those with a coastal location or located on a tidal river. Daily mean water or river level data was extracted from the publically available Hydro-data from the Office of the Public Works (OPW, 2020) for WWTPs 1, 8 and 10. The data is recorded in metres and the daily mean river level was directly available. The vertical reference for both the tidal and the river level data is OD Malin Head Irish Tranverse Mercator.

3.2.2. Future Datasets – CMIP 5 Model Projections:

The projected Irish precipitation climate data were obtained from the High-resolution Climate Projections for Ireland – A Multi-model Ensemble Approach report (Nolan and Flanagan, 2020). The climate projections were generated by downscaling the following CMIP5 GCM data; the UK Met Office's Hadley Centre Global Environment Model version 2 Earth System configuration (HadGEM2-ES) GCM (Collins et al., 2011), the EC-Earth consortium GCM (Hazeleger et al., 2011), the CNRM-CM5 GCM developed by CNRM-GAME (Centre National de Recherches Météorologiques—Groupe d'études de l'Atmosphere Météorologique) and CERFACS (Centre Européen de Recherche et de Formation Avancée) (Voldoire et al., 2012), the Model for Interdisciplinary Research on Climate (MIROC5) GCM developed by the MIROC5 Japanese research consortium (Watanabe et al, 2010) and the MPI-ESM-LR Earth System Model developed by the Max Planck Institute for Meteorology (Giorgetta et al., 2013).

The CMIP5 data were dynamically downscaled using the Consortium for Small-scale Modeling – Climate Limited-area Modelling (COSMO-CLM) and Weather Research Forecasting (WRF) RCMs. The RCMs were initially driven by global boundary conditions with the following nesting strategies; CMIP5 global dataset to 50 km to 18 km to ~ 4 km (for lower resolution CMIP5 data) and CMIP5 to 18 km to ~ 4 km (for higher resolution CMIP5 data). For the current study, only 4 km grid spacing RCM data are considered. The higher resolution data allows sharper estimates of the regional variations of climate projections. To address the issue of uncertainty, a multi-model ensemble approach was employed. Through the ensemble approach, the uncertainty in the projections can be partially quantified, thus providing a measure of confidence in the predictions. To account for the uncertainty arising from the estimation of future global emission of greenhouse gases, downscaled GCM simulations based on two Representative Concentration Pathways (RCP 4.5 and RCP 8.5) were used herein to simulate the future climate of Ireland (Moss et al., 2010; van Vuuren et al., 2011). A full description of the model setup, model validations and future projections is given by Nolan et al. (2017) and Nolan and Flanagan (2020).

The results show that by mid-century, substantial decreases in precipitation are expected for Ireland in the summer months, with reductions ranging from ≈ 0% to 11% for the RCP 4.5 scenario and from 2% to 17% for the RCP 8.5 scenario. Other seasons, and over

the full year, show small projected changes in precipitation. However, the mid-century precipitation climate is expected to become more variable with substantial projected increases in both dry periods and heavy precipitation events (Nolan and Flanagan, 2020).

For this study, three aspects of future precipitation projections were of interest and are summarised in Table 3.3. The location-specific data corresponding to each of the 14 WWTPs were obtained through collaboration with the Irish Centre for High-end Computing [authoring institution of Nolan and Flanagan, (2020)], with a focus on three different datasets as described in Table 3.3. The description of the data, in addition to the purpose of the data in this paper are also included in Table 3.3.

Table 3.3: Rainfall projections from (Nolan and Flanagan, 2020) used in this study

Data from (Nolan and Flanagan, 2020)	Description	Purpose in this research
Projected % change in seasonal mean precipitation	Change in seasonal mean precipitation in 2041 – 2060 as compared to 1981 – 2000	To understand the nature of influent volume variations on a monthly scale as a result of changes in monthly average daily precipitation
33rd and 66th percentiles of the ensemble of RCM projections of mean precipitation for each season	33rd (P33) and 66th (P66) percentiles are calculated of the ensemble of RCM projections for each season. For each RCM ensemble member, the mean change in precipitation is calculated for the period 2041–2060 with respect to 1981–2000	To help capture the impact of climate projection uncertainty on wastewater influent volumes and analyse variability of the findings of the ensembles
Projected % change in the annual number of high and very high precipitation days	Change in the annual number of high precipitation days (days with > 20 mm/day rainfall) and very high precipitation days (days with >30 mm/day rainfall) in 2041 – 2060 as compared to 1981 – 2000	To understand the evolution of influent volume characteristics as an effect of extreme events (defined as high and very high precipitation days for this research)

The three different datasets of mid-century projected % change in seasonal mean precipitation, the 33rd and the 66th percentiles of the ensemble of RCM projections of seasonal mean precipitation and the projected % change in the annual number of high

and very high precipitation days obtained from Nolan and Flanagan (2020) are presented in Figure 3.2, Figure 3.3 and Figure 3.4.

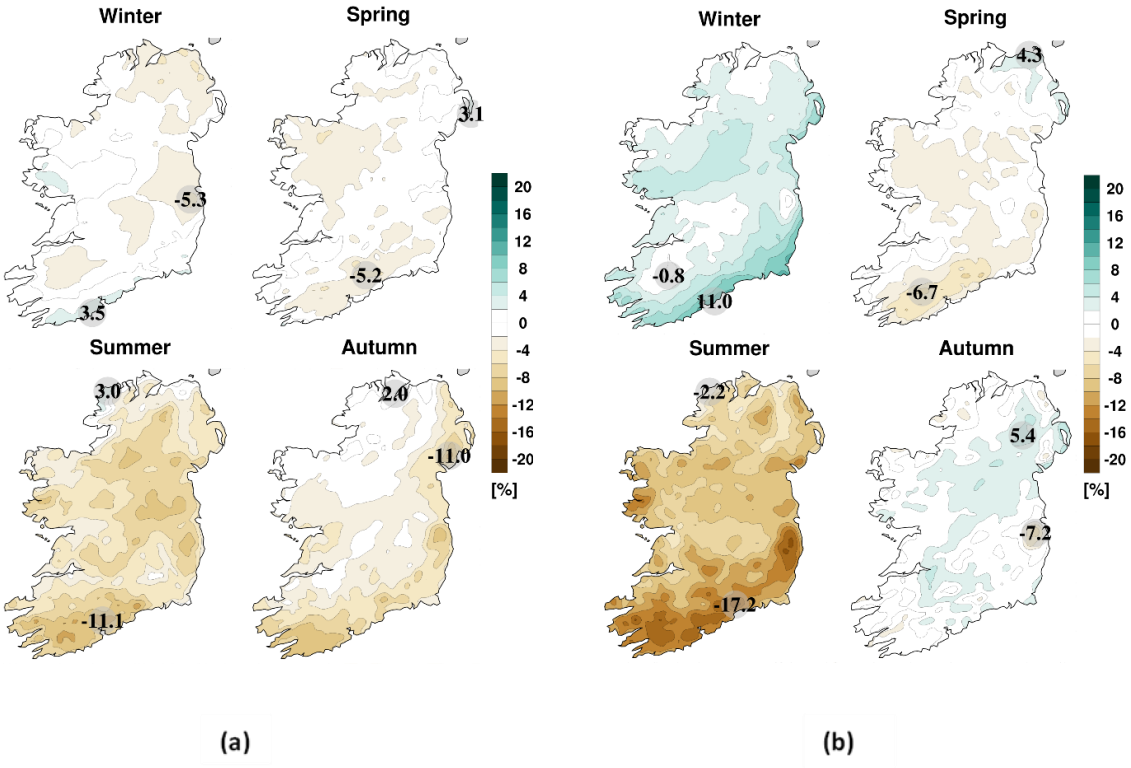

Figure 3.2: Spatial variation in the projected change in ensemble mean seasonal precipitation in Ireland in 2041 – 2060 as compared to 1981 – 2000 under a) RCP 4.5 and b) RCP 8.5. The numbers shown on each plot are the minimum and the maximum projected changes in mean seasonal precipitation displayed at their respective locations

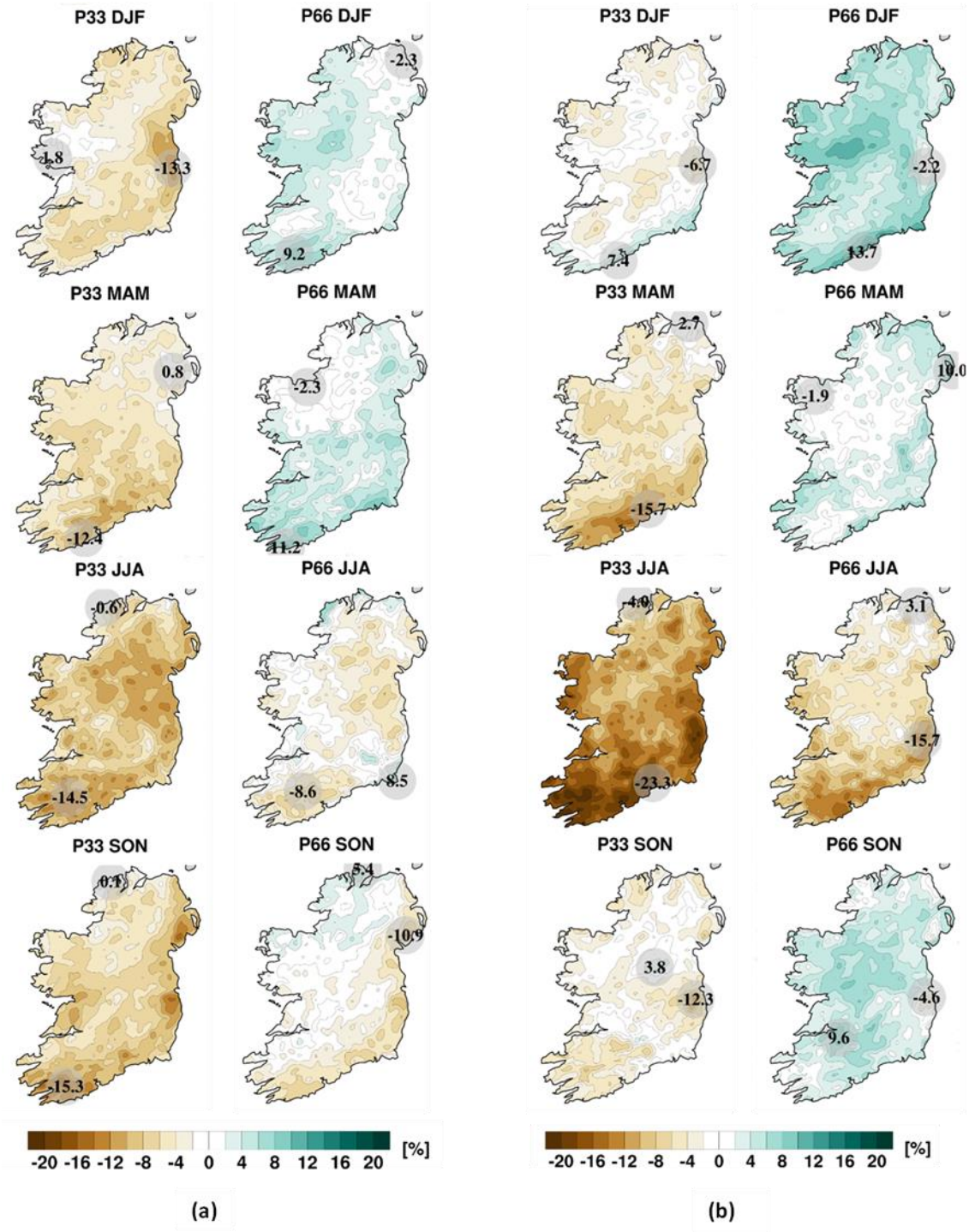

Figure 3.3: The 33rd and 66th percentiles of the projected % change in seasonal mean precipitation in Ireland in 2041 – 2060 as compared to 1981 – 2000 a) under RCP 4.5 and b) under RCP 8.5

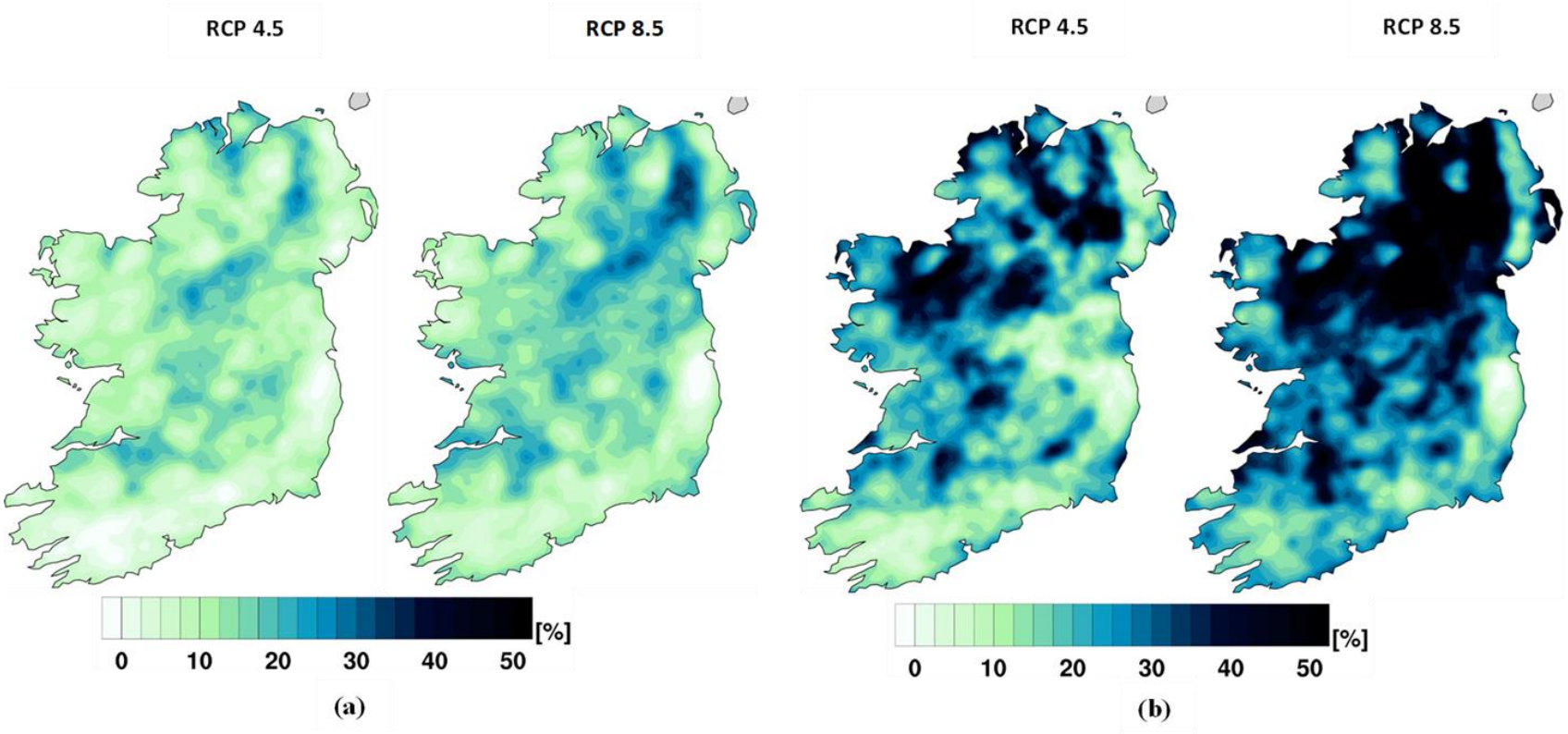

Figure 3.4: Projected % change in annual a) high precipitation days (> 20 mm/day) and b) very high precipitation days (> 30 mm/day), in 2041 – 2060 as compared to 1981 – 2000 under RCP 4.5 and RCP 8.5

3.2.3. Datasets for Land Use Land Cover Analysis

3.2.3.1. Satellite Imageries

As this project is focusing on a timeframe since 2005, Landsat 5 Thematic Mapper (TM) and Landsat 8 images from this timeframe were used in this research in order to maintain a uniformity in the spatial resolution. These images were used across the years for which influent volume data was obtained for each of the agglomerations. Landsat 7 images were not used in this research given the Scan Line Corrector (SLC) of the satellite failed in 2003. Landsat 5 and 8 were previously reviewed in Chapter 2 Section 2.5.1.3. The detailed methodology adopted in the selection of the satellite imageries are mentioned in Chapter 6 Section 6.3.1.

Data sources for the satellite images include the United States Geological Survey (USGS) Earth Explorer and the Google Earth Engine (GEE) Code platform. USGS Earth Explorer is a tool (website) enabling users to search for satellite images and aerial imageries in their catalogs. It also allows users to download satellite data in chronological timelines according to user-defined criteria as shown in Figure 3.5. Tier 1 (T1) Landsat imagery which refers to the data that meets the USGS radiometric and geometric quality requirements were used for this research.

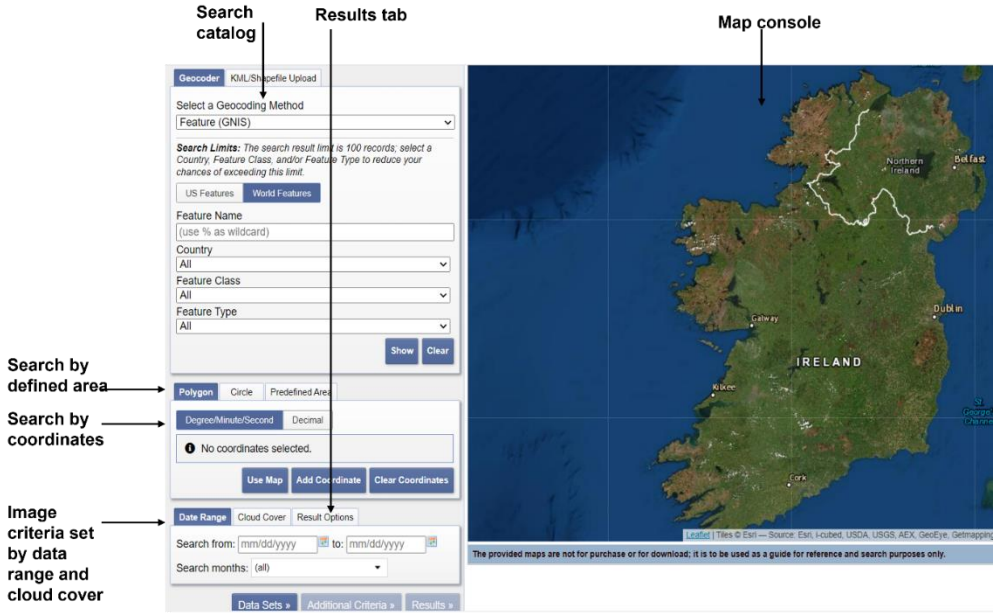

Figure 3.5: USGS Earth Explorer platform and its various components (Source: USGS Earth Explorer, 2022)

Once the satellite images were selected, the GEE code editor platform was used to import the imageries. An archive of various LANDSAT satellite images (5 and 8) of historical and current data was available online in their Google data catalog. This editor platform aims to simplify complex geospatial workflow and is designed into various components as shown in Figure 3.6. Detailed methodology using this platform to import the satellite images is described in Chapter 6 Section 6.3.2.

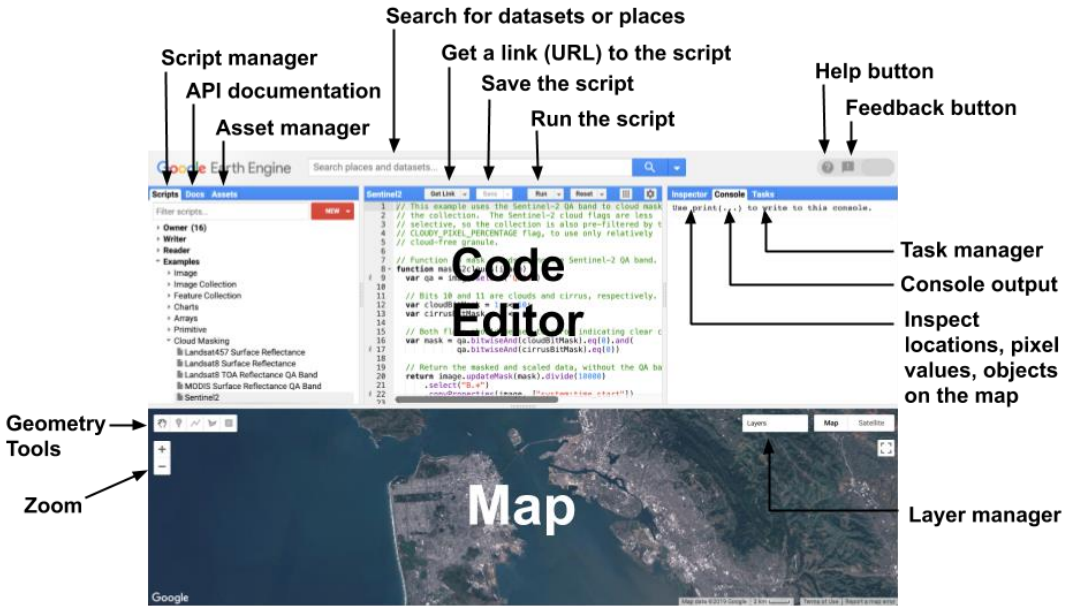

Figure 3.6: Diagram showing the GEE code editor interface with its various components (Source: Google Developers, 2022[16])

Apart from the classification of satellite images, Google Earth Pro software has been used for the validation and accuracy assessment of classified imageries (Refer to Chapter 6 Section 6.3.3). This is a freely available software that allows users to create, overlay, assess and visualize geospatial information. It provides a time slider that helps users to analyse historical data of the area of interest.

3.2.3.2. Shapefiles

The agglomeration boundaries required to assess the urban dynamics and its impacts on WWTPs with CSSs were acquired from Irish Water in shapefile (.shp) format. These

[16] https://developers.google.com/earth-engine/guides/playground (Accessed in Apr, 2022)

shapefiles have polygon features that represent the boundary of each agglomeration as shown in Figure 3.7.

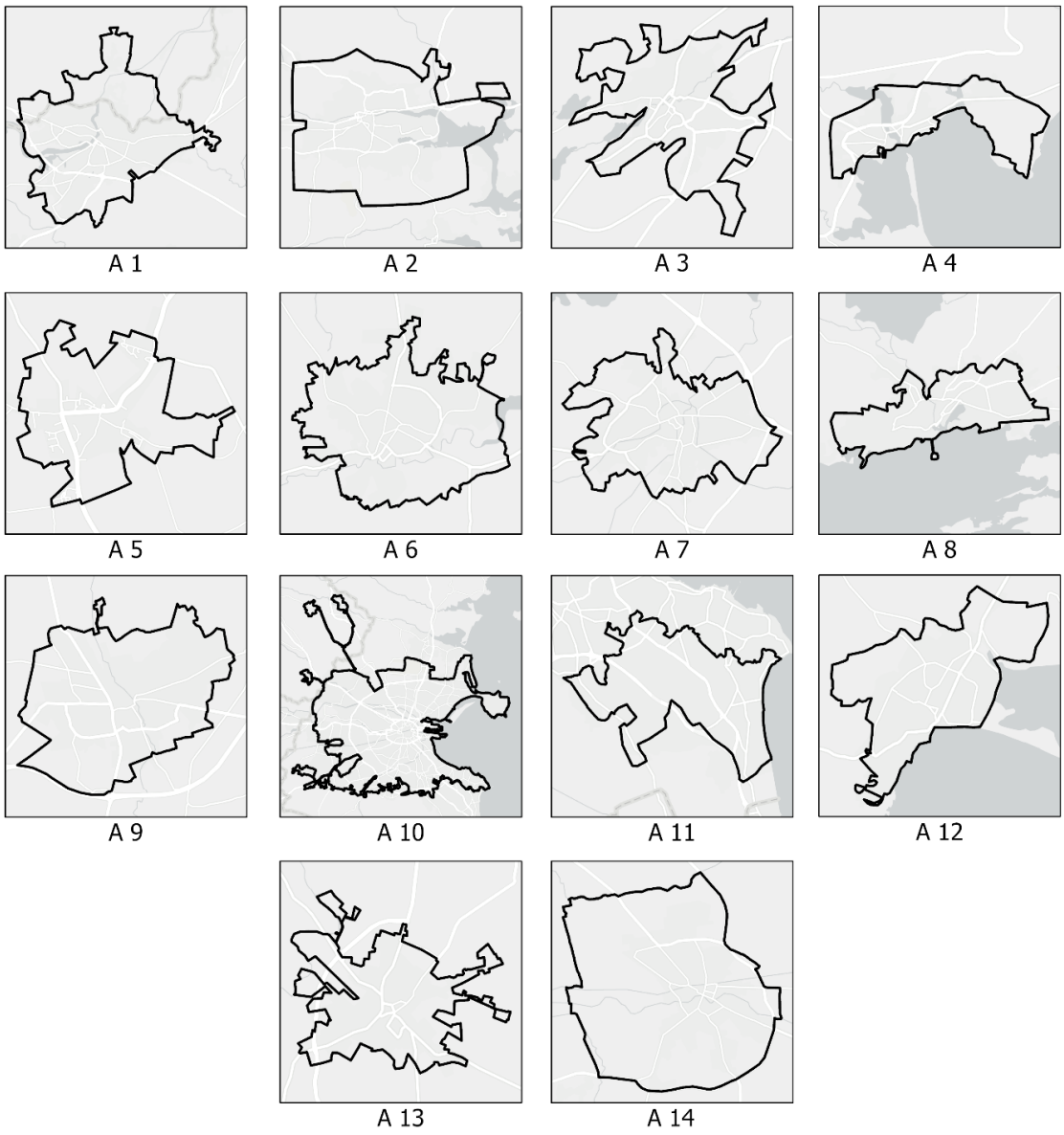

Figure 3.7: The agglomeration boundary shapefiles

3.3. Analysis and Model Building:

The relationship between wastewater influent volumes and variables such as precipitation, tidal level, river level and urban land cover was investigated by undergoing statistical analysis. Statistical modelling of the response variable aids in explaining the behaviour of the variable of interest by a model represented by an algebraic equation. Linear regression is one of the simplest and the most effective method to analyse trends

and detect the non-stationarity nature of local precipitation data and hence often used in urban design studies (Jung et al., 2015). Moreover, when the nature of the function of the regression equations are unknown, linear regression is often considered as first approximation of regression function (Kutner et al., 2005). Urban drainage design studies use annual maximum precipitation data or rainfall extremes and hence use modelling techniques such as generalized extreme value model, Mann Kendall test etc (Arnbjerg-Nielsen, 2012; Willems, 2013; Willems et al., 2012). These tests do not take into consideration the strong temporal variability of daily or sub-daily datasets (Willems et al., 2012). In addition, the studies that investigated the impacts of precipitation variables on influent volumes (Langeveld et al., 2013; Li et al., 2018; Mines et al., 2007) have already established that linear regression modelling approach could be efficiently used to model influent volume characteristics at daily, monthly and event-based scales on the basis of precipitation variables (Chapter 2 Section 2.3.1.2). This thesis did not consider WWTP design, but focused on the influent volume characteristics, at daily scale, hence, in this research, linear regression modelling was adopted and the methodologies were developed based on regression analysis to understand the trends and variations of wastewater influent volumes as a response variable with respect to the above-mentioned predictor variables. There are five main assumptions underlying linear regression analysis: i) linearity, i.e., the variables must be linearly related, ii) homoscedasticity, i.e., equal variances between residuals and predicted values, iii) normality, iv) residuals are independent and v) the predictor variables should not be highly correlated. These assumptions are checked, and it was found that the data satisfies four out of the five assumptions. The data did not follow a normal distribution and had a skewness factor of approximately 0.3 – 0.8 across all the WWTPs. This indicated that the data is slightly positively skewed. However, since Least Squares Regression method (a linear model represented by a line to fit the data) is a linear unbiased estimator, i.e., the data need not be normally distributed (Tellinghuisen, 2008), but rather the residuals and their mean should be zero. This was further checked, and the errors satisfied this condition across all the WWTPs. It is to be noted that it is normal to find influent volume data to not follow a normal distribution due to the presence of extreme values (outliers) that might skew the distribution. However, removal of extreme values will not represent the data in its true sense and thereby, the model will fail to take into account extreme events leading to higher values of influent volumes which are required in studies related to wastewater infrastructure.

R Studio free open-source software was used to perform regression analysis. It is an integrated development environment (IDE) that uses the R programming language for statistical computing[17].

Simple linear regression (SLR) modelling technique is used when one predictor variable is considered at a time in a regression equation to evaluate its impacts on the dependent or response variable. On the other hand, multiple linear regression (MLR) modelling technique is carried out when more than one predictor variables influence the dependent variable. MLR is useful to estimate the combined impacts of predictor variables. SLR (Equation 1) and MLR equations can be represented as follows:

$$y_p = \beta x + c + \in \quad \text{(Eq. 3.1)}$$

$$y_p = \beta_1 x_1 + \beta_2 x_2 + \cdots + \beta_n x_n + c + \in \quad \text{(Eq. 3.2)}$$

Where y_p represents the predicted values of the response variable y, x, x_1, x_2, …, x_n are the predictor variables, n is the number of predictor variables, β, β_1, β_2, …, β_n are the coefficients of the variables respectively, c is the intercept. However, each regression model has an associated model error ∈. This term, representing the error originates from sources beyond the control of the user and can be calculated in terms of various error metrics that that can determine the differences between predicted and actual values of the response variable. However, it does not indicate how much the error has contributed to the discrepancy. For each of the SLR and MLR models, the coefficient of regression/determination (denoted by R^2 or adjusted-R^2 in case of MLR), p value, slope coefficient of each independent variable, residual standard error (RSE) and model error were also determined. RSE or sigma of a model provides a measure of prediction error; lower its value, higher is the accuracy of the model. RSE is expressed in terms of residual sum of squares and degrees of freedom (Equation 3.3).

$$RSE = \frac{\sqrt{\sum (y - y_p)^2}}{o - k - 1} \times 100 \quad \text{(Eq. 3.3)}$$

[17] https://www.rstudio.com/ (Accessed in June, 2022)

where o represents the number of observations, and k represents the number of model parameters.

The model error denotes the total number of incorrect predictions out of all the predictions made and is estimated by Equation 3.4.

$$Model\ error\ = \frac{RSE}{mean\ of\ the\ dependent\ variable} \times 100 \qquad \text{(Eq. 3.4)}$$

Another error metric that was been considered in this study are root mean square error (**RMSE**) which is analogous to standard deviation and provides a measure of the spread of the residuals. It also takes into account outliers (if any) present in the dataset. The unit of RMSE is similar to the response variable, making it easier for a user to interpret the results. In this case, the unit of RMSE is m^3/day.

The statistical significance of the model p and of each explanatory variable was also estimated. p value showing less than 0.05 (5% level of significance or 95% level of confidence) were considered significant variables.

3.4. Development of methodologies

This section discusses the inception of the methodologies developed to study the response of wastewater influent volumes to different variables addressed in this research as discussed in Section 3.1. In order to analyse the impacts on wastewater influent volumes based on observed precipitation, tidal and river levels, the future precipitation projections under various climate change scenarios, and lastly, the change in urban land cover, the methodologies developed are presented in the following sub-sections.

3.4.1. Impact assessment on wastewater influent volumes using observed datasets – a pilot case study

This section discusses the use of observed datasets elaborated in Section 3.2.1. WWTP 8 was selected as a "case-study" to help identify the variables that were most likely to have an impact on wastewater influent volumes. It is 1) a large sized network in an urban area, 2) located near the coast, and 3) has a tidal river in close proximity to the WWTP. As such, it provided an ideal opportunity to test a long list of rainfall variables for significance in relation to their impacts on influent volumes. The variables that were

found to have a significant impact on influent volumes are defined in Table 3.4. All other variables that were tested but had no significant impact on influent volumes are presented in Appendix I.

All variables defined in Table 3.4 were tested separately for statistical significance at a 95% level of confidence using simple linear regression (SLR) analysis, grouped by impact of 1) precipitation, 2) tidal levels, and 3) river levels. Multiple linear regression (MLR) was also performed to estimate the effects of more than one variable on influent volume. For every MLR analysis (daily, monthly, and pooled), bivariate correlation analysis and Variance Inflation Factor (VIF) estimation were conducted to check for multi-collinearity amongst the predictor variables. Variable(s) with correlation coefficients greater than 0.80 signified high correlation between the variables. This was followed by a check of variables with VIF greater than 5. After following up with these two procedures, the variables satisfying both these criteria were discarded (Tay, 2017).

Lag-time (i.e., difference in time between the day that precipitation event occurs and the day the related response or surge in influent volume is observed at the WWTP) was also analysed to understand the response characteristics of influent volumes better. Precipitation categories were determined by categorizing daily precipitation across all years based on percentile evaluation (Schär et al., 2016); and probability of exceedance curves (PoE) represented the likelihood of exceeding certain influent volumes across all years under each precipitation category. Details of the application of this methodology on the rest of the WWTPs and the results are described in Chapter 4.

Table 3.4: List of significant variables/terminologies used in this research, their definition and unit

Variables	Dependent/Predictor variable	Description	Unit
Variables at daily scale			
Daily influent volume (Q)	Dependent	Daily influent volume to the WWTP	m^3/day
Daily precipitation (P)	Predictor	Total daily precipitation	mm/day
Precipitation for 1,2 and 3 days before the corresponding influent volume	Predictor	For influent volume at any given day (d), daily precipitation at day d-1, d-2, and d-3	mm/day
Daily maximum tidal level (T)*	Predictor	Maximum tidal height recorded for each day	m
Daily mean river level (RL)*	Predictor	River level readings averaged for each day	m
Dry weather flow (DWF)	Predictor	Influent volume corresponding to a zero rainfall day	m^3/day
Variables at monthly scale			
Average daily influent volume (ADIV) over a month	Dependent	Average daily influent volume over a given month	m^3/day
Number of wet days (WD) in a month	Predictor	Days with precipitation greater than or equal to 1 mm in a month	days
Number of dry/ zero rainfall days (ZRD) in a month	Predictor	Days with no precipitation in a month	days

Average daily precipitation (ADP) over a month	Predictor	Average daily precipitation over a given month	mm/day
*Relevant only for WWTPs close to rivers and/or sea			

The methodology to analyse the different aspects of precipitation, i.e., intensity, frequency and duration in conjunction at daily and monthly scale is presented in Figure 3.8. The timescale at which WWTP assessments are carried out is of primary importance. Daily flows are much more variable during wet weather days whereas maximum monthly average daily flow is used for the hydraulic design capacity (Mines et al., 2007). Whereas (Li et al., 2018) reported that the relationship between rainfall and inflow rate of combined sewer systems at a monthly scale can be very well depicted by linear models.

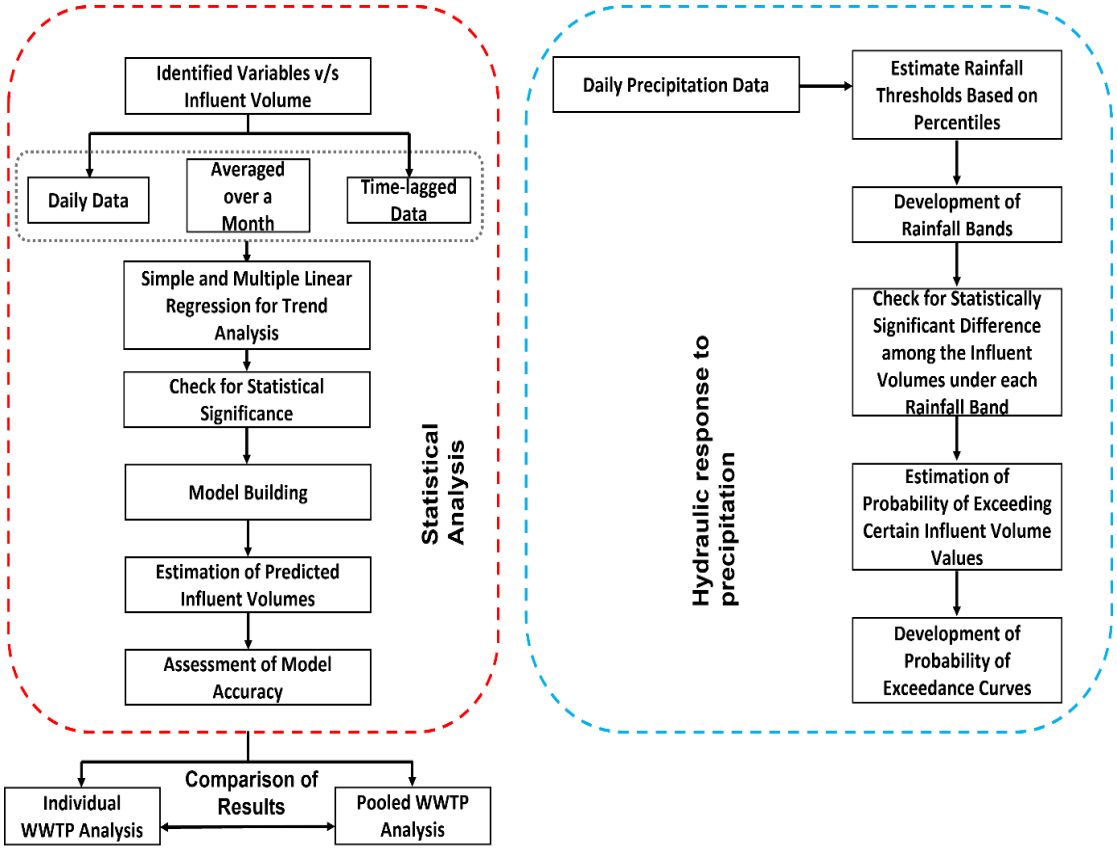

Figure 3.8: Methodology of analysing historical impacts of precipitation variables on wastewater influent volumes

In order to investigate the influence of all the other identified statistically significant variables, a similar approach was carried out. However, tidal level and river level were analysed at a daily scale only.

3.4.2. Impact assessment on wastewater influent volumes using future datasets

Seasonal mid-century projected changes for 2041 – 2060 (Future Period) as compared to 1981 – 2000 (Past Period) were available for Ireland across 4 seasons (i) December, January and February (DJF – winter); (ii) March, April and May (MAM – spring), (iii) June, July and August (JJA – summer) and (iv) September, October and November (SON – autumn) (Nolan and Flanagan, 2020). The models (Equation 3.1 and 3.2) at a monthly scale established using the observed datasets of influent volumes and precipitation for the current period (Table 3.2) for all the WWTPs (details in Chapter 4) are leveraged in this study for future projections of influent volumes. Thus the methodology adopted in this part of the research exploring the future impacts of projected precipitation (described below) included the following assumptions due to the nature of the available climate change projection data: (i) the seasonal projected data were representative of each month of the season; for example, the value of the projected % change in the winter season was applied to the months of December, January and February, which constitutes that season; (ii) change was assumed to have occurred linearly from the past period (1981 – 2000) to the future period (2041 – 2060) (Figure 3.9); and (iii) the projected wastewater influent volume characteristics did not account for demographic changes within the urban areas – thus the impacts are those induced by changes in rainfall patterns only.

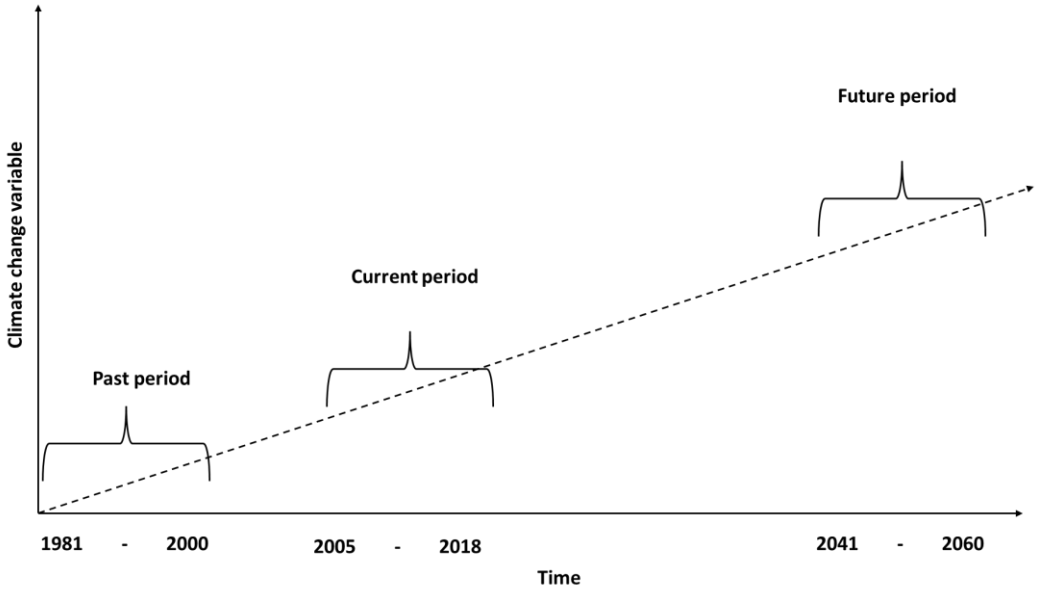

Figure 3.9: Assumption of linear change for a variable showing increase in the future due to climate change

It is to be noted that, if the climate change variable of interest is shown to decrease in future, the linear interpolation plot can be produced similarly. As shown in Figure 3.9, with the assumption of linear change in precipitation variables between the past period (1981 – 2000) and the future period (2041 – 2060), projected precipitation changes for the current period could be estimated using linear interpolation. This is discussed in detail in Chapter 5.

The methodology (Figure 3.10) for analysis of wastewater influent volumes with respect to mid-century projected changes in precipitation variables was based on the regression models of the historical analysis, the background to which are presented in Section 3.4.1. Detailed methodologies using data in Sections 3.2.2 are illustrated in Chapter 5.

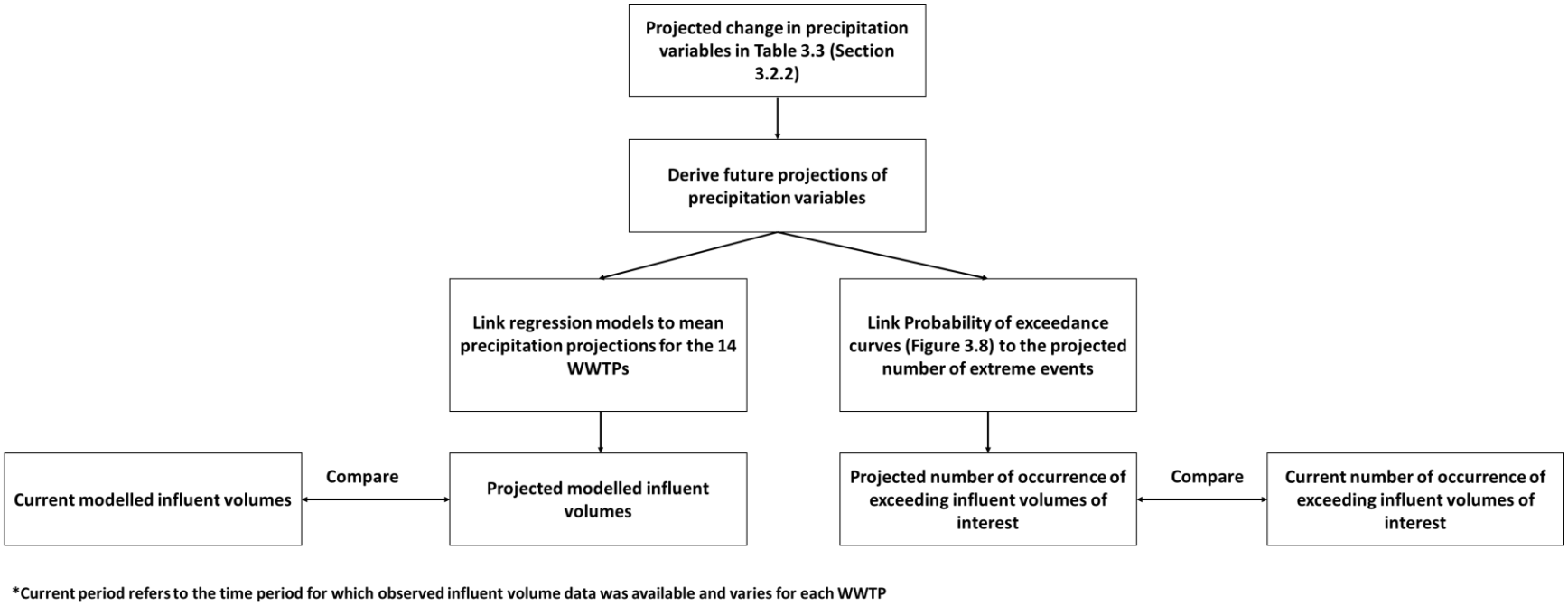

Figure 3.10: Broad methodology of analysing future impacts of precipitation projections on wastewater influent volumes

3.4.3. Impact assessment on wastewater influent volumes using land use land cover datasets

LULC classification technique was performed to classify the satellite images obtained (Detailed in Chapter 6 Section 6.3.2). For this research the random forest classification technique was adopted. Random forest is a machine learning classifier algorithm which performs classification based on decision trees which are its building blocks. It is one of the most commonly used classifiers (Kulkarni et al., 2016) that uses data features to classify into desired number of classes. The random forest algorithm builds numerous decision tree classifiers using bagging and feature randomness on several sub samples of the dataset. Decision tree classifiers are more efficient than single stage classifiers as decisions are being made at multiple levels (Kulkarni et al., 2016). It uses averaging to control overfitting and to improve the predictive accuracy. One of the main advantages of this classification method is its accuracy, which is considered the best among all the current classification algorithms such as support vector machines, artificial neural networks etc (Kulkarni et al., 2016).

Hence random forest classifier was used to classify landuse classes of Landsat 5 and 8 satellite images were classified, with a focus on built-up areas. A time-series analysis of the built-up areas was carried out to estimate the change in urban cover over the years in ArcGIS Pro. This urban dynamic was assessed to understand the relationship between impermeable surface area and the amount of wastewater influent volume incoming into the inlets of the WWTPs resulting from surface runoff. The detailed methodology of LULC classification and the trend analysis are presented in this thesis in Chapter 6. The broad methodology for impact assessment of LULC change on influent volumes followed in this research is shown in Figure 3.11.

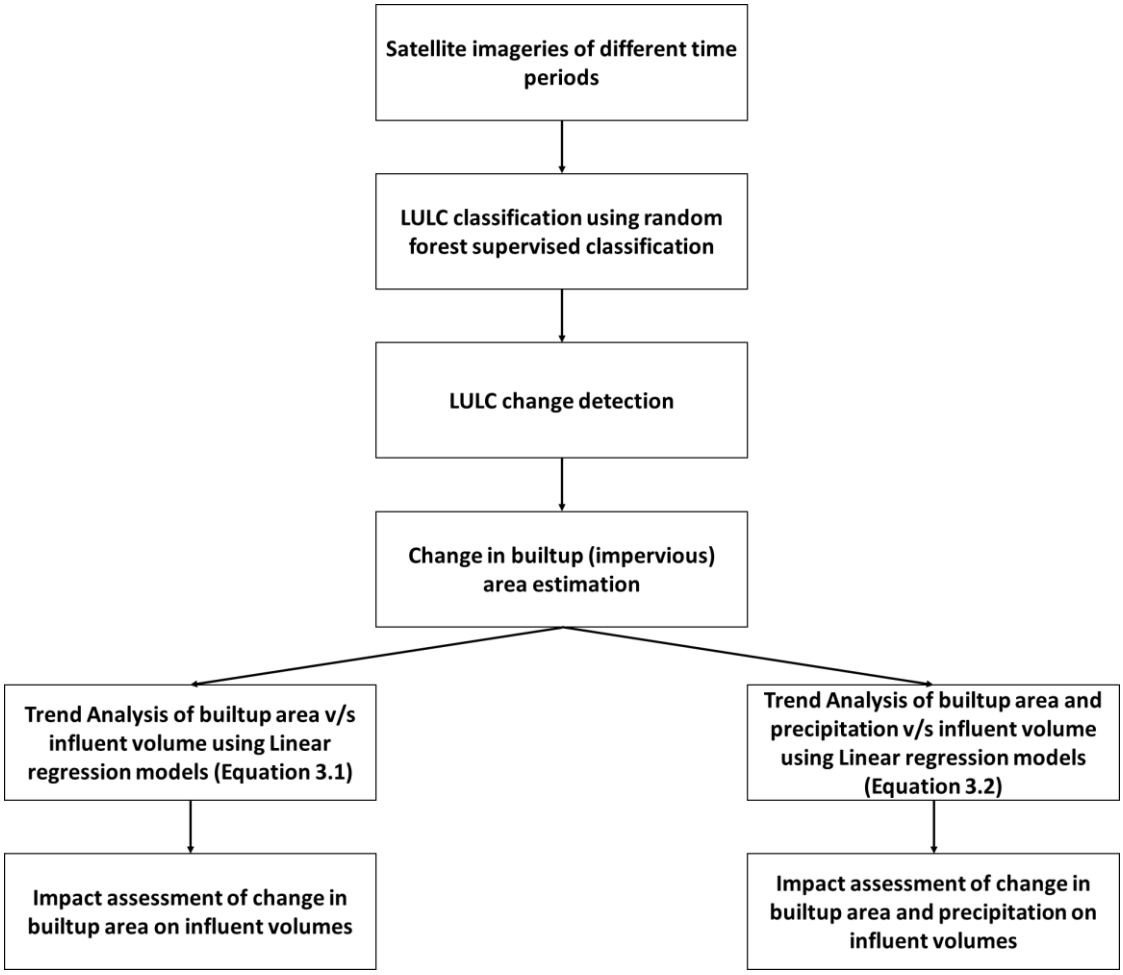

Figure 3.11: Broad methodology of analysing the impacts of urbanisation on influent volumes

3.5. Conclusions

The literature review in Chapter 2 established that studying the influent volume characteristics is very crucial to understand the impacts of various drivers on WWTPs. The novelty of this research lies in the investigation of the impacts of the different aspects of precipitation change (current and future), tidal levels, river levels, and urbanisation on influent volumes. Chapter 2 also revealed that literature is dominated by the use of computer-based software/ models which are pre-defined with artificially derived sewer system characteristics. This has emerged from the challenge of data unavailability of observed influent volumes. However, these models are not effective because they do not cater to the specific local characteristics of each WWTP and therefore, are associated with large uncertainties. The datasets used in this study are typical of what are available from WWTPs and thus, the objective was to develop these methodologies described in

this chapter using these available observed datasets in the best way possible to build models. These models could detect trends in influent volumes based on the different parameters, under practical data constraints. One of the key contributions of these models was the ability to capture local influent volume characteristics at local WWTP scale as a function of specific local features of precipitation, tidal and river levels, and land use land cover change. Another significant contribution of these models was that they could be linked to future precipitation projections under different climate change scenarios. As the significance of wastewater influent volume characteristics has already been established, it essentially demonstrates how future changes in precipitation variables would drive these characteristics and eventually impact WWTP operations in future. Hence the future impact analysis methodology in this research introduces the concept of using data driven models to investigate the evolution of wastewater influent volumes in the future, a novelty of this study. This will be very helpful for the wastewater utilities to take informed decision in their planning and implementation of adaptation strategies to fulfil the sustainable vision of building resilient wastewater infrastructure, thereby contributing towards good health of the communities and the environment. Moreover, these methodologies could be adapted to perform similar analyses globally.

4. PRECIPITATION, TIDAL AND RIVER LEVEL IMPACTS ON INFLUENT VOLUMES OF COMBINED WASTEWATER COLLECTION SYSTEMS: A REGIONAL ANALYSIS

4. Precipitation, tidal and river level impacts on influent volumes of combined wastewater collection systems: A regional analysis

4.1. Overview

The aim of this chapter was to analyse the variations of precipitation and their link with influent volumes. The chapter adopts a new approach to understand influent volume variations by taking into consideration, the combined and individual impacts of tidal and river levels in addition to precipitation; a topic that has not been examined in literature to date. The chapter presents the detailed methodology of using the observed spatio-temporal datasets of the 14 WWTPs with combined sewerage systems, discussed in Chapter 3, to develop models and curves that could be used to determine the response characteristics of influent volumes specific to each WWTP and across all WWTPs. The effectiveness and predictive capacity of these models and the usability of the curves are discussed with the help of examples.

This chapter has been published in Results in Engineering (Saikia, S.D., Ryan, P., Nuyts, S., Clifford, E. (2022). Precipitation, tidal and river level impacts on influent volumes of combined wastewater collection systems: A regional analysis. *Results in Engineering*, 15, 100588. https://doi.org/10.1016/j.rineng.2022.100588

4.2. Introduction

Wastewater treatment plants (WWTPs) that treat both foul and storm wastewater (combined sewerage systems) will experience significant pressure due to changing precipitation patterns and other geophysical parameters. A majority of the studies in the wastewater industry related to precipitation impacts are limited to investigating CSOs and performance of the sewer network (Astaraie-Imani et al., 2012; Butler et al., 2007; Gooré Bi et al., 2015; Hussain et al., 2022; Mailhot et al., 2015; Mohammed et al., 2021; Shakeri et al., 2021; Schroeder et al., 2011). However, influent volumes are also an important parameter to consider (Langeveld et al., 2013; Li et al., 2018; Mines et al., 2007). On days with heavy precipitation intensity, the influent volumes do not match with the effluent volumes due to overflow of untreated wastewater or diversion of excess water to storage tanks as discussed in Chapter 2 Section 2.3.1. Since influent volumes are measured at the inlet of WWTPs, managing this parameter will help ensure the smooth functioning of WWTPs with CSSs and reduce the incidences of CSOs.

Limited work has been done to understand the links between factors such as tidal and river levels, precipitation, and influent volumes to WWTPs (Chapter 2). Another key challenge was data unavailability and hence conventional methods of investigating impacts on WWTPs and their associated sewer systems use hydraulic models and limited observed data for model calibration and validation. This chapter uses extensive range of observed datasets of precipitation, tidal level, river level and influent volumes (Chapter 3, Section 3.2.1) to define the relationships among these variables. This will help stakeholders in wastewater management with long-term planning and investment including responses to changing precipitation patterns and their impact on wastewater infrastructure.

4.3. Methods

4.3.1. Daily data analysis

Regression analyses of daily influent volume was carried out based on three predictor variables at a daily scale 1) daily precipitation, 2) maximum tidal level and 3) mean river level.

4.3.1.1. Precipitation regression analysis

SLR was carried out to assess the relationship between daily precipitation and daily influent volume data for each WWTP. Lag-time was analysed by comparing influent volume at any given day (d) to precipitation of up to 3 previous days (i.e., daily precipitation at day d-1, d-2, and d-3) for all WWTPs individually. Lag time was studied in intervals of 1 day to match the resolution of influent data.

4.3.1.2. Tidal level regression analysis

SLR was used to analyse the relationship between daily maximum tidal level and daily influent volume for all relevant WWTPs, on all days and for zero rainfall days separately (as defined in Chapter 3 Section 3.2.1.2).

4.3.1.3. River level regression analysis

SLR analysis was carried out to assess the potential impact of daily mean river levels (wherever relevant) on daily influent volumes for all days and zero rainfall days separately.

4.3.1.4. Multiple variable regression analysis

MLR was used to analyse the variation of influent wastewater volumes for all days and separately for zero rainfall days (i.e., dry weather flow to the WWTP), with respect to the potential combined influence of 1) daily precipitation and daily maximum tidal levels, 2) daily precipitation and daily mean river level, 3) daily maximum tidal level and daily mean river level and, 4) daily precipitation, daily maximum tidal level and daily mean river level.

4.3.1.5. WWTP influent volumes response to precipitation intensity

Daily precipitation was categorised for each WWTP as outlined in Table 4.1. The influent volumes under each precipiation category were then checked for statistically significant differences using the Kruskal Wallis test. A Pairwise Wilcoxon test was performed as a post-hoc or a posteriori statistical analysis to determine statistically significant differences between each pair of categories.

Table 4.1: Precipitation categories based on percentile values for all WWTPs

Category	Percentile range for daily precipitation	Category Name
1	25^{th} percentile	No precipitation
2	$>25^{th}$ percentile $\leq 50^{th}$ percentile	Very low precipitation
3	$>50^{th}$ percentile $\leq 75^{th}$ percentile	Low precipitation
4	$>75^{th}$ percentile $\leq 95^{th}$ percentile	Moderate precipitation
5	$>95^{th}$ percentile $\leq 99^{th}$ percentile	Heavy precipitation
6	$>99^{th}$ percentile	Extreme precipitation

Categories were later merged if there were no statistically significant differences between the daily mean influent volumes for precipitation categories. For example, in the case of some WWTPs where the frequency of heavy intensity precipitation events was limited for some agglomerations, bands 5 and 6 (categories heavy and extreme precipitation respectively) were merged. Therefore these precipitation categories were unique to each WWTP and represented its local precipitation characteristics.

Because the daily influent volumes observed were also distinctive to the treatment capacities and sizes of each WWTP, the unique response characteristics of each WWTP to their individual precipitation categories were also studied in detail. This was carried out by developing a method to determine the likelihood that influent volumes would exceed any given limit as the result of specific precipitation events.

4.3.2. Monthly data analysis

Daily data analysis focusing on precipitation, river, and tidal level, can give insights into the impacts of these variables on influent data, however they can be quite variable and monthly analysis can be used to help determine long-term hydraulic issues at a WWTP. Li et al., (2018) previously reported that the relationship between precipitation and influent data of CSOs at a monthly scale can be depicted by linear models. In addition, maximum monthly average daily influent flows are often used for the hydraulic design capacity (Mines et al., 2007).

In this study, SLR was used to assess the separate impacts of; 1) monthly average daily precipitation, 2) number of wet days in a month and, 3) number of zero rainfall days in a month on monthly average daily influent volume. These precipitation parameters were also analysed together as predictor variables in an MLR model, to estimate their combined effects on monthly average daily influent volume. However, as discussed in Chapter 3 Section 3.4.1, bivariate correlation analysis and VIF estimation was carried out to assess multicollinearity. This resulted in the removal of number of wet days from the MLR analysis which considered the monthly average daily precipitation and number of zero rainfall days as predictor variables.

In the case of all analysis, the coefficient of regression/determination (denoted by R^2 or adjusted-R^2 in case of MLR), p value, slope coefficient of each predictor variable, and root mean square error (RMSE) were evaluated. The RMSE is in the units of the response

variable, in this case m^3/day. For both simple and multiple linear regression, R^2 (or adjusted R^2) values obtained were compared and qualitatively assessed based on Table 4.2, in line with Mines et al., (2007). The Time Web (2006) also depicts similar correlation coefficient data. The values of correlation coefficients between similar variables for similar studies also represent similarities (Li et al., 2018; Mines et al., 2007).

Table 4.2: R^2 values and degree of correlation (Mines et al., 2007 after Franzblau, 1958)

R^2	Degree of Correlation
0 to 0.04	No or negligible correlation
0.04 to 0.16	Low degree of correlation
0.16 to 0.36	Moderate degree of correlation
0.36 to 0.64	Marked degree of correlation
0.64 to 1	High degree of correlation

4.3.3. Pooled data analysis

To develop models at daily and monthly scales, that could be used across all the WWTPs, all datasets for each WWTP, irrespective of the different temporal range of data, were pooled together for two separate models. These models corresponded to two different time periods, 1) across all years of data for all WWTPs and 2) across 2016 – 2018, which represents the time period of data availability for all the WWTPs facilitating equal influence for each WWTP. Only precipitation variables were considered for this analysis because these were available across all the WWTPs. However, because the influent volume varies by orders of magnitude between some of the WWTPs in terms of treatment capacity/design population, the daily influent volume (on daily basis) and average daily influent volume (on monthly basis) data were normalised using Equation 4.1 and 4.2 respectively.

$$Q'_D = \frac{Q - Q_{min}}{Q_{max} - Q_{min}} \quad \text{(Eq. 4.1)}$$

where $\boldsymbol{Q'_D}$ is the normalised daily influent volume, ranging between 0 – 1, $\boldsymbol{Q}$, $\boldsymbol{Q_{min}}$ and $\boldsymbol{Q_{max}}$ represent the observed values of daily influent volume, the minimum and maximum values of the observed daily influent volumes of each plant respectively.

$$Q'_M = \frac{ADIV - ADIV_{min}}{ADIV_{max} - ADIV_{min}} \quad \text{(Eq. 4.2)}$$

where $\boldsymbol{Q'_M}$ is the normalised monthly average daily influent volume, ranging between 0 – 1, $\boldsymbol{ADIV}$ represents the observed values of monthly average daily influent volume, $\boldsymbol{ADIV_{min}}$ and $\boldsymbol{ADIV_{max}}$ means the minimum and maximum values of the observed monthly average daily influent volumes respectively.

SLR and MLR were used to analyse the relationship between daily precipitation and $\boldsymbol{Q'_D}$ (daily scale) and average daily precipitation, number of wet and zero rainfall days in a month (individually and combined) and $\boldsymbol{Q'_M}$ (monthly scale) across all the WWTPs respectively. Modelled values of normalised daily influent volume and normalised monthly average daily influent volume were then calculated using Equations 4.3 and 4.4 respectively. However, as mentioned in Chapter 3 Section 3.4.1 and section 4.3.2 of this chapter, number of wet days in a month was discarded from the pooled monthly MLR model (Equation 4.4) due to presence of multicollinearity.

$$Q'_{Dwdy} = \beta P_{wdy} + c + \in \quad \text{(Eq. 4.3)}$$

where $\boldsymbol{Q'_{Dwdy}}$ is the predicted normalised influent volume of WWTP $\boldsymbol{w}$ in day d and year y, P is daily precipitation and $\boldsymbol{\beta}$ is its coefficient.

$$Q'_{Mwmy} = \beta_1 ADP_{wmy} + \beta_2 ZRD_{wmy} + c + \in \quad \text{(Eq. 4.4)}$$

$\boldsymbol{Q'_{Mwmy}}$ is the predicted normalised monthly average daily influent volume of WWTP $\boldsymbol{w}$ in month $\boldsymbol{m}$ and year $\boldsymbol{y}$; $\boldsymbol{ADP}$, and $\boldsymbol{ZRD}$ are average daily precipitation and number of

zero rainfall days in a month respectively; $\boldsymbol{\beta_1}$ and $\boldsymbol{\beta_2}$ are the coefficients related to these variables obtained from the pooled regression analysis. $\boldsymbol{c}$ is the intercept and $\in$ is the residual of the model in both the equations. The model coefficents can be interpreted as the change in normalised influent volume with unit change in each of the predictor variables.

From these modelled normalised values, daily influent volume and monthly average daily influent volume were then calculated as per Equations 4.5 and 4.6 respectively.

$$Q_{PD} = Q'_{Dwdy} * [(Q_{max} - Q_{min})] + Q_{min} \quad \text{(Eq. 4.5)}$$

$$Q_{PM} = Q'_{Mwmy} * [(ADIV_{max} - ADIV_{min})] + ADIV_{min} \quad \text{(Eq. 4.6)}$$

where, Q_{PD} and Q_{PM} are the predicted daily influent volume and monthly average daily influent volume respectively. RMSE was estimated by analysing the difference between Q_{PD} and Q and Q_{PM} and ADIV. Linear regression analysis was carried out between the observed and predicted average daily influent volume for the two time periods to assess the predictive capacity of the two pooled models.

Additionally, in order to assess the performance of the pooled model in making generalisable predictions, the Leave One Out Cross Validation technique was used. This method is a commonly used approach where each set of observations, in this case, WWTPs, is considered as the validation set whereas the remaining sets of observations are considered as the training set. Hence, in order to carry out this technique, a regression model is developed using the ADP, ZRD (predictor variables) and ADIV data (response variable) of 13 WWTPs, leaving one WWTP at a time. The observed values of ADP and ZRD of the WWTP which was left out (the validation set) was then incorporated into the regression model to predict ADIV values. This can be explained with the help of an example. In the first run, WWTP 1 was left out and a pooled regression model ws developed with data of WWTP 2 to 13. The observed data of WWTP 1 was then incorporated into this model to predict the ADIV values of WWTP 1. This was repeated

13 more times for the remaining WWTPs. Model error and RMSE values were recorded for each run.

4.4. Results and discussion

The full daily and monthly results of the analysis for each of the 14 WWTPs are discussed in this section with an initial focus on WWTP 8 as an example. The response of influent volume characteristics and pooled WWTP results are also described. As mentioned in Chapter 3 Section 3.4.1, all MLR analysis results presented in this paper has taken into account multi-collinearity amongst variables and only demonstrates the variables with bivariate correlation coefficient and VIF less than 0.80 and 5 respectively.

4.4.1. Daily analysis results

As described in Chapter 3 Section 3.4.1, WWTP 8 was used to identify the initial variables that would have a significant impact on the daily influent volumes. The daily scale results for WWTP 8 are summarised in Table 4.3. All model results were found to be statistically significant at a 95% level of confidence. The impact of the various variables from Table 4.3 are discussed in-turn in the sub sections below.

Table 4.3: Regression results at daily scale for WWTP 8 (pilot case-study) for all years 2011 – 2018

Variables modelled	R^2/Adjusted R^{2***}	Model Error	RMSE (m^3/day)
Precipitation Analysis			
Precipitation v/s influent volume	0.27	18%	10364
Precipitation v/s influent volume with 1-day lag-time	0.23	19%	10687
Tidal Level Analysis			
Maximum tidal level* v/s influent volume	0.16	20%	11170
Maximum tidal level* v/s dry weather flow	0.37	11%	5009

River Level Analysis			
Mean river level* v/s influent volume	0.53	18%	8385
Mean river level* v/s dry weather flow	0.46	13%	6264
Multiple Variable Analysis			
Precipitation and maximum tidal level* v/s influent volume	0.37	17%	9632
Precipitation and mean river level* v/s influent volume	0.67	12%	6962
Maximum tidal level and mean river level** v/s influent volume	0.53	15%	8382
Maximum tidal level and mean river level** v/s dry weather flow	0.46	13%	6222
Precipitation, maximum tidal level, and mean river level** v/s influent volume	0.67	12%	6961
*** For the relevant WWTPs with maximum tidal level or mean river level data**			
**** For the relevant WWTPs with both maximum tidal and mean river level data**			
***** Adjusted R^2 is reported for all the multiple variable analysis**			

4.4.1.1. Precipitation regression analysis results

For WWTP 8, the relationship between daily precipitation (with and without lag-time – see Section 4.3.1.1) and daily influent volumes indicated a moderate degree of correlation without lag-time (18% model error and $R^2 = 0.27$) and with one day lag-time (19% model error and $R^2 = 0.23$). As such, the regression analysis between daily precipitation and daily influent volume resulted in a higher degree of correlation and lower model error when compared to the application of a 1 day lag-time (i.e. no lag-time effect was identified, in the case of this WWTP). The R^2 and model errors for the daily analysis indicate that there are several other factors (e.g., soil moisture content, level of infiltration into the sewer network, evapotranspiration, water consumption) which may influence the

changing influent volume at a daily basis. These factors are, however, outside the scope of the paper.

In relation to the daily precipitation and influent volume analysis for the remaining 13 WWTPs, daily precipitation was found to be statistically significant in explaining the variation in daily influent values. However, the relationship between these two variables, defined by R^2, was observed to range from very low to marked correlation (R^2 = 0.03 – 0.38) and model errors ranged from 18% – 56% across all plants (Appendix I). In relation to lag-time analysis, it was observed that for 7 of the remaining 13 WWTPs, representing all the network categories (refer to Chapter 3 Table 3.2), a 1-day lag-time between precipitation and daily influent volume improved model error and R^2 values (full details in Appendix I). Due to the differences in the relative capacity of stormwater storage across the WWTPs, and the presence of impervious surfaces, it is logical that the the lag-time characteristics would vary. However, for all WWTPs, lag-time greater than 1-day resulted in a decrease in the R^2 and an increase in model error between daily precipitation and daily influent volume. Sub-daily data, which was not available for this study, would facilitate a more thorough investigation into lag-time.

4.4.1.2. Tidal level regression analysis results

For all relevent WWTPs (2, 4, 8, 10, and 12), on all weather days, daily maximum tidal level showed a low degree of correlation (R^2 = 0.04 – 0.16) with daily infuent volume. However, the analysis did indicate that examining the impact of tidal elevation may be a good means of predicting variations in dry weather flow. Indeed, for WWTP 8, the lowest model error (11%) occurred when assessing the relationship between the dry weather flow with the daily maximum tidal level. This may be due to infiltration of saline water into the sewer system at high tides. For the other four WWTPs (WWTPs 2, 4, 10 and 12) with tidal data, model errors ranged between 13% and 38% when analysing the impacts of maximum daily tidal level on dry weather flow. This can reflect site-specific infrastructure issues such as the height above sea level of any storm overflows, the location of the WWTP relative to any storm overflows to the sea or the presence of backflow prevention valves.

4.4.1.3. River level regression analysis results

For WWTP 8, the relationship between daily mean river level and daily influent volume had a marked degree of correlation ($R^2 = 0.53$) for all weather days, and decreased to $R^2 = 0.46$ when only taking into account dry weather flow. WWTP 8 is located in a city that is relatively flat with some low hills in suburban areas, has a short tidal river which is fed by a lake with a relatively large catchment (> 3,100 km2) and thus a surcharge to the sewerage system due to high river levels is not unexpected. However, for WWTP 8, flooding in the urban area does not occur despite frequent occasions of high river levels. Therefore its is more likely that the backflow of due to absence of non-return valves for this specific WWTP.

For the remaining two WWTPs with local rivers (WWTPs 1 and 10), daily mean river level showed a marked to high degree of correlation with daily influent volume (R^2 values 0.49 – 0.61 and model errors 16% – 24%). For dry weather flows, R^2 values were observed to be 0.57 – 0.60 with model errors 13% - 18%. The rivers for these two agglomerations are also tidal rivers and hence show similar characteristics to WWTP 8. The reason for the comparatively weaker tidal effect (as opposed to river level) might be because the invert levels of storm overflows are possibly higher than the maximum tidal level for this WWTP, which would explain the minimum impact of tidal level on wastewater influent volumes. Additionally, as mentioned in Section 4.4.1.1, there are several other factors such a soil moisture content, evapotranspiration etc. that may influence the effect of daily precipitation on wastewater influent volumes. As these variables are not considered in this research, variation in daily influent volumes can only be partially explained using daily precipitation alone. Daily mean river level is found to better explain the variation in daily influent volume than the daily precipitation and the daily maximum tidal level. It is to be noted that rain and river level were found to be not correlated for all the WWTPs.

4.4.1.4. Multiple variable regression analysis results

The previous sub-section showed that precipitation, tidal level, and river level explain to some degree the variation in daily influent volume. If all three variables are considered together, daily precipitation and river level were found to be statistically significant and a high degree of correlation is found between the MLR predictor variables and influent

volumes for the relevant WWTPs: adjusted R^2 = 0.67 for WWTP 8, and adjusted R^2 = 0.52 for WWTP 10. In addition, model errors are lowest when all three variables are considered together for WWTP 10 (23%). It was observed that for WWTP 8, the R^2 and model error remain unchanged when predictor variables influent volume and river level were considered as compared to when all the three variables were considered. It indicated that river level is a stronger contributor when compared to tidal level for this agglomeration for reasons discussed in Section 4.4.1.3 (Refer to Section 4.4.1.3).

As such, the analysis shows that precipitation, tidal level, and river level are very likely to explain a significant component of daily variations in influent volume for the selected WWTPs. This insight can be used to examine additional WWTPs with similar characteristics or for hydraulic design capacity of future WWTPs. The full set of tidal and river level analysis for the relevant WWTPs are presented in Appendix I.

4.4.1.5. Response of WWTP influent volumes to precipitation intensity

This analysis categorised daily precipitation and investigated the "probability" of a given daily precipitation, resulting in exceedance of a daily influent volume, in the monitoring period of each WWTP. This section details the response characteristics of influent volume to precipitation intensity (Table 4.1) for WWTP 8 with the remaining 13 WWTPs presented in Appendix I. The specific precipitation categories for WWTP 8 are detailed in Table 4.4. The Kruskal Wallis test and the Pairwise Wilcoxon test confirmed a statistically significant difference between the daily influent volumes under each category.

Table 4.4: The daily precipitation categories for WWTP 8 based on percentile evaluation

Bands	Thresholds	Category Name
1	Rain (mm/day) = 0	No precipitation
2	0 < Rain (mm/day) <= 1.2	Very low precipitation
3	1.2 < Rain (mm/day) <= 5.4	Low precipitation

4	5.4 < Rain (mm/day) <= 15	Moderate precipitation
5	15 < Rain (mm/day) <= 25.6	Heavy precipitation
6	Rain (mm/day) > 25.6	Extreme precipitation

Figure 4.1 depicts all daily precipitation plotted against daily influent volume for WWTP 8. While there is significant spread in the data (which might occur due to seasonal factors such as influx of tourists, but also river and tidal levels, ground water conditions, soil moisture content, etc.) a clear upward trend in influent volume with increasing precipitation intensity is apparent, albeit with notable variations in influent volumes during zero or low precipitation categories. The maximum daily influent under each precipitation category is observed to be around 80,000 – 85,000 m^3/day (with a small number of higher values observable). This may indiciate some level of storm overflow occuring beyond this point.

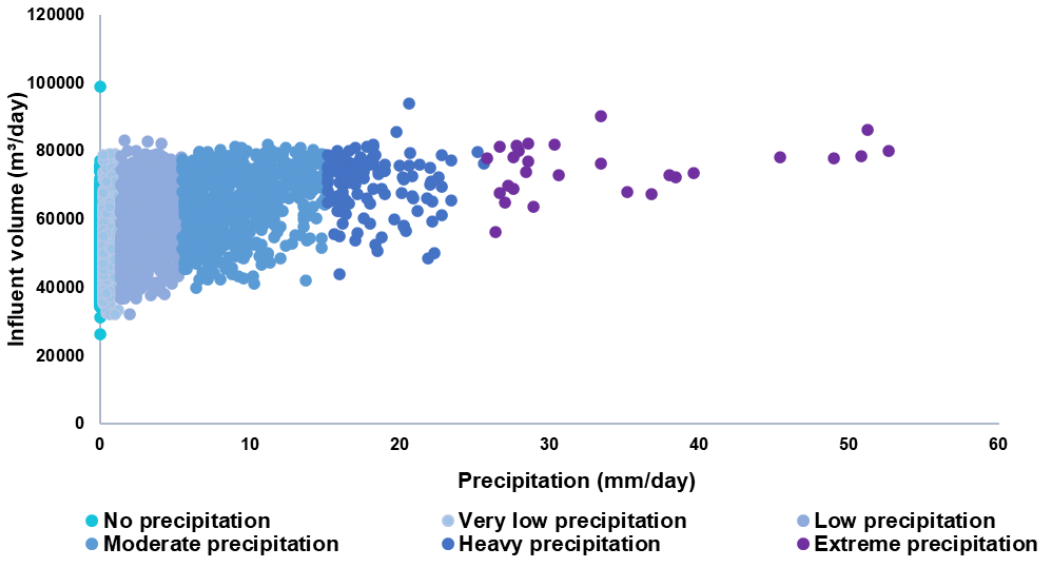

Figure 4.1: Daily precipitation v/s Daily influent volume plot depicting the precipitation categories for WWTP 8 across 2011 – 2018

Figure 4.2 shows the probability of exceedance curves which indicate the percentage of data points that exceed a given influent flow volume for any precipitation category in the 2011 – 2018 period for WWTP 8. For example, on zero rainfall days (category 1) less than 20% of influent flows were above 60,000 m^3/day whereas for days with high precipitation (category 5) more than 80% of influent flows were above 60,000 m^3/day.

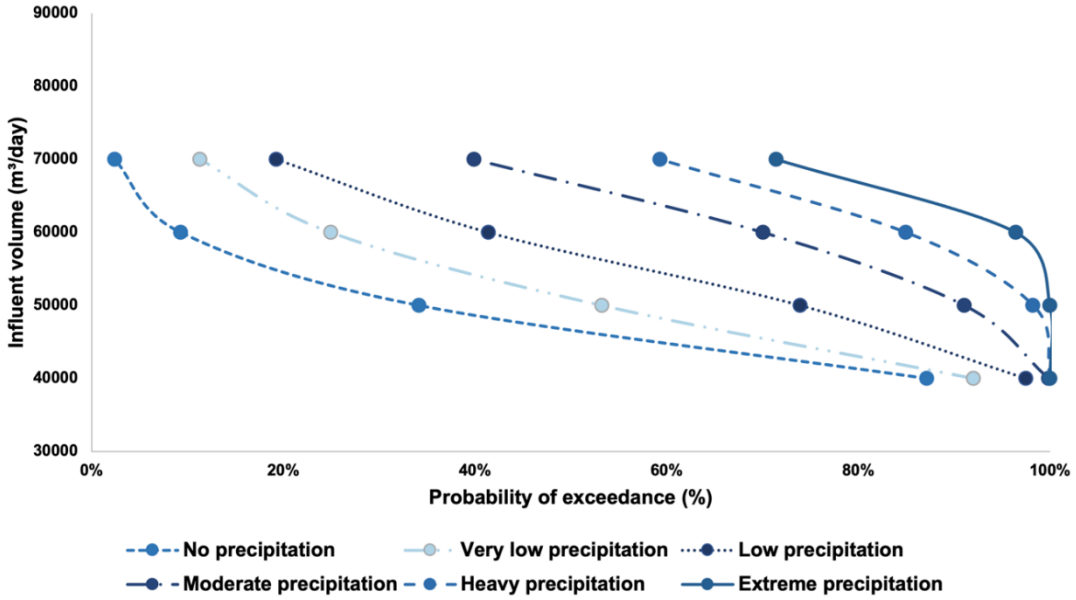

Figure 4.2: PoE curves showing likelihood, in percentage, of influent volumes exceeded by the different precipitation categories for WWTP 8 across 2011 – 2018

The frequency of occurrence of various influent volumes or storm overflows, from a particular WWTP, can be analysed using these probability of exceedance curves developed for a particular WWTP and account for future projected changes in heavy precipitation events. Indeed, the curves are helpful in representing the different characteristics of the WWTPs that are reflected in their precipitation patterns and hydraulic response characteristics. In addition, they illustrate the link between heavy precipitation events and CSO, which can be damaging to receiving waterbody ecosystems and public health (O'Sullivan, 2020). Precipitation categories and probability of exceedance curves were developed for all the 14 WWTPs and are presented in Appendix I.

4.4.2. Monthly analysis results

In order to take into account the impacts of monthly patterns of precipation, monthly average daily data is analysed here. This does not account for daily variation but can account for seasonal factors such as tourism, rainfall, presence of university students, festivals etc. Figure 4.3 highlights the R^2 and RMSE of these three variables independently. As mentioned in Section 4.3.2, the number of wet days per month was omitted from the MLR , hence the results demonstrating the influence on monthly

average daily influent volume took into account only the remaining two predictor variables.

It is clear that all WWTPs showed marked to high degree of correlation between the three variables independently and influent volumes, except for WWTP 4 which showed a moderate degree of correlation between monthly average daily precipitation and monthly average daily influent volume. Although several factors will have an influence on the correlation for WWTP 4, it is most likely caused by; 1) a number of incidents of stormwater overflow during moderate and high precipitation events as reported in the Annual Environmental Report (AER) by Irish Water (Irish Water, 2018) and 2) upgrades and improvements carried out in the CSS of WWTP 4 during the monitoring period.

Overall, when looking at the impact of precipitation on influent volumes, the monthly analysis shows higher R^2 values compared to the daily analysis across all WWTPs. In particular, the daily R^2 values ranged between 0.03 and 0.38, whereas the monthly R^2 values ranged between 0.26 and 0.83; this is not unexpected given the variations in daily data.

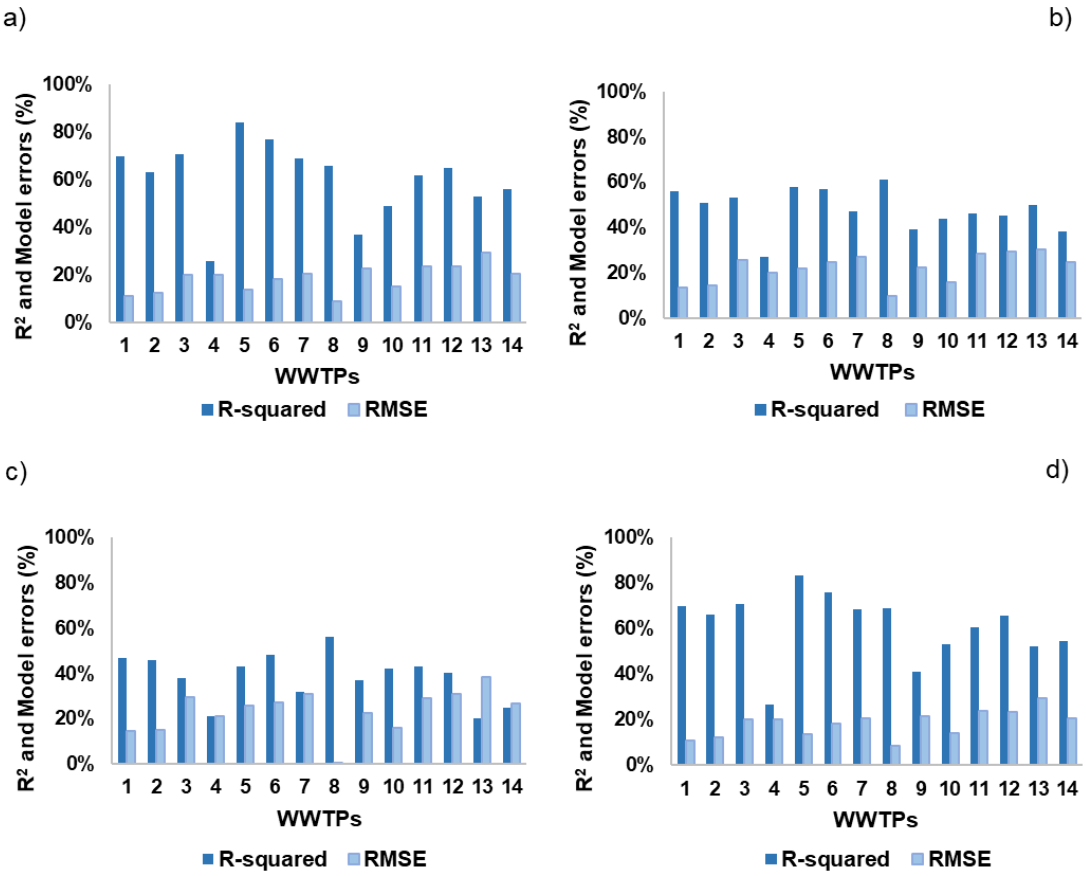

Figure 4.3: Monthly analysis results across all WWTPs, with a) Monthly average daily precipitation v/s monthly average daily influent volume, b) Number of wet days in a month v/s monthly average daily precipitation over a month, c) Number of zero rainfall days in a month v/s monthly average daily influent volumes, and d) Monthly average daily precipitation and number of zero rainfall days in a month v/s monthly average daily influent volume

Six out of the 14 WWTPs (WWTPs 2, 4, 8, 9, 10 and 12) showed higher R^2 values or lower model errors when monthly average daily precipitation and number of zero rainfall days in a month were considered together to explain the variation in monthly average daily influent volumes as opposed to SLR analysis when these variables were considered separately. The remaining WWTPs showed approximately equal model statistics (R^2 and model errors) when compared to the single variable analysis results of monthly average daily precipitation and monthly average daily influent volumes. The results reiterate that although monthly average daily precipitation is the strongest significant contributor and positively correlated to influent volumes, the number of zero rainfall days (negatively correlated) can aid in explaining variations in monthly average daily influent volumes. It

is likely it can help explain some impacts due to rainfall intensity i.e., for any given monthly precipitation a reduced number of zero rainfall days would indicate lower intensity rainfall. This is in line with (Li et al., 2018), taking into account the varying precipitation and hydraulic characteristics across the WWTPs.

4.4.3. Pooled WWTP analysis results

Pooled models were developed to provide regional/national level insights into the impact of precipitation on influent volumes across all WWTPs. As stated in Section 4.3.3, two separate models were developed with different temporal datasets: 1) across all available years of data for the different WWTPs, and 2) across 2016 – 2018, which representes the time period of data availability covering all WWTPs. Taking into account the previous findings (i.e. the variability of precipitation on a daily basis compared to a montly basis), the impact of these two models are highlighted by comparing them with the results of individual daily model (Section 4.4.1.1) and individual monthly model (Section 4.4.2). It should be noted that only precipitation analysis is taken into account in the models as this is the only parameter available for all 14 WWTPs.

4.4.3.1. Daily Pooled Model

The daily pooled models were developed using Equation 4.3, with model regression coefficient of $\beta = 0.0135724$, $c = 0.2523078$, p value = <0.001 and $\in = 0.001769$. Daily precipitation was found to be statistically significant at a 95% level of confidence. Table 4.5 shows the model errors of the individual daily model (from Section 4.4.1.1), and the pooled daily models for all years, and the pooled model for 2016-2018.

The model errors for the daily pooled models are observed to be significantly high and probably render these pooled models unsuitable for further use at this scale. This may be due to factors such as the variability of precipitation between WWTPs, differences in the sewer networks and urban population density. Indeed, it may be very challenging to develop pooled models at a daily level basis for WWTPs. Hence RMSE was also not reported further for the daily model.

Table 4.5: Model errors of multiple linear regression analysis of Individual v/s Pooled daily WWTP models

WWTP	Individual Daily Model	Pooled Daily Model	
		All years	2016-2018
1	24%	39%	25%
2	23%	36%	27%
3	40%	50%	42%
4	26%	53%	24%
5	47%	82%	48%
6	47%	64%	46%
7	39%	59%	37%
8	18%	24%	27%
9	32%	37%	36%
10	32%	44%	33%
11	47%	100%	63%
12	51%	100%	80%
13	56%	100%	100%
14	48%	100%	88%

4.4.3.2. Monthly Pooled Model

The monthly pooled models were developed using Equation 4.4. Table 4.6 shows details about the model regression coefficients of the Equation, where β1 and β2 are the model regression coefficients of monthly average daily precipitation and number of zero rainfall days in a month respectively.

Table 4.6: Model coefficients (Equation 4.4) of the Pooled monthly multiple linear regression models developed in this research

	Pooled all-years model			Pooled 2016-2018 model		
	Coefficient	***Error***	***p-value***	***Coefficient***	***Error***	***p-value***
β_1	0.08458	0.00401	<0.001	0.09882	0.00674	<0.001
β_2	-0.00172	0.00127	0.17357	-0.00597	0.00191	<0.01
Intercept	-0.081667			0.086451		
Datapoints	1097			495		

Table 4.7 highlights the model errors of the individual monthly model (from Section 4.4.2), and the pooled monthly models for all years and for 2016-2018, from the adapted Equation 4.4.

Table 4.7: Model errors and RMSE of multiple linear regression analysis of Individual v/s Pooled monthly WWTP models

WWTP	**Individual Monthly Model**		**Pooled Monthly Model**			
			All years		**2016-2018**	
	Model error	**RMSE (m^3/day)**	**Model error**	**RMSE (m^3/day)**	**Model error**	**RMSE (m^3/day)**
1	11%	5097	14%	6806	16%	7369
2	12%	12106	12%	12484	10%	10567
3	20%	1776	30%	2640	29%	2499
4	20%	1782	38%	3376	9%	913
5	14%	33	27%	66	14%	34
6	18%	1768	21%	2095	21%	1959
7	21%	1918	26%	2441	21%	1829
8	8%	4671	9%	5123	9%	5428
9	22%	2496	23%	2649	25%	2457
10	14%	57412	16%	67680	18%	73048
11	24%	7101	26%	7873	25%	7553
12	23%	1234	28%	1478	23%	1243
13	29%	811	31%	907	31%	911

14	21%	1241	24%	1494	21%	1220

The model errors reveal that, in general, individual WWTP models showed better accuracy, as they take into account WWTP specific factors rather than the generic pooled WWTP model, i.e., model errors are lower for individual monthly models compared to both pooled models. Nevertheless, for 10 out of 14 WWTPs the pooled models showed only a 3% difference in model error when compared to individual WWTP models, with large and medium WWTPs representing the best results accross all the pooled models. The RMSE values of the pooled models also reflect comparable errors to individual WWTP models. For example for WWTP 1, the RMSE was found out to 6806 m^3/day for the all years pooled model. This was considered a good measure of error because the observed data for WWTP 1 was in the range of 32000 – 72000 m^3/day. The model errors above are similar to those reported in Mines et al., (2007), Steinschneider et al., (2013) and Li et al., (2018) – albeit there are different variables being analysed.

The 2016 – 2018 pooled model showed lower model error and RMSE when compared to the all-years pooled model for almost all WWTPs. This may be explained by a number of factors including (i) the all-years pooled model is more heavily influenced by WWTPs with the maximum amount of data and (ii) the 2016 – 2018 model represents the most updated/recent networks which accounts for recent changes (if any) to the networks and potential changes in weather patters experienced in recent years.

Figure 4.4 shows the 2016 – 2018 pooled monthly model across all the WWTPs and separately for very large, large, medium, and small sized WWTPs. Overall, the predictive capacity of the pooled models was found to be strong, as also cross validated by the Leave One Out Cross Validation (Table 4.8). R^2 values ranged from 0.43 – 0.94, representing marked to high degree of correlation (as Table 4.2). The pooled monthly models across different sized WWTPs for both the time periods and their correlation coefficients are presented in Appendix I.

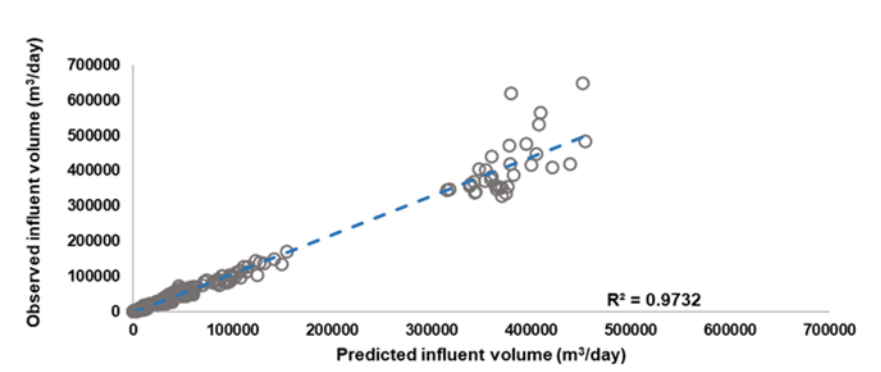
Observed influent volume (m³/day)
700000
600000
500000
400000
300000
200000
100000
0
0
100000
200000
300000
400000
500000
600000
700000
Predicted influent volume (m³/day)
R² = 0.9732

(a)

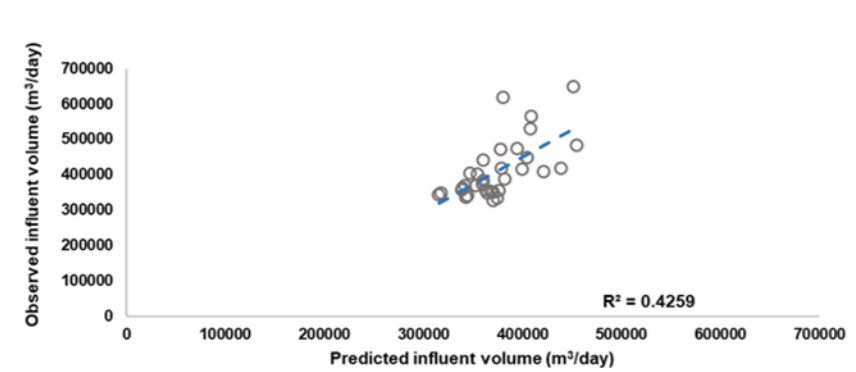
Observed influent volume (m³/day)
700000
600000
500000
400000
300000
200000
100000
0
0
100000
200000
300000
400000
500000
600000
700000
Predicted influent volume (m³/day)
R² = 0.4259

(b)

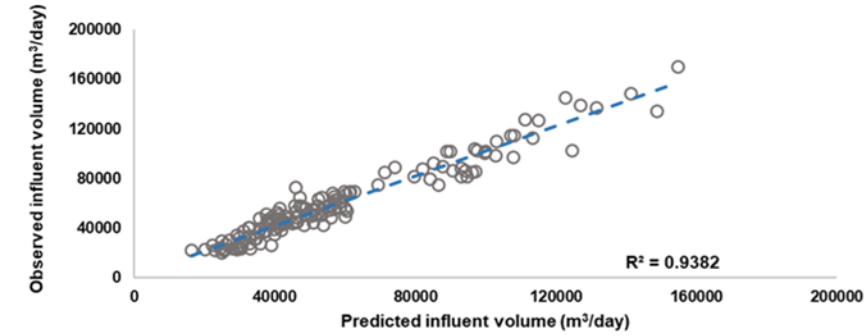
Observed influent volume (m³/day)
200000
160000
120000
80000
40000
0
0
40000
80000
120000
160000
200000
Predicted influent volume (m³/day)
R² = 0.9382

(c)

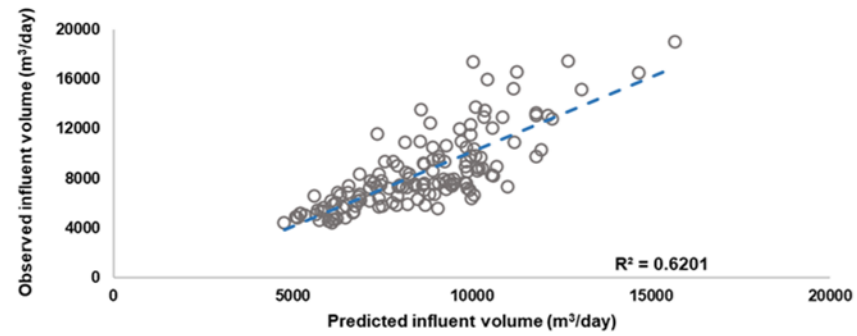
Observed influent volume (m³/day)
20000
16000
12000
8000
4000
0
0
5000
10000
15000
20000
Predicted influent volume (m³/day)
R² = 0.6201

(d)

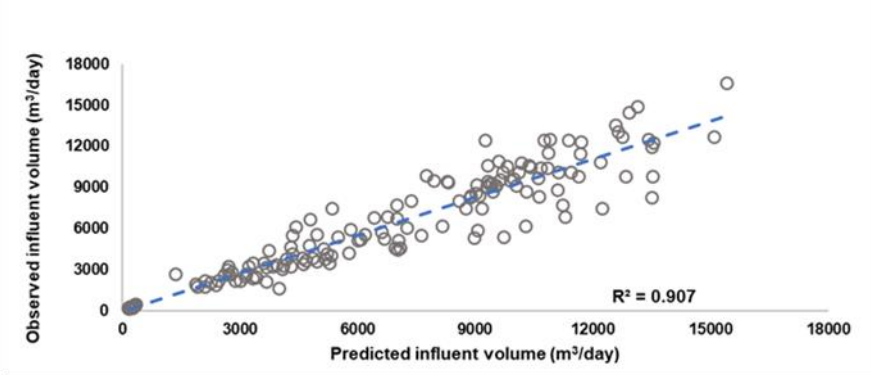

(e)

Figure 4.4: Observed v/s predicted average daily influent volume on a monthly basis across (a) all WWTPs, (b) 1 very large WWTP, (c) 4 large WWTPs, (d) 4 medium WWTPs, and (e) 5 small WWTPs using the built 2016 - 2018 pooled model data

The Leave One Out Cross Validation results are presented in Table 4.8.

Table 4.8: Model errors and RMSE for the 14 WWTPs calculated by the Leave One Out Cross Validation method

WWTPs	Pooled Monthly Model for Cross Validation			
	All years		2016-2018	
	Model error	RMSE (m^3/day)	Model error	RMSE (m^3/day)
1	15%	7009	16%	7677
2	12%	12632	10%	10617
3	32%	2857	32%	2767
4	41%	3741	9%	925
5	28%	69	14%	34
6	21%	2118	21%	1989
7	27%	2527	21%	1833
8	9%	5187	10%	5561
9	23%	2689	25%	2461
10	16%	67978	18%	74830
11	26%	7945	25%	7562
12	29%	1560	23%	1259
13	31%	912	32%	929
14	25%	1556	21%	1252

The predictions made for each WWTP by the regression models developed by excluding them using the Leave One Out Cross Validation method showed approximately equal model errors and RMSE for 7 of the 14 WWTPs as compared to the model errors and RMSE when all the 14 WWTPs were considered, for both the all years and 2016 – 2018 pooled models. The predictions for the remaining 7 WWTPs showed only a difference of 1 – 3 % model errors as compared to the predictions from the pooled regression model when all the 14 WWTPs were considered. As the model error of the pooled model showed high predictive capacity (Figure 4.4), and the cross validation also indicated similar model errors, it can be concluded that the pooled model could be adapted to derive genric trends of influent volumes across any WWTP.

In conclusion, these pooled models can enable modelling of hydraulic responses to rainfall of other WWTPs with similar characteristics. In addition, the model errors from Leave One Out Cross Validation analysis shows that the pooled models can be used across urban CSOs in Ireland as they capture the variability of hydraulic characteristics across different plants, in particular for for medium and large WWTPs (model error is more pronounced for smaller WWTPs). Furthermore, the models can be linked with regional climate change projections to better understand how changing precipitation patterns may impact storm overflows and influent wastewater volumes.

4.5. Conclusion

This study analysed wastewater collection systems with foul water and stormwater collected together (i.e., combined sewerage system) to understand the impact of different variables (i.e., precipitation, tidal level, and river level) on wastewater treatment plant (WWTP) influent volume. The degree to which key variables such as precipitation, tidal and river levels impact influent wastewater influent volumes has received limited attention to date. Given the importance of wastewater infrastructure and their vulnerability to climate impacts, this is an area that requires further research. Uniquely for this application, this study leverages data from a number of regionally spread WWTP of various sizes and treatment capacities. Furthermore precipitation, tidal and river levels (at daily scale) of between 3 and 14 years has been used for each WWTP. Influent volumes for 14 WWTPs over the above time period was also collated at a daily scale (the highest frequency available).

When considering the daily scale analysis, the key conclusions of the study are as follows:

- At the daily scale, precipitation, and mean river level, when considered separately, are significant contributors to changes in influent volumes. In addition, examining the impact of tidal elevation proved to be a good means of predicting variations in dry weather flow.
- Precipitation intensity bands were developed for each WWTP. When analysed with influent volume this enabled key hydraulic responses to rainfall to be elucidated. For example, for WWTP on days with zero rainfall, less than 20% of the influent volumes was above 60,000 m^3/day, whereas for days with high precipitation, more than 80% influent flows were above 60,000 m^3/day. This

analysis was completed for all WWTPs investigated and is a simple, but robust means of estimating the response of a network to rainfall. This analyses could be adopted for other WWTPs and allow utilities to rapidly identify vulnerabilities in their networks to precipitation; for example in relation to increasing storm overflows drive by precipitation changes.

At the monthly scale, monthly average daily precipitation, number of wet per month and number of zero rainfall days per month (when considered separately) were all significant contributors to average daily influent volumes. The analysis also showed that, although monthly average daily precipitation is the strongest contributor to variations in influent volumes, number of zero rainfall days aids in explaining variations in monthly average daily influent volumes.

A novel pooled WWTP model, based on a spatio-temporal analysis, was also developed to study the characteristics of wastewater influent volume. This model consisting of WWTPs of varying capacities was also established to build an optimized model with high predictive capacity, which could be adapted to model other WWTPs with CSOs to improve understanding of network responses to rainfall while accounting for regional characteristics in WWTP or CSS design.

Future research should focus on analysing issues how other variables can be used to reduce model error. These may include soil moisture deficit, evapotranspiration, use of water consumption data, use of sub-daily data and analysis of land use and land cover in urban areas.

5. IMPACTS OF PROJECTED FUTURE CHANGES IN PRECIPITATION ON THE WWTP INFLUENT VOLUMES CONNECTED BY COMBINED SEWER COLLECTION SYSTEMS

5. Impacts of projected future changes in precipitation on the WWTP influent volumes connected by combined sewer collection systems

5.1. Overview

The aim of this chapter was to study the evolution of wastewater influent volume characteristics of WWTPs with combined sewerage systems in future as an impact of climate change, a topic that has not been investigated to date. Impacts of two main aspects of climate change are focused in this chapter, i.e., the projected change in mean precipitation intensity in future and the projected change in the frequency of extreme precipitation events. The work described herein leverages data driven models of observed precipitation variables and influent volumes for 14 Irish WWTPs described in Chapter 4, to project monthly wastewater influent volumes in 2041 – 2060 using Ireland's most up-to-date high resolution multi-model RCM projections under RCPs 4.5 and 8.5, that are described in Chapter 3. In addition to this, the probability of exceedance curves introduced in Chapter 4, are used in this chapter to link them to projected extreme events, to identify events exceeding the peak design capacities of each of the 14 WWTPs.

This chapter has been submitted in Climate Services (Saikia, S.D., Ryan, P., Nuyts, S., Nolan, P. Clifford, E., (2023). Impacts of projected future changes in precipitation on the WWTP influent volumes connected by combined sewer collection systems. *Climate Services (Under Review)* and is currently under review.

5.2. Introduction

With the changing climate, as human-water interaction changes, the amount of municipal wastewater generated will be impacted (Shakeri et al., 2021), which will eventually end up entering WWTPs (Zouboulis and Tolkou, 2015), influencing such infrastructure with increased instances of CSOs and hydraulic overloading. However, infrastructure in many cases, will not have been designed for these changes (Meyer et al., 2012). While there have been detailed studies identifying precipitation variables impacting wastewater influent volumes in CSSs (for example Gooré Bi et al., 2015; Langeveld et al., 2013; Li et al., 2016; Mines et al., 2007; Saikia et al., 2022), the response characteristics of the influent volumes with respect to future change in precipitation induced by climate change have, to the best knowledge of the author, yet to be analysed. Therefore, it is likely that, if future projections are not considered, new and existing infrastructure may not be

resilient to future climates, making it important to consider climate change impacts in the planning and management of wastewater utilities (Vogel et al., 2016).

Conventionally, studies have investigated the impact of potential changes in rainfall patterns on the hydraulic response characteristics of wastewater infrastructure or focused on sanitary sewers (Gooré Bi et al., 2015; Hlodversdottir et al., 2015; Jung et al., 2015; Kleidorfer et al., 2009; ; Shakeri et al., 2021). Historically, based on the strong relationship between wastewater influent volumes for WWTPs with CSSs and precipitation (Saikia et al., 2022), climate change induced precipitation events will also likely impact influent volumes in the future in countries which utilise CSS systems. As the influent volumes approach the design capacity of the WWTP, there is an increased likelihood of occurrences of system failures. However, there has been no research focused on future change in precipitation as the climate change variable of interest, to evaluate the effects it might have on the evolution of wastewater influent volume characteristics at a WWTP scale. In addition to this, all the above-mentioned studies considering the future impacts of climate change on the hydraulic response characteristics of wastewater infrastructure take into account one case-study at a time. With the latest IPCC 6th Assessment Report stating that there is a high confidence that precipitation change in future will exhibit substantial regional differences and seasonal contrasts (IPCC, 2021), the importance of considering the spatial and temporal scales (Rubio-Martin et al., 2023) in identifying the differences in the response of WWTPs to future climate change scenarios has been ignored.

In order to fill this gap in literature, this chapter has been built on Chapter 4, by leveraging historical analysis of precipitation impacts on wastewater influent volumes of 14 WWTPs of varying treatment capacities, connected to CSSs, and spatially distributed across Ireland. Having established the models and relationships between precipitation variables and wastewater influent volumes at monthly and daily scales, this chapter predicts the evolution of wastewater influent volume characteristics in the mid- 21st century (2041 – 2060) as compared to the current period based on future precipitation projections under the two climate change scenarios of RCP 4.5 and RCP 8.5. By focusing at detailed WWTP scale, this chapter intends to present the findings as a climate service for wastewater utility managers as end-users (Swart et al., 2021), to help them towards better

understanding of the problems and challenges that WWTPs are likely to face with the changing climate at a regional and local scale, with particular focus on CSSs.

5.3. Methods

5.3.1. Impact of projected changes in mean precipitation on influent volumes

The linear regression models developed in Chapter 4 that described the relationship between monthly average daily influent volume and monthly average daily precipitation is presented in Equation 5.1:

$$Q_m = \beta ADP + c + \in \qquad \text{(Eq. 5.1)}$$

where, Q_m represents the observed monthly average daily influent volume, β is the coefficient of the predictor variable ADP (monthly average daily precipitation), c is the intercept and $\in$ is the residual. The projected percentage change in monthly average daily precipitation between the current and future time periods, computed on the basis of linear interpolation (Chapter 3 Figure 3.9) for emission scenarios RCP 4.5 and RCP 8.5, were incorporated into the existing linear regression models (Equation 5.1) for each of the WWTPs to give a new projected monthly average daily influent volume $Q_{m,p}$ for each time period based on each emission scenario. The methodology to derive future changes in monthly average daily influent volumes as a function of monthly average daily precipitation is depicted in Figure 5.1.

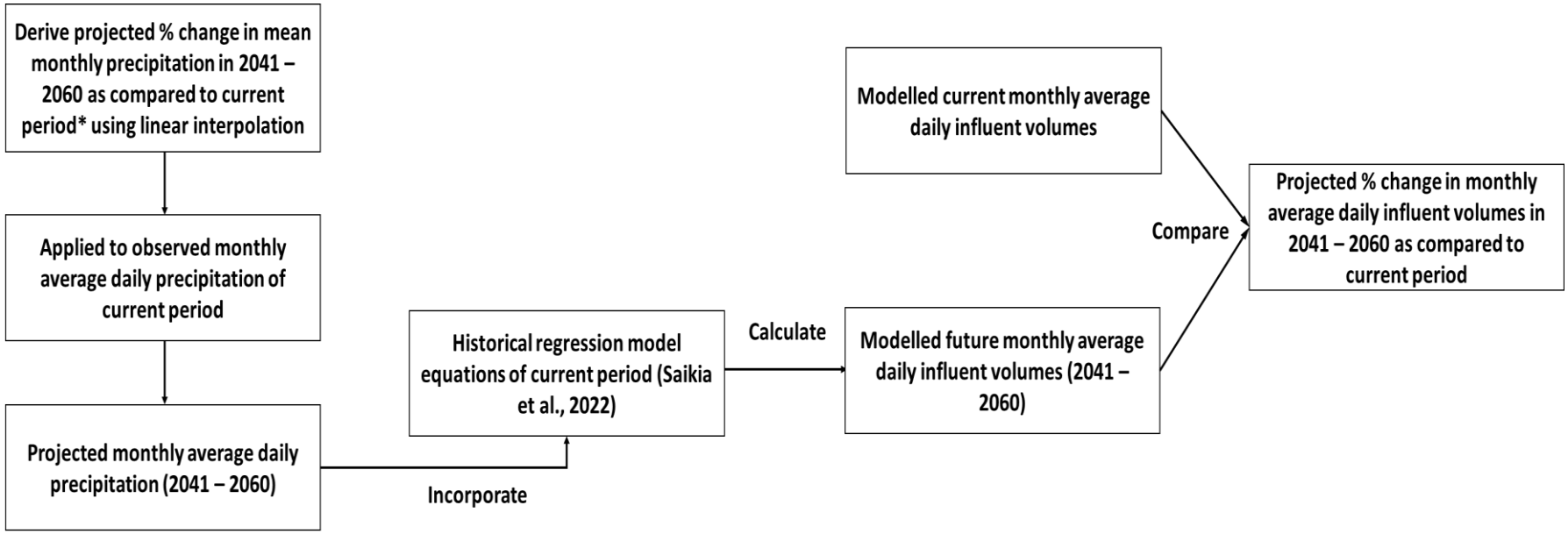

Figure 5.1: Methodology depicting the estimation of projected % change in monthly average daily influent volume based on change in monthly average daily precipitation for the 14 WWTPs to 2041 – 2060

In order to analyse the variability in the projected influent volume findings, as mentioned in Chapter 3 Table 3.3, the 33rd (P33) and 66th (P66) percentile values of the projected % change in monthly average daily influent volumes were also estimated using the methodology described above and in Figure 5.1.

The impact of climate change on each WWTP is assessed in terms of the change in the reserve capacity of a WWTP. The reserve capacity of a WWTP, was defined as the portion of the peak design capacity which is not used under normal circumstances and can be affected by climate change induced change in precipitation events (Equation 5.2).

$$RC_{O,m} = PD - Q_m \qquad \text{(Eq. 5.2)}$$

Where $RC_{O,m}$ is the observed reserve capacity for the month m, PD is the peak design capacity (a fixed value for each WWTP) which is obtained from the Annual Environmental Reports (Environmental Protection Agency, Ireland) and Q_m is the observed average daily influent volume for month m as mentioned in Equation 5.1. If the projected climate change impacts upon the calculated influent capacities, resulting in a new monthly average daily influent volume (defined as $Q_{m,p}$), it will alter the observed reserve capacity. This % change in reserve capacity under RCP 4.5 and RCP 8.5, is expressed as a new metric introduced in this paper which provides an insight into the impact of climate change, and can be calculated as (Equation 5.3):

$$\%\ change\ in\ reserve\ capacity = \frac{(PD - Q_{m,p}) - RC_{o,m}}{RC_{o,m}} * 100 \qquad \text{(Eq. 5.3)}$$

5.3.2. Impact of high and very high precipitation days on influent volumes

In order to assess the impact of extreme events on the influent volume response characteristics, the projected % change in annual number of days with high (> 20 mm/day) and very high precipitation (> 30 mm/day) in 2041 – 2060 as compared to current period were also computed on the basis of the assumption of linear interpolation as shown in Chapter 3 Figure 3.9.

Using the observed daily influent volume data under high and very high precipitation days, the proportion of times a high or very high precipitation day led to influent volumes

to the WWTP of greater than 25%, > 50%, > 75% and > 100% of the peak design capacity was calculated annually for each of the 14 WWTPs. It is to be noted that the daily influent volumes, and thereby the peak design capacities were unique to each of the WWTP (Chapter 3 Table 3.2). Hence the nature of response characteristics of the influent volumes to the individual precipitation categories were also unique to each of the WWTP.

It was assumed that for any given rainfall event, the probability of exceedance of any given proportion of peak design capacity (e.g., flows > 100% as per above) of each WWTP in the future period remains unchanged as compared to current period. Thus, the change in the number of incidences of flows exceeding a particular level of design capacity, during the future period, would be directly related to the change in the number of occurrences in high and very high precipitation days under the RCP 4.5 and RCP 8.5 scenarios. The methodology for calculating this change is summarised in Figure 5.2.

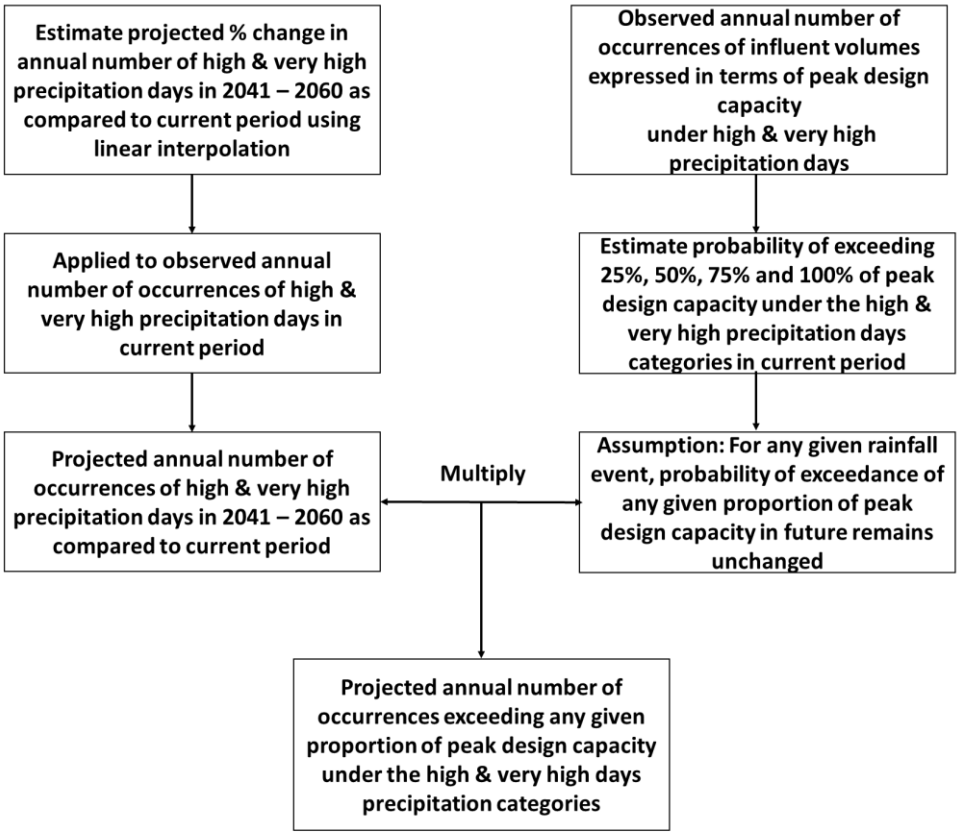

Figure 5.2: Methodology depicting the estimation of mid-century projected annual number of occurrences exceeding any given proportion of peak design capacity under high and very high precipitation days as compared to current period for each of the 14 WWTPs

In order to highlight the impact of extreme events on the WWTP influent volumes, the return period for exceeding 100% of peak design capacities were also estimated for each of the WWTP under RCP 4.5 and RCP 8.5. Any difference between the current and the future return period of events characterized by exceedance of 100% of the peak design capacity would reflect the climate change impact.

5.4. Results

This section presents the results depicting the evolution of influent volume characteristics across all the 14 WWTPs by 2041 – 2060, due to change in precipitation characteristics induced by climate change. Results for both the emission scenarios RCP 4.5 and RCP 8.5 are demonstrated. In some cases, specific results for individual WWTPs are presented to illustrate trends.

5.4.1. Response of influent volumes to projected change in monthly mean precipitation

The changes in monthly average daily influent volumes in the future period (2041 – 2060) compared to the current period (somewhere between 2005 – 2018 depending on WWTP) under RCP 8.5 and RCP 4.5 are summarised in Figure 5.3 and Figure 5.4 respectively. The shades in blue denote reductions in influent volume to the WWTP in the future period with respect to the current period, green denotes no change in influent volume and the shades in orange represent increase in influent volume. During the winter months, the high emission RCP 8.5 scenario showed increases in monthly average daily influent volumes (due to changes in rainfall) across all WWTPs, ranging from +0.3% to +3%. Under RCP 4.5 the monthly average daily influent volume showed mixed trends in winter months across the 14 WWTPs, with projected increases in monthly average daily influent volumes ranging from +0.2% to +0.6% for 6 WWTPs with the remaining showing decreases ranging from -0.9% to -0.2%. It was found that, for the spring months, 13 out of the 14 WWTPs showed a decrease in monthly average daily influent volumes, with the exception showing an almost negligible increase of +0.1% under both RCPs 8.5 and 4.5. As seen in Figure 5.3 and Figure 5.4, these decreases are marginal, ranging from -1% to -0.1% for the 13 WWTPs across the RCP 8.5 and RCP 4.5 scenarios. In the summer months, projected decreases in monthly average daily influent volumes across all WWTPs under both RCP 8.5 and RCP 4.5, ranged from -3.2% to -0.8% and -2.7% to -0.5% respectively. During the autumn months under RCP 8.5, the majority of the WWTPs (9 out of 14) showed an increase in influent volume (+0.1% to +0.9%), 4 WWTPs showed negligible decreases ranging from -0.4% to -0.1%, and the remaining one showed no change. Under RCP 4.5, a reduction was projected ranging from -1.9% to -0.1% across all WWTPs. Overall, the winter months showed the maximum increases and summer months showed maximum decreases in the monthly average daily influent volumes under both RCP 4.5 and RCP 8.5.

	Winter			Spring			Summer			Autumn		
	December	January	February	March	April	May	June	July	August	September	October	November
WWTP 1	0.5	0.5	0.5	-0.1	-0.1	-0.1	-0.8	-1.1	-1.3	0.7	0.5	0.9
WWTP 2	1.6	1.6	1.2	-0.6	-0.5	-0.6	-2.1	-2.1	-1.8	0.3	0.3	0.3
WWTP 3	0.9	0.8	0.8	-1.0	-0.9	-0.9	-3.0	-3.0	-3.4	0.6	0.6	0.7
WWTP 4	1.4	1.3	1.1	-0.4	-0.4	-0.3	-1.2	-1.2	-1.1	0.1	0.2	0.2
WWTP 5	1.8	1.7	1.6	-0.7	-0.5	-0.6	-1.7	-2.1	-2.1	0.5	0.5	0.6
WWTP 6	0.8	0.9	0.8	-0.5	-0.4	-0.4	-1.5	-1.9	-2.0	-0.1	-0.1	-0.1
WWTP 7	1.2	1.2	1.1	-0.6	-0.5	-0.7	-2.7	-2.5	-3.1	0.7	0.8	0.9
WWTP 8	0.9	0.8	0.6	-0.1	-0.1	-0.1	-1.0	-1.0	-1.0	0.1	0.1	0.1
WWTP 9	0.3	0.3	0.3	-0.2	-0.2	-0.2	-1.1	-0.9	-1.1	-0.4	-0.4	-0.5
WWTP 10	0.7	0.6	0.4	0.1	0.1	0.1	-1.2	-0.9	-0.9	0.0	0.0	0.0
WWTP 11	1.4	1.2	0.9	-0.4	-0.3	-0.4	-1.5	-1.7	-1.7	-0.1	-0.1	-0.2
WWTP 12	3.0	2.7	2.3	-0.2	-0.2	-0.2	-3.1	-3.2	-3.0	0.3	0.3	0.4
WWTP 13	1.6	1.6	1.7	-0.9	-0.5	-0.6	-2.1	-1.9	-2.5	0.9	0.8	0.9
WWTP 14	0.6	0.6	0.5	-0.3	-0.3	-0.4	-1.7	-1.5	-1.8	-0.3	-0.3	-0.4

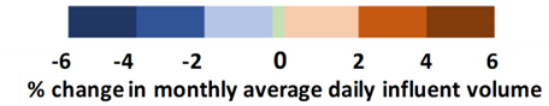

Figure 5.3: Projected % change in monthly average daily influent volume as compared to current period under RCP 8.5 based on monthly average daily precipitation projections (Equation 5.1)

	Winter			Spring			Summer			Autumn		
	December	January	February	March	April	May	June	July	August	September	October	November
WWTP 1	-0.2	-0.2	-0.1	-0.2	-0.1	-0.2	-0.5	-0.6	-0.8	-0.2	-0.1	-0.2
WWTP 2	0.4	0.4	0.3	-0.4	-0.3	-0.3	-1.3	-1.3	-1.2	-1.2	-1.2	-1.2
WWTP 3	-0.3	-0.2	-0.2	-0.9	-0.8	-0.8	-1.1	-1.2	-1.3	-0.8	-0.7	-0.9
WWTP 4	0.3	0.3	0.2	-0.1	-0.1	-0.1	-0.7	-0.7	-0.6	-0.6	-0.9	-1.0
WWTP 5	0.6	0.6	0.5	-0.8	-0.6	-0.7	-1.2	-1.5	-1.5	-0.8	-0.8	-1.0
WWTP 6	-0.7	-0.7	-0.6	-0.1	-0.1	-0.1	-1.1	-1.4	-1.4	-0.1	-0.1	-0.1
WWTP 7	-0.5	-0.5	-0.4	-0.4	-0.3	-0.4	-2.4	-2.2	-2.7	-0.9	-1.0	-1.2
WWTP 8	0.3	0.3	0.2	-0.1	-0.1	-0.2	-0.5	-0.5	-0.6	-0.6	-0.6	-0.7
WWTP 9	-0.6	-0.5	-0.4	-0.1	-0.1	-0.1	-0.9	-0.7	-0.9	-0.2	-0.3	-0.3
WWTP 10	-0.3	-0.3	-0.2	0.1	0.1	0.1	-0.7	-0.5	-0.5	-0.7	-0.5	-0.8
WWTP 11	-0.9	-0.7	-0.6	-0.2	-0.2	-0.2	-0.6	-0.7	-0.7	-1.4	-1.2	-1.6
WWTP 12	0.5	0.4	0.4	-0.2	-0.2	-0.2	-1.3	-1.4	-1.3	-1.5	-1.8	-1.9
WWTP 13	0.3	0.3	0.3	-1.0	-0.6	-0.7	-1.4	-1.3	-1.8	-0.9	-0.8	-0.9
WWTP 14	-0.6	-0.5	-0.5	-0.4	-0.3	-0.4	-1.6	-1.5	-1.8	-0.5	-0.4	-0.6

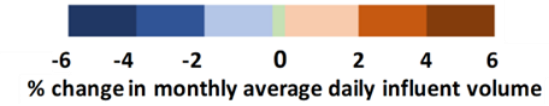

Figure 5.4: Projected % change in monthly average daily influent volume as compared to current period under RCP 4.5 based on monthly average daily precipitation (Equation 5.1)

No spatial trend was apparent with respect to the projected change in influent volumes. However, the data used to produce the influent volumes results, i.e., the projected change in seasonal mean precipitation, showed a strong spatial trend as demonstrated in Chapter 3 Figure 3.2. This strong spatial signal did not translate into the influent volumes findings due to the following reasons: i) The precipitation projections are obtained at the seasonal

scale as opposed to the influent volume projections which are estimated at the monthly scale, ii) some of the WWTPs studied in this paper are not precisely located in the areas where a strong spatial trend in seasonal mean precipitation is observed, and iii) in addition to change in precipitation in future, other variables such as urbanisation and demographics which might have an impact on wastewater influent volumes, were not considered. The only exceptions were observed under RCP 8.5, when i) WWTP 12, located in the southeast of Ireland showed the maximum increase in influent volumes during the winter months, coinciding with Winter map shown in Chapter 3 Figure 3.2 b and ii) WWTPs 2 (southeast), 7 (midlands), 12 (southeast) and 13 (midlands), which showed decreases in the summer months coinciding with the Summer map shown in Chapter 3 Figure 3.2 b.

The 33rd and 66th percentiles of the projected % change in monthly average daily influent volume for each of the 14 WWTPs in future period as compared to the current period were also reported to help analyse the climate projection related uncertainty associated with the future influent volume findings (Figure 5.5 and Figure 5.6). The variability or spread in the projected findings was determined by the range between the 33rd and the 66th percentile values. As observed from Figure 5.5, under RCP 8.5, summer months showed the least variability in monthly average daily influent volumes with spread (difference between P66 and P33) ranging from 0.6% (WWTPs 5 and 9) to 2.8% (WWTP 7). Winter months showed maximum spread in the projected findings ranging from 0.7% (WWTP 4) to 4.5% (WWTP 13). The variability in the spring and autumn months was observed to lie between the variability in the winter and summer months. This might be because extreme events such as storms and dry spells are more likely to occur in winter and summer months resulting in increased uncertainty associated with the projected % change in monthly average daily influent volumes. Similarly, Figure 5.6 shows the variability associated with the influent volume projections under RCP 4.5. Under RCP 4.5, contrary to RCP 8.5, maximum spread of 4.4% was observed for the spring months and minimum spread of 3.1% for autumn months. Variability in the influent volume findings of summer and winter months lied between that of spring and autumn months.

	Winter						Spring						Summer						Autumn					
WWTPs	December		January		February		March		April		May		June		July		August							
	P33	P66	P33	P66	P33	P66	P33	P66	P33	P66	P33	P66	P33	P66	P33	P66	P33	P66	P33	P66	P33	P66	P33	P66
WWTP 1	-0.5	1.1	-0.5	1.1	-0.5	1.1	-0.8	0.4	-0.5	0.3	-0.7	0.4	-1.3	-0.6	-1.6	-0.8	-2.0	-0.9	0.3	1.5	0.2	1.1	0.3	1.8
WWTP 2	0.7	1.9	0.7	1.9	0.5	1.4	-2.1	0.8	-1.8	0.7	-1.9	0.7	-2.9	-1.8	-3.0	-1.8	-2.6	-1.6	-0.6	1.0	-0.6	1.0	-0.6	1.0
WWTP 3	-1.6	2.7	-1.4	2.3	-1.5	2.5	-2.2	0.3	-1.9	0.2	-2.1	0.2	-4.3	-2.2	-4.4	-2.3	-4.9	-2.6	-0.1	1.8	-0.1	1.7	-0.2	2.0
WWTP 4	0.9	1.7	0.8	1.6	0.6	1.3	-1.1	0.5	-1.2	0.5	-1.1	0.5	-1.8	-0.9	-1.8	-0.9	-1.7	-0.9	-0.1	0.5	-0.1	0.6	-0.1	0.8
WWTP 5	0.2	3.6	0.1	3.4	0.1	3.1	-1.9	0.4	-1.4	0.3	-1.6	0.4	-2.0	-1.4	-2.5	-1.7	-2.5	-1.7	-0.3	1.9	-0.3	1.9	-0.3	2.3
WWTP 6	-0.9	2.2	-1.0	2.3	-0.9	2.1	-1.6	0.2	-1.3	0.2	-1.5	0.2	-1.8	-0.2	-2.4	-0.3	-2.4	-0.3	-1.7	0.8	-1.4	0.7	-2.0	1.0
WWTP 7	-0.7	2.5	-0.7	2.3	-0.7	2.3	-1.8	0.2	-1.6	0.2	-1.9	0.2	-3.8	-1.3	-3.5	-1.2	-4.3	-1.5	-0.4	2.3	-0.4	2.4	-0.5	2.9
WWTP 8	0.2	1.6	0.2	1.4	0.2	1.2	-0.3	0.3	-0.3	0.3	-0.4	0.3	-1.6	-0.8	-1.7	-0.8	-1.8	-0.9	-0.6	1.1	-0.7	1.1	-0.8	1.3
WWTP 9	-0.9	1.1	-0.7	0.9	-0.6	0.8	-0.7	0.2	-0.5	0.1	-0.7	0.2	-1.4	-0.6	-1.1	-0.5	-1.4	-0.7	-0.3	0.7	-0.3	0.8	-0.3	0.9
WWTP 10	-0.7	0.8	-0.6	0.6	-0.4	0.4	-0.4	0.5	-0.4	0.4	-0.4	0.5	-2.1	-0.3	-1.6	-0.2	-1.6	-0.2	-0.8	0.4	-0.6	0.3	-0.9	0.5
WWTP 11	-0.7	1.2	-0.6	1.0	-0.5	0.8	-1.4	0.1	-1.1	0.1	-1.2	0.1	-2.4	-0.9	-2.8	-1.1	-2.8	-1.1	-1.2	0.3	-1.0	0.2	-1.4	0.3
WWTP 12	1.5	3.5	1.4	3.1	1.2	2.7	-2.4	1.6	-2.1	1.5	-2.2	1.5	-3.9	-2.6	-4.1	-2.8	-3.8	-2.5	-0.1	0.8	-0.2	1.0	-0.2	1.1
WWTP 13	-0.4	3.8	-0.5	3.9	-0.5	4.0	-1.9	0.2	-1.2	0.1	-1.3	0.1	-2.4	-1.5	-2.3	-1.4	-3.0	-1.8	-0.4	2.7	-0.3	2.4	-0.4	2.6
WWTP 14	-0.7	1.5	-0.6	1.4	-0.6	1.3	-1.0	0.4	-0.8	0.3	-1.0	0.5	-2.6	-1.2	-2.3	-1.1	-2.8	-1.3	-0.8	0.7	-0.7	0.7	-1.1	1.0

-6 -4 -2 <0> 2 4 6

% change in monthly average daily influent volume

Figure 5.5: The 33rd and the 66th percentile values of the projected % change in monthly average daily influent volumes based on the projected % change in monthly average daily precipitation in 2041 – 2060 as compared to current period across all the 14 WWTPs under RCP 8.5

	Winter						Spring						Summer						Autumn					
	December		January		February		March		April		May		June		July		August		September		October		November	
	P33	P66	P33	P66	P33	P66	P33	P66	P33	P66	P33	P66	P33	P66	P33	P66	P33	P66	P33	P66	P33	P66	P33	P66
WWTP 1	-1.1	0.7	-1.1	0.7	-1.0	0.6	-1.0	0.3	-0.7	0.2	-0.9	0.3	-1.0	-0.1	-1.2	-0.1	-1.5	-0.2	-0.8	-0.1	-0.6	-0.1	-1.0	-0.1
WWTP 2	-0.7	1.2	-0.7	1.2	-0.5	0.9	-1.5	0.7	-1.3	0.6	-1.4	0.7	-1.5	-0.8	-1.5	-0.8	-1.3	-0.7	-1.7	-1.0	-1.7	-1.0	-1.7	-1.0
WWTP 3	-0.2	1.3	-0.2	1.1	-0.2	1.2	-2.0	0.2	-1.7	0.2	-1.9	0.2	-2.0	-0.1	-2.0	-0.1	-2.3	-0.1	-2.2	0.3	-2.1	0.3	-2.5	0.3
WWTP 4	-0.5	0.3	-0.5	0.3	-0.4	0.2	-0.6	0.6	-0.7	0.6	-0.6	0.5	-1.2	0.0	-1.2	0.0	-1.1	0.0	-0.9	-0.6	-1.2	-0.8	-1.4	-1.0
WWTP 5	0.1	1.9	0.1	1.8	0.1	1.6	-2.0	0.4	-1.5	0.3	-1.7	0.3	-1.5	-0.4	-1.8	-0.5	-1.8	-0.5	-2.1	-0.4	-2.1	-0.4	-2.6	-0.5
WWTP 6	-2.0	1.3	-2.2	1.4	-1.9	1.2	-0.6	0.6	-0.5	0.5	-0.6	0.5	-2.1	-0.9	-2.6	-1.1	-2.7	-1.2	-2.0	0.5	-1.8	0.4	-2.5	0.6
WWTP 7	-1.5	1.2	-1.4	1.1	-1.4	1.1	-1.9	0.5	-1.7	0.4	-2.0	0.5	-3.3	-1.7	-3.0	-1.5	-3.7	-1.9	-2.1	-0.7	-2.2	-0.8	-2.7	-0.9
WWTP 8	-0.9	1.2	-0.8	1.1	-0.7	0.9	-0.7	0.6	-0.6	0.5	-0.8	0.7	-1.4	0.2	-1.4	0.2	-1.5	0.2	-1.5	0.0	-1.5	0.0	-1.8	0.0
WWTP 9	-1.3	0.1	-1.2	0.1	-1.0	0.1	-0.8	0.5	-0.7	0.4	-0.8	0.5	-1.4	-0.4	-1.2	-0.3	-1.5	-0.4	-0.9	0.0	-1.0	0.0	-1.1	0.0
WWTP 10	-2.0	0.7	-1.6	0.6	-1.0	0.4	-0.5	0.6	-0.5	0.6	-0.5	0.7	-1.3	-0.1	-1.0	-0.1	-1.0	-0.1	-1.4	-1.0	-1.0	-0.7	-1.6	-1.1
WWTP 11	-3.1	0.5	-2.6	0.4	-2.1	0.3	-1.5	1.0	-1.2	0.8	-1.3	0.9	-1.3	-0.1	-1.5	-0.1	-1.5	-0.1	-2.8	-1.6	-2.4	-1.4	-3.4	-1.9
WWTP 12	-1.3	0.3	-1.2	0.2	-1.0	0.2	-2.1	2.3	-1.9	2.0	-1.9	2.1	-2.6	0.7	-2.8	0.7	-2.5	0.7	-2.2	-1.6	-2.6	-2.0	-2.8	-2.1
WWTP 13	-0.4	1.8	-0.4	1.9	-0.4	2.0	-2.2	0.5	-1.3	0.3	-1.5	0.3	-2.4	0.0	-2.2	0.0	-3.0	0.0	-2.7	-0.6	-2.3	-0.5	-2.6	-0.6
WWTP 14	-1.3	0.8	-1.2	0.7	-1.1	0.7	-1.7	1.0	-1.4	0.8	-1.8	1.0	-2.1	-0.6	-1.9	-0.6	-2.3	-0.7	-1.2	-0.5	-1.1	-0.4	-1.6	-0.6

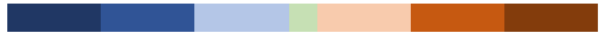

-6 -4 -2 <0> 2 4 6

% change in monthly average daily influent volume

Figure 5.6: The 33rd and the 66th percentile values of the projected % change in monthly average daily influent volumes based on the projected % change in monthly average daily precipitation in 2041 – 2060 as compared to current period across all the 14 WWTPs under RCP 4.5

From these results, it can be concluded that the influent volume findings are more reliable in summer months under RCP 8.5 and in summer and winter months under RCP 4.5. However it is to be kept in mind that the uncertainty calculated from the 33rd and the 66th percentiles reported in Figure 5.5 and Figure 5.6 is associated with the climate model projections used to calculate the influent volume projections. These values do not take into account the model errors of the regression equations of each of these WWTPS, where the monthly average daily precipitation projections were fed into, to estimate the monthly average daily influent volume projections. These model errors of the individual WWTPs are provided in Appendix I Table I.7. Thus the calculation of total uncertainty is demonstrated with the help of an example. Under RCP 8.5, the variability in influent volume projections for WWTP 1 in the month of January is 1.6% (Refer to Appendix II Table II.2). The model error associated with the regression model of WWTP 1 is 11% (Refer to Appendix I Table I.7). Therefore the total uncertainty associated with the average daily influent volume projection for the month of January under RCP 8.5 is 12.6%. The full results showing the model errors of the regression equations and the range of the projected influent volume findings for all the 14 WWTPs are included in Appendix I and Appendix II respectively.

In addition to the above results, the % change in reserve capacity of these WWTPs was estimated from Equation 5.3 for RCP 8.5 and RCP 4.5. Among all the 14 WWTPs, influent volumes of WWTP 13 showed to be the most susceptible to the effects of change in precipitation in future induced by climate change, with a reduction in reserve capacity by and 18.1% under RCP 4.5 108.4% under RCP 8.5 for the month of January. In the span of three years of observed data for WWTP 13 from 2016 – 2018 (Chapter 3 Table 3.2), the observed monthly average daily influent volume in the month of January exceeded the peak design capacity for two years in 2016 and in 2018. Hence the plant has in recent times being operating a maximum capacity in come more recent years. The projected change in reserve capacity was also demonstrated to further reduce in future under both the RCP 4.5 and RCP 8.5. Results for all the other WWTPs are presented in Appendix II.

5.4.2. Response of influent volumes to projected change in number of high and very high precipitation days

Table 5.1 summarises the change in the return period of each WWTP exceeding its peak design capacity (PD) due to high or very high rainfall events under RCP 4.5 and RCP 8.5 (as outlined in Section 5.3.2).

Table 5.1: Return periods of exceedance of 100% of the peak design capacity under high and very high precipitation days

WWTPs	High precipitation days			Very high precipitation days		
	Current (years)	RCP 4.5 (years)	RCP 8.5 (years)	Current (years)	RCP 4.5 (years)	RCP 8.5 (years)
WWTP 1	5	4.6	4.4	5	4.2	4.1
WWTP 2	-	-	-	-	-	-
WWTP 3	-	-	-	-	-	-
WWTP 4	2.5	2.4	2.35	-	-	-
WWTP 5	-	-	-	-	-	-
WWTP 6	-	-	-	-	-	-
WWTP 7	-	-	-	-	-	-
WWTP 8	-	-	-	-	-	-
WWTP 9	1.8	1.6	1.6	7	5.74	5.67
WWTP 10	1	0.97	0.97	4	3.64	3.52
WWTP 11	1	0.98	0.97	2.5	2.38	2.37
WWTP 12	0.22	0.21	0.21	0.65	0.61	0.59
WWTP 13	0.38	0.36	0.34	1	0.87	0.85
WWTP 14	-	-	-	-	-	-

As shown in Table 5.1, the return periods of events exceeding 100% of peak design capacity in 2041 under RCPs 4.5 and 8.5 reduced as compared to the current period across all 7 of the 14 WWTPs for which the return periods could be computed. For the remaining 7 WWTPs, there were no observed occurrences of such events in the current period and hence projected return periods could not be estimated. For better illustration of the

response of the WWTPs to the projected change in the number of high and very high precipitation days, WWTP 11 is elaborated as an example.

The observed exceedance of 25%, 50%, 75% and 100% of the peak design capacity of WWTP 11 under high and very high precipitation conditions is shown in Figure 5.7.

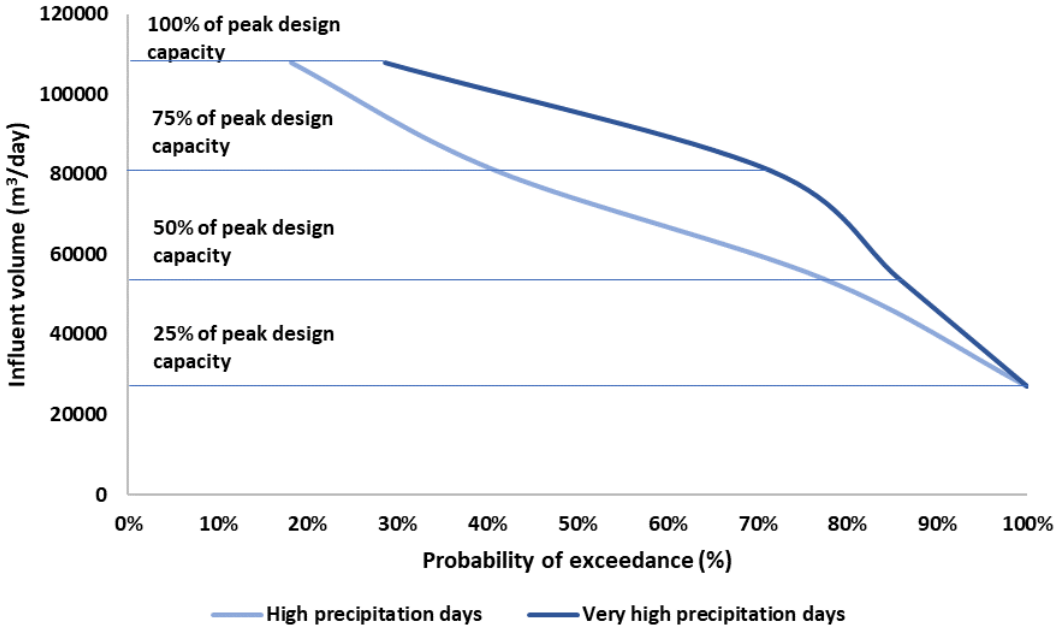

Figure 5.7: Observed probability of exceedance curves showing the likelihood, in percentage, of influent volumes exceeding any given proportion of peak design capacity under high and very high precipitation days for WWTP 11

As mentioned in Section 5.3.2, on the basis of the assumption that the probability of exceedance (%) under both high and very high precipitation days remains unchanged from the current period to future period (2041 – 2060), using the projected % change in the number of high and very high precipitation days from current period to 2041 – 2060 (Figure 5.8), the number of occurrences of events exceeding 25%, 50%, 75% and 100% of the peak design capacity for WWTP 11 were estimated as shown below in Table 5.2.

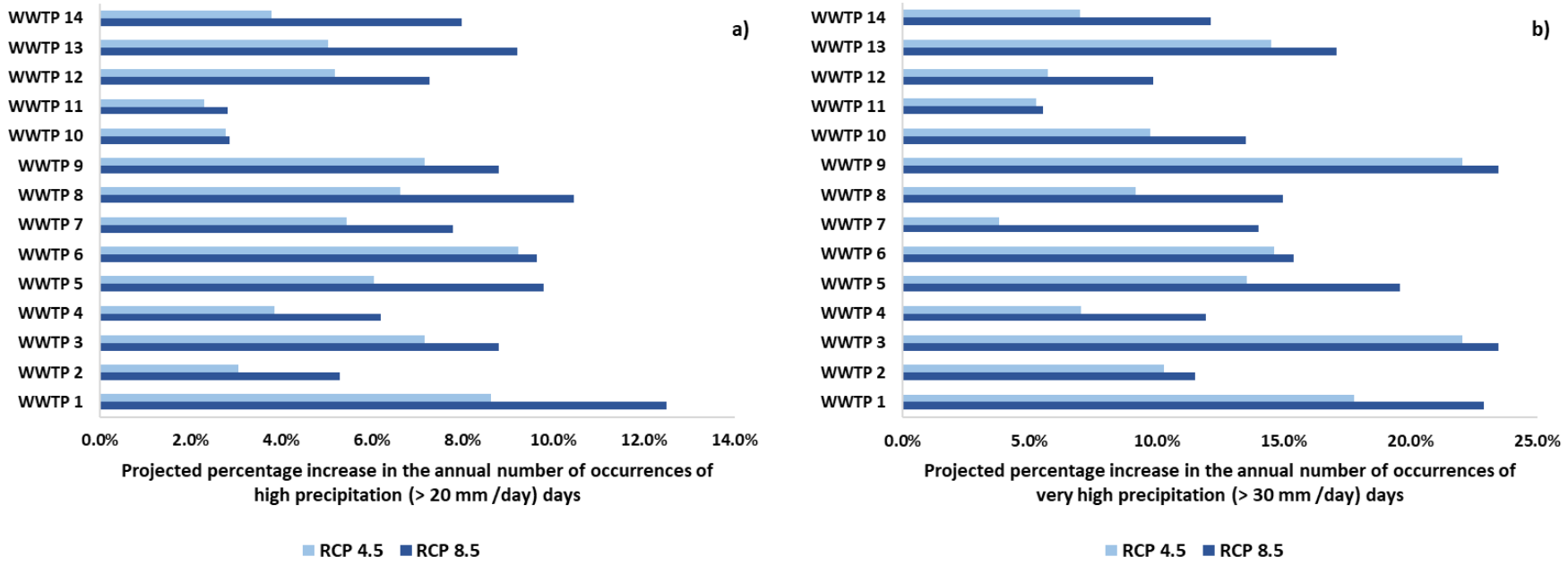

Figure 5.8: Projected % change in the annual number of occurrences of a) high precipitation days marked by > 20 mm/day and b) very high precipitation days marked by >30 mm/day across all the 14 WWTPs under RCP 4.5 and RCP 8.5

Table 5.2: Estimation of number of events exceeding any given proportion of peak design capacity of WWTP 11 based on observed probability of exceedance and the projected % change in high and very high precipitation days in 2041 – 2060 as compared to current period under RCP 4.5 and RCP 8.5

		> 25% of PD		> 50% of PD		> 75% of PD		> 100% of PD	
Time period	**Annual number of occurrences**	**Observed PoE**	**Annual no. of events exceeding 25% of PD**	**Observed PoE**	**Annual no. of events exceeding 50% of PD**	**Observed PoE**	**Annual no. of events exceeding 75% of PD**	**Observed PoE**	**Annual no. of events exceeding 100% of PD**
High precipitation days									
Current	5.5	100%	5.5	77%	4.25	41%	2.25	18%	1
2041 – 2060 (RCP 4.5)	5.6		5.6		4.33		2.29		1.02
2041 – 2060 (RCP 8.5)	5.7		5.7		4.4		2.33		1.04
Very high precipitation days									
Current	1.4	100%	1.4	86%	1.2	71%	1	29%	0.4

2041 – 2060 (RCP 4.5)	1.47	1.47	1.26	1.05	0.42
2041 – 2060 (RCP 8.5)	1.48	1.48	1.27	1.06	0.42
*PD refers to the peak design capacity and PoE refers to Probability of Exceedance					

This analysis for each of the 14 WWTPs is provided in Appendix II. The results indicate that with projected increase in high and very high precipitation days in Ireland, the operations and maintenance of WWTPs with CSSs will be challenged as the frequency of days exceeding a given proportion of peak design capacity increases under both the medium and high emission scenarios RCP 4.5 and RCP 8.5 respectively. It will also impact the return period of occurrence of challenging operational events such as exceedance of 100% of the peak design capacity. This suggests that WWTP infrastructure may need to adapt to handling more intense precipitation to avoid occurrence of combined sewer overflows.

5.5. Conclusions

Precipitation is one of the strongest variables influencing the response of influent volumes, particularly for combined sewerage systems. With climate change, changing precipitation patterns, may impact influent volume characteristics and present infrastructure operators and designers with new challenges. To date, research studying how precipitation changes predicted in climate change models may impact wastewater influent volumes of combined sewerage systems is not found. This chapter analyses the evolution of wastewater influent volume characteristics in the mid-21st century (2041 – 2060) as compared to recent data using (i) precipitation projections under two climate change scenarios, namely RCP 4.5 and RCP 8.5 and (ii) influent data from 14 WWTPs in Ireland.

The outputs of the analyses show that there is an expected increase in monthly average daily influent volumes during autumn and winter months, particularly under RCP 8.5. On the other hand, during the spring and summer months, some WWTPs could face challenges associated with reduced influent volumes. The research presents a new metric to indicate the change in reserve hydraulic capacity of WWTPs from predicted changes to precipitation patterns. In this context most of the WWTPs examined, currently have sufficient reserve capacity with one being more vulnerable.

Projected impacts of extreme events such as high and very high precipitation days on the influent volumes in relation to the peak design capacities of the WWTPs were also quantified. The annual number of occurrences of exceedance of peak daily WWTP hydraulic design capacities was projected to increase in future under both RCP 4.5 and

RCP 8.5. Overall, this chapter provides an insight into the degree to which the wastewater influent volumes might be impacted by precipitation. This research also assists wastewater utility managers in making informed decision towards establishing resilient wastewater infrastructure under climate change conditions. Promising future research in this area could examine additional temporally dynamic parameters such as urbanisation and demographics.

6. IMPACTS OF URBANISATION ON INFLUENT VOLUMES

6. Impacts of urbanisation on influent volumes

6.1. Overview

This chapter presents a detailed investigation into the impacts of urbanisation and the combined impacts of urbanisation and precipitation on wastewater influent volumes. The estimation of urbanisation is based on land use land cover (LULC) changes using Remote Sensing. This analysis focuses on the agglomerations corresponding to the 14 WWTPs with combined collection systems which are discussed in detail in Chapter 4 and 5. Section 6.2 outlines a brief introduction on the topic of urbanisation impacts on urban water and wastewater management systems. Section 6.3 describes the LULC classification techniques adopted in this thesis and the methodology involved in analysing the impact of urbanisation on influent volume. Section 6.4 presents detailed results and discussion with a focus on case-studies to illustrate key points. The results for all WWTPs analysed (and associated images) are included in Appendix III of this thesis.

6.2. Introduction

In addition to climate change, rapid growth in urbanisation is a crucial variable affecting the hydraulic and hydrologic processes of urban water management systems (Zhou et al., 2019). In the context of this research, "urbanisation" is defined as the increase in built-up area. Urban or built-up LULC mainly consists of impermeable surfaces such as concrete, asphalt, etc. When the surface area of impervious surfaces increases, in conjunction with changes in precipitation variables, such as precipitation intensity and frequency, it can change stormwater runoff characteristics (Yao et al., 2016). This happens because the degree of contribution of urbanisation to stormwater runoff depends on the precipitation intensity, peak location and duration of a rainfall event (Yao et al., 2016). That is why, in terms of wastewater infrastructure, particularly CSSs, it is crucial to understand the dynamics between precipitation, urbanisation and influent volumes, as an increase in stormwater runoff can increase the hydraulic loading to WWTPs leading to increased release of untreated wastewater into the environment (Kleidorfer et al., 2009; Semadeni-Davies et al., 2008).

Conventionally, as discussed in Chapter 2 Section 2.5.3, studies have extensively investigated the impacts of increase in impervious areas on the varied response of stormwater runoff characteristics and eventually on the performance of the sewerage

systems (Hussain et al., 2022; Kleidorfer et al., 2009; Loperfido et al., 2014; Miller et al., 2014; Paule-Mercado et al., 2017; Ravagnani et al., 2009; Semadeni-Davies et al., 2008; Yao et al., 2016; Zhou et al., 2019). The findings of these studies indicate that, the impact of urbanisation on CSSs extend to the WWTPs connected to these networks by default. Moreover many studies suggest that newer developments need to consider features such as sustainable drainage systems, green blue infrastructure, rainwater storage, low development impact techniques and other best management practices that are shown to efficiently manage stormwater runoff (Loperfido et al., 2014; Miller et al., 2014; Paule-Mercado et al., 2017). However, there is a key gap in understanding the influence of urbanisation (and its nature) and precipitation on wastewater influent volumes. Hence, this chapter uses LULC change as a measure of urbanisation at a WWTP scale for 14 agglomerations across Ireland to analyse its impacts individually, and combined with precipitation on wastewater influent volumes.

6.3. LULC classification techniques and association of urbanisation with influent volumes

The data used for this Chapter and the broad methodology was described in Chapter 3 Section 3.4.3. This section presents a detailed description of the methods adopted to estimate urban land cover and analyse the impacts of (a) urbanisation and (ii) the combined impacts of precipitation and urbanisation on wastewater influent volumes. Landuse land cover changes, for each WWTP, were analysed to align with the years for which influent volume data was available for each WWTP (Table 3.2, Chapter 3). The LULC classification methodology applied is summarised and described in the sections below.

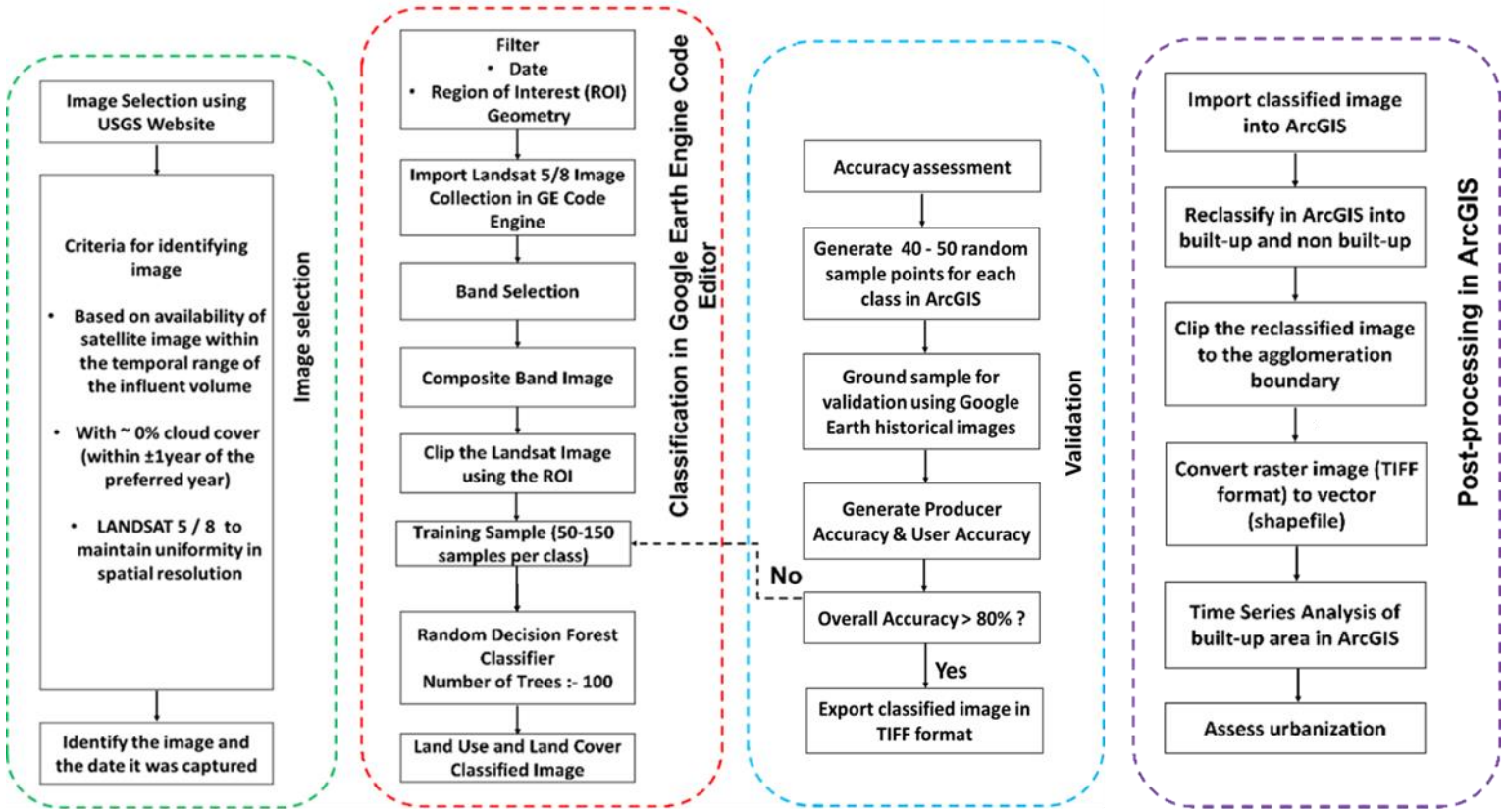

Figure 6.1: Detailed methodology of LULC classification and LULC change detection in GEE code editor and ArcGIS

6.3.1. Selection of Satellite Images

Initially, for the selection of satellite images for each agglomeration, the time period corresponding to each satellite image was identified based on the following criteria:

1. The time period for the satellite images for each agglomeration should be available within the temporal range of influent volume data availability for each corresponding WWTP (Table 3.2, Chapter 3).

2. A minimum of two sampling points (i.e., satellite images) for each agglomeration were considered to analyse change in urban patterns.

3. Changes in urbanisation could be estimated over a minimum 2-year period (e.g., from 2014 – 2016 but not from 2014 – 2015). For agglomerations with a longer temporal range of WWTP influent volume data, the number of sampling points were greater than two.

Once the particular years of interest for each agglomeration was delineated based on the above-mentioned criteria, search for the corresponding satellite images was carried out in USGS Earth Explorer platform. This was performed keeping in mind the following eligibility criteria:

1. Each scene/ tile of satellite image (Chapter 2 Section 2.5.1.3) should be sufficiently clear (i.e., minimal cloud cover), in order to be chosen for further study. Cloud cover within the extent of the agglomeration boundary (known as the Area of Interest or the AOI) inside each satellite image should be preferably 0%. For example, if a satellite image has approximately 10% of cloud cover over some parts or areas, it could still be used, provided the AOI within the image is cloud-free. In order to minimise misclassification of pixels, this task was performed manually, as any cloud cover or cloud shadow could affect the accuracy of classification (Section 6.4.1). An exception was made where no cloud-free satellite image was found within the years of preference. In that case, ± 1 year was considered to expand the temporal range and increase the possibility to find a cloud-free image.

2. An image was selected such that the AOI was covered completely under one scene of satellite image. If the extent of the study area was divided in more than one scene, then

another scene consisting of the entire study area extent was considered. This is because two different scenes captured on different days would be dissimilar due to several external environmental factors such as variation in atmospheric conditions, sun reflectance intensity etc. Hence, this step was carried out to ensure that the spectral signature of the ground features was uniform, which is an important consideration during the image classification process.

Based on all the above-mentioned criteria, either Landsat 5 (1984 – 2012) or Landsat 8 (2013 – Present) (Chapter 2 Section 2.5.1.3 and Chapter 3 Section 3.2.3.1) satellite images were selected. For example, for the agglomeration with WWTP 2, for which influent volume data was available for the period 2005 – 2018 (Table 3.2, Chapter 3), 4 satellite images were selected in order to analyse the change in urbanisation patterns. These images were spaced at different intervals from 3 years to 5 years in 2006, 2011, 2015 and 2018, based on all the criteria previously described. While Landsat 5 images were selected for 2006 and 2011, Landsat 8 images were selected for 2015 and 2018. On the contrary for WWTP 5, for which influent volume data was available from 2014 – 2018, Landsat 8 satellite images at 2-year intervals from 2014, 2016 & 2018 were selected. For all the remaining WWTPs, a similar exercise was carried out with a minimum of 2-year interval between consecutive images.

6.3.2. Classification of satellite images using Google Earth Engine Code Editor

The script for LULC classification was developed within the code editor section in the Google Earth Engine (GEE) code editor platform. The script was developed with the help of online tutorials and Google repositories and is presented in Appendix III.

6.3.2.1. Defining the study area extent

Using GEE code editor, a geometric layer (polygon type) of rectangular shape was created with the variable name ROI (Region of Interest) that was specified by the coordinates of its boundary. The ROI is defined with a buffer of approximately 5 km around the agglomeration boundary (thus the agglomeration boundary is within the ROI boundary). The purpose of defining this layer was to aid in loading the portion of the satellite imagery that corresponds to the specific study area extent in the Map section (Refer to Figure 3.7 in Chapter 3 Section 3.2.3.1), of the GEE code editor platform. This ensured that the classification was carried out within the ROI boundary (rather than for

the whole image) and reduced algorithm processing time by focusing on the area within the coordinates specified in the script.

6.3.2.2. Loading the satellite image

The next part of the script was used to load the satellite image within the ROI into the Map section of the GEE code editor. In order to execute this step, the date that was identified in Section 6.3.1 was incorporated to filter that specific image from the repository of the LANDSAT 5/8 collection of images as shown in Figure 6.2.

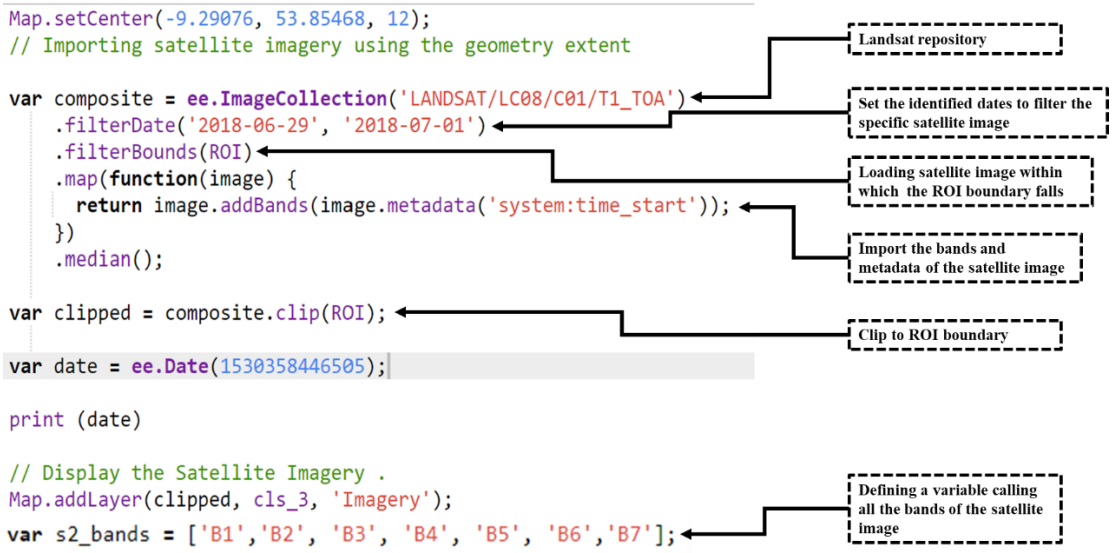

Figure 6.2: Code using JavaScript in GEE code editor for displaying satellite imagery

For better visual interpretation, the satellite image was loaded in False Colour Composite (FCC) (Refer to Figure 2.11, Chapter 2 Section 2.5.1.3) using the function 'map.addlayer'. All the bands for the satellite image (LANDSAT 5/8), that are required to carry out LULC classification, were stored in the variable s2_bands.

6.3.2.3. Creating and training the classes

For the purpose of this research, four types of feature classes (Chapter 2, Section 2.5.2) were created, i.e., built-up, water, green cover and open spaces (Table 6.1).

Table 6.1: The geographical features based on which LULC classes were assigned

Classes	On-ground geographical features	Colour
Built-up	Rooftops, house, carparks, roads	Red
Water	River bodies, estuaries, ponds etc.	Blue
Green cover	Agricultural vegetation, forests, land with bushes/trees etc.	Green
Open spaces	Open land such as football grounds, public open spaces, barren land, marshland, wetlands, sediments, sand etc.	Brown

Training samples for each feature class were created to train the satellite image. All the samples were created based on the following image interpretation techniques (Table 6.2).

Table 6.2: Colour Signature of different geographical features in Standard FCC[18]

S. No.	Earth Surface Feature	Colour (In Standard FCC)
1	**Built-up area**	
	High density	Dark blue to bluish green
	Low density	Light blue
2	**Water**	
	Clear water	Dark blue to black
	Turbid waterbody	Light blue
3	**Green cover**	
	Evergreen forests	Red to magenta
	Deciduous forests	Brown to red
	Scrubs	Light brown with red patches
	Cropped land	Bright red
	Fallow land	Light blue to white
4	**Open spaces**	
	Rock outcrops	Light brown
	Sandy deserts/River sand/Salt affected	Light blue to white
	Deep ravines	Dark green
	Shallow ravines	Light green

[18] Introduction to Remote Sensing, Chapter 7, (https://ncert.nic.in/textbook/pdf/kegy307.pdf) (Accessed in June, 2022)

Wetlands	Motelled black

Based on supervised classification method (Refer to Chapter 2, Section 2.5.2.2), around 50 – 150 samples were selected for each class to capture the different spectral signatures across all the pixels belonging to each class. The selection of the amount of samples for each class depends on the type of class. For example, because water is a fairly homogeneous landuse class, lesser number of samples are taken. In case the water is turbid or has sediments in it, the reflection of such pixels vary from a pure water pixel. But since both the turbid or pure water pixels belong to the water body, samples from each type of these pixels are taken if present. On the contrary, for a class such as built-up, different kinds of features (roads, roofs, parking spaces) might have different reflectance values of pixels. In such a scenario, care must be taken that samples from each and every type of pixel is taken and allocated to the built-up class. Therefore, training samples for built-up class were greater than that of water.

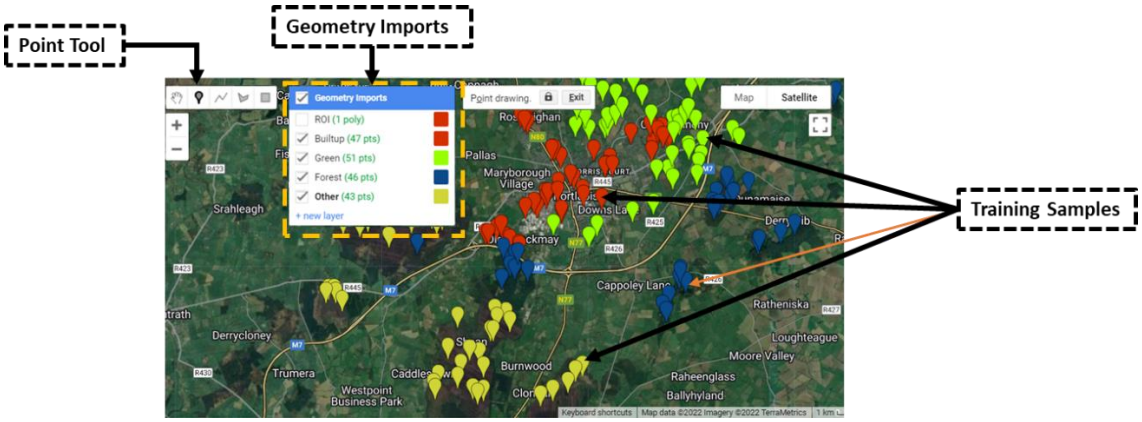

Figure 6.3: The point training samples for one agglomeration

Training samples were unique to each agglomeration. For example, as shown in the "Geometry Imports" in Figure 6.3 above, this particular agglomeration did not have any water body within the limits of the ROI boundary. Hence no training samples for water class were provided for this agglomeration. Similarly, in some cases, two or more classes were created to represent the same geographical feature. In the Figure 6.3, "Green" and "Forest", both represent green cover, but while selecting the training samples, agricultural vegetation was assigned to class "Green" and larger tree covers were assigned to class

"Forest". These would be later reclassified into one class during the post-processing stage as discussed in Section 6.3.4.

6.3.2.4. Classification algorithm

After the training samples were created, these were then overlaid on the satellite image. A random forest classifier (Chapter 3, Section 3.4.3) was used to classify the satellite image into different classes based on these training samples. Based on the optimum number of decision trees – generally shown to range from 64 to 128, and the number of training samples, 100 decision trees were used in the classifier (Oshiro et al., 2012). Finally, a classified image was generated and added to the GEE code editor.

6.3.3. Validation of the classified images:

The objective of accuracy assessment was to evaluate the accuracy with which the pixels were classified into each of the appropriate land cover classes. Accuracy assessment was carried out initially using two methods for one agglomeration as a pilot study. This was performed to check which method would provide better accuracy. In the first method, for one pilot case-study (agglomeration), validation of the classified satellite image was carried out in GEE code editor. Before executing the code, the same feature classes, i.e., built-up, green cover, water and open spaces, had to be created again. New sampling points had to be manually created for each class which was time consuming. Moreover, manual selection of sampling points could be biased which could overestimate the accuracy. Given these disadvantages, this method was not executed on the remaining agglomerations. In the second method 40 – 50 samples were generated randomly for each class on the classified image in ArcGIS. In total, for the four different classes, 160 samples for each satellite image were generated. These points were then imported into the Google Earth Pro platform and manually checked and validated against the images in those respective years since they are of higher quality as compared to the original satellite image used for classification (Figure 6.4). In case a particular satellite image of interest is not available in Google Earth Pro, the original satellite image was used as the reference.

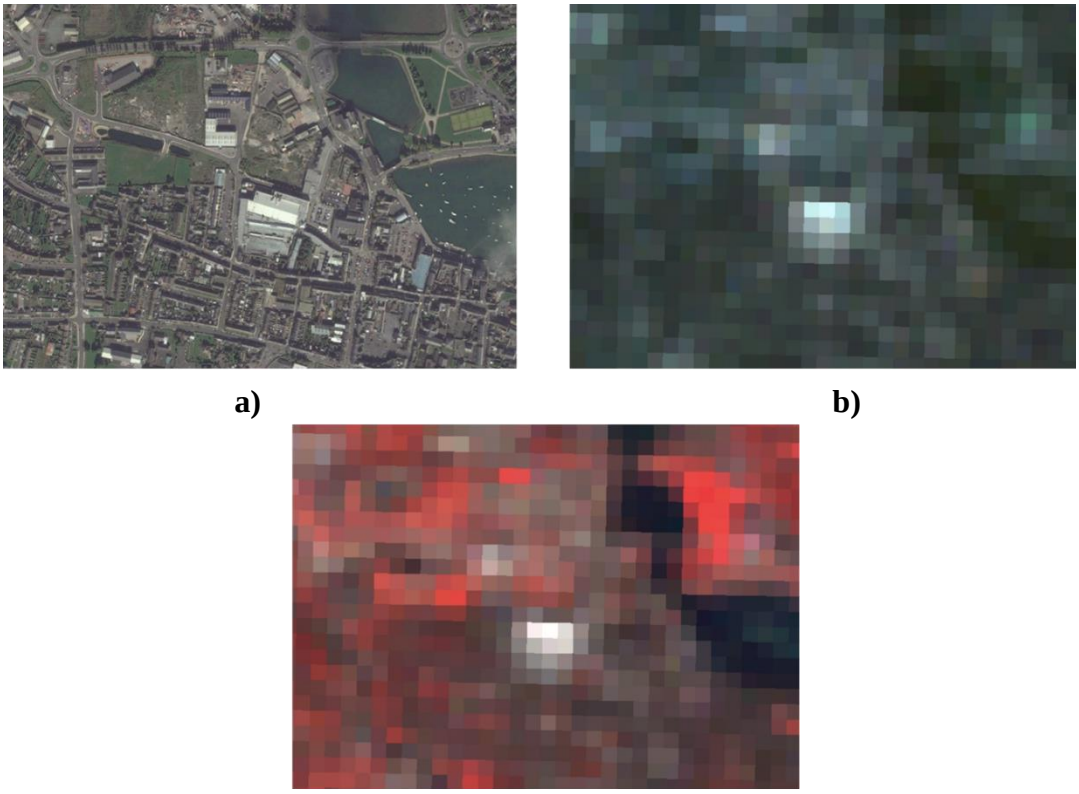

a) **b)**

c)

Figure 6.4: a) Google Earth Pro Satellite image 2010, b) Landsat 5 Image 2010 True Colour Composite (TCC), c) Landsat 5 Image 2010 False Colour Composite (FCC)

At this stage, two types of accuracy measures were computed using a confusion or error matrix; the user and producer accuracies (Equation 6.1 and 6.2). User accuracy is the measure of the pixels that are incorrectly classified and is also known as the Type I error or the error of commission (Eq. 6.1). Producer accuracy is the measure of pixels that are omitted from the correct class and also known as the Type II error or the error of omission (Eq. 6.2). These two errors provide an accuracy assessment of each class individually.

$$User\ Accuracy\ (\%) = \frac{Number\ of\ correctly\ classified\ pixels\ of\ each\ class}{Total\ number\ of\ reference\ points\ of\ each\ class} * 100 \quad \text{(Eq. 6.1)}$$

$$Producer\ Accuracy\ (\%) = \frac{\frac{Number\ of\ correctly\ classified\ pixels\ of\ each\ class}{Total\ number\ of\ points\ classified\ as\ the\ known\ class}}{} * 100 \quad \text{(Eq. 6.2)}$$

The quality of the classified image was then assessed by calculating the overall accuracy as per Equation 6.3

$$Overall\ Accuracy\ (\%) = \frac{Number\ of\ correctly\ classified\ pixels}{Total\ number\ of\ reference\ points} * 100 \quad \text{(Eq. 6.3)}$$

The classified images were finally exported in TIFF format with the condition that the overall accuracy of the classified images was ≥ 80% which can be considered as a successful accuracy for random forest classifier (Matarira et al., 2022). If the accuracy was below this threshold, resampling of training sets of each class was carried out to ensure higher accuracy on the next run.

6.3.4. Post processing

After the required overall accuracy was achieved, all the classified images were imported into ArcGIS platform. This comprised 39 images in total across 14 WWTPs. The 4 classes were then reduced to 2 classes using the Reclassify tool (under Spatial Analyst Tool) in ArcToolbox – (i) Built-up and (ii) Other. The class "Other" included all the classes initially assigned in GEE code editor except built-up class. This was performed because urbanisation demonstrated by the change in built-up area (impervious surfaces) over the years was the primary focus of this Chapter. All the classified images from the different years were then overlaid on one another to analyse the change in urban land cover over the period of time. The reclassified images (originally set to the extent of the ROI) were eventually clipped according to the agglomeration boundary of each of the 14 WWTPs. The clipped reclassified images were converted to vector (shapefile) format.

Finally, the surface areas of the vector classes: “Built-up” and “Other”, were calculated using the Calculate Geometry Tool.

6.3.5. Analysis of impacts of change in urban areas on wastewater influent volumes

The change in built-up area was estimated by comparing an image for a specific agglomeration to the previous image (e.g., if an agglomeration had images for 2014, 2016 and 2018 – the change in built-up area between 2014 and 2016 was measured, similarly for 2016 and 2018 etc.) and was analysed in three different ways as follows:

1. Percentage change in built-up area as shown in Equation 6.4

$$BU_t\% = \frac{BU_{ts} - BU_{tp}}{BU_{tp}} * 100 \qquad \text{(Eq. 6.4)}$$

where, $\boldsymbol{BU_t}$% refers to the percentage change in built-up area over a particular time interval $\boldsymbol{t}$ specific to each agglomeration; $\boldsymbol{BU_{ts}}$ and $\boldsymbol{BU_{tp}}$ refers to the built-up area of the subsequent year $\boldsymbol{ts}$ and the antecedent year $\boldsymbol{tp}$ respectively.

2. Change in the ratio of the built-up area to total agglomeration area as shown in Equation 6.5

$$BU_{tA}\% = \frac{BU_{ts} - BU_{tp}}{A} * 100 \qquad \text{(Eq. 6.5)}$$

where, $\boldsymbol{BU_{tA}}$% represents the percentage change in built-up area to total agglomeration area in time interval $\boldsymbol{t}$, $\boldsymbol{BU_{ts}}$ and $\boldsymbol{BU_{tp}}$ represent the same variables as in Equation 6.4 and $\boldsymbol{A}$ is the total agglomeration area which is constant over the years.

3. Rate of urbanisation as shown in Equation 6.6

$$BU_{tR}\% = \frac{\frac{BU_{tf} - BU_{ti}}{BU_{ti}} * 100}{tf - ti} \qquad \text{(Eq. 6.6)}$$

where, $\boldsymbol{BU_{tf}}$ is the built-up area in the final year tf, $\boldsymbol{BU_{ti}}$ is the built-up area in the initial/first year ti and $\boldsymbol{BU_{tR}}\%$ is the average annual rate of change in built-up or the rate of urbanisation/year during the monitoring period.

Since the 14 agglomerations considered vary with respect to i) the size of their surface area and ii) the temporal range of data availability; all the built-up variables in the three equations mentioned above are expressed as percentages for standardisation purpose. Finally, the response of influent volumes to $\boldsymbol{BU_t}\%$, $\boldsymbol{BU_{tA}}\%$ and $\boldsymbol{BU_{tR}}\%$ individually and combined with the % change in precipitation (for $\boldsymbol{BU_t}\%$ and $\boldsymbol{BU_{tA}}\%$) and rate of change in average annual precipitation (for $\boldsymbol{BU_{tR}}\%$) was assessed by linear regression analysis in R and visual interpretation.

6.4. Results and Discussion

This section presents the results of the different stages of LULC classification and the results of analysing the relationship between the built-up variables with and without the precipitation variable and influent volume. Results are demonstrated with examples of agglomerations and WWTPs.

6.4.1. Results for LULC classification

After accounting for cloud cover and other criteria outlined in Section 6.3.1, between 2 and 4 images were found to be suitable for each agglomeration. The final classified images after multiple runs of resampling and classification algorithm for the different years for agglomeration A4 are demonstrated in Figure 6.5 as an example.

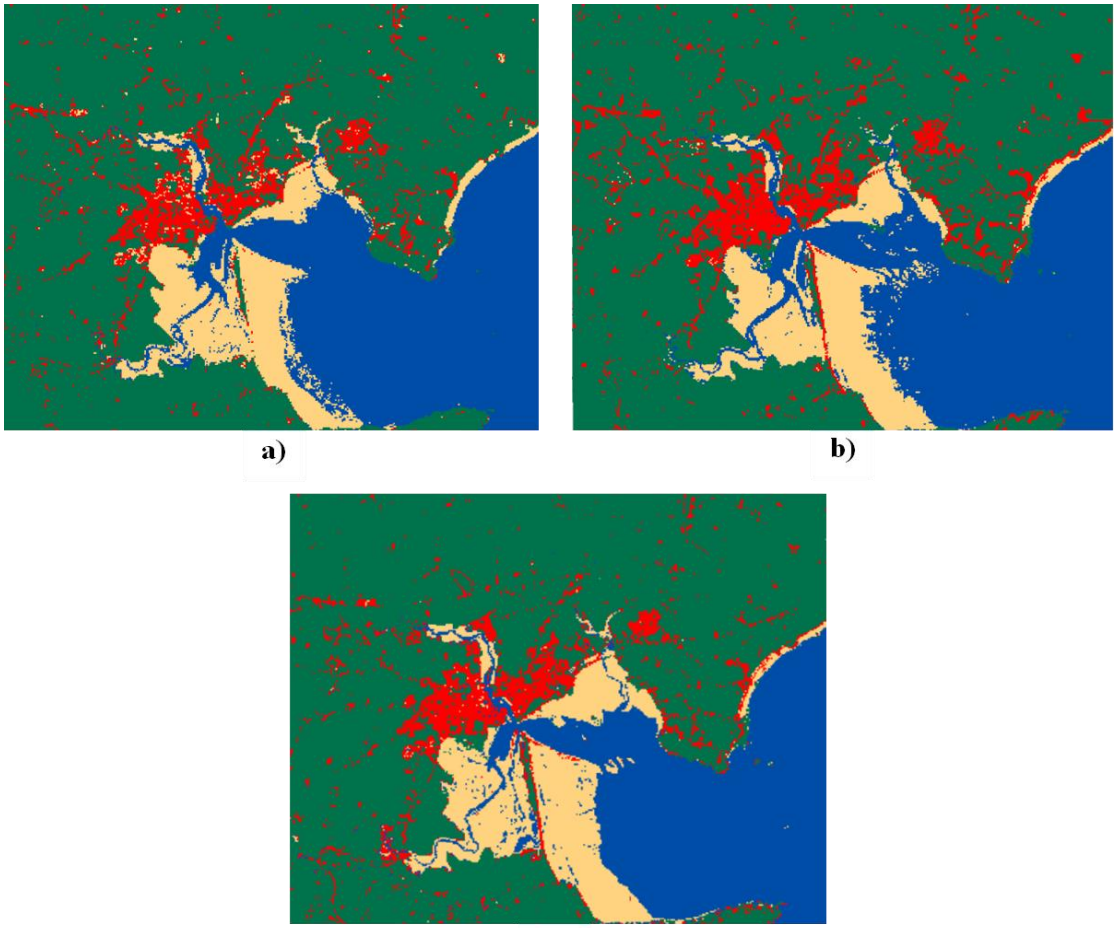

Figure 6.5: LULC classified images set to the ROI boundary in GEE code editor for agglomeration A4 for the years a) 2010 (LANDSAT 5), b) 2015 (LANDSAT 8) and c) 2018 (LANDSAT 8)

As mentioned in Section 6.3.3, accuracy assessment in ArcGIS with the help of random sampling eliminated the possibilities of any bias induced by the user and therefore, was found to be a better technique in validating the classified images. The user and producer accuracies of each of the class for agglomeration A4 is shown in Table 6.3.

Table 6.3: Error matrix of the classified images for agglomeration A4

2010						
Class	**Built-up**	**Water**	**Green cover**	**Open Spaces**	**Total**	**User Accuracy**
Built-up	**35**	1	2	2	40	87.5%
Water	0	**33**	2	5	40	82.5%
Green cover	1	0	**37**	2	40	92.5%
Open spaces	0	3	2	**35**	40	87.5%
Total	36	37	43	44	160	
Producer accuracy	97.2%	89.2%	86.0%	79.5%		

2015						
Class	**Built-up**	**Water**	**Green cover**	**Open Spaces**	**Total**	**User Accuracy**
Built-up	**34**	1	4	1	40	85.0%
Water	0	**34**	0	6	40	85.0%
Green cover	1	0	**39**	0	40	97.5%
Open spaces	0	3	1	**36**	40	90.0%
Total	35	38	44	43	160	
Producer accuracy	97.1%	89.5%	88.6%	83.7%		

2018						
Class	**Built-up**	**Water**	**Green cover**	**Open Spaces**	**Total**	**User Accuracy**
Built-up	**33**	0	5	2	40	82.5%
Water	0	**34**	0	6	40	85.0%
Green cover	2	0	**38**	0	40	95.0%
Open spaces	0	1	0	**39**	40	97.5%
Total	35	35	43	47	160	
Producer accuracy	94.3%	97.1%	88.4%	83.0%		

Each column of this table refers to the total number of samples classified under each LULC class. Each row refers to the total number of reference samples. For example, for the year 2010, a total of 36 samples were classified as built-up out of a total of 40 reference built-up training samples. Out of the 36 classified built-up samples, 35 were correctly classified, 1 sample which was green cover was incorrectly classified as built-up. Therefore, the producer accuracy for built-up as per Equation 6.2 is the ratio of 35 to 36 multiplied by 100, which equates to 97.2%. On the other hand, as we go across the row, for the year 2010, it was observed that, out of 40 reference samples of built-up, 35 were correctly classified, 1 was classified as water, 2 were classified as green cover and 2 were classified as open spaces. As per Equation 6.3, the user accuracy for built-up is the ratio of 35 to 40 multiplied by 100, which equates to 87.5%. Similarly, producer and user accuracies of each of the LULC class for each year are shown in Table 6.3. The overall accuracies as per Equation 6.4, for each of the 14 agglomerations were found to be greater than 80% (Table 6.4).

Table 6.4: Overall accuracy of all agglomeration as per Equation 6.3

Agglomeration	Year of the classified image	Overall accuracy
A1	2014	86.6%
	2016	87.0%
	2018	85.5%
A2	2006	81.2%
	2011	83.7%
	2015	84.4%
	2018	86.2%
A3	2011	90.1%
	2015	90.1%
	2018	91.6%
A4	2010	87.5%
	2015	89.3%
	2018	90.0%
A5	2014	89.2%
	2016	90.0%
	2018	91.7%
A6	2015	85.0%
	2018	83.1%
A7	2014	89.5%
	2016	84.0%
	2018	89.0%
A8	2011	82.5%
	2015	84.2%
	2018	84.2%
A9	2011	91.0%
	2015	90.0%
	2018	89.0%
A10	2015	86.9%
	2018	86.2%
A11	2015	86.9%
	2018	86.2%

A12	2010	88.8%
	2015	91.8%
	2018	86.2%
A13	2016	82.0%
	2018	85.0%
A14	2014	83.0%
	2016	84.0%
	2018	81.0%

The accuracy of the classified images is impacted by the presence of mixed pixels on ground characterised by two or more LULC types. Such pixels are difficult to classify, particularly in moderate resolution LANDSAT images of 30 m x 30 m pixel sizes. Moreover, built-up pixels and pixels of sediments or sand particles have similar reflectance values. In case of agglomeration A4, the open spaces include sediments as shown in Figure 6.5. As a result, they are interchangeably misclassified by the algorithm. This is the most common reason why misclassification occurred during the LULC classification process in this research. There are also certain errors inherently present in the imagery that are caused due to factors such as technical errors while capturing the image, atmospheric conditions etc., that are beyond the control of the user. The classified image with the ROI boundary overlaid with the agglomeration boundary is shown in Figure 6.6.

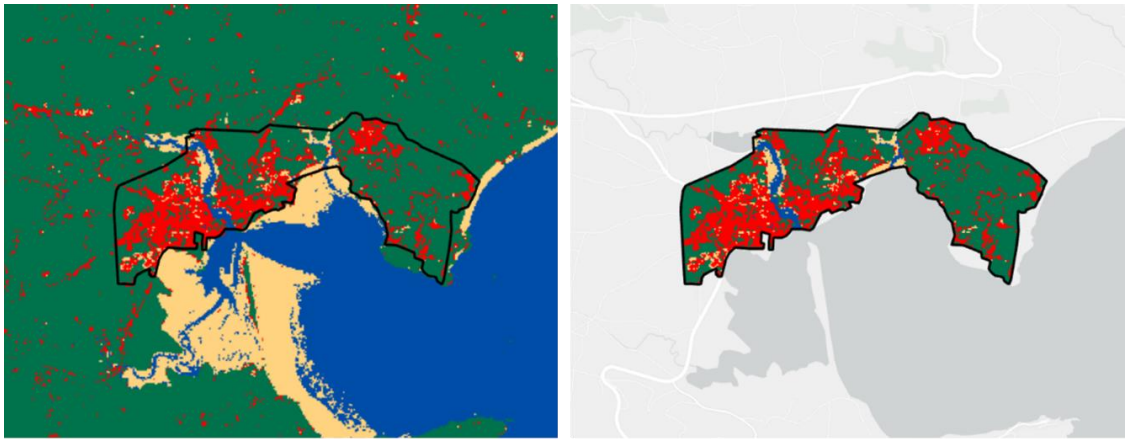

Figure 6.6: a) Classified image set to ROI with overlaid agglomeration boundary of A4 and b) Classified image clipped to agglomeration boundary of A4

Finally, the vector shapefiles of the reclassified images clipped to the agglomeration boundaries in ArcGIS for all the agglomerations were created as demonstrated by an example in Figure 6.7.

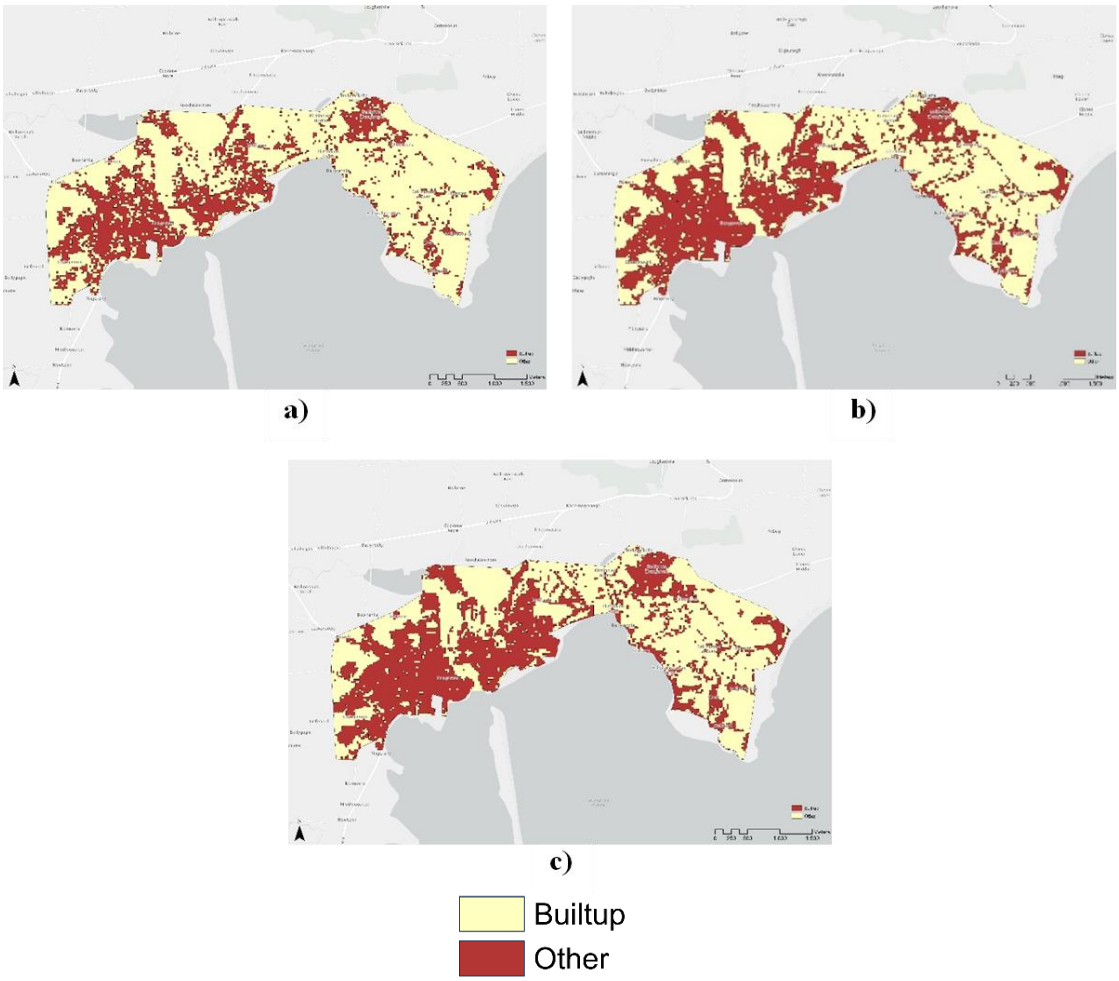

Figure 6.7: Reclassified vector shapefiles of agglomeration A4 into built-up areas represented by red, and other landuse areas represented by yellow for a) 2010, b) 2015 and c) 2018

6.4.2. Built-up Cover Change detection

The surface area of built-up class increased across all the time intervals for each of the agglomerations (Appendix III). An example of the change in built-up area from 2014 to 2018 in a 2-year interval period is shown in Table 6.5.

Table 6.5: Estimation of change in built-up area for agglomeration A4 (example) over 2010 – 2018

Year	Area in sq. m	Time interval	% Change in built-up area
2010	4161552	-	-
2015	4777729	2010 – 2015	14.80%
2018	5215966	2015 - 2018	9.20%

As shown in Table 6.5, in agglomeration A4, urban area increased from 2010 to 2015 by 14.8% and from 2015 – 2018 by 9.2%.

6.4.3. Comparative response of influent volumes to urbanisation and change in precipitation

Out of the three urbanisation variables, i.e., % change in built-up area ($\boldsymbol{BU_t}$%), % change in the built-up to agglomeration area ($\boldsymbol{BU_{tA}}$%) and rate of urbanisation/year ($\boldsymbol{BU_{tR}}$%), $\boldsymbol{BU_{tA}}$% was found to be a statistically significant variable at a 95% level of confidence, in helping explain changes in influent volume over each interval period across all agglomerations. This variable estimated the change in built-up area in each agglomeration relative to its agglomeration area and thereby, provided a greater degree of insight into the changes in influent volume contributed by the existing urban to non-urban area ratio within each agglomeration. This might be the reason why R^2 value was the highest ($R^2 = 0.17$ showing a moderate degree of correlation as per Table 4.2, Chapter 4) for $\boldsymbol{BU_{tA}}$% (Table 6.6). On the contrary, $\boldsymbol{BU_t}$% for each agglomeration indicates just the absolute value of the change in built-up area but does not account for the degree to which urbanisation occurred relative to total agglomeration area and hence showed a lower R^2 value with influent volumes. The difference in outcomes between $\boldsymbol{BU_t}$% and $\boldsymbol{BU_{tA}}$% can be explained with the help of an example. Let us suppose agglomeration AX has a total surface area of 500 m^2 and initial built-up area of 100 m^2 and agglomeration AY has a total surface area of 5000 m^2 with an initial built-up area of 500 m^2. As per Equation 6.4, a 50% increase in built-up area ($\boldsymbol{BU_t}$%) would mean that the built-up increased from 100 m^2 to 150 m^2 for agglomeration AX and from 500 m^2 to 750 m^2 for agglomeration AY. However, since AY is ten times greater in size than AX, a 50% increase in built-up area in AY (250 m^2 increase out of 5000 m^2 agglomeration area) will not have a significant impact on influent volumes as compared to a 50% increase in built-

up area in AX (50 m^2 increase out of 500 m^2 agglomeration area) which is much smaller in size. As per Equation 6.5, when the surface area of each agglomeration is accounted for, $\boldsymbol{BU_{tA}}$% can be computed to be 10% and 5% respectively for agglomerations AX and AY. Hence, $\boldsymbol{BU_{tA}}$% makes more sense while considering all the agglomerations together as the consequences of the same value for $\boldsymbol{BU_t}$% for two agglomerations might vary if the agglomerations differ in size. This result implies that influent volumes are affected by the degree of urbanisation relative to total space in each agglomeration, rather than urbanisation itself.

On the other hand, BU_{tR}% accounts for the difference in the temporal range of data availability across the 14 agglomerations. However, R^2 between BU_{tR}% and rate of change of influent volume was the lowest. This might be because rate of urbanisation/year is small and hence, insignificant in contributing towards influent volumes. New urban developments over the years might be connected to sanitary sewers which will not contribute to influent volumes resulting in dissociation of urbanisation and influent volumes. Moreover, BU_{tR}% does not consider the relative changes in built-up area to other LULC types over the years within each agglomeration area which might have a higher degree of influence on influent volumes as indicated by $\boldsymbol{BU_{tA}}$%.

Table 6.6: R^2 values of change in influent volume v/s change in built-up area and precipitation

Variables	R^2/ Adjusted-R^2	p-value
$\boldsymbol{BU_t}$% v/s % change in influent volume	0.04	0.3348
$\boldsymbol{BU_{tA}}$%* v/s % change in influent volume	0.17	0.0432
$\boldsymbol{BU_{tR}}$% v/s rate of change (%) of influent volume	0.03	0.3012
% change in precipitation* v/s % change in influent volume	0.30	0.0060
rate of change in precipitation* (%) v/s rate of change of influent volume	0.49	0.0063
$\boldsymbol{BU_t}$% and % change in precipitation* v/s % change in influent volume	0.23	0.0114

$\boldsymbol{BU_{tA}}$% and % change in precipitation* v/s % change in influent volume	0.28	0.0126
$\boldsymbol{BU_{tR}}$% and rate of change in precipitation* (%) v/s rate of change of influent volume	0.48	0.0047
Adjusted- R^2 is only reported for the multiple linear regression model results		

Precipitation was found to be statistically significant throughout all the results. In all the cases the predictor variables were positively correlated with influent volume (intercept was negative across all the models). The model errors and RMSEs of all the regression models indicated that their predictive powers were low. When both urbanisation and precipitation variables were considered, the adjusted-R^2 (which compensates for the overestimation of the goodness-of-fit of the model) decreased as compared to R^2 when precipitation was considered alone. This is because urbanisation is only slightly correlated to influent volumes as compared to precipitation and including urbanisation in the multiple linear regression model does not necessarily improve the model fit. This indicates that precipitation is a stronger contributor to influent volumes as compared to urbanisation.

Generally, the expected response to increase in impervious surfaces is also amplified influent volumes due to the increase in stormwater runoff as evident from the numerous studies discussed in the literature review. Despite the marginal impact of urbanisation on influent volumes, as observed from the regression analysis results, a number of case-specific examples are highlighted in more detail below (Figure 6.8, Figure 6.9 and Figure 6.10).

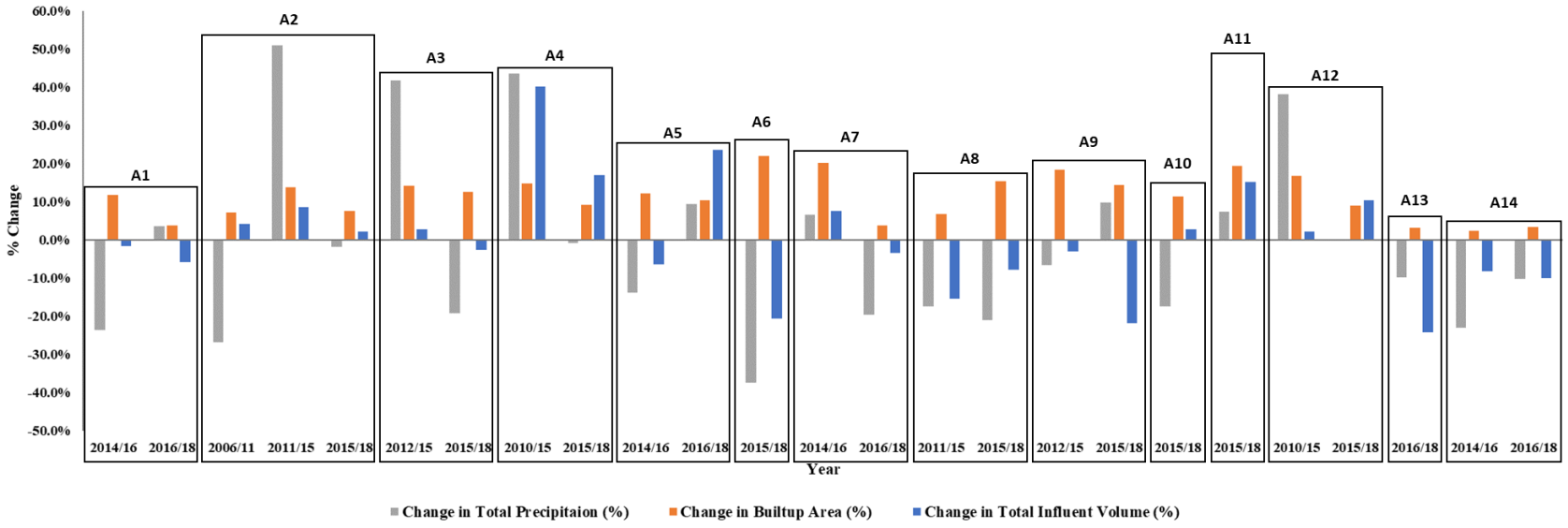

Figure 6.8: Percentage change (y-axis) in precipitation (grey bars), built-up area (orange bars) and influent volume (blue bars) over the different time periods (x-axis) particular to each agglomeration

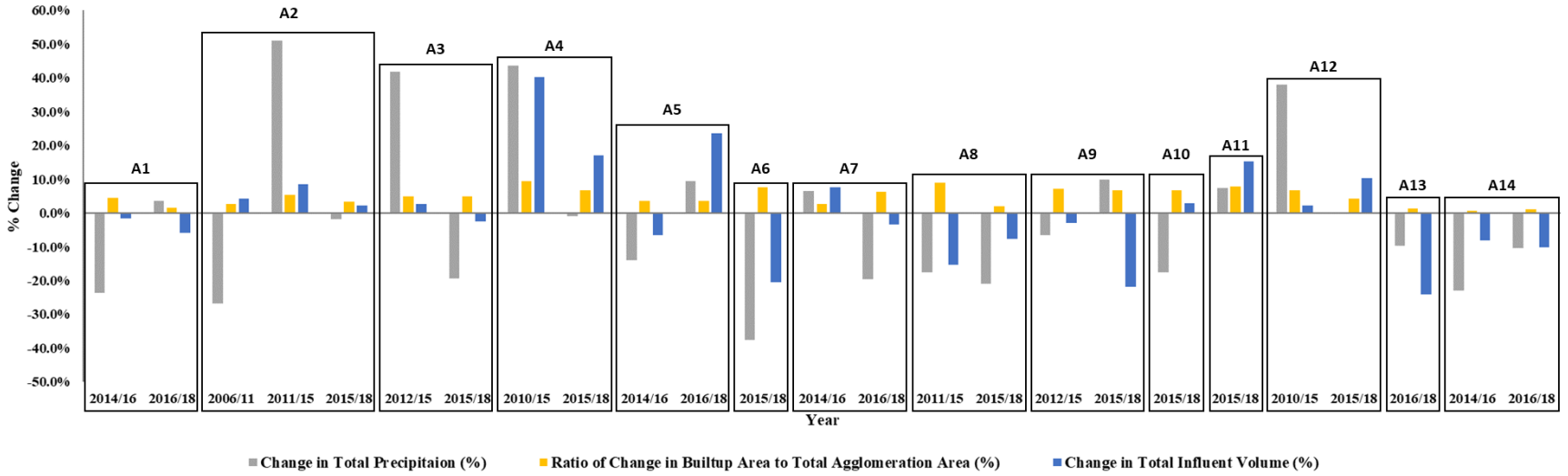

Figure 6.9: Percentage change (y-axis) in precipitation (grey bars), built-up are with respect to agglomeration area (yellow bars) and influent volume (blue bars) over the different time periods (x-axis) particular to each agglomeration

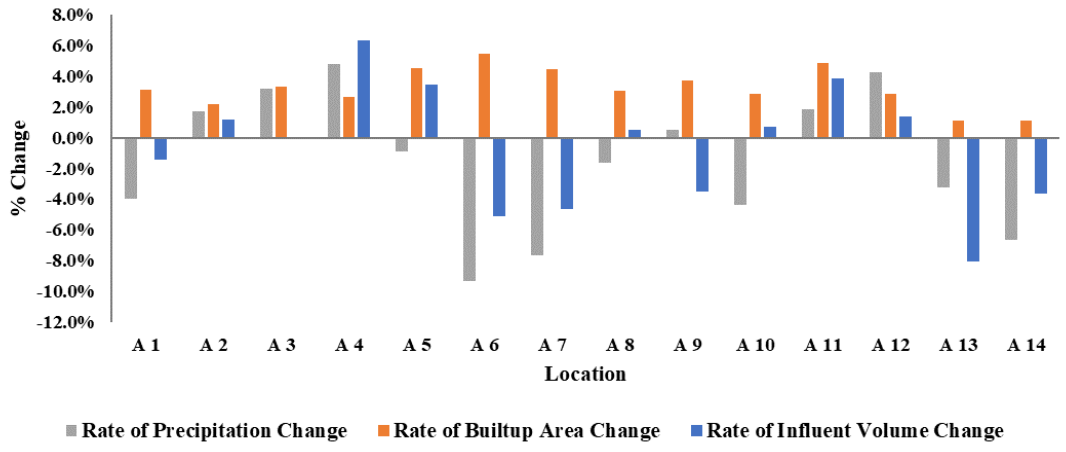

Figure 6.10: Rate of change (%) in precipitation/year (grey bars), built-up area/year (orange bars) and influent volume/year (blue bars) across all agglomerations

There were four different outcomes of influent volumes observed from Figure 6.8, Figure 6.9 and Figure 6.10 which were triggered by both the change in built-up variable and change in precipitation: i) increase in built-up area and precipitation leading to increase in influent volume, ii) increase in built-up area and precipitation leading to decrease in influent volume, iii) increase in built-up area and decrease in precipitation leading to increase in influent volumes and iv) increase in built-up and decrease in precipitation leading to decrease in influent volumes. For the purpose of comparison of these mixed trends (different hydraulic response characteristics), the results for agglomerations A1, A2, A4, and A14 in Figure 6.8 are discussed in detail.

For agglomeration A1, during the time period 2014 – 2016, there was a reduction in the precipitation amount by more than 20% accompanied by an increase in built-up area by 10%. It was observed that the influent volumes decreased by around 1%. The slight change in influent volume may reflect the reduced precipitation which off-sets the increase in built-up area in agglomeration A1. However, during 2016 – 2018, both built-up area and precipitation increased by 3 – 4% but influent volume declined by 5%. The reason for this outcome might be because the increase in built-up area and precipitation was marginal and some other factors such as soil moisture deficit, evapotranspiration rate etc. might play a bigger role which are not analysed. In addition to that, there might be the occurrence of possible overflows in the sewer network which might mask the influent volume increases (if any) during this period. For example, there was one incident in

agglomeration A1 in 2017 when surcharge of the sewer network resulted in spillage of wastewater onto the road (Annual Environmental Report for agglomeration A1, EPA Ireland, 2017). This factor could also be the reason why, during 2011 – 2015 for agglomeration A2, when there was a significant increase in precipitation amount by around 50% and built-up area by just more than 10%, influent volumes increased by only 8% which was relatively low. Agglomeration A2 also had a number of overflow events during this period which might have resulted from hydraulic overloading of the sewer network (Annual Environmental Report for agglomeration A2, EPA Ireland, 2015).

Agglomeration A4 showed an increase in precipitation by around 40% and increase in built-up area by approximately 12% during the period 2010 – 2015. Influent volume increased by around 40% during the same period. The significantly high percentage change in influent volume could be the combined effects of precipitation and urbanisation, but based on the results above, mostly due to precipitation. In case of agglomeration A14, for all the time periods (2014 – 2016 and 2016 – 2018), there was reduction in precipitation, although the built-up cover increased. Influent volumes were observed to decrease during both the periods. These results indicate that, out of the two predictor variables, precipitation was a stronger contributing factor towards variation in influent volumes. Lastly, there have been recent changes to storm water management in Ireland. New developments are required to have separate storm drainage systems which might result in reduced stormwater ingress at the inlets of the WWTPs (Irish Water, 2020). These developments might have already taken place in many agglomerations across Ireland which could be an explanation for the disasscociation of impervious areas with influent volumes. Moreover, these newer developments might have taken into consideration low impact developments such sustainable drainage systems, green blue infrastructure, rainwater storage etc. and might have adopted best management practices. The different outcomes in the relationship between urbanisation, precipitation and influent volumes across the different agglomerations highlight individual characteristics and scenarios specific to each agglomeration.

Overall, the marginal impact of urbanisation on the influent volumes across all the agglomerations considered in this thesis might be attributed to additional factors such as soil moisture deficit and evapotranspiration rates. In Ireland, the soil moisture deficit in the east (e.g., Dublin Airport) is generally lower than in the west (e.g. Valentia) (Allen et

al., 1998; Schulte et al., 2005; Garcia et al., 2022). According to EPA, the average annual mean soil moisture deficit (1981 – 2016) for poorly drained soil ranges from -5 mm to +15 mm from west to east (Werner et al., 2016). The same report states that actual evapotranspiration is highest along the western coast of Ireland. Depending on the soil type, poorly, moderately or well-drained soil types, evapotranspiration rate, and soil moisture deficit, the runoff might be impacted, which will eventually impact influent volumes. For example for a highly saturated soil and high water table, depending on the season of the year, urbanisation might not have as much effect on runoff due to lower percolation of water into the sub-surface layers of the soil (Zope et al., 2016).

6.5. Conclusions

This Chapter conducted a comprehensive investigation of the possible impacts of urbanisation on wastewater treatment plants. This analysis was enhanced by the inclusion of change in precipitation as one of the additional variables to explain the variation in influent volume. LULC classification of remotely sensed satellite images was carried out using coding in JavaScript programmimg languange in Google Earth Engine Code Editor. Accuracy assessment showed more than 80% accuracy for all the classfied images. Although this platform has been used for LULC change detection in various studies, it has been used in a study of WWTP influent volumes for the first time in this thesis.

Trend analysis of LULC change in the 14 agglomerations and their corresponding influent volumes of the 14 WWTPs was carried out. The results indicated that, in order to detect the trend in influent volumes, the % change of built-up area relative to agglomeration area was a stronger indicator as compared to the percentage change in built-up area and the rate of urbanisation/year. Precipitation change was found to be statistically significant and the stronger contributor to influent volumes as compared to urbanisation. Additional factors that were identified as potential influencers contributing towards variation in influent volumes are lag-time, hydraulic overloading and overflow of untreated wastewater, developments of sewer networks etc., that might have led to the dissociation of stormwater runoff (from impervious areas) and influent volumes. As the findings could not fully demonstrate the impacts of urbanisation on influent volumes, additional parameters such as soil moisture deficit and evapotranspiration data, will aid in further understanding the response characteristics of WWTP influent volumes connected with combined collection systems. Information about wastewater networks,

connections, pipelines etc. can be promising in terms of improving the understanding of urbanisation impacts on WWTPs.

7. CONCLUSIONS AND RECOMMENDATIONS

7. Conclusions and recommendations

7.1. Overview

The operations of wastewater treatment plants (WWTPs), particularly ones connected to combined sewerage systems, can often encounter challenges such as hydraulic overloading and combined sewer overflows. In the case of hydraulic overloading, the WWTP can no longer treat the incoming wastewater effectively. On days with heavy precipitation intensity, combined sewer overflows can result in untreated wastewater being released into the environment leading to serious pollution. With factors such as climate change (current and future) and urbanisation, the frequency of occurrence of such events may be amplified. As stricter environmental regulations towards releasing of treated and untreated wastewater are enforced to protect the receiving waters, it has become increasingly important to identify crucial variables that impact the maintenance and operations of WWTPs. A critical parameter to consider is influent volume at the inlet of a WWTP. Due to factors downstream of the CSO during and after skills, there is still variations in the wastewater inflow which is accounted for in influent volumes. Therefore influent volumes have a significant impact on subsequent WWTP processes, and their management can prevent occurrences of overflows. Given WWTPs can have a design life of between 20 and 50 years projecting future influent volumes is key to both efficient design and operation of such facilities.

In this research, the importance of influent volumes has been thoroughly established. An extensive temporal range of precipitation and influent volume data were obtained for 14 WWTPs (population equivalents ranging from 3,000 to 1,640,000), spatially distributed across Ireland. The data was analysed to determine the impacts of precipitation on influent wastewater volumes. In addition to this, out of the 14 WWTPs, location-specific information such as daily maximum tidal level and daily mean river level were collected for WWTPs located near coasts or rivers, respectively. The relationships between these variables and influent volumes were explored. Future high-resolution regional climate model projections of precipitation variables under RCP 4.5 and RCP 8.5 emission scenarios were obtained for each of the 14 WWTPs to project the evolution of influent volumes, based on the predicted changes in precipitation to mid-century. Lastly, Landsat satellite images for each of the 14 agglomerations corresponding to each WWTP were also obtained to analyse how urbanisation might impact wastewater influent volumes.

7.2. Conclusions

The main conclusions of this research are as follows:

- Regression analyses revealed that local daily precipitation, and daily mean river level, when considered separately, were statistically significant at a 95% level of confidence in explaining some of the variation in influent volumes at a daily scale for each of the 14 WWTPs. R^2 values between daily precipitation and daily influent volume ranged from very low to marked correlation (R^2 = 0.03 – 0.38). Seven out of the 14 WWTPs showed better correlation between daily precipitation and 1-day lagged influent volumes, when compared with 0-day lag. River level and influent volume showed marked to high degrees of correlation (R^2 = 0.49 – 0.61) for the 3 WWTPs with local rivers. Daily maximum tidal level was found to be a significant variable in relation to dry weather flow for treatment plants close to the sea.
- On a monthly basis, for each of the 14 WWTPs individually, monthly average daily precipitation, number of wet days in a month and number of zero rainfall days in a month were found to be statistically significant contributors at a 95% level of confidence, when considered separately. Moderate to high degrees of correlation were observed between each of the predictor variables individually (R^2 = 0.26 – 0.84 for monthly average daily precipitation and R^2 = 0.20 – 0.56 for number of zero rainfall days in a month) with monthly average daily influent volumes. When considered together, monthly average daily precipitation and number of zero rainfall days were statistically significant. However, monthly average daily precipitation was found to be the stronger contributor towards influent volumes.
- A novel pooled model across all the 14 WWTPs linking the monthly average daily influent volume to monthly average daily precipitation and number of zero rainfall days in a month was developed through spatio-temporal analysis which demonstrated a high predictive capacity. This model accounted for the spatial and temporal variation of rainfall and influent volume characteristics by using observed datasets across the 14 WWTPs. This pooled model consisting of WWTPs of varying sizes, was cross validated with the Leave One Out Cross Validation method and the model errors indicated that the pooled model could be

adapted to model the generic trend in influent volumes of any WWTP, connected with CSS, while also accounting for the local characteristics of the WWTP.

- Probability of exceedance curves were developed from observed daily datasets of precipitation and influent volumes. These curves allow for analysis of the likelihood that influent volume would exceed a given limit under a range of precipitation categories. The probability of exceedance curves thereby, enables the explanation of key hydraulic responses to rainfall, allowing utilities to identify potential vulnerabilities (e.g., exceedance of peak design capacities) in their networks. These curves can also be considered in the context of future rainfall projections (e.g. extreme events) to identify specific influent volume events of interest, giving indications as to the exceedance of peak design capacity of WWTPs.
- Future climate change impacts based on high-resolution multi-model RCM projected monthly precipitation data were observed to be seasonally variable with the highest decrease in influent volumes during the summer months and the highest increase during the winter months, particularly under the high greenhouse gas emission scenario RCP 8.5. While 13 of the 14 WWTPs examined were found to have sufficient reserve hydraulic capacity under RCP 4.5 and RCP 8.5, one of the 14 WWTPs was found to be particularly vulnerable to climate change impacts
- The probability of exceedance curves when applied to projected extreme events in the future, showed that increases in expected high (< 20 mm/day) and very high precipitation (> 30 mm/day) would reduce the return period of overflow events across all WWTPs under both RCPs 4.5 and 8.5. For example, the return period for annual exceedance of peak design capacity of WWTP 1 under high precipitation days was found to reduce from 5 years under current conditions to 4.6 years and 4.4 years under RCP 4.5 and RCP 8.5, respectively. On the other hand, under very high precipitation days, the return period of such events was shown to reduce from 5 years (current) to 4.2 years (RCP 4.5) and 4.1 years (RCP 8.5).
- Despite the strong correlation between urbanisation and stormwater runoff from various literature discussed in Chapter 2, urbanisation was found to have negligible to moderate degree of correlation with influent volumes. Rate of urbanisation per year showed negligible correlation (R^2 = 0.03) with rate of

change of influent volume per year. Similarly, there was negligible correlation between the percentage change in urban area and percentage change in influent volume for a given time ($R^2 = 0.04$). It is noted however that percentage change in built-up area relative to total agglomeration area was found to be statistically significant at a 95% level of confidence across all agglomerations with $R^2 = 0.17$ with influent volumes. There was dissociation between stormwater runoff and influents potentially arising from a number of factors such as lag-time, recent developments of sewer networks and possible transition from combined to separate sewer systems, hydraulic overloading and overflow of untreated wastewater etc.

Despite have a high degree of uncertainty associated with precipitation projections, a significant contribution of this research is that the high-quality multi-model RCM projections could be used to derive meaningful cause-impact relationships between extreme events and exceedance of peak design capacities in future. The impact of the climate projection uncertainty on the influent volume projections estimated in this research could be captured to an extent with the help of the 33rd and 66th percentiles of the ensemble of RCM projections of mean precipitation. This would help wastewater utility managers in enhancing the understanding of network response characteristics to rainfall. This research will assist them in making informed decisions in mitigating risks and vulnerabilities in the network and developing adaptation strategies to combat the effects of climate change. The methodology enables users to adapt it to different WWTPs across the world, while also keeping in mind the local characteristics specific to each WWTP as derived from the individual WWTP models.

7.3. Recommendations for future work

Some of the recommendations for future work are as follows:

- The understanding of the relationship between precipitation and influent volume characterised by lag-time should be improved by integrating sub-daily level datasets and network information about directly connected areas to the WWTPs etc. Access to such data will enhance the existing model and will also help to focus on the response characteristics of influent volumes at a much-detailed time scale.

- Because of the adaptability of the pooled model derived from spatio-temporal analysis across a range of WWTPs of various sizes, further study can update the model by including data from other WWTPs. However, this model is likely only suitable only for WWTPs with combined sewerage systems. As rainfall characteristics change spatially and characteristics of influent volumes change with WWTPs, the coefficients of the model would change. Nonetheless, future studies have the scope of updating the model with additional information, thereby increasing the robustness of the model.
- Investigation of impacts on influent volumes in future could leverage precipitation variables at a finer scale, where access to higher temporal resolution (monthly and daily, as opposed to seasonal) RCM projections are available. Additionally, higher spatial resolution (< 4 km) projection datasets with higher accuracy from updated climate models from more recent reports will provide a deeper insight into evolution of influent volumes in future.
- Better understanding of the evolving dynamics of wastewater influent characteristics can also be achieved by integrating other variables such as projected sea level rise, demographics, etc.
- Future work should also take into consideration other additional variables such as soil moisture deficit, evapotranspiration, water consumption etc. at different time scales to assess their impacts on wastewater influent volumes.

REFERENCES

References

Abdellatif, M., Atherton, W., & Alkhaddar, R. (2014). Assessing combined sewer overflows with long lead time for better surface water management. In *Environmental Technology (United Kingdom)* (Vol. 35, Issue 5, pp. 568–580). https://doi.org/10.1080/09593330.2013.837938

Amani, M., Ghorbanian, A., Ahmadi, S. A., Kakooei, M., Moghimi, A., Mirmazloumi, S. M., Moghaddam, S. H. A., Mahdavi, S., Ghahremanloo, M., Parsian, S., Wu, Q., & Brisco, B. (2020). Google Earth Engine Cloud Computing Platform for Remote Sensing Big Data Applications: A Comprehensive Review. *IEEE Journal of Selected Topics in Applied Earth Observations and Remote Sensing*, *13*, 5326–5350. https://doi.org/10.1109/JSTARS.2020.3021052

Arnbjerg-Nielsen, K.Arnbjerg-Nielsen, K. (2011). Past, present, and future design of urban drainage systems with focus on Danish experiences. Water Science and Technology, 63(3), 527–535. https://doi.org/10.2166/wst.2011.253. (2011). Past, present, and future design of urban drainage systems with focus on Danish experiences. *Water Science and Technology*, *63*(3), 527–535. https://doi.org/10.2166/wst.2011.253

Arnbjerg-Nielsen, K. (2012). Quantification of climate change effects on extreme precipitation used for high resolution hydrologic design. *Urban Water Journal*, *9*(2), 57–65. https://doi.org/10.1080/1573062X.2011.630091

Astaraie-Imani, M., Kapelan, Z., & Butler, D. (2013). Improving the performance of an integrated urban wastewater system under future climate change and urbanisation scenarios. *Journal of Water and Climate Change*. https://doi.org/10.2166/wcc.2013.078

Astaraie-Imani, M., Kapelan, Z., Fu, G., & Butler, D. (2012). Assessing the combined effects of urbanisation and climate change on the river water quality in an integrated urban wastewater system in the UK. *Journal of Environmental Management*, *112*, 1–9. https://doi.org/10.1016/j.jenvman.2012.06.039

Berggren, K., Olofsson, M., Viklander, M., Svensson, G., & Gustafsson, A.-M. (2012).

Hydraulic Impacts on Urban Drainage Systems due to Changes in Rainfall Caused by Climatic Change. *Journal of Hydrologic Engineering*, *17*(1), 92–98. https://doi.org/10.1061/(asce)he.1943-5584.0000406

Bo, W. (2014). *Environmental Science Use of online water quality monitoring for assessing the e ff ects of WWTP over fl ows in rivers*. 1510–1518. https://doi.org/10.1039/c3em00449j

Budd, E., Babcock, R. W., Spirandelli, D., Shen, S., & Fung, A. (2020). Sensitivity analysis of a groundwater infiltration model and sea-level rise applications for coastal sewers. *Water (Switzerland)*, *12*(3). https://doi.org/10.3390/w12030923

Butler, D., McEntee, B., Onof, C., & Hagger, A. (2007). Sewer storage tank performance under climate change. *Water Science and Technology*, *56*(12), 29–35. https://doi.org/10.2166/wst.2007.760

Cahoon, L. B., & Hanke, M. H. (2017). Rainfall effects on inflow and infiltration in wastewater treatment systems in a coastal plain region. *Water Science and Technology*, *75*(8), 1909–1921. https://doi.org/10.2166/wst.2017.072

Cahoon, L. B., & Hanke, M. H. (2019). Inflow and infiltration in coastal wastewater collection systems: Effects of rainfall, temperature, and sea level. *Water Environment Research*, *91*(4), 322–331. https://doi.org/10.1002/wer.1036

Chaolin, G. (2020). Definitions of Urbanization. *International Encyclopedia of Human Geography*, *12*, 112–118. https://doi.org/10.1016/B978-0-08-102295-5.10355-5

Coffey, R., Benham, B., Wolfe, M. L., Dorai-Raj, S., Bhreathnach, N., O'Flaherty, V., Cormican, M., & Cummins, E. (2016). Sensitivity of streamflow and microbial water quality to future climate and land use change in the West of Ireland. *Regional Environmental Change*, *16*(7), 2111–2128. https://doi.org/10.1007/s10113-015-0912-0

Colson, M. G. T. L., Gagnon, M. P. C., & Houde, P. G. M. (2019). A major release of urban untreated wastewaters in the St . Lawrence River (Quebec , Canada) altered growth , reproduction , and redox status in experimentally exposed Daphnia magna. *Ecotoxicology*, 843–851. https://doi.org/10.1007/s10646-019-02084-4

Dawson, R. J., Thompson, D., Johns, D., Wood, R., Darch, G., Chapman, L., Hughes, P. N., Watson, G. V. R., Paulson, K., Bell, S., Gosling, S. N., Powrie, W., & Hall, J. W. (2018). A systems framework for national assessment of climate risks to infrastructure. *Philosophical Transactions of the Royal Society A: Mathematical, Physical and Engineering Sciences*, *376*(2121). https://doi.org/10.1098/rsta.2017.0298

Draude, S., Keedwell, E., Hiscock, R., & Kapelan, Z. (2019). A statistical analysis on the effect of preceding dry weather on sewer blockages in South Wales. In *Water Science and Technology* (Vol. 80, Issue 12, pp. 2381–2391). https://doi.org/10.2166/wst.2020.063

European Communities. (2007). *Terms and Definitions of the Urban Waste Water Treatment Directive (91/271/EEC). January*, 1–34. http://nl.wikipedia.org/wiki/Bestand:Waterzuivering_in_Madurodam.jpg

Farjad, B., Gupta, A., Razavi, S., Faramarzi, M., & Marceau, D. J. (2017). An integrated modelling system to predict hydrological processes under climate and land-use/cover change scenarios. *Water (Switzerland)*, *9*(10). https://doi.org/10.3390/w9100767

Flood, J. F., & Cahoon, L. B. (2019). *Linked references are available on JSTOR for this article : Risks to Coastal Wastewater Collection Systems Sea-Level Rise and Climate Change*. *27*(4), 652–660.

Fortier, C., & Mailhot, A. (2015). Climate Change Impact on Combined Sewer Overflows. *Journal of Water Resources Planning and Management*, *141*(5), 04014073. https://doi.org/10.1061/(asce)wr.1943-5452.0000468

Fung, A., & Babcock, R. (2020). A flow-calibrated method to project groundwater infiltration into coastal sewers affected by sea level rise. *Water (Switzerland)*, *12*(7). https://doi.org/10.3390/w12071934

García-Ávila, F., Valdiviezo-Gonzales, L., Iglesias-Abad, S., Gutiérrez-Ortega, H., Cadme-Galabay, M., Donoso-Moscoso, S., & Arévalo, C. Z. (2021). Opportunities for improvement in a potabilization plant based on cleaner production: Experimental

and theoretical investigations. *Results in Engineering*, *11*. https://doi.org/10.1016/j.rineng.2021.100274

Giokas, D., Vlessidis, A., Angelidis, M., Tsimarakis, G., & Karayannis, M. (2002). Systematic analysis of the operational response of activated sludge process to variable wastewater flows. A case study. *Clean Technologies and Environmental Policy*, *4*(3), 183–190. https://doi.org/10.1007/s10098-002-0145-z

Gooré Bi, E., Gachon, P., Vrac, M., & Monette, F. (2017). Which downscaled rainfall data for climate change impact studies in urban areas? Review of current approaches and trends. *Theoretical and Applied Climatology*, *127*(3–4), 685–699. https://doi.org/10.1007/s00704-015-1656-y

Gooré Bi, E., Monette, F., Gachon, P., Gaspéri, J., & Perrodin, Y. (2015). Quantitative and qualitative assessment of the impact of climate change on a combined sewer overflow and its receiving water body. *Environmental Science and Pollution Research*, *22*(15), 11905–11921. https://doi.org/10.1007/s11356-015-4411-0

Hawchar, L., Naughton, O., Nolan, P., Stewart, M. G., & Ryan, P. C. (2020). Climate Risk Management A GIS-based framework for high-level climate change risk assessment of critical infrastructure. *Climate Risk Management*, *29*(May 2019), 100235. https://doi.org/10.1016/j.crm.2020.100235

Hlodversdottir, A. O., Bjornsson, B., Andradottir, H. O., Eliasson, J., & Crochet, P. (2015). Assessment of flood hazard in a combined sewer system in Reykjavik city centre. *Water Science and Technology*, *71*(10), 1471–1477. https://doi.org/10.2166/wst.2015.119

Huang, J., Mendoza, B., Daniel, J. S., Nielsen, C. J., Rotstayn, L., & Wild, O. (2013). Anthropogenic and natural radiative forcing. *Climate Change 2013 the Physical Science Basis: Working Group I Contribution to the Fifth Assessment Report of the Intergovernmental Panel on Climate Change*, *9781107057*, 659–740. https://doi.org/10.1017/CBO9781107415324.018

Hughes, J., Cowper-Heays, K., Olesson, E., Bell, R., & Stroombergen, A. (2021). Impacts and implications of climate change on wastewater systems: A New Zealand

perspective. *Climate Risk Management*, *31*, 100262. https://doi.org/10.1016/j.crm.2020.100262

Hussain, S. N., Zwain, H. M., & Nile, B. K. (2022). Modeling the effects of land-use and climate change on the performance of stormwater sewer system using SWMM simulation: case study. *Journal of Water and Climate Change*, *13*(1), 125–138. https://doi.org/10.2166/wcc.2021.180

Jones, E. R., Van Vliet, M. T. H., Qadir, M., & Bierkens, M. F. P. (2021). Country-level and gridded estimates of wastewater production, collection, treatment and reuse. *Earth System Science Data*, *13*(2), 237–254. https://doi.org/10.5194/essd-13-237-2021

Jung, M., Kim, H., Mallari, K. J. B., Pak, G., & Yoon, J. (2015). Analysis of effects of climate change on runoff in an urban drainage system: A case study from Seoul, Korea. *Water Science and Technology*, *71*(5), 653–660. https://doi.org/10.2166/wst.2014.341

Kaźmierczak, B., & Kotowski, A. (2014). The influence of precipitation intensity growth on the urban drainage systems designing. *Theoretical and Applied Climatology*, *118*(1–2), 285–296. https://doi.org/10.1007/s00704-013-1067-x

Kiely, G. (1999). *Climate change in Ireland from precipitation and stream ¯ ow observations*. *23*, 141–151.

King County Department of Natural Resources and Parks. (2008). *Vulnerability of Major Wastewater Facilities to Flooding from Sea-Level Rise Tidally Influenced Facilities in King County ' s System*. *July*.

Kirchhoff, C. J., & Watson, P. L. (2019). Are Wastewater Systems Adapting to Climate Change? *Journal of the American Water Resources Association*. https://doi.org/10.1111/1752-1688.12748

Kleidorfer, M., Moderl, M., Sitzenfrei, R., Urich, C., & Rauch, W. (2009). A case independent approach on the impact of climate change effects on combined sewer system performance. *WATER SCIENCE AND TECHNOLOGY*, *60*(6), 1555–1564. https://doi.org/10.2166/wst.2009.520 WE - Science Citation Index Expanded (SCI-

EXPANDED)

Kollat, J. B., Kasprzyk, J. R., Thomas, W. O., Miller, A. C., & Divoky, D. (2012). Estimating the Impacts of Climate Change and Population Growth on Flood Discharges in the United States. *Journal of Water Resources Planning and Management*, *138*(5), 442–452. https://doi.org/10.1061/(asce)wr.1943-5452.0000233

Kulkarni, A. D., Lowe, B., Kulkarni, A. D., & Lowe, B. (2016). *Random Forest Algorithm for Land Cover Classification Random Forest Algorithm for Land Cover Classification*.

Kutner, M. H., Nachtsheim, C. J., Neter, J., & Li, W. (2005). *Applied Linear Statistical Models.*

Langeveld, J. G., Schilperoort, R. P. S., & Weijers, S. R. (2013). Climate change and urban wastewater infrastructure: There is more to explore. *Journal of Hydrology*, *476*, 112–119. https://doi.org/10.1016/j.jhydrol.2012.10.021

Li, W. W., Sheng, G. P., Zeng, R. J., Liu, X. W., & Yu, H. Q. (2012). China's wastewater discharge standards in urbanization: Evolution, challenges and implications: Evolution, challenges and implications. *Environmental Science and Pollution Research*, *19*(5), 1422–1431. https://doi.org/10.1007/s11356-011-0572-7

Li, Y., Hou, X., Zhang, W., Xiong, W., Wang, L., Zhang, S., Wang, P., & Wang, C. (2016). Integration of life cycle assessment and statistical analysis to understand the influence of rainfall on WWTPs with combined sewer systems. *Journal of Cleaner Production*, *172*, 2521–2530. https://doi.org/10.1016/j.jclepro.2017.11.158

Lian, J. J., Xu, K., & Ma, C. (2013). Joint impact of rainfall and tidal level on flood risk in a coastal city with a complex river network: A case study of Fuzhou City, China. *Hydrology and Earth System Sciences*, *17*(2), 679–689. https://doi.org/10.5194/hess-17-679-2013

Loperfido, J. V., Noe, G. B., Jarnagin, S. T., & Hogan, D. M. (2014). Effects of distributed and centralized stormwater best management practices and land cover on urban stream hydrology at the catchment scale. *Journal of Hydrology*, *519*(PC),

2584–2595. https://doi.org/10.1016/j.jhydrol.2014.07.007

Mailhot, A., Talbot, G., & Lavallée, B. (2015). Relationships between rainfall and Combined Sewer Overflow (CSO) occurrences. *Journal of Hydrology*, *523*, 602–609. https://doi.org/10.1016/j.jhydrol.2015.01.063

Marlow, D. R., Moglia, M., Cook, S., & Beale, D. J. (2013). Towards sustainable urban water management: A critical reassessment. *Water Research*, *47*(20), 7150–7161. https://doi.org/10.1016/j.watres.2013.07.046

Mascher, F., Mascher, W., Pichler-semmelrock, F., Reinthaler, F. F., Id, G. E. Z., & Kittinger, C. (2017). *Impact of Combined Sewer Overflow on Wastewater Treatment and Microbiological Quality of Rivers for Recreation*. https://doi.org/10.3390/w9110906

Matarira, D., Mutanga, O., & Naidu, M. (2022). Google Earth Engine for Informal Settlement Mapping: A Random Forest Classification Using Spectral and Textural Information. *Remote Sensing*, *14*(20). https://doi.org/10.3390/rs14205130

McDonnell, B., Hayslett, R. W., & Tetrick, N. J. (2014). Dry Weather Channel Impacts on Wet Weather Combined Sewer Overflow Pollution Rates. *Journal of Water Management Modeling*, 1–10. https://doi.org/10.14796/jwmm.c384

Miller, J. D., Kim, H., Kjeldsen, T. R., Packman, J., Grebby, S., & Dearden, R. (2014). Assessing the impact of urbanization on storm runoff in a peri-urban catchment using historical change in impervious cover. *Journal of Hydrology*, *515*, 59–70. https://doi.org/10.1016/j.jhydrol.2014.04.011

Mines, R. O., Lackey, L. W., & Behrend, G. H. (2007). The impact of rainfall on flows and loadings at Georgia's wastewater treatment plants. *Water, Air, and Soil Pollution*, *179*(1–4), 135–157. https://doi.org/10.1007/s11270-006-9220-0

Mohammed, M. H., Zwain, H. M., & Hassan, W. H. (2021). Modeling the impacts of climate change and flooding on sanitary sewage system using SWMM simulation: A case study. *Results in Engineering*, *12*, 100307. https://doi.org/10.1016/j.rineng.2021.100307

Morgan, D., Xiao, L., & McNabola, A. (2017). *Technologies for monitoring, detecting and treating overflows from urban wastewater networks (2014-W-DS-19). 240*, 69. http://epa.ie/pubs/reports/research/water/Research_Report_240.pdf

Mushtaq, F., & Lala, M. G. N. (2017). Assessment of hydrological response as a function of LULC change and climatic variability in the catchment of the Wular Lake, J&K, using geospatial technique. *Environmental Earth Sciences*, *76*(22), 1–19. https://doi.org/10.1007/s12665-017-7065-z

Nesmerak, I., & Blazkova, S. D. (2014). Analysis of the time series of waste water quality at the inflow of the wastewater treatment plant and transfer functions. *Journal of Hydrology and Hydromechanics*, *62*(1), 55–59. https://doi.org/10.2478/johh-2014-0009

Nolan, A. P., & Flanagan, J. (n.d.). *High-resolution Climate Projections for Ireland – A Multi- model Ensemble Approach* (Issue 339).

Nolan, P., O'Sullivan, J., & McGrath, R. (2017). Impacts of climate change on mid-twenty-first-century rainfall in Ireland: a high-resolution regional climate model ensemble approach. *International Journal of Climatology*, *37*(12), 4347–4363. https://doi.org/10.1002/joc.5091

Ohba, M. (2021). *Chapter 2 - Precipitation under climate change* (J. B. T.-P. Rodrigo-Comino (Ed.); pp. 21–51). Elsevier. https://doi.org/https://doi.org/10.1016/B978-0-12-822699-5.00002-1

Olds, H. T., Corsi, S. R., Dila, D. K., Halmo, K. M., Bootsma, M. J., & McLellan, S. L. (2018). High levels of sewage contamination released from urban areas after storm events: A quantitative survey with sewage specific bacterial indicators. *PLoS Medicine*, *15*(7), 1–23. https://doi.org/10.1371/journal.pmed.1002614

Pachauri, R. K. (2014). Climate change 2014 synthesis report summary chapter for policymakers. *Ipcc*, 31. https://doi.org/10.1017/CBO9781107415324

Paule-Mercado, M. A., Lee, B. Y., Memon, S. A., Umer, S. R., Salim, I., & Lee, C. H. (2017). Influence of land development on stormwater runoff from a mixed land use and land cover catchment. *Science of the Total Environment*, *599–600*, 2142–2155.

https://doi.org/10.1016/j.scitotenv.2017.05.081

Peleg, N., Blumensaat, F., Molnar, P., Fatichi, S., & Burlando, P. (2016). Partitioning spatial and temporal rainfall variability in urbandrainage modelling. *Hydrology and Earth System Sciences Discussions*. https://doi.org/10.5194/hess-2016-530

Peng, S., Wang, C., Li, Z., Mihara, K., Kuramochi, K., Toma, Y., & Hatano, R. (2023). Climate change multi-model projections in CMIP6 scenarios in Central Hokkaido, Japan. *Scientific Reports*, *13*(1), 230. https://doi.org/10.1038/s41598-022-27357-7

Ravagnani, F., Pellegrinelli, A., & Franchini, M. (2009). Estimation of urban impervious fraction from satellite images and its impact on peak discharge entering a storm sewer system. *Water Resources Management*, *23*(10), 1893–1915. https://doi.org/10.1007/s11269-008-9359-0

Read, J. M., & Torrado, M. (2009). *Remote Sensing* (R. Kitchin & N. B. T.-I. E. of H. G. Thrift (Eds.); pp. 335–346). Elsevier. https://doi.org/https://doi.org/10.1016/B978-008044910-4.00508-3

River, V., Heikkinen, M., Schönach, P., & Massa, I. (2016). *Politicization of wastewater overflows : the case of the*. *18*, 1454–1472. https://doi.org/10.2166/wp.2016.011

Roy, D. P., Wulder, M. A., Loveland, T. R., C.E., W., Allen, R. G., Anderson, M. C., Helder, D., Irons, J. R., Johnson, D. M., Kennedy, R., Scambos, T. A., Schaaf, C. B., Schott, J. R., Sheng, Y., Vermote, E. F., Belward, A. S., Bindschadler, R., Cohen, W. B., Gao, F., … Zhu, Z. (2014). Landsat-8: Science and product vision for terrestrial global change research. *Remote Sensing of Environment*, *145*, 154–172. https://doi.org/10.1016/j.rse.2014.02.001

Rubio-Martin, A., Llario, F., Garcia-Prats, A., Macian-Sorribes, H., Macian, J., & Pulido-Velazquez, M. (2023). Climate services for water utilities: Lessons learnt from the case of the urban water supply to Valencia, Spain. *Climate Services*, *29*(May 2022), 100338. https://doi.org/10.1016/j.cliser.2022.100338

Ryu, J., Oh, J., Snyder, S. A., & Yoon, Y. (2014). *Determination of micropollutants in combined sewer overflows and their removal in a wastewater treatment plant (Seoul , South Korea)*. 3239–3251. https://doi.org/10.1007/s10661-013-3613-5

Sahu, O. (2019). Sustainable and clean treatment of industrial wastewater with microbial fuel cell. *Results in Engineering*, *4*(October), 100053. https://doi.org/10.1016/j.rineng.2019.100053

Saikia, S. D., Ryan, P., Nuyts, S., & Clifford, E. (2022). Results in Engineering Precipitation , tidal and river level impacts on influent volumes of combined wastewater collection systems : A regional analysis. *Results in Engineering*, *15*(August), 100588. https://doi.org/10.1016/j.rineng.2022.100588

Sanyal, J., Densmore, A. L., & Carbonneau, P. (2014). Analysing the effect of land-use/cover changes at sub-catchment levels on downstream flood peaks: A semi-distributed modelling approach with sparse data. *Catena*, *118*, 28–40. https://doi.org/10.1016/j.catena.2014.01.015

Saraswat, C., Kumar, P., & Mishra, B. K. (2016). Assessment of stormwater runoff management practices and governance under climate change and urbanization: An analysis of Bangkok, Hanoi and Tokyo. *Environmental Science and Policy*, *64*, 101–117. https://doi.org/10.1016/j.envsci.2016.06.018

Schär, C., Ban, N., Fischer, E. M., Rajczak, J., Schmidli, J., Frei, C., Giorgi, F., Karl, T. R., Kendon, E. J., Tank, A. M. G. K., O'Gorman, P. A., Sillmann, J., Zhang, X., & Zwiers, F. W. (2016). Percentile indices for assessing changes in heavy precipitation events. *Climatic Change*, *137*(1–2), 201–216. https://doi.org/10.1007/s10584-016-1669-2

Schroeder, K., Riechel, M., Matzinger, A., Rouault, P., Sonnenberg, H., Pawlowsky-Reusing, E., & Gnirss, R. (2011). Evaluation of effectiveness of combined sewer overflow control measures by operational data. *Water Science and Technology*, *63*(2), 325–330. https://doi.org/10.2166/wst.2011.058

Semadeni-Davies, A., Hernebring, C., Svensson, G., & Gustafsson, L. G. (2008). The impacts of climate change and urbanisation on drainage in Helsingborg, Sweden: Combined sewer system. *Journal of Hydrology*, *350*(1–2), 100–113. https://doi.org/10.1016/j.jhydrol.2007.05.028

Shakeri, H., Motiee, H., & Mcbean, E. (2021). Forecasting impacts of climate change on

changes of municipal wastewater production in wastewater reuse projects. *Journal of Cleaner Production*, *329*(December 2020), 129790. https://doi.org/10.1016/j.jclepro.2021.129790

Shukla, A. K., Shukla, S., Ojha, C. S. P., Buytaert, W., Mijic, A., Pathak, S., & Garg, R. D. (2018). Population growth, land use and land cover transformations, and water quality nexus in the Upper Ganga River basin. *Hydrology and Earth System Sciences*, *22*(9), 4745–4770. https://doi.org/10.5194/hess-22-4745-2018

Steinschneider, S., Yang, Y. C. E., & Brown, C. (2013). Panel regression techniques for identifying impacts of anthropogenic landscape change on hydrologic response. *Water Resources Research*, *49*(12), 7874–7886. https://doi.org/10.1002/2013WR013818

Swart, R., Celliers, L., Collard, M., Prats, A. G., Huang-Lachmann, J. T., Sempere, F. L., de Jong, F., Máñez Costa, M., Martinez, G., Velazquez, M. P., Martín, A. R., Segretier, W., Stattner, E., & Timmermans, W. (2021). Reframing climate services to support municipal and regional planning. *Climate Services*, *22*(May). https://doi.org/10.1016/j.cliser.2021.100227

Tang, Y., Guo, Q., Su, C., & Chen, X. (2017). Flooding in delta areas under changing climate: Response of design flood level to non-stationarity in both inflow floods and high tides in South China. *Water (Switzerland)*, *9*(7). https://doi.org/10.3390/w9070471

Tay, R. (2017). Correlation, variance inflation and multicollinearity in regression model. *Journal of the Eastern Asia Society for Transportation Studies*, *12*, 2006–2015.

Tebaldi, C., O'Neill, B., & Lamarque, J. F. (2015). Sensitivity of regional climate to global temperature and forcing. *Environmental Research Letters*, *10*(7). https://doi.org/10.1088/1748-9326/10/7/074001

Teklehaimanot, G. Z., Kamika, I., Coetzee, M. A. A., & Momba, M. N. B. (2015). Population Growth and Its Impact on the Design Capacity and Performance of the Wastewater Treatment Plants in Sedibeng and Soshanguve, South Africa. *Environmental Management*, *56*(4), 984–997. https://doi.org/10.1007/s00267-015-

0564-3

Tellinghuisen J. Least squares with non-normal data: estimating experimental variance functions. Analyst. 2008 Feb;133(2):161-6. doi: 10.1039/b708709h. Epub 2007 Nov 2. PMID: 18227936.

The Impacts of Climate Change on Wastewater Treatment Costs: Evidence from the Wastewater Sector in China. (2020). *Water*, *12*(11), 3272. https://doi.org/http://dx.doi.org/10.3390/w12113272

Tuohy, P., O' Loughlin, J., Peyton, D., & Fenton, O. (2018). The performance and behavior of land drainage systems and their impact on field scale hydrology in an increasingly volatile climate. *Agricultural Water Management*, *210*(December 2017), 96–107. https://doi.org/10.1016/j.agwat.2018.07.033

Vogel, J., McNie, E., & Behar, D. (2016). Co-producing actionable science for water utilities. *Climate Services*, *2–3*, 30–40. https://doi.org/10.1016/j.cliser.2016.06.003

Vousdoukas, M. I., Mentaschi, L., Voukouvalas, E., Verlaan, M., & Feyen, L. (2017). Extreme sea levels on the rise along Europe's coasts. *Earth's Future*, *5*(3), 304–323. https://doi.org/10.1002/2016EF000505

Wi, S., Ray, P., Demaria, E. M. C., Steinschneider, S., & Brown, C. (2017). A user-friendly software package for VIC hydrologic model development. *Environmental Modelling and Software*, *98*, 35–53. https://doi.org/10.1016/j.envsoft.2017.09.006

Willems, P. (2013). Revision of urban drainage design rules after assessment of climate change impacts on precipitation extremes at Uccle, Belgium. *Journal of Hydrology*, *496*, 166–177. https://doi.org/10.1016/j.jhydrol.2013.05.037

Willems, P., Arnbjerg-Nielsen, K., Olsson, J., & Nguyen, V. T. V. (2012). Climate change impact assessment on urban rainfall extremes and urban drainage: Methods and shortcomings. *Atmospheric Research*, *103*, 106–118. https://doi.org/10.1016/j.atmosres.2011.04.003

Williams, J., Horsburgh, K. J., Williams, J. A., & Proctor, R. N. F. (2016). Tide and skew surge independence: New insights for flood risk. *Geophysical Research Letters*,

43(12), 6410–6417. https://doi.org/10.1002/2016GL069522

Willuweit, L., & O'Sullivan, J. J. (2013). A decision support tool for sustainable planning of urban water systems: Presenting the dynamic urban water simulation model. *Water Research*, *47*(20), 7206–7220. https://doi.org/10.1016/j.watres.2013.09.060

Yao, L., Wei, W., & Chen, L. (2016). How does imperviousness impact the urban rainfall-runoff process under various storm cases? *Ecological Indicators*, *60*, 893–905. https://doi.org/10.1016/j.ecolind.2015.08.041

Yazdanfar, Z., & Sharma, A. (2015). Urban drainage system planning and design - Challenges with climate change and urbanization: A review. *Water Science and Technology*, *72*(2), 165–179. https://doi.org/10.2166/wst.2015.207

Yin, J., Yin, Z. e., Hu, X. meng, Xu, S. yuan, Wang, J., Li, Z. hua, Zhong, H. dong, & Gan, F. bin. (2011). Multiple scenario analyses forecasting the confounding impacts of sea level rise and tides from storm induced coastal flooding in the city of Shanghai, China. *Environmental Earth Sciences*, *63*(2), 407–414. https://doi.org/10.1007/s12665-010-0787-9

Zhang, Y., & Ayyub, B. M. (2021). *Chapter 2 - Temperature extremes in a changing climate* (A. B. T.-C. C. and E. E. Fares (Ed.); pp. 9–23). Elsevier. https://doi.org/https://doi.org/10.1016/B978-0-12-822700-8.00001-9

Zhou, Q. (2014). A review of sustainable urban drainage systems considering the climate change and urbanization impacts. *Water (Switzerland)*, *6*(4), 976–992. https://doi.org/10.3390/w6040976

Zhou, Q., Leng, G., Su, J., & Ren, Y. (2019). Comparison of urbanization and climate change impacts on urban flood volumes: Importance of urban planning and drainage adaptation. *Science of the Total Environment*, *658*, 24–33. https://doi.org/10.1016/j.scitotenv.2018.12.184

Zope, P. E., Eldho, T. I., & Jothiprakash, V. (2016). Impacts of land use-land cover change and urbanization on flooding: A case study of Oshiwara River Basin in Mumbai, India. *Catena*, *145*, 142–154. https://doi.org/10.1016/j.catena.2016.06.009

APPENDICES

Appendices

Appendix I

Appendix I contains the supplementary information for Chapter 3 Section 3.4.1 and Chapter 4 of the thesis.

Table I.1: Variables assessed during the initial analysis on WWTP 8

Variables at daily scale	
Sl. No.	**List of variables**
1	Daily precipitation v/s Daily influent volume
2	Wet day precipitation v/s Wet day influent volume
3	Precipitation v/s 1 day lagged influent volume
4	Precipitation v/s 2 days lagged influent volume
5	Precipitation v/s 3 days lagged influent volume
6	Precipitation v/s 1 day lagged influent volume excluding zero rainfall days
7	Precipitation v/s 2 days lagged influent volume excluding zero rainfall days
8	Precipitation v/s 3 days lagged influent volume excluding zero rainfall days
9	Precipitation v/s 1 day lagged influent volume excluding all days with rainfall < 1 mm
10	Precipitation v/s 2 days lagged influent volume excluding all days with rainfall < 1 mm
11	Precipitation v/s 3 days lagged influent volume excluding all days with rainfall < 1 mm
12	Daily maximum tidal level v/s Daily influent volume
13	Daily maximum tidal level during wet days v/s Wet day influent volume
14	Daily maximum tidal level v/s Dry weather flow

15	Daily mean river level v/s Daily influent volume
16	Daily mean river level during wet days v/s Wet day influent volume
17	Daily maximum tidal level v/s Dry weather flow
18	Daily precipitation v/s Daily maximum tidal level
19	Daily precipitation v/s Daily mean river level
20	Daily maximum tidal level v/s Daily mean river level
	Variables at monthly scale
Sl. No.	**List of variables**
1	Average daily precipitation over a month v/s Average daily influent volume over a month
2	Number of wet days in a month v/s Average daily influent volume over a month
3	Number of zero rainfall days in a month v/s Average daily influent volume over a month
4	Average wet day precipitation in a month v/s Average wet day influent volume in a month
5	Number of rainy days (with precipitation > 0.2 mm and less than 1 mm) in a month v/s Average daily influent volume in a month
6	Average rainy day precipitation in a month v/s Average rainy day influent volume in a month
7	Number of wet days v/s Average daily influent volume of wet days
8	Number of zero rainfall days v/s Average daily influent volume of zero rainfall days
9	Total monthly precipitation v/s Total monthly influent volume
10	Number of wet days v/s Total monthly influent volume
11	Number of zero rainfall days v/s Total monthly influent volume
12	Number of rainy days v/s Total monthly influent volume

13	Number of consecutive zero rainfall days v/s Average influent volume of that period
14	Number of consecutive wet days v/s Average influent volume of that period

Table I.2: Comparison of regression results of daily precipitation v/s daily influent volume with and without 1 day lag-time

Daily precipitation v/s daily influent volume				
WWTPs	**R^2**		**Model Error**	
	Without Lag-time	**With 1 day Lag-time**	**Without Lag-time**	**With 1 day Lag-time**
WWTP 1	0.14	0.31	24%	21%
WWTP 2	0.28	0.21	23%	24%
WWTP 3	0.38	0.26	40%	44%
WWTP 4	0.06	0.16	26%	25%
WWTP 5	0.21	0.44	47%	40%
WWTP 6	0.21	0.45	47%	39%
WWTP 7	0.34	0.27	39%	41%
WWTP 8	0.27	0.23	18%	19%
WWTP 9	0.17	0.16	32%	32%
WWTP 10	0.13	0.37	32%	27%
WWTP 11	0.17	0.34	47%	41%
WWTP 12	0.32	0.28	51%	52%
WWTP 13	0.28	0.16	56%	57%
WWTP 14	0.03	0.32	48%	40%

Table I.3: Tidal level analysis results for all the WWTPs located near coast

Plants	Daily Maximum Tidal level v/s Dry weather flow		Daily Maximum Tidal Level v/s Daily influent volume		Daily maximum tidal level and Daily precipitation v/s Daily influent volume	
	R^2	Model Error	R^2	Model Error	R^2	Model Error
WWTP 2	0.17	13%	0.16	24%	0.36	21%
WWTP 4	0.09	15%	0.16	18%	0.23	17%
WWTP 8	0.37	11%	0.16	20%	0.37	17%
WWTP 10	0.02	26%	0.04	36%	0.16	31%
WWTP 12	0.01	38%	0.08	61%	0.32	53%

Table I.4: River level analysis results for all the WWTPs located near river

Plants	Daily mean river level v/s Dry weather Flow		Daily mean river level v/s Daily influent volume		Daily mean river level and Daily precipitation v/s Daily influent volume	
	R^2	Model Error	R^2	Model Error	R^2	Model Error
WWTP 1	0.57	13%	0.61	16%	0.65	15%
WWTP 8	0.46	13%	0.53	18%	0.67	12%
WWTP 10	0.6	18%	0.49	24%	0.51	24%

Table I.5: Tidal and river level analysis results for all the WWTPs located near both coast and river

Plants	Daily mean river level and Daily maximum tidal level v/s Dry weather flow		Daily mean river level and Daily maximum tidal level v/s Daily influent volume		Daily mean river level, Daily maximum tidal level and Daily Precipitation v/s Daily influent volume	
	R^2	Model Error	R^2	Model Error	R^2	Model Error
WWTP 8	0.46	13%	0.53	15%	0.67	12%
WWTP 10	0.6	18%	0.51	24%	0.52	23%

Table I.6: Daily Precipitation categories for all WWTPs based on percentile evaluation (Refer to Table 4.1 for the percentile values)

Plants	No rainfall	Very low	Low	Moderate	High	Extreme event
WWTP 1	0	>0 <= 0.7	>0.7 <= 3.7	>3.7 <= 11.8	>11.8 <= 21.1	>21.1
WWTP 2	0	>0 <= 0.3	>0.3 <= 3.1	>3.1 <= 14.9	>14.9 <= 28.3	>28.3
WWTP 3	<=0.1	>0.1 <= 2	>2 <= 6.7	>6.7 <= 16.6	>16.6 <= 26.7	>26.7
WWTP 4	0	>0 <= 0.4	>0.4 <= 3.6	>3.6 <= 16.6	>16.6 <= 31.4	>31.4
WWTP 5	0	>0 <= 1.2	>1.2 <= 4.7	>4.7 <= 15.1	>15.1 <= 25.7	>25.7
WWTP 6	0	>0 <= 1.2	>1.2 <= 4.8	>4.8 <= 13.6	>13.6 <= 23.4	>23.4
WWTP 7	0	>0 <= 0.7	>0.7 <= 3.8	>3.8 <= 12.1	>12.1 <= 23	>23
WWTP 9	0	>0 <= 0.8	>0.8 <= 2.9	>2.9 <= 10.2	>10.2 <= 18.7	>18.7
WWTP 10	0	0	>0 <= 1.8	>1.8 <= 8.8	>8.8 <= 17.9	>17.9
WWTP 11	0	<=0.1	>0.1 <= 2	>2 <= 10.5	>10.5 <= 24.2	>24.2
WWTP 12	0	>0 <= 0.2	>0.2 <= 2.8	>2.8 <= 13.2	>13.2 <= 26.8	>26.8
WWTP 13	0	>0 <= 0.6	>0.6 <= 4	>4 <= 12.4	>12.4 <= 21.3	>21.3
WWTP 14	0	>0 <= 0.6	>0.6 <= 3	>3 <= 11.4	>11.4 <= 19.9	>19.9

In case of some WWTPs where influent volumes under two precipitation categories were not statistically significantly different, they were merged in order to plot the probability of exceedance curves. All the probability of exceedance curves for all the WWTPs are presented in the set of figures below. Probability of exceedance curves for WWTP 8 is already presented in Chapter 4.

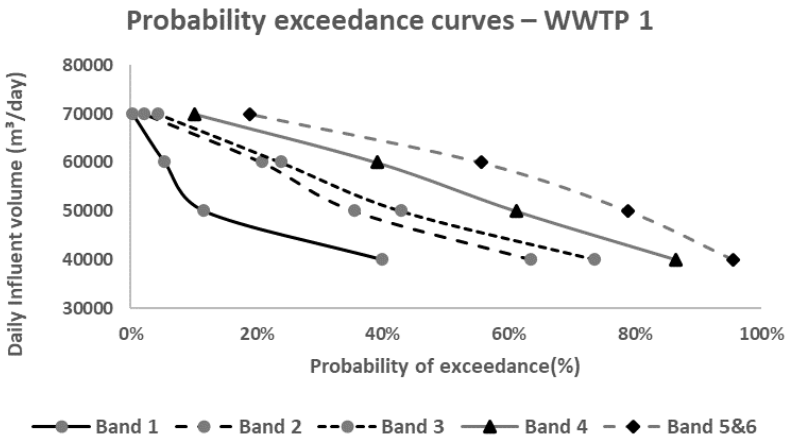
Probability exceedance curves – WWTP 1
Daily Influent volume (m³/day)
80000
70000
60000
50000
40000
30000
0%
20%
40%
60%
80%
100%
Probability of exceedance(%)
Band 1
Band 2
Band 3
Band 4
Band 5&6

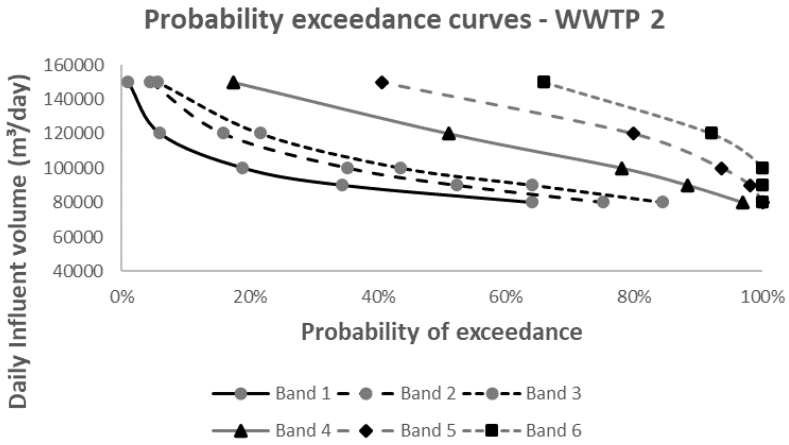
Probability exceedance curves - WWTP 2
Daily Influent volume (m³/day)
160000
140000
120000
100000
80000
60000
40000
0%
20%
40%
60%
80%
100%
Probability of exceedance
Band 1
Band 2
Band 3
Band 4
Band 5
Band 6

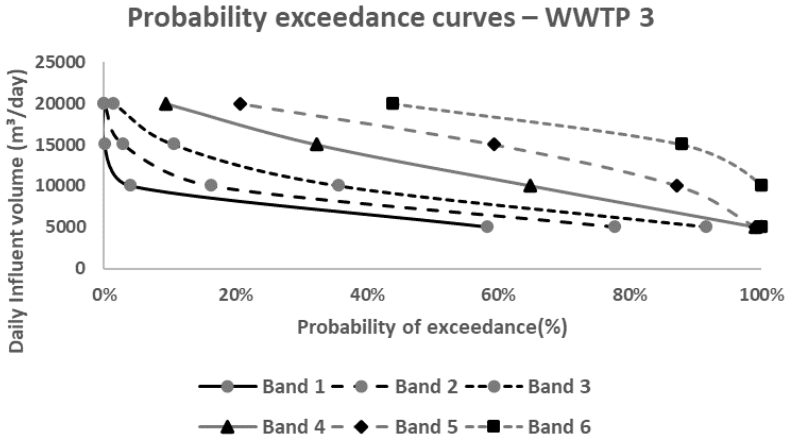
Probability exceedance curves – WWTP 3
Daily Influent volume (m³/day)
25000
20000
15000
10000
5000
0
0%
20%
40%
60%
80%
100%
Probability of exceedance(%)
Band 1
Band 2
Band 3
Band 4
Band 5
Band 6

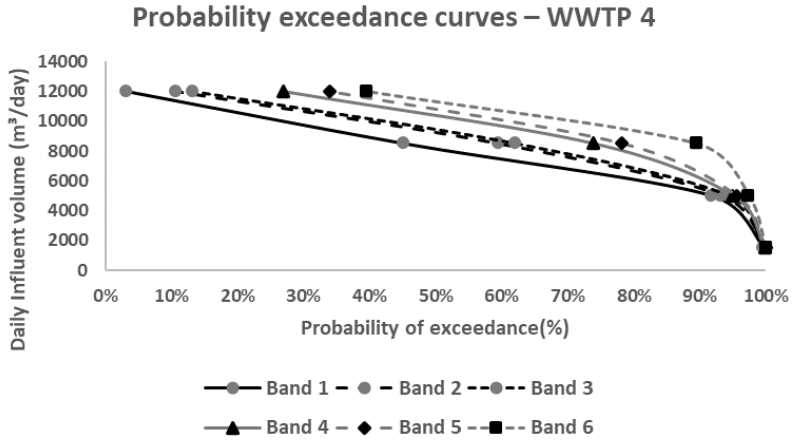
Probability exceedance curves – WWTP 4
Daily Influent volume (m³/day)
14000
12000
10000
8000
6000
4000
2000
0
0%
10%
20%
30%
40%
50%
60%
70%
80%
90%
100%
Probability of exceedance(%)
Band 1
Band 2
Band 3
Band 4
Band 5
Band 6

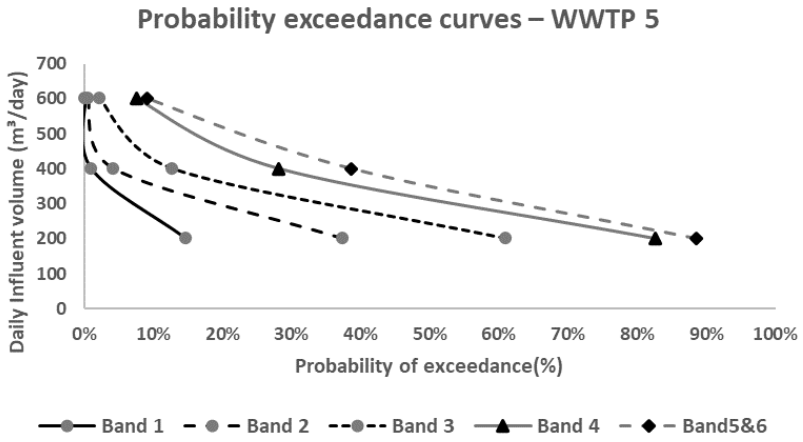
Probability exceedance curves – WWTP 5
Daily Influent volume (m³/day)
700
600
500
400
300
200
100
0
0%
10%
20%
30%
40%
50%
60%
70%
80%
90%
100%
Probability of exceedance(%)
Band 1
Band 2
Band 3
Band 4
Band5&6

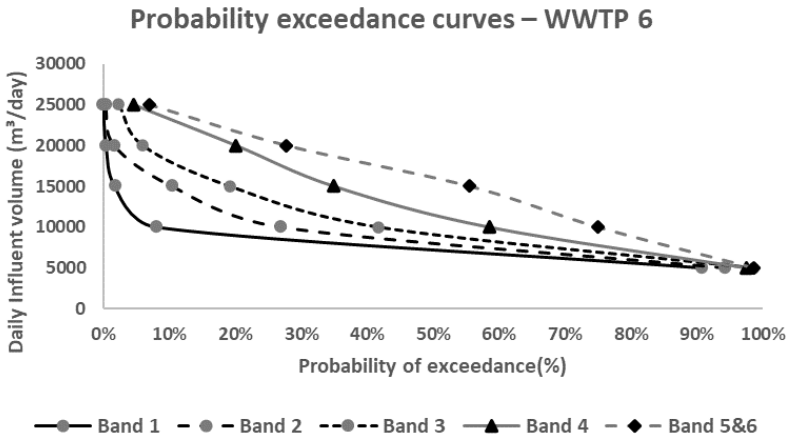
Probability exceedance curves – WWTP 6
Daily Influent volume (m³/day)
30000
25000
20000
15000
10000
5000
0
0%
10%
20%
30%
40%
50%
60%
70%
80%
90%
100%
Probability of exceedance(%)
Band 1
Band 2
Band 3
Band 4
Band 5&6

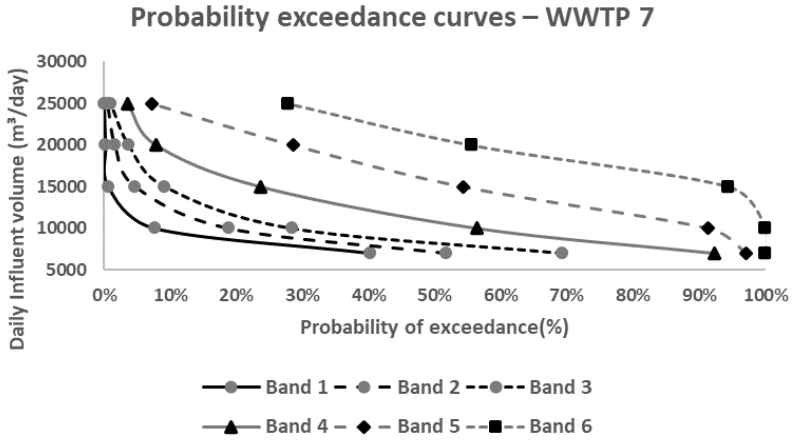
Probability exceedance curves – WWTP 7
Daily Influent volume (m³/day)
30000
25000
20000
15000
10000
5000
0%
10%
20%
30%
40%
50%
60%
70%
80%
90%
100%
Probability of exceedance(%)
Band 1
Band 2
Band 3
Band 4
Band 5
Band 6

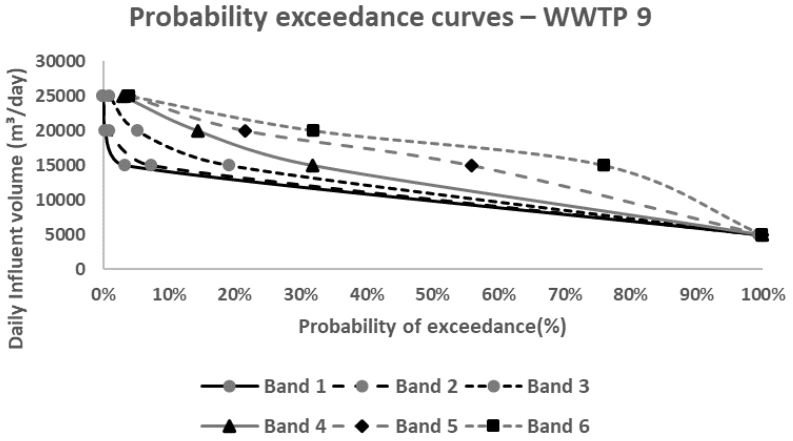
Probability exceedance curves – WWTP 9
Daily Influent volume (m³/day)
30000
25000
20000
15000
10000
5000
0
0%
10%
20%
30%
40%
50%
60%
70%
80%
90%
100%
Probability of exceedance(%)
Band 1
Band 2
Band 3
Band 4
Band 5
Band 6

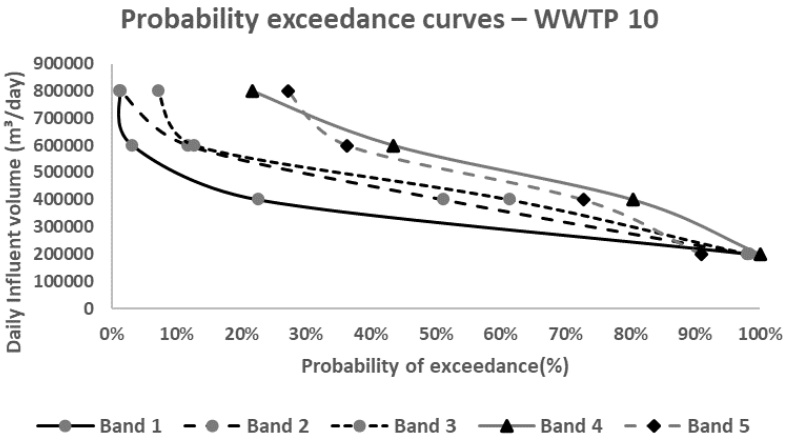
Probability exceedance curves – WWTP 10
Daily Influent volume (m³/day)
900000
800000
700000
600000
500000
400000
300000
200000
100000
0
0%
10%
20%
30%
40%
50%
60%
70%
80%
90%
100%
Probability of exceedance(%)
Band 1
Band 2
Band 3
Band 4
Band 5

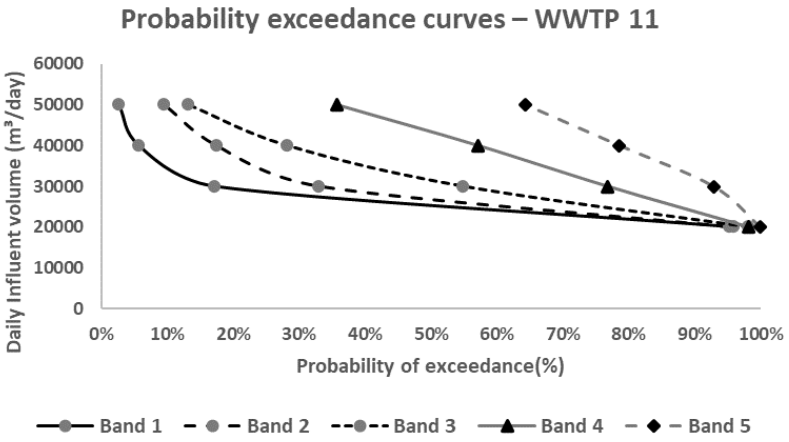
Probability exceedance curves – WWTP 11
Daily Influent volume (m³/day)
60000
50000
40000
30000
20000
10000
0
0%
10%
20%
30%
40%
50%
60%
70%
80%
90%
100%
Probability of exceedance(%)
Band 1
Band 2
Band 3
Band 4
Band 5

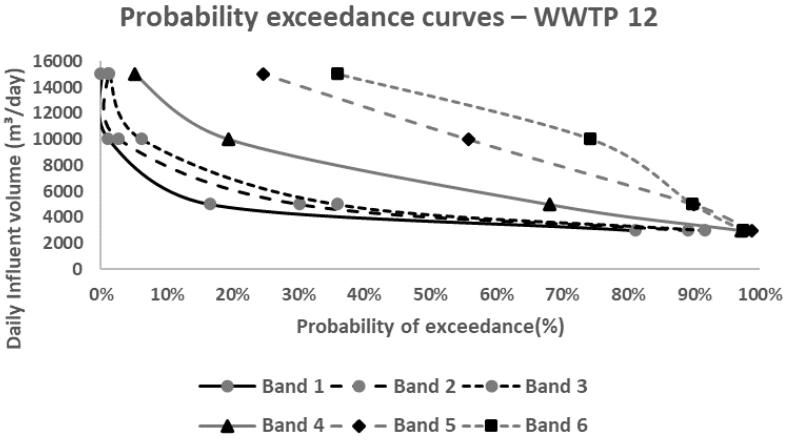
Probability exceedance curves – WWTP 12
Daily Influent volume (m³/day)
16000
14000
12000
10000
8000
6000
4000
2000
0
0%
10%
20%
30%
40%
50%
60%
70%
80%
90%
100%
Probability of exceedance(%)
Band 1
Band 2
Band 3
Band 4
Band 5
Band 6

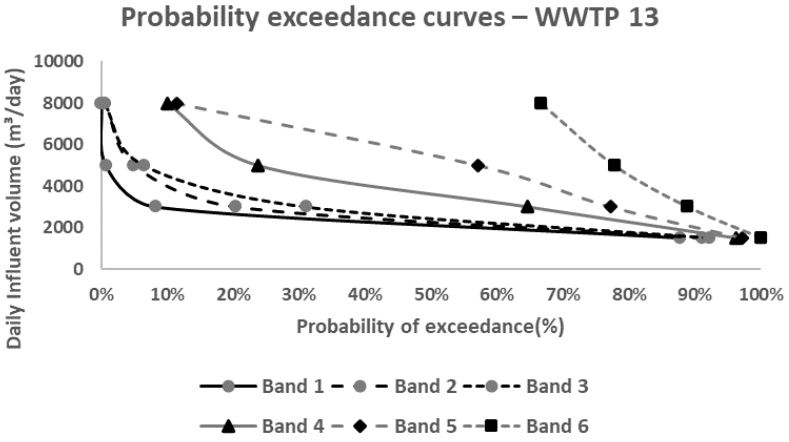
Probability exceedance curves – WWTP 13
Daily Influent volume (m³/day)
10000
8000
6000
4000
2000
0
0%
10%
20%
30%
40%
50%
60%
70%
80%
90%
100%
Probability of exceedance(%)
Band 1
Band 2
Band 3
Band 4
Band 5
Band 6

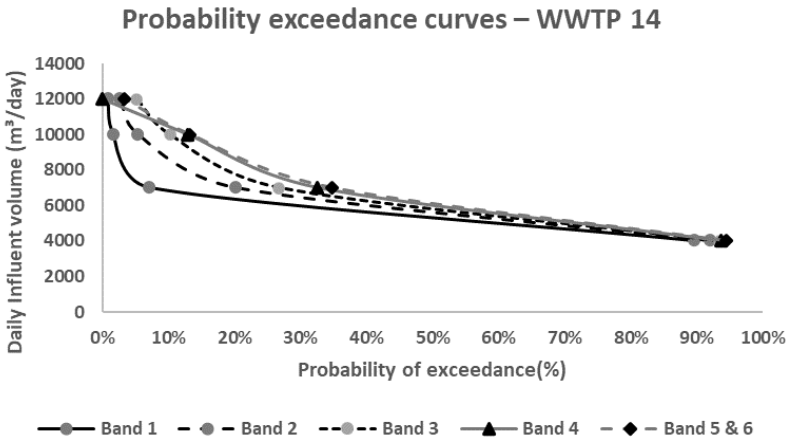

Figure I.1: Probability of exceedance curves for all the WWTPs based on the different precipitation categories

Table I.7: Monthly regression analysis results of monthly average daily influent volumes (ADIV) v/s monthly average daily precipitation (ADP), number of wet days in a month (WD) and number of zero rainfall days in a month (ZRD) considered individually and together for all the WWTPs

Monthly Analysis summary across all WWTPs								
Plants	**ADP v/s ADIV**		**WD v/s ADIV**		**ZRD v/s ADIV**		**ADP and ZRD v/s ADIV**	
	R^2	**Model Error**	**R^2**	**Model Error**	**R^2**	**Model Error**	**Adjusted-R^2**	**Model Error**
WWTP 1	0.70	11%	0.56	13%	0.47	14%	0.70	11%
WWTP 2	0.63	12%	0.51	14%	0.46	15%	0.66	12%
WWTP 3	0.71	20%	0.53	26%	0.38	30%	0.71	20%
WWTP 4	0.26	20%	0.27	20%	0.21	21%	0.27	20%
WWTP 5	0.84	14%	0.58	22%	0.43	26%	0.83	14%
WWTP 6	0.77	18%	0.57	25%	0.48	27%	0.76	18%
WWTP 7	0.69	21%	0.47	27%	0.32	31%	0.68	21%
WWTP 8	0.66	9%	0.61	9%	0.56	10%	0.69	9%
WWTP 9	0.37	22%	0.39	22%	0.37	23%	0.41	22%
WWTP 10	0.49	15%	0.44	16%	0.42	16%	0.53	14%
WWTP 11	0.62	24%	0.46	28%	0.43	29%	0.61	24%
WWTP 12	0.65	23%	0.45	29%	0.40	31%	0.66	23%
WWTP 13	0.53	29%	0.50	30%	0.20	38%	0.52	29%
WWTP 14	0.56	21%	0.38	24%	0.25	27%	0.54	21%

Table I.8: Model errors of Individual v/s pooled models at daily and monthly scales

Plants	Daily Scale Model accuracy in terms of model errors for Individual v/s Pooled Daily WWTP model			Monthly Scale Model accuracy in terms of model errors for Individual v/s Pooled Monthly WWTP model		
	Individual Daily Model	**Pooled Daily all-years Model**	**Pooled Daily 2016 - 2018 Model**	**Individual Monthly Model**	**Pooled Monthly all-years Model**	**Pooled Monthly 2016 - 2018 Model**
WWTP 1	24%	39%	25%	11%	14%	16%
WWTP 2	23%	36%	27%	12%	12%	10%
WWTP 3	40%	50%	42%	20%	30%	29%
WWTP 4	26%	53%	24%	20%	38%	9%
WWTP 5	47%	82%	48%	14%	27%	14%
WWTP 6	47%	64%	46%	18%	21%	21%
WWTP 7	39%	59%	37%	21%	26%	21%
WWTP 8	18%	24%	27%	9%	9%	9%
WWTP 9	32%	37%	36%	22%	23%	25%
WWTP 10	32%	44%	33%	14%	16%	18%
WWTP 11	47%	100%	63%	24%	26%	25%
WWTP 12	51%	100%	80%	23%	28%	23%
WWTP 13	56%	100%	100%	29%	31%	31%
WWTP 14	48%	100%	88%	21%	24%	21%

Individual model represents the analysis done for each WWTP separately whereas pooled model represents the analysis done across all WWTPs.

All WWTPs

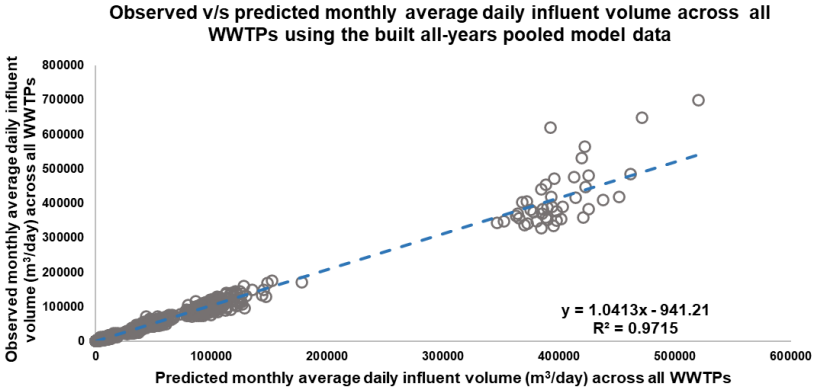

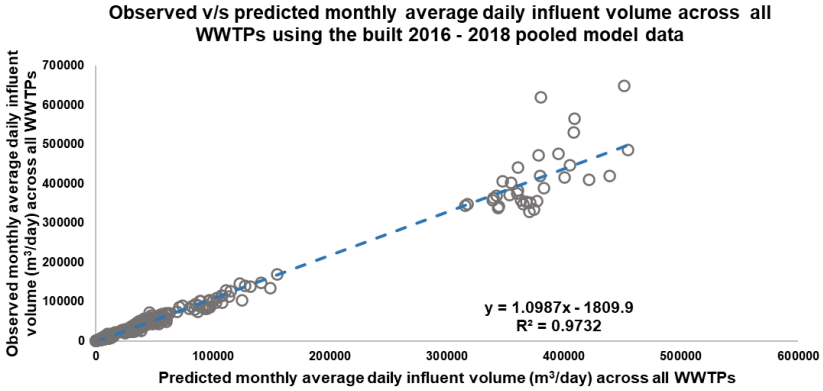

Very Large WWTP

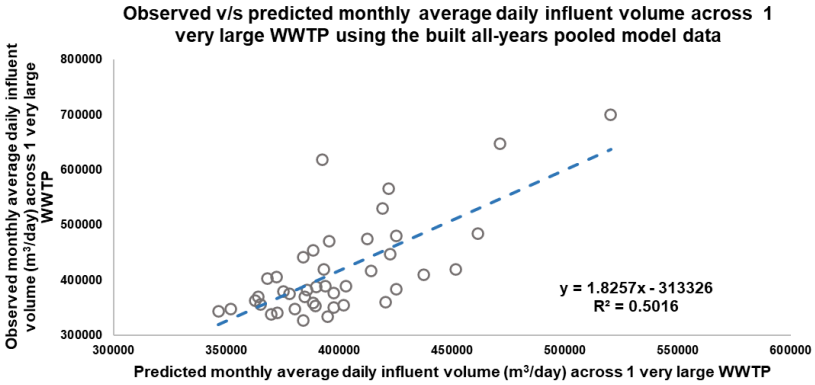

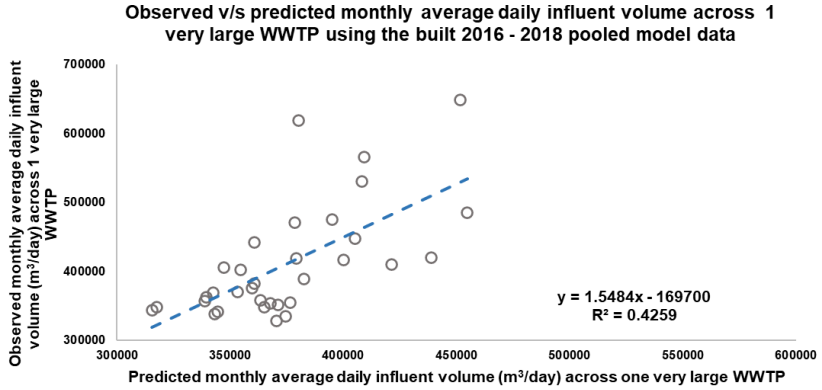

Large WWTPs

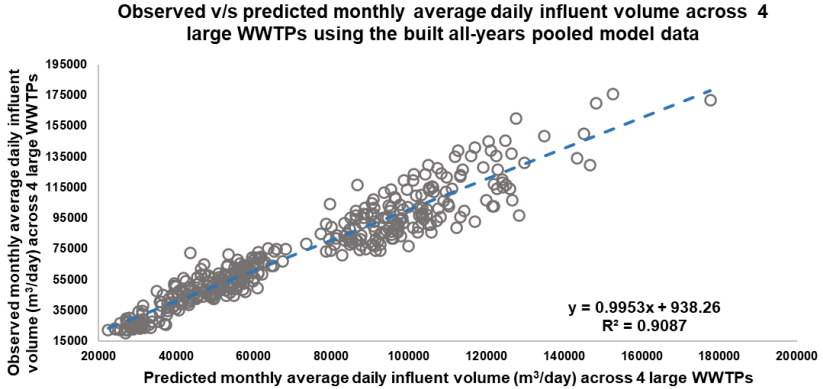

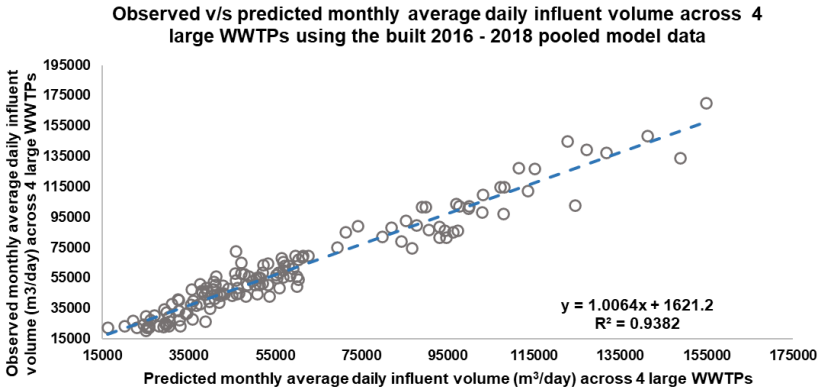

Medium WWTPs

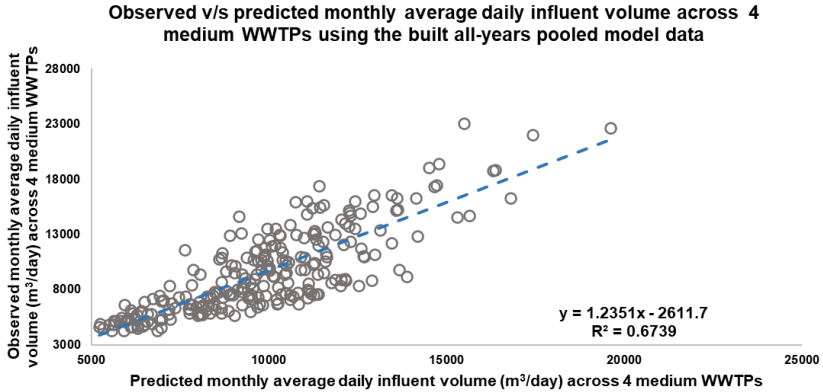

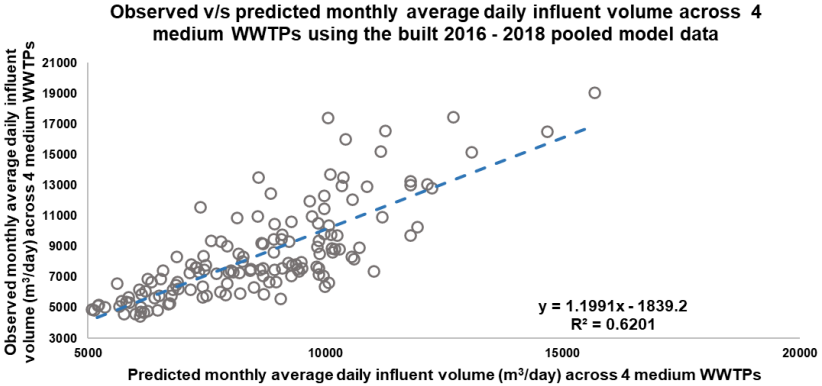

Small WWTPs

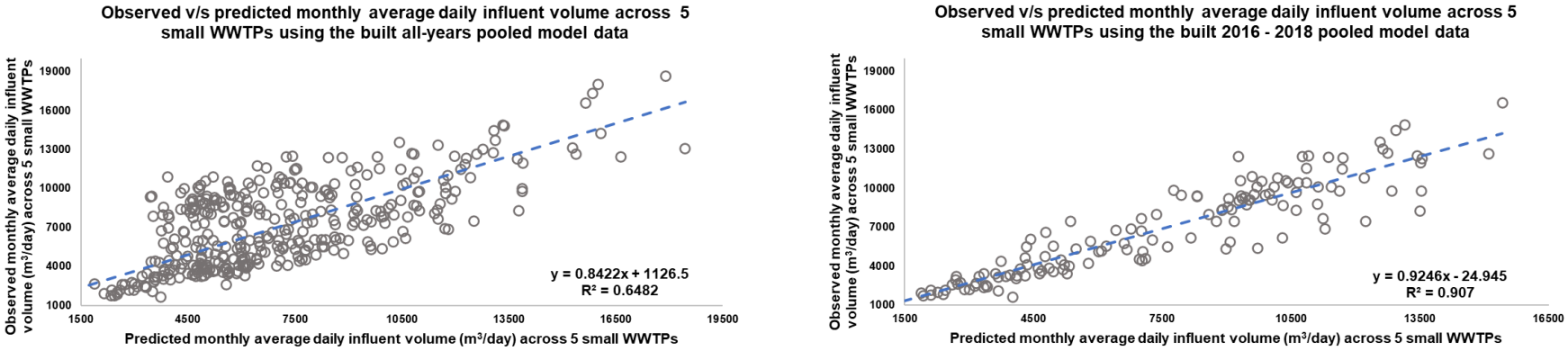

Figure I.2: Observed v/s predicted monthly average daily influent volume from pooled models (all-years and 2016 – 2018) for all WWTPs

Appendix II

This section refers to the supplementary information of Chapter 5 of the thesis.

Table II.1: Difference between 33rd and 66th percentile of the projected % change in monthly average daily influent volumes in 2041 - 2060 as compared to current period under RCP 4.5 (%)

WWTPs	Winter			Spring			Summer			Autumn		
	D	J	F	M	A	M	J	J	A	S	O	N
WWTP 1	1.8	1.8	1.6	1.4	0.9	1.2	0.9	1.1	1.3	0.7	0.5	0.9
WWTP 2	1.9	1.9	1.4	2.2	1.9	2.1	0.7	0.7	0.6	0.7	0.7	0.7
WWTP 3	1.5	1.3	1.4	2.2	1.9	2.1	1.9	1.9	2.2	2.5	2.4	2.8
WWTP 4	0.8	0.8	0.6	1.2	1.3	1.1	1.2	1.2	1.1	0.3	0.4	0.4
WWTP 5	1.8	1.7	1.5	2.4	1.8	2.0	1.1	1.3	1.3	1.7	1.7	2.1
WWTP 6	3.3	3.6	3.1	1.2	1.0	1.1	1.2	1.5	1.5	2.5	2.2	3.1
WWTP 7	2.7	2.5	2.5	2.4	2.1	2.5	1.6	1.5	1.8	1.4	1.4	1.8
WWTP 8	2.1	1.9	1.6	1.3	1.1	1.5	1.6	1.6	1.3	1.5	1.5	1.8
WWTP 9	1.4	1.3	1.1	1.3	1.1	1.3	1.0	0.9	1.1	0.9	1.0	1.0
WWTP 10	2.7	2.2	1.4	1.1	1.1	1.2	1.2	0.9	0.9	0.4	0.3	0.5
WWTP 11	3.6	3.0	2.3	2.5	2.0	2.2	1.2	1.4	1.4	1.2	1.0	1.5
WWTP 12	1.6	1.4	1.2	4.4	3.9	4.0	3.3	3.5	3.2	0.6	0.6	0.7
WWTP 13	2.2	2.3	2.4	2.7	1.6	1.8	2.4	2.2	3.0	2.1	1.8	2.0
WWTP 14	2.1	1.9	1.8	2.7	2.2	2.8	1.5	1.3	1.6	0.7	0.7	1.0

Table II.2: Difference between 33rd and 66th percentile of the projected % change in monthly average daily influent volumes in 2041 - 2060 as compared to current period under RCP 8.5 (%)

WWTPs	Winter			Spring			Summer			Autumn		
	D	J	F	M	A	M	J	J	A	S	O	N
WWTP 1	1.6	1.6	1.6	1.2	0.8	1.1	0.7	0.8	1.1	1.2	0.9	1.5
WWTP 2	1.2	1.2	1.1	2.9	2.5	2.6	1.1	1.2	1.0	1.6	1.6	1.6
WWTP 3	4.3	3.7	4.0	2.5	2.1	2.3	2.1	2.1	2.3	1.9	1.8	2.2
WWTP 4	0.8	0.8	0.7	1.6	1.7	1.6	0.9	0.9	0.8	0.6	0.7	0.9
WWTP 5	3.4	3.3	3.0	2.3	1.7	2.0	0.6	0.8	0.8	2.2	2.2	2.6
WWTP 6	3.1	3.3	3.0	1.8	1.5	1.7	1.6	2.1	2.1	2.5	2.1	3.0
WWTP 7	3.2	3.0	3.0	2.0	1.8	2.1	2.5	2.3	2.8	2.7	2.8	3.4
WWTP 8	1.4	1.2	1.0	0.6	0.6	0.7	0.8	0.9	0.9	1.7	1.8	2.1
WWTP 9	2.0	1.6	1.4	0.9	0.6	0.9	0.8	0.6	0.7	1.0	1.1	1.2
WWTP 10	1.5	1.2	0.8	0.9	0.8	0.9	1.8	1.4	0.4	1.2	0.9	1.4
WWTP 11	1.9	1.6	1.3	1.3	1.2	1.3	1.5	1.7	1.7	1.5	1.2	1.7
WWTP 12	2.0	1.7	1.5	4.0	3.6	3.7	1.3	1.3	1.3	0.9	1.2	1.3
WWTP 13	4.2	4.4	4.5	2.1	1.3	1.4	0.9	0.9	1.2	3.1	2.7	3.0
WWTP 14	2.2	2.0	1.9	1.4	1.1	1.5	1.4	1.2	1.5	1.5	1.4	2.1

WWTPs	Winter			Spring			Summer			Autumn		
	Dec	Jan	Feb	Mar	Apr	May	Jun	Jul	Aug	Sep	Oct	Nov
WWTP 1	0.3	0.3	0.3	0.3	0.1	0.1	0.4	0.5	0.7	0.2	0.1	0.3
WWTP 2	-0.2	-0.2	-0.1	0.1	0.1	0.1	0.4	0.4	0.4	0.5	0.5	0.6
WWTP 3	0.3	0.1	0.2	0.5	0.3	0.3	0.4	0.4	0.6	0.3	0.4	0.8
WWTP 4	-0.7	-0.6	-0.4	0.2	0.2	0.2	0.9	0.8	0.8	0.8	1.2	2.0
WWTP 5	-0.1	-0.1	-0.1	0.1	0.1	0.1	0.1	0.1	0.2	0.1	0.1	0.1
WWTP 6	0.5	0.7	0.4	0.1	0.0	0.0	0.3	0.4	0.4	0.0	0.0	0.0
WWTP 7	0.3	0.3	0.3	0.2	0.1	0.1	0.7	0.6	0.8	0.3	0.3	0.7
WWTP 8	-0.3	-0.2	-0.2	0.1	0.1	0.1	0.3	0.3	0.4	0.4	0.4	0.6
WWTP 9	0.9	1.0	0.7	0.2	0.1	0.1	0.8	0.5	0.7	0.2	0.2	0.3
WWTP 10	0.4	0.3	0.1	-0.1	0.0	0.0	0.5	0.3	0.3	0.5	0.3	0.7
WWTP 11	0.6	0.5	0.2	0.1	0.1	0.1	0.2	0.2	0.2	0.4	0.3	0.6
WWTP 12	-0.7	-0.6	-0.4	0.1	0.1	0.1	0.8	0.9	0.9	0.8	1.4	2.4
WWTP 13	-0.4	-18.1	-1.1	1.8	0.5	0.5	1.0	0.9	1.4	1.2	0.7	1.4
WWTP 14	0.2	0.2	0.1	0.1	0.1	0.1	0.3	0.2	0.3	0.1	0.1	0.2

Figure II.1: Percentage change in reserve capacity for all the WWTPs in 2041-2060 as compared to current period under RCP 4.5

WWTPs	Winter			Spring			Summer			Autumn		
	Dec	Jan	Feb	Mar	Apr	May	Jun	Jul	Aug	Sep	Oct	Nov
WWTP 1	-1.0	-1.1	-0.9	0.2	0.1	0.1	0.6	0.8	1.2	-0.7	-0.5	-1.2
WWTP 2	-0.8	-0.8	-0.5	0.3	0.2	0.2	0.7	0.7	0.6	-0.1	-0.1	-0.1
WWTP 3	-1.1	-0.5	-0.8	0.5	0.4	0.4	1.0	1.0	1.5	-0.3	-0.3	-0.7
WWTP 4	-3.3	-2.9	-1.8	0.6	0.6	0.5	1.5	1.3	1.4	-0.2	-0.3	-0.5
WWTP 5	-0.4	-0.3	-0.2	0.1	0.0	0.1	0.2	0.2	0.2	-0.1	0.0	-0.1
WWTP 6	-0.6	-0.8	-0.5	0.2	0.1	0.2	0.4	0.6	0.6	0.0	0.0	0.1
WWTP 7	-0.9	-0.8	-0.7	0.3	0.2	0.2	0.8	0.6	0.9	-0.2	-0.2	-0.5
WWTP 8	-0.8	-0.7	-0.5	0.0	0.0	0.0	0.5	0.6	0.7	0.0	0.0	-0.1
WWTP 9	-0.5	-0.5	-0.4	0.2	0.2	0.2	0.9	0.6	0.8	0.3	0.4	0.5
WWTP 10	-0.7	-0.6	-0.3	-0.1	-0.1	-0.1	0.8	0.5	0.6	0.0	0.0	0.0
WWTP 11	-1.0	-0.8	-0.4	0.2	0.1	0.1	0.5	0.5	0.5	0.0	0.0	0.1
WWTP 12	-4.6	-3.7	-2.3	0.2	0.1	0.1	1.8	2.1	2.2	-0.2	-0.3	-0.4
WWTP 13	-2.5	-108.4	-6.4	1.6	0.5	0.5	1.5	1.2	2.1	-1.2	-0.7	-1.4
WWTP 14	-0.2	-0.2	-0.2	0.1	0.1	0.1	0.3	0.2	0.3	0.1	0.1	0.1

Figure II.2: Percentage change in reserve capacity for all the WWTPs in 2041-2060 as compared to current period under RCP 8.5

Table II.3: Estimation of annual number of events exceeding any given proportion of peak design capacity based on observed (obs.) probability of exceedance and the projected % change in high and very high precipitation days in 2041 – 2060 as compared to current period for all WWTPs [Note: All numbers displayed in the table are estimated annually]

WWTPs	Precipitation days	Time period	No. of occurrences	> 25% of PD		> 50% of PD		> 75% of PD		> 100% of PD	
				Obs. PoE	No. of events exceeding 25% of PD	Obs. PoE	No. of events exceeding 50% of PD	Obs. PoE	No. of events exceeding 75% of PD	Obs. PoE	No. of events exceeding 100% of PD
WWTP 1	High precipitation days	Current	4.2	100 %	4.2	95%	4.0	71%	3.0	5%	0.2
		2041 - 2060 RCP 4.5	4.56		4.56		4.35		3.26		0.22
		2041 - 2060 RCP 8.5	4.72		4.72		4.5		3.37		0.23

	Very high precipitation days	**Current**	0.4	100 %	0.4	100 %	0.4	50%	0.2	50%	0.2
		2041 - 2060 RCP 4.5	0.47		0.47		0.47		0.24		0.24
		2041 - 2060 RCP 8.5	0.49		0.49		0.49		0.25		0.25
WWTP 2	**High precipitation days**	**Current**	9.9	99%	9.9	4%	0.4	0%	0.0	0%	0
		2041 - 2060 RCP 4.5	10.2		10.2		0.44		0.0		0.0
		2041 - 2060 RCP 8.5	10.5		10.4		0.45		0.0		0.0
	Very high precipitation days	**Current**	3.00	100 %	3.00	10%	0.29	0%	0.0	0%	0.0
		2041 - 2060 RCP 4.5	3.31		3.31		0.31		0.0		0.0

		2041 - 2060 RCP 8.5	3.35		3.35		3.32		0.0		0.0	
WWTP 3	**High precipitation days**	**Current**	9.6	100 %	9.6	85%	8.1	51%	4.9	0%	0.0	
		2041 - 2060 RCP 4.5	10.3		10.3		8.7		5.2		0.0	
		2041 - 2060 RCP 8.5	10.4		10.4		8.9		5.3		0.0	
	Very high precipitation days	**Current**	2	100 %	2	100 %	2	79%	1.6	0%	0.0	
		2041 - 2060 RCP 4.5	2.4		2.4		2.4		1.9		0.0	
		2041 - 2060 RCP 8.5	2.5		2.5		2.5		1.9		0.0	

WWTP 4	**High precipitation days**	**Current**	12.2	98%	12.0	87%	10.6	46%	5.6	3%	0.4
		2041 - 2060 RCP 4.5	12.7		12.5		11		5.8		0.42
		2041 - 2060 RCP 8.5	13.0		12.7		11.3		5.9		0.42
	Very high precipitation days	**Current**	4.5	100 %	4.5	96%	4.3	53%	2.4	0%	0.0
		2041 - 2060 RCP 4.5	4.8		4.8		4.6		2.6		0.0
		2041 - 2060 RCP 8.5	5.0		5.0		4.8		2.7		0.0
WWTP 5	**High precipitation days**	**Current**	7.8	26%	2.0	0%	0.0	0%	0.0	0%	0.0
		2041 - 2060 RCP 4.5	8.3		2.1		0.0		0.0		0.0

		2041 - 2060 RCP 8.5	8.6		2.2		0.0		0.0		0.0
	Very high precipitation days	**Current**	2	50%	1	100 %	0.0	0%	0.0	0%	0.0
		2041 - 2060 RCP 4.5	2.3		1.1		0.0		0.0		0.0
		2041 - 2060 RCP 8.5	2.4		1.2		0.0		0.0		0.0
WWTP 6	**High precipitation days**	**Current**	6.3	92%	5.8	76%	4.8	32%	2.0	0%	0.0
		2041 - 2060 RCP 4.5	6.8		6.3		5.2		2.2		0.0
		2041 - 2060 RCP 8.5	6.9		6.3		5.2		2.2		0.0
		Current	1.8	100 %	1.8	100 %	1.8	71%	1.3	0%	0.0

	Very high precipitation days	**2041 - 2060 RCP 4.5**	2.0		2.0		2.0		1.4		0.0	
		2041 - 2060 RCP 8.5	2.0		2.0		2.0		1.4		0.0	
WWTP 7	**High precipitation days**	**Current**	5.0	100 %	5.0	64%	3.2	12%	0.60	0%	0.0	
		2041 - 2060 RCP 4.5	5.3		5.3		3.4		0.63		0.0	
		2041 - 2060 RCP 8.5	5.4		5.4		3.4		0.65		0.0	
	Very high precipitation days	**Current**	0.8	100 %	0.8	75%	0.6	0%	0.0	0%	0.0	
		2041 - 2060 RCP 4.5	0.8		0.8		0.6		0.0		0.0	

		2041 - 2060 RCP 8.5	0.9		0.9		0.7		0.0	0.0
WWTP 8	**High precipitation days**	**Current**	7.3	100 %	7.3	71%	5.1	0%	0.0	0% 0.0
		2041 - 2060 RCP 4.5	7.7		7.7		5.5		0.0	0.0
		2041 - 2060 RCP 8.5	8.0		8.0		5.7		0.0	0.0
	Very high precipitation days	**Current**	1.8	100 %	1.8	93%	1.6	0%	0.0	0% 0.0
		2041 - 2060 RCP 4.5	1.9		1.9		1.8		0.0	0.0
		2041 - 2060 RCP 8.5	2.0		2.0		1.9		0.0	0.0

WWTP 9	**High precipitation days**	**Current**	2.9	100 %	2.9	85%	2.43	55%	1.60	20%	0.57
		2041 - 2060 RCP 4.5	3.06		3.06		2.60		1.68		0.61
		2041 - 2060 RCP 8.5	3.11		3.11		2.64		1.70		0.62
	Very high precipitation days	**Current**	0.29	100 %	0.29	100 %	0.29	100 %	0.29	50%	0.14
		2041 - 2060 RCP 4.5	0.35		0.35		0.35		0.35		0.17
		2041 - 2060 RCP 8.5	0.35		0.35		0.35		0.35		0.18
WWTP 10		**Current**	2.0	100 %	2.0	88%	1.75	75%	1.50	50%	1.00

	High precipitation days	**2041 - 2060 RCP 4.5**	2.1		2.1		1.80		1.54		1.03	
		2041 - 2060 RCP 8.5	2.1		2.1		1.80		1.54		1.03	
	Very high precipitation days	**Current**	0.5	100 %	0.5	100 %	0.5	100 %	0.5	50%	0.30	
		2041 - 2060 RCP 4.5	0.55		0.55		0.55		0.55		0.27	
		2041 - 2060 RCP 8.5	0.57		0.57		0.57		0.57		0.28	
WWTP 12	**High precipitation days**	**Current**	7.2	99%	7.1	86%	6.2	77%	5.5	62%	4.5	
		2041 - 2060 RCP 4.5	7.6		7.5		6.5		5.8		4.7	

		2041 - 2060 RCP 8.5	7.7		7.6		6.6		5.9		4.8	
	Very high precipitation days	**Current**	2.5	100 %	2.5	89%	2.2	78%	1.9	63%	1.5	
		2041 - 2060 RCP 4.5	2.6		2.6		2.3		2.0		1.6	
		2041 - 2060 RCP 8.5	2.7		2.7		2.4		2.1		1.7	
WWTP 13	**High precipitation days**	**Current**	3.3	100 %	3.3	100 %	3.3	90%	3.0	80%	2.7	
		2041 - 2060 RCP 4.5	3.5		3.5		3.5		3.2		2.8	
		2041 - 2060 RCP 8.5	3.6		3.6		3.6		3.3		2.9	

	Very high precipitation days	**Current**	1.3	100 %	1.3	100 %	1.3	75%	1.0	75%	1.0
		2041 - 2060 RCP 4.5	1.5		1.5		1.5		1.1		1.1
		2041 - 2060 RCP 8.5	1.6		1.6		1.6		1.2		1.2
WWTP 14	**High precipitation days**	**Current**	3.40	94%	3.20	41%	1.40	12%	0.40	0%	0.0
		2041 - 2060 RCP 4.5	3.53		3.32		1.45		0.42		0.0
		2041 - 2060 RCP 8.5	3.67		3.46		1.51		0.43		0.0
	Very high precipitation days	**Current**	0.40	100 %	0.40	100 %	0.40	50%	0.20	0%	0.0
		2041 - 2060 RCP 4.5	0.43		0.43		0.43		0.21		0.0

		2041 - 2060 RCP 8.5	0.45	0.45	0.45	0.22	0.0

***PD refers to the peak design capacity and PoE refers to Probability of Exceedance**

Appendix III

This section contains the supplementary information relevant to Chapter 6.

Following is the JavaScript code used in Google Earth Engine to perform landuse landcover classification for all the WWTPs. The lines starting with "//" refers to a comment that describes the steps following it.

Script:

```
Map.setCenter(-9.29076, 53.85468, 12);
// Importing satellite imagery using the satellite imagery extent
var composite = ee.ImageCollection('LANDSAT/LC08/C01/T1_TOA')
    .filterDate('2018-06-29', '2018-07-01')
    .filterBounds(ROI)
    .map(function(image) {
      return image.addBands(image.metadata('system:time_start'));
    })
    .median();
var clipped = composite.clip(ROI);
// Inster System data (1530358446505) from metadata using inspect option
var date = ee.Date(1530358446505);
print (date)
// Display satellite imagery
Map.addLayer(clipped, cls_3, 'Imagery');
var s2_bands = ['B1','B2', 'B3', 'B4', 'B5', 'B6','B7'];
var TrainingImage = composite.select(s2_bands);
// set the selection bands
var predictionBands = TrainingImage.bandNames();
print (TrainingImage.bandNames());
```

```
// Merge all into a single Feature collection
var trainingFeatures1=Builtup.merge(Water).merge(Green);
var classifierTraining = TrainingImage.select(predictionBands)
.sampleRegions({collection: trainingFeatures1, properties: ['Class'], scale: 10 });
var classifier = ee.Classifier.smileRandomForest({
        numberOfTrees: 100,
});
var classifyer = classifier.train({features:classifierTraining,
classProperty:'Class', inputProperties: predictionBands});
var classified = TrainingImage.select(predictionBands).classify(classifyer);
var ClassifiedClip = classified.clip(ROI);
Map.addLayer(ClassifiedClip, cls, 'Classified');
Export.image.toDrive({
  image: classified,
  description: 'Castlebar_L8_2018_Classified',
  scale: 10,
  region: ROI,
  maxPixels: 1e11
});
```

Classified Images

The following figures and tables refer to the classified images and change in built-up area for all the agglomerations within each time interval. The results for agglomeration A4 are already in Chapter 6.

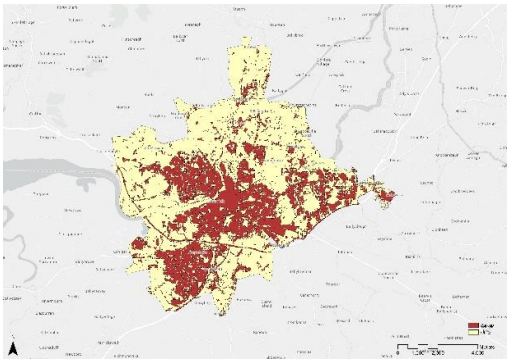

2014

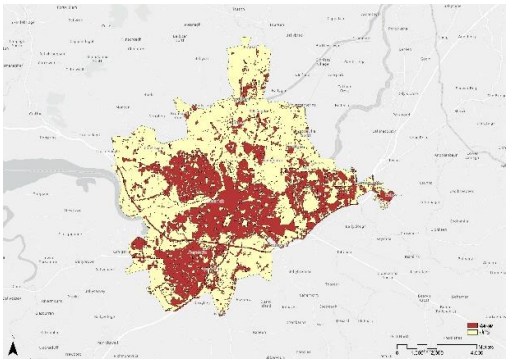

2016

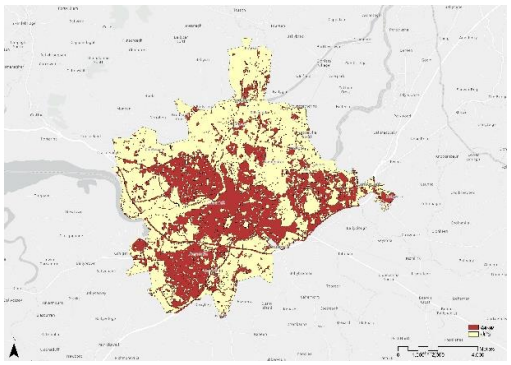

2018

Figure III.1: Classified images of agglomeration A1

Table III.1: Change in built-up area for agglomeration A1

Year	Area in sq. m	Time interval	% Change in built-up area
2014	29767155	-	-
2016	33267652	2014 – 2016	11.8%
2018	34524554	2016 – 2018	3.9%

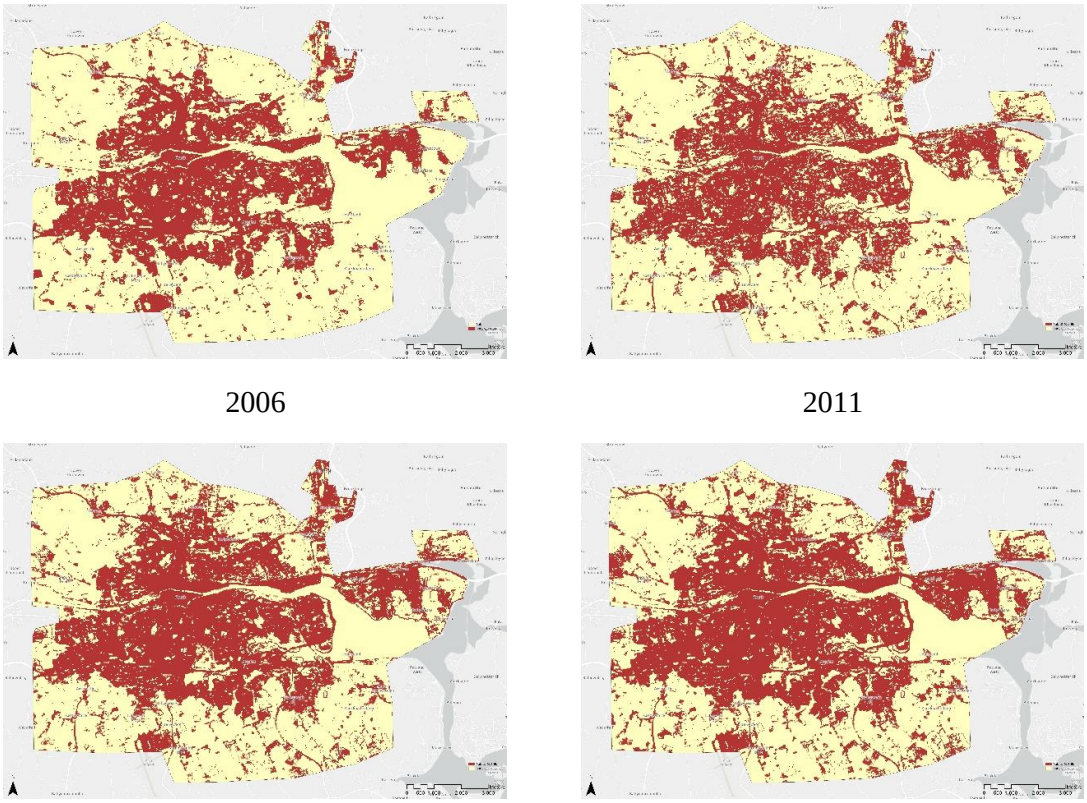

2006 2011

2015 2018

Figure III.2: Classified images of agglomeration A2

Table III.2: Change in built-up area for agglomeration A2

Year	Area in sq. m	Time interval	% Change in built-up area
2006	50707123	-	-
2011	54399667.17	2006 – 2011	7.3%
2015	61906975.75	2011 – 2015	13.8%
2018	66579507.35	2015 – 2018	7.5%

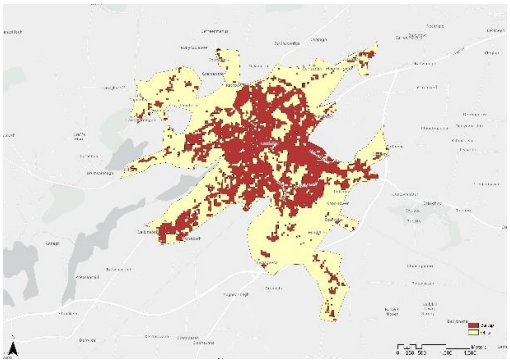

2012

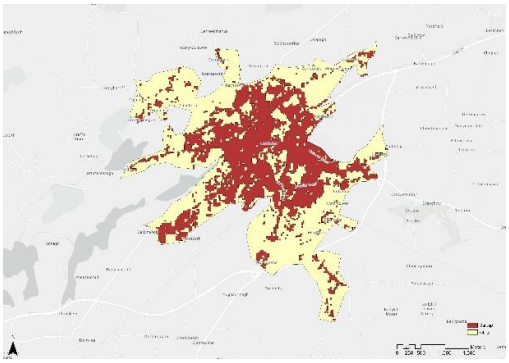

2015

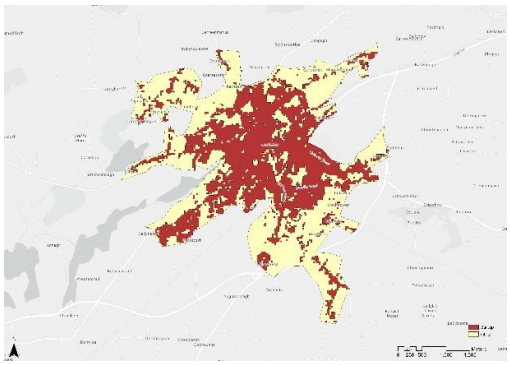

2018

Figure III.3: Classified images of agglomeration A3

Table III.3: Change in built-up area for agglomeration A3

Year	Area in sq. m	Time interval	% Change in built-up area
2012	4946759	-	-
2015	5652319	2012 – 2015	14.3%
2018	6360817	2015 – 2018	12.5%

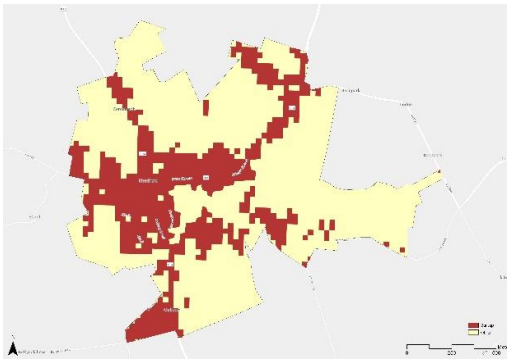

2014

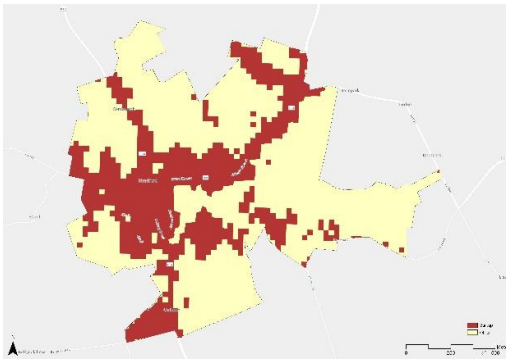

2016

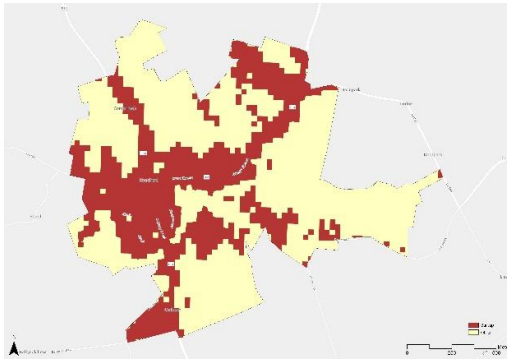

2018

Figure III.4: Classified images of agglomeration A5

Table III.4: Change in built-up area for agglomeration A5

Year	Area in sq. m	Time interval	% Change in built-up area
2014	587644.4962	-	-
2016	658957.9656	2014 – 2016	12.1%
2018	727430.8012	2016 – 2018	10.4%

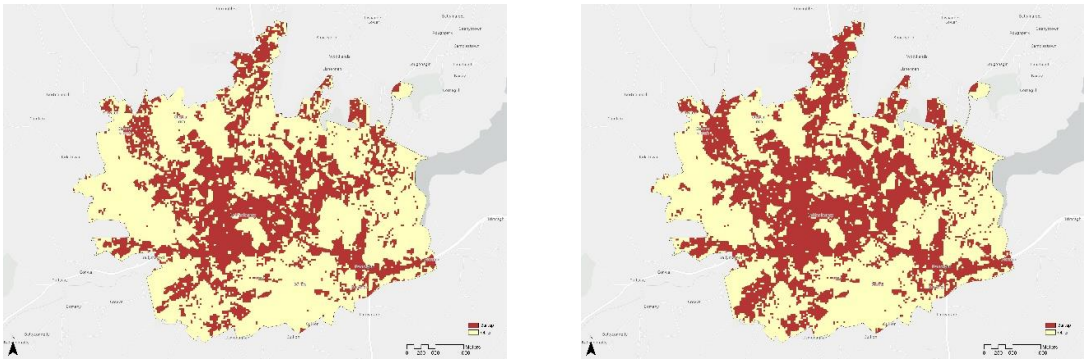

2015 2018

Figure III.5: Classified images of agglomeration A6

Table III.5: Change in built-up area for agglomeration A6

Year	Area in sq. m	Time interval	% Change in built-up area
2015	7330511.304	-	-
2018	8938004.292	2015 – 2018	21.9%

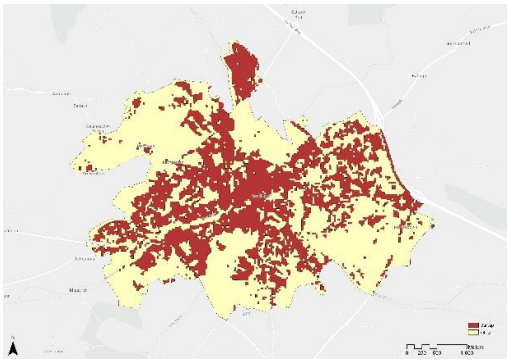

2014

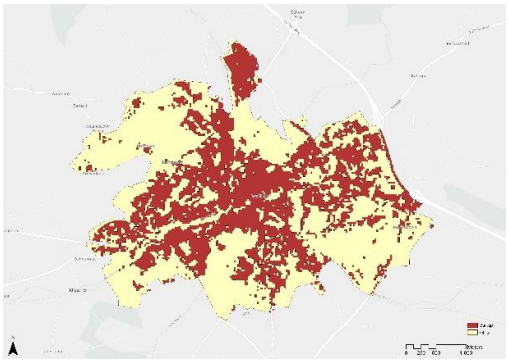

2016

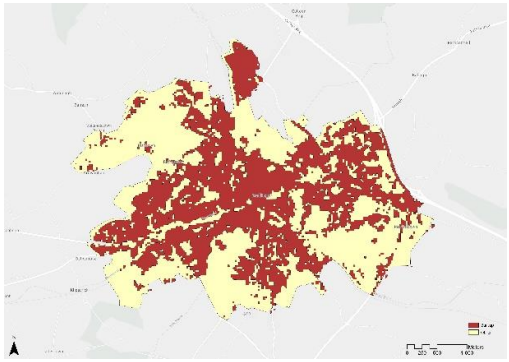

2018

Figure III.6: Classified images of agglomeration A7

Table III.6: Change in built-up area for agglomeration A7

Year	Area in sq. m	Time interval	% Change in built-up area
2014	5856560	-	-
2016	6253100	2014 – 2016	6.8%
2018	7215996	2016 – 2018	15.4%

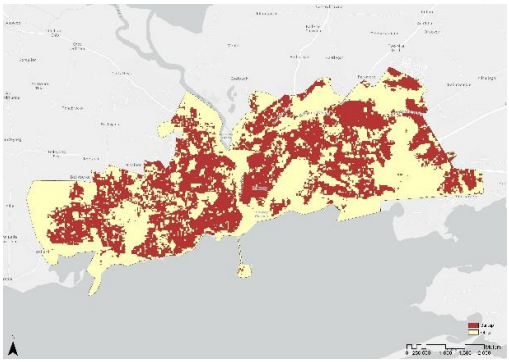

2011

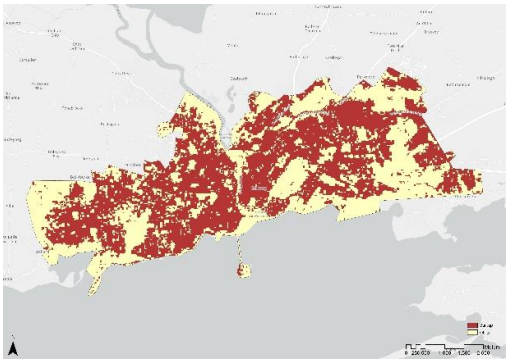

2015

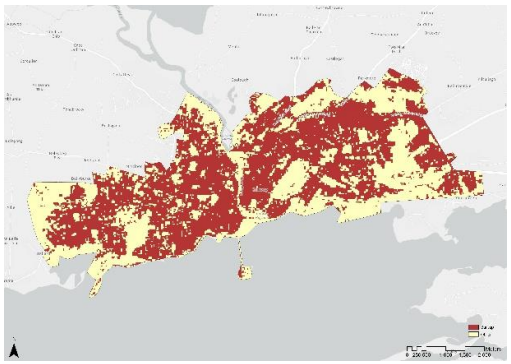

2018

Figure III.7: Classified images of agglomeration A8

Table III.7: Change in built-up area for agglomeration A8

Year	Area in sq. m	Time interval	% Change in built-up area
2011	13956239.8	-	-
2015	16789311.81	2011 – 2015	20.3%
2018	17441316.39	2015 – 2018	3.9%

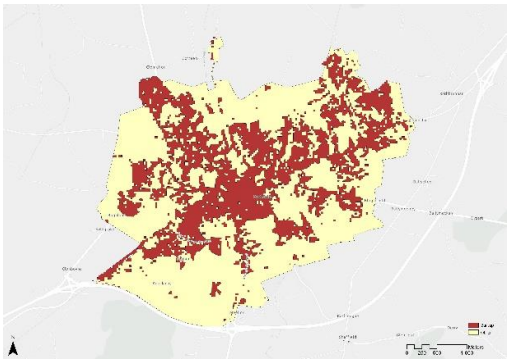

2011

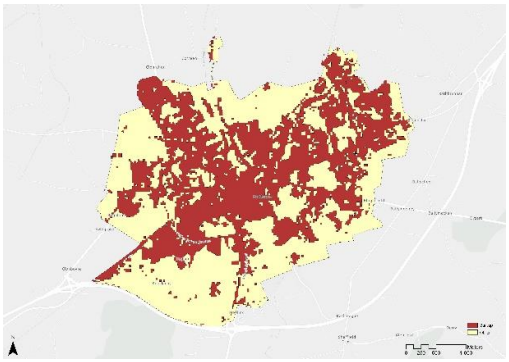

2015

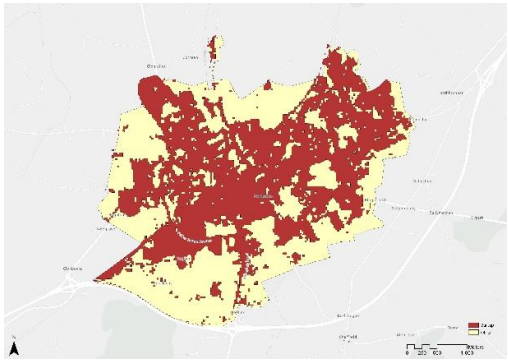

2018

Figure III.8: Classified images of agglomeration A9

Table III.8: Change in built-up area for agglomeration A9

Year	Area in sq. m	Time interval	% Change in built-up area
2011	6082515	-	-
2015	7200470	2011 – 2015	18.4%
2018	8240562	2015 – 2018	14.4%

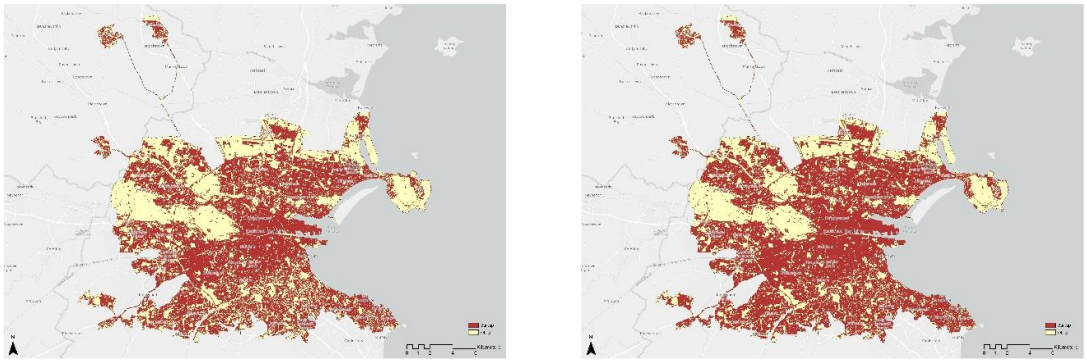

2015 2018

Figure III.9: Classified images of agglomeration A10

Table III.9: Change in built-up area for agglomeration A10

Year	Area in sq. m	Time interval	% Change in built-up area
2015	189692508.1	-	-
2018	211502456.4	2015 – 2018	11.5%

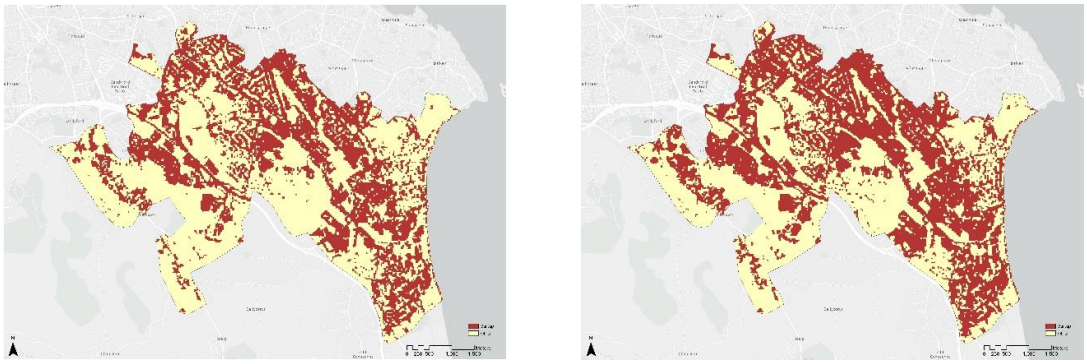

2015 2018

Figure III.10: Classified images of agglomeration A11

Table III.10: Change in built-up area for agglomeration A11

Year	Area in sq. m	Time interval	% Change in built-up area
2015	12303947.78	-	-
2018	14680329.32	2015 – 2018	19.3%

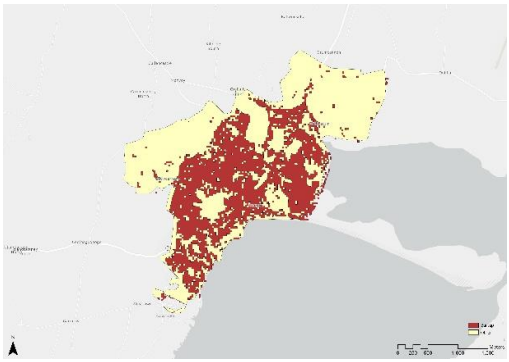

2010

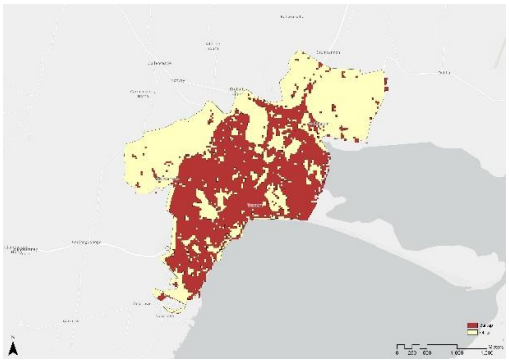

2015

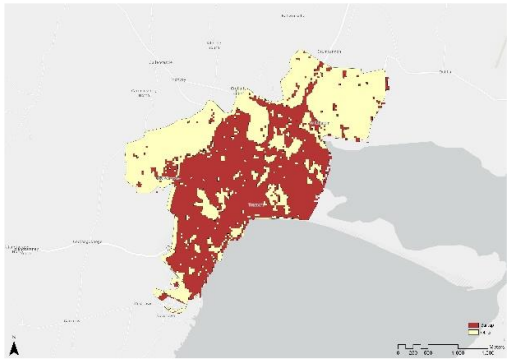

2018

Figure III.11: Classified images of agglomeration A12

Table III.11: Change in built-up area for agglomeration A12

Year	Area in sq. m	Time interval	% Change in built-up area
2010	3347277	-	-
2015	3907893	2010 – 2015	16.8%
2018	4261501	2015 – 2018	9.1%

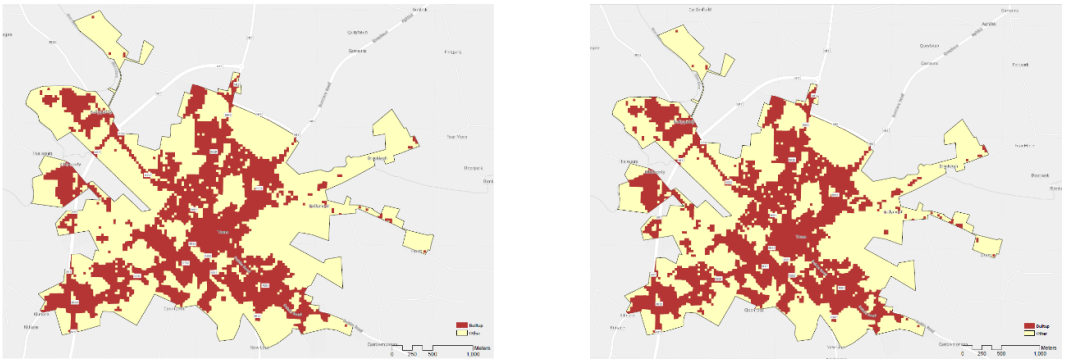

2016 2018

Figure III.12: Classified images of agglomeration A13

Table III.12: Change in built-up area for agglomeration A13

Year	Area in sq. m	Time interval	% Change in built-up area
2016	3418032	-	-
2018	3529107	2016 – 2018	3.2%

2014 2016

2018

Figure III.13: Classified images of agglomeration A14

Table III.13: Change in built-up area for agglomeration A14

Year	Area in sq. m	Time interval	% Change in built-up area
2014	8170230	-	-
2016	8362440	2014 – 2016	2.3%
2018	8640393	2016 – 2018	3.3%